ISAS - INTERNATIONAL SCHOOL
FOR ADVANCED STUDIES

Interplay between surface in-plane ordering and roughening

Thesis submitted for the degree of

"Doctor Philosophiæ"

CANDIDATE

Giorgio Mazzeo

SUPERVISORS

Prof. Giancarlo Jug

Prof. Erio Tosatti

November 1992

TRIESTE

SISSA - SCUOLA
INTERNAZIONALE
SUPERIORE
STUDI AVANZATI
TRIESTE
Strada Costiera 11

SISSA ISAS

SCUOLA INTERNAZIONALE SUPERIORE DI STUDI AVANZATI
INTERNATIONAL SCHOOL FOR ADVANCED STUDIES

Interplay between surface in-plane ordering and roughening

Thesis submitted for the degree of

"Doctor Philosophiæ"

CANDIDATE

Giorgio Mazzeo

SUPERVISORS

Prof. Giancarlo Jug

Prof. Erio Tosatti

November 1992

Index

Introduction 1

1. Surface phase transitions and surface scattering 5

1.1 The Solid on Solid description 7

1.2 Deconstruction of a (2×1) reconstructed surface 9

1.3 Roughening 10

1.3.1 The BCSOS model (and the six vertex model) 13

1.3.2 Step free energy and the equilibrium shape of crystals . 16

1.4 Scattering 18

1.4.1 Scattering nomenclature 18

1.4.2 Atom and X-rays scattering 21

1.4.3 Coherent and incoherent scattering intensity 24

1.4.4 Scattering and order parameters 28

1.4.5 Scattering and critical exponents 30

1.4.6 Scattering from a rough surface 33

1.4.7 Other considerations about scattering 34

2. Phenomenology of (110) surfaces 37

2.1 Reconstructed surfaces 37

2.1.1 Au(110) 37

2.1.2 Pt(110) 43
2.1.3 Ir(110) 46
2.2 Uneconstructed surfaces 47
2.2.2 Ag(110) 47
2.2.2 Pb(110) 48
2.2.3 Cu(110) 49
2.2.4 Ni(110) 51
2.2.5 Other (110) surfaces 52
2.3 An overview on fcc(110) surfaces 52

3. Theoretical models 57
3.1 The preroughening transition 57
3.2 Scenarios for the reconstructed surfaces:
the Bernasconi analysis 62
3.2.1 The parity restoring transition 64
3.2.2 Experiments and scenarios for Au(110) 65
3.3 The model of Levi and Touzani 67
3.4 The models of Kohanoff, Jug and Tosatti 69
3.5 The models of Villain and Vilfan 71
3.6 The four-state clock step model of den Nijs 76
3.7 The strong chirality limit and the global phase diagram . . . 79

4. The model and the method 87
4.1 A description of the model 87
4.2 Ground state considerations 88
4.3 Energy parameters 90

4.4 The Monte Carlo algorithm 95
4.5 The relevant quantities 96
4.6 Order parameters 98

5. The BCSOS model 102
5.1 The sublattice order parameter 104
5.2 Exacts results verified 107
5.3 The staggered fields susceptibility 110
5.4 The exponent ω 111

6. Gold(110) 120
6.1 Deconstruction and roughening 120
6.2 Scattering intensities results 123
6.3 Discussion 125

7. Silver(110) 142
7.1 Sublattice disordering and roughening 142
7.2 Scattering intensities results 146

Conclusions 161

Appendix 166

Bibliography 172

Ringraziamenti

Introduction

Clean single-crystal metal surfaces usually possess a well defined two dimensional periodicity closely resembling the atomic ordering in the bulk. In some cases, however, the surface lattice reconstructs into a phase with a new symmetry: this can occur spontaneously or it can be induced by small coverages of adsorbed atoms or molecules. In this respect, the fcc (110) surfaces of noble and near-noble metals belong to two different classes †. The first class includes the lighter metals (Cu, Ag, Ni, Pd), whose (110) surface remains unreconstructed when clean (although a suitable coverage of alkali adatoms causes their reconstruction), but which are expected to show a roughening transition. The second class includes the heavier metals (Au, Pt, Ir). Of these, two reconstruct in the (2×1) missing-row phase at low temperatures while for Ir the situation is more complex and even a (3×1) reconstruction does not seem to properly represent its ground state and more complex structures have been proposed. As the temperature is raised, excitations start to disorder the ideally reconstructed (2×1) surface until a continuous deconstruction transition takes place, where (2×1) long-range order is lost. At still higher temperatures a roughening transition is likely to occur, due to proliferation of steps; hence the interplay between steps and other defects gives rise to a connection between the two transitions which has been the subject of much recent experimental and theoretical work.

Fcc metal surfaces like (100) and (111) generally show reconstructing features at low temperatures but no roughening phase transition at high temperature, at

† By near-noble one means nearly filled d-band metals.

least sufficiently below the melting point. More open surfaces like (113), (115), (117) lose reconstruction but gain roughening. The rich phenomenology of (110) surfaces is due to their position "in between" the two quoted examples, i.e. to their nature of open surfaces showing reconstruction but also a roughening and, eventually, a melting transition at higher temperatures. In addition, from the statistical mechanics point of view, their sublattice structure and the interplay between different phase transitions open a wide variety of scenarios for the behaviour of the correlation functions and the drawing of phase diagrams.

This thesis is intended to present a detailed theoretical study of some of the above mentioned scenarios, both for the unreconstructed and for the reconstructed (110) surfaces, by means of Monte Carlo simulations performed on a suitably chosen Hamiltonian. It is organized as follows.

Chapter 1 is roughly divided in two parts. The first leads into the structural and geometrical aspects of the surfaces examined in the thesis and introduces the Solid-On-Solid (SOS) description appropriate for them, since the model adopted for the study of the fcc (110) phenomenology belongs to the SOS class of Hamiltonians. A section is dedicated to the deconstruction transition (of the reconstructed surfaces), with particular regards to its critical behaviour, and another to the roughening transition. The latter, after some historical review, presents some important results characterizing the transition, especially from the point of view of the universal features shared by the various models thus far proposed. Amongst them, a position of outstanding importance is attached to the BCSOS model, of which a detailed description is given in connection with the six vertex model. The section is concluded by some phenomenological argument about the vanishing of the step free energy (and of the corresponding facet in the equilibrium crystal shape) at the roughening transition.

The second part of the chapter is dedicated to scattering. It is in fact essential to introduce the main concepts concerning this important experimental tool, since many investigations on surfaces are performed by means of scattering experiments. An introductory section tries to clarify the sometimes confusing scattering terminology, then the most relevant physical quantities, such as the scattering intensities, are introduced and discussed both for atom and X-ray scattering (in the kinematic approximation). Decomposition into coherent and incoherent scatter-

ing is presented in connection with critical behaviour near a second order surface phase transition. Extraction of information about the physics of the surface under consideration is finally implemented by the study of scattering from a rough surface, since its features strongly differ both from those of an ordered surface and from those of a randomly disordered one.

The aim of Chapter 2 is to offer a concise but comprehensive review of the phenomenology of the (110) surfaces, both reconstructed and unreconstructed, from the point of view of their low temperature symmetries and their thermal phase transitions. Each section is devoted to a particular metal and a final section tries to summarize the general most relevant features in an overview.

In Chapter 3 a review is presented of the most recent and relevant theoretical models of the phase transitions which can occur on the fcc(110) surfaces: preroughening on the unreconstructed surface, deconstruction for the reconstructed ones, and roughening. The presence on the "hot" surface of many kinds of defects, from vacancies and adatoms to bound or free arrays of steps, may lead to an intriguing interplay between the various transitions which gives rise to the formulation of different disordering scenarios. The main source is represented by the work by Marcel den Nijs, starting from the idea of a preroughening transition on a model for a simple cubic (100) surface, then evolving into the study of the connections between deconstruction and roughening for (2×1) reconstructed fcc(110) surfaces. On this second line, important contributions have been provided by the works of Villain and Vilfan (and, very recently, of Balents and Kardar), all of these comprehensively reviewed in a "global" paper by Bernasconi, who presents some new ideas and puts forward new possible scenarios; their detailed description will be the main subject of Chapter 3.

In Chapter 4 the model from which all the new results of the thesis are drawn is presented. Two different real systems, the (2×1) reconstructed surface of gold and the (1×1) unreconstructed surface of silver, are chosen for investigation of their low temperature symmetries and their high temperature critical behaviour, while particular emphasis is given to the physical motivations underlying the structure of the model itself as well as to the choice of the energy parameters adopted to describe what will be henceforth called "gold" and "silver" (110). Then, a short account of the Monte Carlo algorithm set up in order to study the properties of the chosen Hamiltonian is provided, together with a list of the relevant quanti-

ties which have been examined for understanding the physics embodied by the model. Particular stress is given to the definition and significance of surface order parameters.

Chapter 5 is dedicated to the study of the roughening transition on the BCSOS model. Its aim is threefold. First, it can be seen as a check for the techniques and, in general, for the global simulation procedure against an exactly solvable model. Secondly, an important concept like that of sublattice order parameter is introduced and studied in connection with known exact results. Lastly, a deeper insight into a quantity which has remained hitherto unexplored, the staggered susceptibility, is provided.

In Chapter 6 the results of the Monte Carlo simulation for Au(110) are presented. Evidence for a second order Ising-like phase transition and of a distinct (separated in temperature) roughening transition is given, in accordance with the most recent experimental results. Scattering calculations are able to reproduce a temperature dependent shift in the half integer order peaks, a feature which provides a deep insight into the nature of the flat but disordered phase between the two transitions. A discussion follows where one of the scenarios proposed in Chapter 3 for the two transitions is chosen and its nature and occurrence on the simulated surface justified.

Chapter 7 provides results for the unreconstructed fcc(110) surface which has been called "silver". Data analysis runs parallel to that in the preceeding Chapter, also form the point of view of the scattering calculation. For the first time in a Monte Carlo simulation, a new transition, apart form roughening, is found and characterized. It can be ascribed to the class of preroughening transitions introduced (in Chapter 3) by theoretical analysis, though up to now no direct experimental evidence has been clearly detected it on a real surface.

An Appendix shows the exact relations between order parameters and scattering intensities, while the final section summarizes the situation of the fcc(110) surfaces arisen from the present Monte Carlo simulations.

Chapter 1

Surface phase transitions and surface scattering

The outermost layer of a (110) surface of an fcc crystal has an anisotropic structure which can be described as made up of atomic rows a distance a apart in the [001] direction (a being the fcc lattice parameter) and with the atoms separated by the close-packing distance $a/\sqrt{2}$ in the $[1\bar{1}0]$ direction of each row. It is useful to superimpose on the surface a cartesian system of axis: from now on the x direction will coincide with [001] and the y direction with $[1\bar{1}0]$, so that the surface atomic spacings will result $a_x = a$ and $a_y = a/\sqrt{2}$ (fig. 1.1).

The surface of the heavier metals (Au, Pt) tends to increase its atomic density by means of formation of (111) microfacets and the resulting structure is a more closely packed surface with lower surface energy than the (1×1), despite the increase in microscopic surface area. The lowest order possibility of such microfaceting is the (2×1) reconstruction where every second row is missing. The unit cell is doubled in the [001] direction, and the resulting surface structure is thus made up by a sequence of local (111) facets which form a 35° angle with the surface plane (fig. 1.2).

Apart from such reconstruction phenomena, real surfaces show other minor relaxation effects like small lateral atomic displacements and inward relaxation of the top layers with respect to an ideal, bulk-truncated structure. Such effects are both experimentally observed and theoretically predicted. In the case of Au(110) missing-row phase, for example, results from various diffraction experiments indicate a contraction of the top interlayer spacing, together with distortions of the

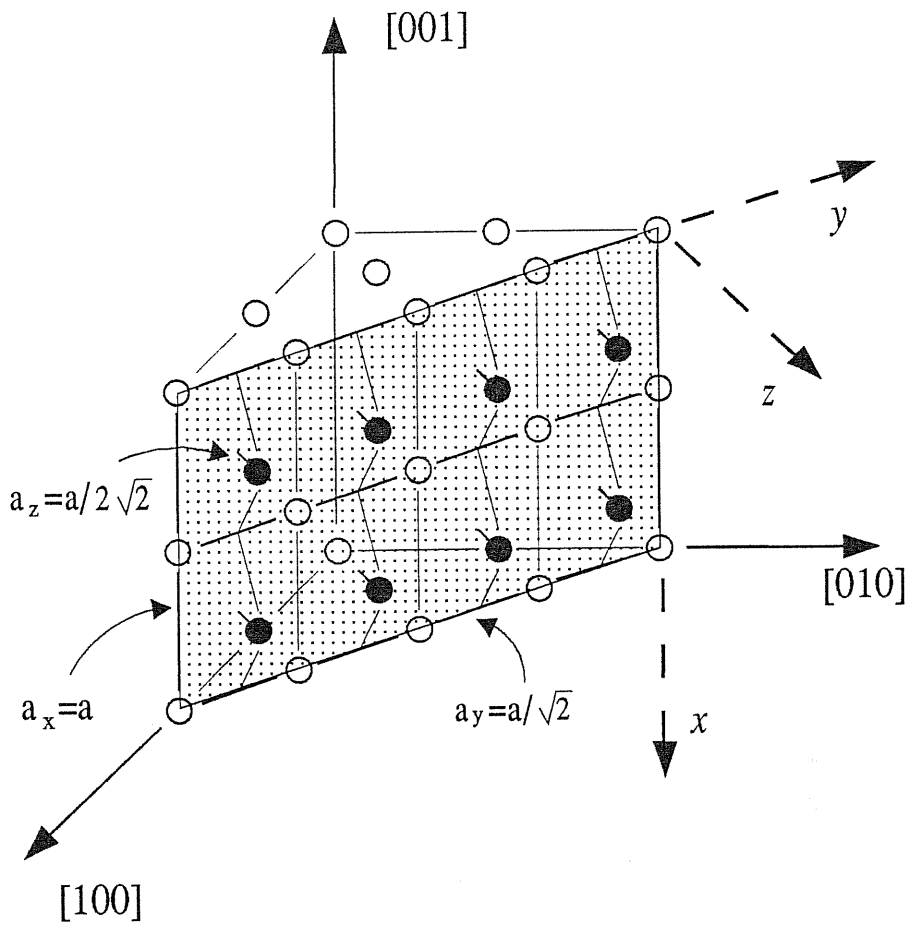

Figure 1.1. The fcc lattice, cut so as to show the (110) surface, with the surface reference system $x-y-z$, the atomic spacings and the two sublattices (black and white) which the surface is made of.

inner layers including lateral displacements of the second layer atoms and a buckling of the third atomic layer (see chapter 2 for details and references). These relaxation of the atomic position from an ideal (2×1) structure are also confirmed both by the first principles calculations of Ho and Bohnen [1,2] and by more empirical many body approaches, such as the "glue model" of Ercolessi *et al.* [3–5]. Nonetheless, the model presented in this thesis is directed towards the understanding of the different phase transitions shown by the fcc (110) surfaces rather than of their detailed structural aspects; thus, it is chosen to be a Solid On Solid model.

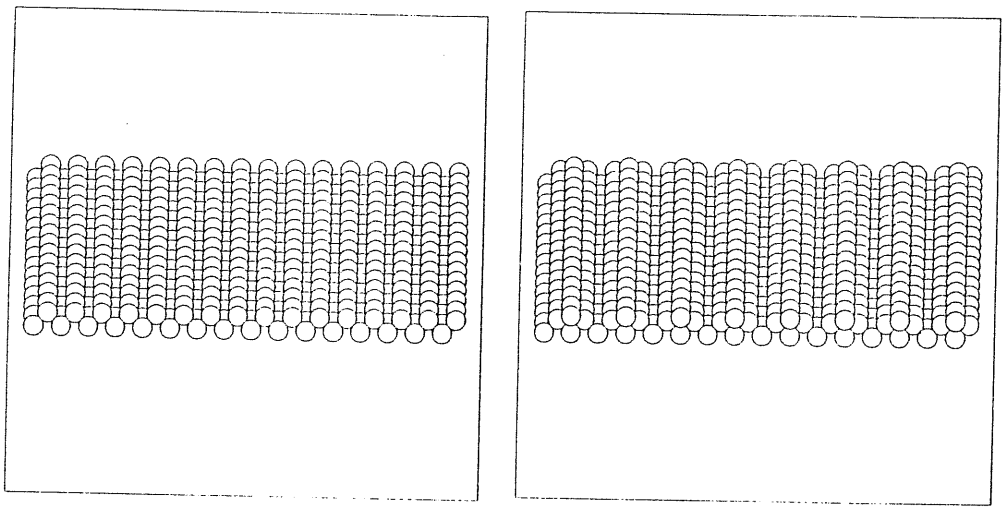

Figure 1.2. Ground state configuration for: (left) the unreconstructed surface; (right) the 2×1 missing row reconstructed surface.

1.1 The Solid On Solid description

In the microscopic description of a surface, a certain class of models are grouped together under the Solid On Solid (SOS) designation, from a particular restriction imposed on their Hamiltonians. First of all, the atoms are constrained to lie on the sites of a rigid three dimensional lattice, moreover the further requirement is imposed so that every atom (i.e. lattice occupied site) is directly above another occupied site (thus excluding "overhangs" in the surface shape, as well as voids in the solid phase or "bubbles" in the vapor phase). A SOS model can thus be thought of as an array of interacting columns of variable integer heights. The surface configuration is represented by the 2D array of integers specifying the number of atoms in each column perpendicular to the chosen surface or, equivalently, by the heights of the columns relative to a flat reference surface. Growth or evaporation of the crystal involves just the "surface atoms" on the top of their columns. In this way, an SOS Hamiltonian is expressed in terms of a set of integer height variables $\{m_i\}$ defined at each site i of a two dimensional lattice, and the surface energy is a function of the number of broken bonds due to the existence of surface fluctuations. A wide variety of SOS models can be considered, in which

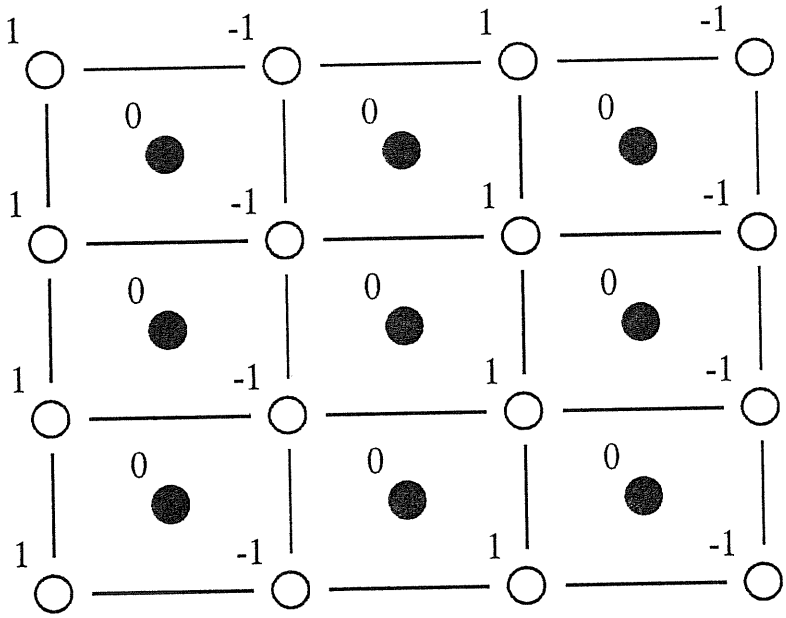

Figure 1.3. The fcc(110) lattice viewed from above. The numbers refer to the height variables associated to each site, in units of vertical lattice spacing a_z, with reference to a perfectly ordered 2×1 missing row phase.

the interaction energy between neighbouring columns is some increasing function V of their height difference, which is proportional to the number of broken bonds, so that the Hamiltonian can be written as follows:

$$H_{SOS} = \sum_{\langle i<j \rangle} V(m_i - m_j) \tag{1.1}$$

where $\langle i < j \rangle$ means i and j are nearest neighbour sites.

Specifying now to the case of interest, i.e. that of a fcc (110) surface, the SOS description will be given in terms of a set of discrete column heights $\{h(\mathbf{R})\}$ (see fig. 1.3) defined on the sites $\mathbf{R}$ of a lattice made up of two interpenetrating plane rectangular sublattices (which from now on will be called "black" and "white" sublattices for convenience's sake, as they are completely equivalent from the physical

point of view). The height values $h(\mathbf{R})$ may be written as $h(\mathbf{R}) = a_z m(\mathbf{R})$, where a_z is the lattice spacing perpendicular to the surface, $a_z = a/2\sqrt{2}$, and $m(\mathbf{R})$ are integers, odd on the sites on one sublattice (say, the white one) and even on those of the other (the black one), as required in addition by the geometry of the surface itself.

This SOS description will be presented in more details in Chapter 4, but it will prove immediately useful in Section 1.4, when scattering quantities will be introduced and the main formulas for scattering intensities derived. It is now time to talk about some of the surface phase transitions of interest in the present thesis: deconstruction and roughening.

1.2 Deconstruction of a (2×1) reconstructed surface

At low temperature, a surface like Au or Pt (110) is ideally made up of an infinite array of atoms arranged in the (2×1) reconstructed phase with no defects of any kind. In reality, the long-range order is guaranteed by a succession of terraces of the right symmetry but of finite extension, separated by finite steps and by closed islands if not by other defects (dislocations, etc...).

When the temperature of the system is increased, the ordered in-plane structure starts to develop defects due to the excited states now made thermally available. Creation of vacancies and adatoms, of new steps, etc..., reduce the terrace width and the increase in the amount of disorder present on the surface can be monitored by looking at the thermal behaviour of some suitably defined order parameter. All these effects may be responsible, at a certain temperature T_D, for a phase transition from the (2×1) symmetry to some other phase, called *deconstruction*, the nature of which can be investigated through scattering experiments. Scattering intensities are in fact directly related to thermodynamical quantities (see Section 1.4.3), and the corresponding critical exponents which usually become experimentally accessible are:

- β, related to the order parameter vanishing at the critical temperature as $\mathcal{P} \sim t^{\beta}$ (with $t = |\frac{T-T_D}{T_D}|$);
- γ, related to the divergence of the susceptibility χ of that order parameter at T_D, $\chi \sim t^{-\gamma}$;

- ν, related to the divergence of the correlation length ξ of the system at T_D, $\xi \sim t^{-\nu}$.

1.3 Roughening

While deconstruction is a phase transition which involves the surface in-plane degrees of freedom, i.e. those related to the two dimensional symmetries and ordering, roughening instead takes into account the off-plane degrees of freedom, those related to the mean surface thickness.

In 1949 Burton and Cabrera[6] first put forward the idea (further developed in a now classic article by Burton, Cabrera and Frank[7]) that a phase transition may occur in the equilibrium structure of crystal surfaces. They conjectured that low index crystal faces in equilibrium with vapor, melt or solution, would become rough above a certain transition temperature T_R: this can have important consequences for the speed of growth and the equilibrium shape of the crystal. The transition is characterized by the interface becoming infinitely "rough" in the sense of a divergent interfacial width. The argument used by Burton, Cabrera and Frank for the existence of such transition was partly based on a mapping of the interface problem onto the 2D Ising model, which had just recently been solved by Onsager[8] and which could lead to large fluctuations in the surface structure at the critical temperature T_C^{2D}. The idea is undoubtedly valid at low temperatures, but breaks down near the transition temperature, when the interface tends to delocalize before becoming infinite in width and any mapping onto a model which takes into account only a finite number of atomic layers is no longer valid. This failure ends up in a wrong prediction about the universality class to which a correct roughening model should belong, which is not of the 2D Ising type.

Since 1949, a wealth of theoretical work (reviewed in ref. [9,10]) was produced, especially after a certain class of models was introduced, imposing the SOS restriction on the Hamiltonian. In this regard, one of the most important SOS models is the Discrete Gaussian model (DG), first studied by Chui and Weeks[11], where the building blocks lie on a square lattice, and the interaction energy between adjacent columns is taken to be as the quadratic form (see eq. (1.1))

$$H_{DG} = \sum_{i<j} J(m_i - m_j)^2 \tag{1.2}$$

The partition function of Hamiltonian (1.2) was rewritten, via a duality transformation, into the partition function of a neutralized 2D Coulomb gas, but with the ratio J/T inverted. In this way the existence of a transition was established between a smooth, low-temperature phase, and a rough, high- temperature one and, which was placed in the Kosterlitz-Thouless universality class [12,13]. Different forms of the interaction energy V will not change the universality class because the roughening transition involves long-wavelength fluctuations in the position of different parts of the interface, hence changes in the interaction energy between columns that affect only short-wavelength properties should be irrelevant at the roughening point [9].

It is now useful to present some of the results of the Renormalization Group calculations for thermodynamical quantities near T_R [10].

The singular part of the free energy is not analytic at T_R, its form being

$$F_S \approx B \exp\left(-\frac{C}{\sqrt{|T - T_R|}}\right) \tag{1.3}$$

for T in the neighbourhood of T_R (B and C are non-universal constants). The singularity is a very weak one as all the derivatives of F_S with respect to T are smooth functions of T vanishing at T_R. In particular, there is no specific heat anomaly at T_R, in contrast with the Ising model: the transition is said to be of infinite order.

The correlation length, which is the characteristic length for correlations between thermal excitations of the crystal surface, is finite well below T_R, while it diverges at T_R like

$$\xi \approx \begin{cases} \xi^0 \exp\left(\frac{A}{\sqrt{T_R - T}}\right), & T < T_R \\ \infty, & T \geq T_R \end{cases} \tag{1.4}$$

with ξ^0 and A again non-universal constants.

But the most striking result concerns the behaviour of the height-height correlation function,

$$G(R) \equiv \langle [h(\mathbf{R}_i) - h(\mathbf{R}_0)]^2 \rangle \tag{1.5}$$

where $R \equiv |\mathbf{R}_i - \mathbf{R}_0|$, and the angular brackets denote an ensemble average in the SOS system. This function gives a measure of the delocalization of the interface due to fluctuations in height between different regions of the surface. Its full expression is

$$G(R) = K(T) a_\perp^2 \ln \left[a_\parallel^2 \left(\frac{1}{R^2} + \frac{1}{\xi^2} \right) \right]^{-1} \tag{1.6}$$

where $a_\perp$ and $a_\parallel$, respectively, are the lattice constants in the direction orthogonal and parallel to the plane of the surface under consideration (where it is implicitly assumed that $a_\parallel$ is the same for different principal directions in this plane). ξ is the correlation length introduced in (1.4), hence for $T > T_R$ one has $\xi^{-1} = 0$ and a logarithmic divergence of $G(R)$. The coefficient $K(T)$ is an increasing function of temperature, whose behaviour is specifically predicted by Renormalization Group calculations. At the roughening temperature, $K(T)$ assumes the universal value

$$K(T_R) = \frac{1}{\pi^2} \tag{1.7}$$

approached from above in the following way:

$$K(T) \simeq \frac{1}{\pi^2} + C \, [T - T_R]^{\frac{1}{2}} \ , \ T \to T_R^+ \tag{1.8}$$

where the power $\frac{1}{2}$ is universal, but the constant C is not[10]. The correlation function is clearly related to the fluctuations in height of a point of the interface about its average value $\langle h(\mathbf{R}_0) \rangle$, being

$$\langle \delta h^2 \rangle \equiv \langle h^2(\mathbf{R}_0) \rangle - \langle h(\mathbf{R}_0) \rangle^2 = \lim_{R_i \to \infty} \frac{1}{2} \langle [h(\mathbf{R}_i) - h(\mathbf{R}_0)]^2 \rangle \tag{1.9}$$

so that

$$\langle \delta h^2 \rangle \approx \begin{cases} K(T) \ln\left(\xi/a_{\parallel}\right), & T < T_R \\ K(T) \ln\left(L/a_{\parallel}\right), & T \geq T_R \end{cases} \tag{1.10}$$

thus saturating to a constant value for temperatures below T_R (smooth phase), while logarithmically diverging with the size L of the system for $T > T_R$. This delocalization of the interface is the concept more closely related to the statistical mechanics idea of roughening. It should also be remarked that (1.6) and subsequent formulæ should hold for anisotropic surfaces as well, at least in the limit of large R.

1.3.1 The BCSOS model (and the six vertex model)

Another type of SOS model presenting a roughening transition and, moreover, exactly solvable, is the BCSOS (Body Centered Solid-on-Solid) model introduced by van Beijeren[14] in 1977. The system under consideration is the (100) face of a bcc crystal, in which both the atoms at the corner of the cube and those at the center are taken into account. At $T = 0$, nearest neighbour columns differ by one atom (one interlayer spacing) since half the columns terminate in the layer directly below the outermost surface layer. The system is constrained such that at all temperatures these nearest neighbour columns can differ by at most ± 1 interlayer spacing. Thus the higher-energy multiple jumps between neighbouring columns are completely suppressed but, as argued before, this should have no effect on the critical behaviour: the (and actually is) in the same universality class as the other SOS models.

In practice, the system is composed of two standard SOS models defined on two interpenetrating square sublattices, where on one of the sublattices the height variables may assume only odd values ($\pm 1, \pm 3, \ldots$) and on the other sublattice only even values ($0, \pm 2, \pm 4, \ldots$). Also, the additional (and very relevant, as it will be seen later) restriction is imposed that the height jumps between neighbouring sites (belonging to different sublattices) may be just ± 1. Van Beijeren showed with a simple argument that the allowed configurations in the BCSOS model can be placed in exact correspondence with the vertex configurations of Lieb's six vertex model[15–17], which is the 2D version of the ice model, introduced by Pauling[18]

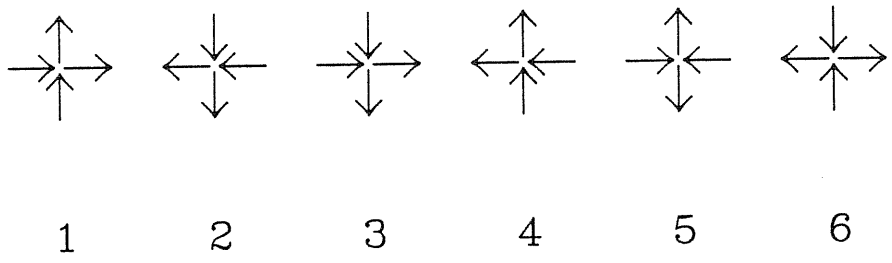

Figure 1.4. The six vertices.

and Slater[19] in order to study the residual entropy of ice at $T = 0$, as well as the ferroelectric phase transition. Hence the two models are isomorphic.

Van Beijeren's construction proceeds by placing arrows across the bonds of the dual lattice, fixing their direction in such a way that the higher of the two neighbouring height variables always lies to the right of an the arrow (the arrow lattice thus results rotated by 45° with respect to the surface lattice). It is easy to see that at the sites of the dual lattice, where four arrows meet, just six of the sixteen possible combinations of four arrows are realised. They are precisely the vertices allowed by the six vertex model (shown in fig. 1.4), satisfying the so called "ice rule" (at each node of the dual lattice two arrows point inwards and two outwards) which is an immediate consequence of the uniqueness of the height variables of the surface system. This also makes one-to-one the correspondence between vertex configurations and BCSOS height configurations (up to an overall vertical shift of the height variables, an arbitrariness which can be removed by fixing the value of a simple height variable).

The six vertex model, which was exactly solved by Lieb and Wu[16], can be divided into different classes according to the values of the energies ε_i assigned to each vertex. If the system is invariant under arrow reversal, the energies satisfy $\varepsilon_1 = \varepsilon_2$, $\varepsilon_3 = \varepsilon_4$ and $\varepsilon_5 = \varepsilon_6$. The exact solution is available for general ε_1, ε_3 and ε_5, and is given in terms of the quantity

$$\Delta = \frac{a^2 + b^2 - c^2}{2ab} \tag{1.11}$$

where a, b and c are the Boltzmann factors associated with ε_1, ε_3 and ε_5 respectively. This quantity has a great relevance in the analytic solution, because most properties of the six vertex model do not depend on a, b and c separately, but on their combination Δ.

The BCSOS model corresponds to the six vertex model in its F version, that is with $\varepsilon_1 = \varepsilon_3 = \varepsilon > 0$, $\varepsilon_5 = 0$. By energetically discouraging vertices 1 to 4 in favour of 5 and 6 one gets an antiferromagnetic long-range order for the low temperature phase. The transition between this phase (with correlation length ξ finite) to a high temperature one (with $\xi = \infty$) is of infinite order, and occurs for $\Delta = -1$, that is when $a+b = c$, which means $k_B T_C = \varepsilon / \ln 2$. In the BCSOS model ε equals the interaction energy J between atoms in each sublattice (isotropic in the x and y directions), while, as said before, interaction between the two sublattices are taken of infinite strength, thus allowing just for a height difference of ± 1. As shown by van Beijeren [14], this model can be thought of as the limit of a lattice gas model on a bcc crystal lattice with strong nearest-neighbour interactions and much weaker next-nearest- neighbour interactions.

From the physical point of view, the complete low T antiferroelectric order of the F model corresponds here to the presence of vertices 5 and 6 only, thus, according to van Beijeren's construction, to a flat surface (one sublattice, for example, with all sites at height 1, the other all at 0). The rise in temperature is accompanied by the appearance of excitations of all the other vertices, that is of steps and adatoms on the surface, leading to the rough phase.

Being exactly solvable, all the properties of this Kosterlitz-Thouless phase transition are known. All the Renormalization Group predictions discussed in the preceeding section for the Discrete Gaussian model (which is in the same universality class as the BCSOS model), are confirmed, in particular the non-analytic behaviour of the free energy at the transition temperature, and the resulting absence of a heat capacity peak at T_R. However, a rounded anomaly is predicted to occur below T_R, due to a rapid continuous change in the surface disorder. In fact, roughening corresponds to an inverted XY model transition (i.e. with an inverted ratio J/T), where the appearance of defects which break short range order occurs above the critical point; the specific heat thus shows a maximum not at T_R but for $T \simeq 0.81 T_R$.

Further developments of van Beijeren's idea are due to Jayaprakash and

Saam[20–22], and by Trayanov *et al.* [23], who specialize to an anisotropic version of the BCSOS model in order to account for the roughening of the (110) face of fcc crystals. This model is again exactly solvable when mapped onto the six vertex model. The details are left to Chapter 4, where the model presented in this thesis is introduced and studied, since the initial underlying physical considerations are the same for all these models.

1.3.2 Step free energy and the equilibrium shape of crystals

From the statistical point of view one can characterize the roughening transition by the divergence of the height-height correlation function. From the phenomenological point of view one can characterize it through the disappearance of a cusp in the so-called γ-plot, microscopically corresponding to the vanishing of the step free energy of the roughening surface.

The γ-plot is nothing but the polar plot of $\gamma(\hat{\mathbf{n}})$, i.e. the surface free energy γ as a function of the surface orientation $\hat{\mathbf{n}}$. Since the crystal, at a fixed volume, tends to achieve minimum total energy by suitably distorting its shape, there is a clear relation between $\gamma(\hat{\mathbf{n}})$ and the equilibrium crystal shape, first mathematically expressed by Wulff[24] in 1901 and completed by Herring[25] 50 years later. Wulff's construction permits to draw the equilibrium shape of the crystal starting from the knowledge of its free energy, or to reconstruct the latter from measurements of the former[26]. In particular, cusps at certain orientations of the γ-plot correspond to facets in the crystal shape, i.e. regions with zero curvature.

In general, the surface of a crystal in equilibrium consists of these facets, which are macroscopically flat and, at $T \neq 0$, of rounded parts between them. The facets are crystal faces in a smooth phase, i.e. below their roughening temperature and the rounded parts may be considered as constructed from infinitesimal pieces of rough faces. So, if the temperature is raised through $T_R(\hat{\mathbf{n}})$ (the roughening temperature of a face of orientation $\mathbf{n}$), the facet size shrinks to zero and the orientation $\mathbf{n}$ becomes part of a rounded area. Therefore, for the relation between the γ-plot and crystal shape, the roughening transition can be characterized by the disappearance of a cusp from the γ-plot.

If one wants to obtain an expression for the surface free energy γ (or f) as a

function of orientation from a simple model, one is lead to study a vicinal surface, that is a surface under a tiny angle from a low index one. Adopting an SOS model on a square lattice to describe the situation, one can build at $T = 0$ the vicinal surface of orientation $(p, 0, 1)$, with $|p| \ll 1$, by creating p straight steps per unit length in the x direction on the (001) flat facet[10]. At non zero temperature the straight steps will develop kinks, and the terraces between them will develop thermal excitations in form of small bumps (adatoms) and pits (vacancies). The surface free energy of the surface per unit area is expressed as

$$f(p, 0, 1) = f(0, 0, 1) + f^S(0)|p| + \dots \tag{1.12}$$

where $f^S(\varphi)$ is the free energy associated to a step forming an angle φ with the y direction per unit length and unit step height, and the dots stand for entropic contributions (ignored because of no interest in what follows), and interaction terms between steps (neglected in the limit $|p| \to 0$ because of order p^2 or greater).

If $f^S(0) > 0$, one sees from (1.12) that $f(p, 0, 1)$ exhibits a cusp as a function of p at $p = 0$. According to the preceeding discussion, this implies that the equilibrium crystal shape exhibits a facet in the (001) direction; furthermore it can be proved that the diameter of this facet in the y direction is proportional to $f^S(0)$. More generally, $f(\lambda \cos\varphi, \lambda \sin\varphi, 1)$ as a function of λ exhibits a cusp at $\lambda = 0$ under a slope given by

$$\left.\frac{\partial f}{\partial \lambda}\right|_{\lambda=0} = f^S(\varphi) \tag{1.13}$$

But, since the roughening transition macroscopically corresponds to a facet in the equilibrium crystal shape shrinking to zero at T_R, that is to the disappearance of a cusp in the Wulff's plot, one can conclude from (1.13) that the roughening transition can be characterized microscopically by the vanishing of the step free energy for steps on the facet that roughens up. Once this happens, steps of arbitrary length will form spontaneously on this face, so that the height $h(r_0)$ of a chosen point on the interface will fluctuate more and more about its average value, thus causing the divergence of the height-height correlation function, as follows from the statistical mechanics definition of roughening of formulæ (1.5)-(1.9).

1.4 Scattering

The present discussion on scattering concepts will be restricted to the kinematic approximation, where there is little difference amongst the various probes, in particular atoms and X-rays: each surface atom is considered as an individual scattering centre, hence LEED (Low Energy Electron Diffraction) and related techniques will be excluded from this review since large multiple-scattering effects arise in this case.

1.4.1 Scattering nomenclature

In the classical derivation of the diffraction pattern from a crystal lattice, it is frequently assumed that the crystal is infinite in extent; the diffraction peaks are then perfect δ functions. When finite-size effects are included, the peaks are found to be broadened by an amount inversely related to the dimension of the diffracting region of the crystal and, in addition, a significant amount of intensity is always scattered far away from the Bragg peaks and is spread right across the Brillouin zone. The order of magnitude of this intensity is the same as that arising from a single (crystalline) layer of atoms, and so diffraction experiments with monolayer sensitivity (possible, e.g., by means of X-rays[27]) are able to detect it.

A primitive parallelepiped crystal of dimensions N_x, N_y and N_z unit cells with lattice parameters a_x, a_y and a_z diffracts X-rays with an intensity proportional to the square of the structure factor,

$$|F(q_x,q_y,q_z)|^2 = \left| \sum_{j_x=1}^{N_x} \sum_{j_y=1}^{N_y} \sum_{j_z=1}^{N_z} \mathrm{e}^{i(q_x a_x j_x + q_y a_y j_y + q_z a_z j_z)} \right|^2 =$$

$$= \frac{\sin^2\left(\frac{1}{2}N_x q_x a_x\right)}{\sin^2\left(\frac{1}{2}q_x a_x\right)} \frac{\sin^2\left(\frac{1}{2}N_y q_y a_y\right)}{\sin^2\left(\frac{1}{2}q_y a_y\right)} \frac{\sin^2\left(\frac{1}{2}N_z q_z a_z\right)}{\sin^2\left(\frac{1}{2}q_z a_z\right)}. \quad (1.14)$$

When N_x, N_y and N_z are large, the function is sharply peaked at the Bragg points where the intensity is $(N_x N_y N_z)^2$. The three Laue conditions for this are

$q_x a_x = 2\pi h$, $q_y a_y = 2\pi k$, $q_z a_z = 2\pi l$ (h, k and l integers), which define the reciprocal lattice. If one of these conditions is relaxed, say on q_z, the intensity tends in the limit of large N_z to

$$\left|F\left(\frac{2\pi h}{a_x}, \frac{2\pi k}{a_y}, q_z\right)\right|^2 = N_x^2 N_y^2 \frac{\sin^2\left(\frac{1}{2}N_z q_z a_z\right)}{\sin^2\left(\frac{1}{2}q_z a_z\right)} \longrightarrow$$

$$\longrightarrow N_x^2 N_y^2 \frac{1}{2\sin^2\left(\frac{1}{2}q_z a_z\right)} \text{ as } N_z \to \infty \text{ for } q_z a_z \neq 2\pi l \quad (1.15)$$

where the rapid oscillations of the numerator are averaged to $\frac{1}{2}$ in the limit. Similar results can be readily obtained by relaxing the conditions on q_x or q_y. Thus the diffraction intensity of the finite-sized crystal has diffuse streaks connecting all the Bragg points. The diffuse intensity far from the nodes is of order of magnitude N^4 compared with N^6 at the nodes.

If one considers now a crystal with the fcc structure, bulk Bragg peaks can always be labeled by means of the set of integers ($h\,k\,l$), but keeping in mind that due to the fcc symmetry, $h\,k\,l$ must be of the the same parity. Peaks for which this condition holds are called *bulk permitted*, they are called *bulk forbidden* otherwise. The distinction has to be made with particular respect to scattering probes like X-rays, which penetrate into the crystal and create a well known bulk diffraction pattern onto which, eventually, a surface diffraction pattern is superimposed.

Scattering that is sharp in two directions and diffuse in the third must thus arise from a crystalline object that is localized in one dimension and extended in the other two, such as the surface of a semi-infinite crystal. The scattering pattern of a surface differs from that of a bulk crystal in the sense that the Bragg points transform into elongated rods in the q_z direction, called *crystal truncation rods*. The distinction between peaks and rods is now clear: a scattering peak is labeled by means of the usual bulk Miller indices ($h\,k\,l$), whereas a rod is instead identified by two "surface" Miller indices ($h_s\,k_s$), which form the two-dimensional reciprocal lattice of the surface structure. The rod includes the whole range of scattering intensities displayed as q_z scans the interval $0 \leq q_z a_z \leq 2\pi$. Again, the symmetry of the fcc (110) surface now plays an important role in the distinction of the various rods.

Three different kinds of rods are in fact present (see figure 1.5)

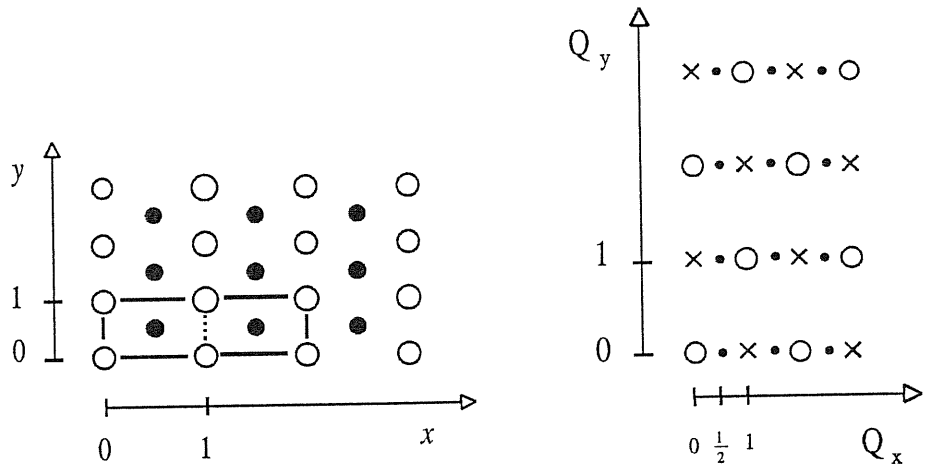

Figure 1.5. The fcc(110) lattice (left) with the usual unit cell (dashed) and the cell doubled due to reconstruction (solid lines), and the corresponding reciprocal lattice (right). The points denote intersection of the various rods with the $Q_x - Q_y$ phase. Open circles indicate principal rods, crosses are superlattice and dots reconstruction rods.

(a) *principal* rods, i.e. $(h_s\, k_s)$ of the same parity, forming the reciprocal lattice of the surface;

(b) *superlattice* rods, i.e. $(h_s\, k_s)$ with different parity, forming the reciprocal lattice of one of the two sublattices characterizing the surface;

(c) *reconstruction* (or half-integer) rods, i.e. h_s assuming half integer order values for the doubling of the unit cell in the [001] direction due to reconstruction (this last kind of course arises only for the reconstructed surfaces, and they are always bulk-forbidden peaks).

The position of a certain peak along a given rod is identified by the value of the momentum transfer perpendicular to the surface, q_z, or $p = q_z a_z$, so that the connection between the bulk Miller indices of a peak and the surface ones is expressed by the relation

$$\begin{aligned} h &= k_s + p \\ k &= -k_s + p \\ l &= h_s \end{aligned} \tag{1.16}$$

valid for an fcc (110) surface . From now on, expressions like "reconstruction peaks" should be read as a short form for "peaks in a reconstruction rod"; in addition, unless otherwise specified, every peak labeled by three indices is to be considered as belonging to bulk notation, i.e. of the form $(h\,k\,l)$.

1.4.2 Atom and X-rays scattering

In the corrugated hard wall model for atom-surface interaction and in the kinematic (or Kirchoff, or eikonal) approximation [28] the elastic scattering probability per unit solid angle is proportional to what will be called from now on scattering intensity, (scattering amplitude squared) that is to [29]

$$\mathcal{I}_A(\mathbf{Q}, q_z) = \left| \sum_{\mathbf{R}} \mathrm{e}^{i\mathbf{Q}\cdot\mathbf{R}} \mathrm{e}^{iq_z h(\mathbf{R})} \alpha(\mathbf{R}) \right|^2 \tag{1.17}$$

where:

- the subscript A stands for "atom scattering ";
- $\mathbf{Q}$ and q_z are the surface parallel and perpendicular momentum transfers, respectively, with $Q_x = \frac{2\pi}{a_x} h_s$ and $Q_y = \frac{2\pi}{a_y} k_s$ in the rod notation;
- $\mathbf{R}$ runs over the surface atom positions in the plane;
- $h(\mathbf{R})$ is the vertical position of the atom at $\mathbf{R}$, measured with respect to an arbitrary reference plane;
- $\alpha(\mathbf{R})$ is a *shadowing factor* depending on the heights of the nearest-neighbours of the atom at $\mathbf{R}$.

Formula (1.17) closely resembles the square of a surface structure factor except for $\alpha(\mathbf{R})$, which is included because atoms surrounding a lower one make the latter less visible to the probing atomic beam, whereas atoms surrounding a higher one leave it very visible, thus $\alpha(\mathbf{R})$ is chosen to be larger or smaller than 1 for a very exposed or poorly exposed surface atom respectively. A reasonable approximation is [30]

$$\alpha(\mathbf{R}) = 2 - \frac{1}{2} n(\mathbf{R}) \tag{1.18}$$

where $n(\mathbf{R})$ is the number of nearest-neighbours of atom $\mathbf{R}$ located to a level higher than the atom itself. Since each (110) surface atom has 4 nearest-neighbours, this form yields in the extreme situations the maximum value $\alpha(\mathbf{R}) = 2$ for a fully isolated adatom, and zero for any "buried' atom, including one below a surface vacancy. It is clearly not exact, and vastly improvable. However, it does reflect the main physics in a simple way, and is quite adequate for a qualitative analysis. Notice that the actual intensity also contains a Debye-Waller factor, an atomic form factor and other factors not relevant to the present discussion, hence omitted in (1.17).

For X-rays scattering the situation is similar. It should be recalled, however, that X-rays also penetrate into the bulk crystal and the overall effect on the surface is obtained by performing the sums over all the crystal atomic positions including an attenuation coefficient which mimics the decay in the X-ray intensity far from the surface into the bulk. The corresponding formula for the intensity is thus

$$\mathcal{I}_X(\mathbf{Q}, q_z) = \left| \sum_{\mathbf{R}} \sum_{z=-\infty}^{h(\mathbf{R})} e^{i\mathbf{Q}\cdot\mathbf{R}} e^{iq_z z} e^{\tilde{\mu}[z-h(\mathbf{R})]} \right|^2 \tag{1.19}$$

where:

- the subscript X stands for "x rays";
- the additional sum over z is over all the atoms lying below a surface atom at position $\mathbf{R}$;
- $\tilde{\mu}$ is the absorption coefficient which causes the decay of the amplitude as $e^{-\tilde{\mu} z}$ into the bulk starting form each surface atom at level $h(\mathbf{R})$.

The formula holds for a crystal whose thickness is L_z, provided $L_z^{-1} \ll \tilde{\mu} \ll a_z^{-1}$, so that that the sum over z can be pushed to $-\infty$. The physical reason for the attenuation is the X-ray absorption due to the excitation of photoelectric processes with the crystal atoms. The order of magnitude of $\tilde{\mu}$ is $\tilde{\mu} a_z \sim 10^{-5}$, a typical value for a 10 KeV beam on Au[31]. It should be noted, however, that in experiments performed under grazing conditions (i.e. with the beam at an angle near to 90° with the surface normal) a different mechanism should be advocated, i.e. total reflection, since the X-ray refraction index is less than 1 and the wave penetrating

into the crystal is actually an evanescent wave. In this case the attenuation length ($\sim \tilde{\mu}^{-1}$) is very much shorter than in the previous case.

At this point it is worth noting that eq. (1.19), as (1.17), is a very general expression valid for a real surface, i.e. including eventual lattice relaxation effects of the kind mentioned at the beginning of this chapter. Such effects are absent, of course, in a SOS description of the (110) surface, where the atoms are considered nothing but geometric building bricks of a structure made up of a juxtaposition of columns infinite in length in one direction (the bulk) but stopping at various levels in the other so as to represent different surface configurations. In this case it is possible to rewrite (1.19) by performing the sum in the vertical direction, since $z = a_z n$, $h(\mathbf{R}) = a_z m(\mathbf{R})$, $m(\mathbf{R})$ and n integers, so that taking into account the parity of the values assumed by the height variables belonging to the two different sublattices, and using the formula

$$\sum_{n=-\infty}^{m} \mathrm{e}^{ipn}\mathrm{e}^{\mu(n-m)} = \frac{\mathrm{e}^{ipm}}{1-\mathrm{e}^{-ip-\mu}}$$

one gets

$$\mathcal{I}_X(\mathbf{Q}, q_z) = \frac{1}{\left|1-\mathrm{e}^{-2(ip+\mu)}\right|^2}\left|\sum_{\mathbf{R}} \mathrm{e}^{i\mathbf{Q}\cdot\mathbf{R}}\mathrm{e}^{iq_z h(\mathbf{R})}\right|^2 \tag{1.20}$$

where $p = q_z a_z$, $\mu = \tilde{\mu} a_z$. When $\mu \ll 1$, as it is in general the case, the prefactor in front of the equation can be rewritten and approximated as

$$\begin{aligned}\left|1-\mathrm{e}^{-2(ip+\mu)}\right|^2 &= \left[\left(1-\mathrm{e}^{-2\mu}\right)^2 + 4\mathrm{e}^{-2\mu}\sin^2 p\right] \simeq \\ &\simeq \left[4\left(1-\mu_I\right)\sin^2 p + \mu_I^2\right]\end{aligned} \tag{1.21}$$

where μ_I is the intensity attenuation factor, $\mu_I = 2\mu$ (μ in fact represents the amplitude attenuation factor).

Before concluding this section, it is worth noting that the kinematic theory is a powerful tool not only for atom but also for X-rays surface scattering: multiple

scattering effects in fact, which would require the much more detailed treatment of dynamical theory [32], play a role only for the bulk-permitted peaks [33], thus can be disregarded in the surface analysis of the present thesis.

1.4.3 Coherent and incoherent scattering intensity

It is now useful to express the intensity of a peak as a sum of two contributions: the *coherent* scattering which is related to the amount of order present on the surface, and the *incoherent* scattering, which is a measure of the fluctuations.

In order to carry out this distinction, it is necessary to rewrite (1.17), for example (but the same would happen for the X-rays formula (1.20)), as follows

$$\mathcal{I}_A(\mathbf{Q}, q_z) = \sum_{\mathbf{R}_1,\mathbf{R}_2} e^{i\mathbf{Q}\cdot(\mathbf{R}_1-\mathbf{R}_2)} e^{iq_z[h(\mathbf{R}_1)-h(\mathbf{R}_2)]} \alpha(\mathbf{R}_1)\alpha^*(\mathbf{R}_2). \tag{1.22}$$

Now three different decompositions are to be made, depending on the nature (principal, superlattice or reconstruction) of the investigated peaks, by renaming the position $\mathbf{R}$ of the surface atom (see fig. 1.5)

principal: $\mathbf{R} = \mathbf{X}$, where $\mathbf{X}$ runs over all the atoms;

superlattice: $\mathbf{R} = \mathbf{X}+\mathbf{x}_\kappa$ ($\kappa = 1, 2$), where $\mathbf{X}$ runs over all the positions of the left corner atom of each cell, and the $\mathbf{x}_\kappa$'s label the coordinates of the atoms in the cell, i.e $\mathbf{x}_1 = 0\hat{\mathbf{x}} + 0\hat{\mathbf{y}}$, $\mathbf{x}_2 = \frac{a_x}{2}\hat{\mathbf{x}} + \frac{a_y}{2}\hat{\mathbf{y}}$;

reconstruction: $\mathbf{R} = \mathbf{X}+\mathbf{x}_\kappa$ ($\kappa = 1, 2, 3, 4$), as in the case above, but $\mathbf{X}$ runs over the positions, e.g, of the left corner atoms of each doubled unit cell, due to reconstruction, while $\mathbf{x}_1 = 0\hat{\mathbf{x}}+0\hat{\mathbf{y}}$, $\mathbf{x}_2 = \frac{a_x}{2}\hat{\mathbf{x}}+\frac{a_y}{2}\hat{\mathbf{y}}$, $\mathbf{x}_3 = a_x\hat{\mathbf{x}} + 0\hat{\mathbf{y}}$, $\mathbf{x}_4 = \frac{3a_x}{2}\hat{\mathbf{x}} + \frac{a_y}{2}\hat{\mathbf{y}}$.

It is thus possible to substitute

$$\sum_{\mathbf{R}} f(\mathbf{R}) \longrightarrow \sum_{\mathbf{X}} \sum_{\kappa=1}^{N} f(\mathbf{X}+\mathbf{x}_\kappa)$$

where the summation symbol $\sum_{\mathbf{X}}$ takes on different meanings and $\hat{N} = 0, 2, 4$ respectively in each one of the three above mentioned cases (in this notation, the sum over $\mathbf{x}_\kappa$ is absent for the principal peaks). In addition, to simplify the formulæ, it is better to define

$$A(\mathbf{X}) = \sum_{\kappa} \mathrm{e}^{i\mathbf{Q}\cdot\mathbf{x}_\kappa} \mathrm{e}^{iq_z h(\mathbf{X}+\mathbf{x}_\kappa)} \alpha(\mathbf{X}+\mathbf{x}_\kappa); \tag{1.23}$$

in this way, eq. (1.22) reads

$$\mathcal{I}_A = \sum_{\mathbf{X}_1,\mathbf{X}_2} \mathrm{e}^{i\mathbf{Q}\cdot(\mathbf{X}_1-\mathbf{X}_2)} A(\mathbf{X}_1)A^*(\mathbf{X}_2) = \\ = \sum_{\mathbf{X}} \mathrm{e}^{i\mathbf{Q}\cdot\mathbf{X}} \sum_{\mathbf{X}_1} A(\mathbf{X}_1)A^*(\mathbf{X}_1-\mathbf{X}) \tag{1.24}$$

where in the second line of (1.24) $\mathbf{X} \equiv \mathbf{X}_1 - \mathbf{X}_2$. At this point, apart from normalization factors, a sum over $\mathbf{X}_1$ can be considered as a spatial average over sites and denoted by the symbol $\overline{(\cdots)}$, that is

$$\sum_{\mathbf{X}_1} (\cdots) \equiv \overline{(\cdots)}. \tag{1.25}$$

The *coherent intensity* is defined as the quantity obtained from (1.24) by decoupling this average as $|\mathbf{X}| = |\mathbf{X}_1 - \mathbf{X}_2| \to \infty$, that is using the factorization

$$\overline{A(\mathbf{X}_1)A^*(\mathbf{X}_1-\mathbf{X})} \to \overline{A(\mathbf{X}_1)}\ \overline{A^*(\mathbf{X}_1-\mathbf{X})} \tag{1.26}$$

By replacing these two spatial averages into (1.24) and considering that the second one is no more dependent on $\mathbf{X}$, one gets

$$\mathcal{I}_A^{\mathrm{coh}} = \delta_{\mathbf{Q},\mathbf{G}} \sum_{\kappa_1,\kappa_2} \mathrm{e}^{i\mathbf{Q}\cdot(\mathbf{x}_{\kappa_1}-\mathbf{x}_{\kappa_2})} \left[\sum_{\mathbf{X}_1} \mathrm{e}^{iq_z h(\mathbf{X}_1,\kappa_1)} \alpha(\mathbf{X}_1,\kappa_1)\right] \\ \left[\sum_{\mathbf{X}_2} \mathrm{e}^{iq_z h(\mathbf{X}_2,\kappa_2)} \alpha(\mathbf{X}_2,\kappa_2)\right]^* \tag{1.27}$$

since, apart from normalization factors,

$$\sum_{\mathbf{X}} e^{i\mathbf{X}\cdot\mathbf{Q}} = \delta_{\mathbf{Q},\mathbf{G}} = \begin{cases} 1 & \text{if } \mathbf{G} = \mathbf{G}_{\mathrm{P}} \text{ (S, R)} \\ 0 & \text{otherwise} \end{cases} \tag{1.28}$$

that is the above Kronecker delta is 1 when $\mathbf{Q}$ belongs to the reciprocal lattice associated with the $\mathbf{X}$'s in the three different cases (P=principal, S=superlattice, R=reconstruction). The $e^{i\mathbf{Q}\cdot(\mathbf{x}_{\kappa_1}-\mathbf{x}_{\kappa_2})}$ phase factors are all 1 for principal peaks, so

$$\mathcal{I}_{\mathrm{A}}^{\mathrm{coh,\ P}} = \delta_{\mathbf{Q},\mathbf{G}_{\mathrm{P}}} \left| \sum_{\mathbf{X}} e^{iq_z h(\mathbf{X})} \alpha(\mathbf{X}) \right|^2 \tag{1.29}$$

while they are $+1$ or -1 for the superlattice peaks, leading to

$$\begin{aligned} \mathcal{I}_{\mathrm{A}}^{\mathrm{coh,\ S}} = \delta_{\mathbf{Q},\mathbf{G}_{\mathrm{S}}} \sum_{\mathbf{X}_1,\mathbf{X}_2} \Big[& e^{iq_z h(\mathbf{X}_1,1)} \alpha(\mathbf{X}_1,1)\, e^{-iq_z h(\mathbf{X}_1,1)} \alpha(\mathbf{X}_1,1) + \\ & e^{iq_z h(\mathbf{X}_1,1)} \alpha(\mathbf{X}_1,1)\, e^{-iq_z h(\mathbf{X}_2,2)} \alpha(\mathbf{X}_2,2) + \\ & e^{iq_z h(\mathbf{X}_2,2)} \alpha(\mathbf{X}_2,2)\, e^{-iq_z h(\mathbf{X}_1,1)} \alpha(\mathbf{X}_1,1) + \\ & e^{iq_z h(\mathbf{X}_2,2)} \alpha(\mathbf{X}_2,2)\, e^{-iq_z h(\mathbf{X}_2,2)} \alpha(\mathbf{X}_2,2) \Big]. \end{aligned} \tag{1.30}$$

In the case of reconstruction peaks, they can also assume complex values, i.e. they will be 1, i, -1, $-i$.

The coherent scattering intensity thus arises from a decoupling of a spatial average in the limit $|\mathbf{X}| \to \infty$. The *incoherent* part of the scattering, on the other hand, arises from the difference between the total average, eq. (1.17), and the above described asymptotic limit.

The procedure described above is correct on general grounds. A problem arises when one has to calculate scattering intensities via a Monte Carlo (MC) simulation procedure, as is done in this thesis. The relation between the spatial average defined by eq. (1.25) and the MC average $\langle \cdots \rangle$, which is an average on

different configurations (taken at different MC "time" steps) of the same surface (see Section 4.4), must be addressed.

In most cases, the correct choice is to define a thermodynamic quantity as a function of the surface configuration, then take its MC average as, for example, for the energy (eq. (4.11)) or the order parameters (eq. (4.18) – (4.20)). Nonetheless their fluctuations (the specific heat, eq. (4.12), the susceptibility eq. (4.21) are not MC averages of well defined quantities but are constructed from other MC averages.

For the total scattering intensity the first choice is the right one (eq. (4.15), (4.16)), but when one has to decouple averages as in eq. (1.26), two possibilities arise. The first is to consider the MC average on the same ground as a spatial average, since the MC procedure is intrinsically not a description of a dynamic evolution of the system, but a study of its equilibrium properties through a great number of replicas which should represent different finite samples of an "infinite" system. The second is to take the MC average at the end of the decorrelation procedure. The former way leads to substitute eq. (1.26) with

$$\langle \overline{A(\mathbf{X})A^*(\mathbf{X}_1 - \mathbf{X})} \rangle \to \langle \overline{A(\mathbf{X})} \rangle \langle \overline{A^*(\mathbf{X}_1 - \mathbf{X})} \rangle \tag{1.31}$$

and, for example, eq. (1.29) with

$$I_A^{\mathrm{coh,\,P}} = \langle \mathcal{I}_A^{\mathrm{coh,\,P}} \rangle = \delta_{\mathbf{Q},\mathbf{G}_\mathrm{P}} \left| \left\langle \sum_{\mathbf{X}} \mathrm{e}^{iq_z h(\mathbf{X})} \alpha(\mathbf{X}) \right\rangle \right|^2 . \tag{1.32}$$

Alternatively, within the latter, eq. (1.29) reads

$$I_A^{\mathrm{coh,\,P}} = \langle \mathcal{I}_A^{\mathrm{coh,\,P}} \rangle = \delta_{\mathbf{Q},\mathbf{G}_\mathrm{P}} \left\langle \left| \sum_{\mathbf{X}} \mathrm{e}^{iq_z h(\mathbf{X})} \alpha(\mathbf{X}) \right|^2 \right\rangle , \tag{1.33}$$

and similar formulæ hold for the other peaks. However, formula (1.33) is not the right one on thermodynamical grounds, since it does not lead to the correct relation between scattering intensities, order parameters and fluctuations (see the following Section). Yet, formula (1.32) contains a feature which makes it unsuitable for the Monte Carlo calculation. Differently from eq. (1.33), the MC average lies

in fact inside the modulus and this makes it sensitive to the average surface width $\overline{h}$, that is to the $k = 0$ – capillary waves which originate on the surface. The substitution $h(\mathbf{X}) \rightarrow h(\mathbf{X}) + \tilde{h}$, $\tilde{h}$ integer, which is nothing but a global shift of the surface by $\tilde{h}$ and which should not influence the quantities defined on the surface configuration, does not leave (1.32) invariant. This bad feature cannot be simply cured by subtracting, for example, $\overline{h}$ to each $h(\mathbf{X})$ value, since (1.32) would lose all the periodicities in q_z (see Section 1.4.7) which exist on physical grounds and should be respected.

The choice made in the present thesis is to assign greater importance to the thermodynamical point of view, and still use formula (1.32) as the correct one. This implies that one must avoid calculating separately coherent and incoherent intensities (due to the above mentioned problems), resorting instead to divide the two contributions by a fitting procedure applied directly to the total intensity.

It is necessary now to show how formula (1.32) includes the right thermodynamic relations: this is the subject of the next Section.

1.4.4 Scattering and order parameters

In this section it is shown that the coherent part of a scattering peak is proportional to the square of a suitably defined order parameter. In addition, the incoherent scattering intensity is proportional to the Fourier transform of the correlation function of the order parameter. In particular, this relation will be shown for the reconstruction peaks.

In every (2×1) unit cell, one can define a local order parameter $\mathcal{P}$ as follows:

$$\mathcal{P}(\mathbf{X}) = \sum_{\kappa=1}^{4} \mathcal{P}_\kappa(\mathbf{X}) = \sum_{\kappa=1}^{4} \mathrm{e}^{i\mathbf{G}\cdot\mathbf{x}_\kappa}\, \alpha(\mathbf{X}, \mathbf{x}_\kappa) \tag{1.34}$$

where $\mathbf{G}$ are reconstruction points in the reciprocal space. The factor α can be taken as the shadowing factor of eq. (1.18) (in this case a relation will arise between the atom scattering reconstruction peaks and the $\mathcal{P}_{2\times1}$ order parameter defined in eq. (4.18), see Appendix), or it can be chosen differently, for example $\alpha = 1$ for top row atoms, 0 otherwise. It is also possible to eliminate every shadowing

effect by taking $\alpha = 1$for all the atoms: different choices of α give rise to different definitions of the local order parameter (1.34), and of the total scattering intensity (1.17).

From the expression (1.24) of the scattering intensity and the definition of the $A(\mathbf{X})$ factors in eq. (1.23), one recognizes that $\mathcal{P}(\mathbf{X})$ and $A(\mathbf{X})$ coincide for $q_z = 0$ and $\mathbf{Q} = \mathbf{G}$, and that (1.24), with $q_z = 0$ and with the MC average, reads

$$\langle \mathcal{I}(\mathbf{Q}) \rangle = \sum_{\mathbf{X}} e^{i\mathbf{Q}\cdot\mathbf{X}} \sum_{\kappa_1,\kappa_2} e^{i(\mathbf{Q}-\mathbf{G})\cdot(\mathbf{x}_{\kappa_1}-\mathbf{x}_{\kappa_2})} \langle \overline{\mathcal{P}_{\kappa_1}(\mathbf{X}_1)\mathcal{P}^*_{\kappa_2}(\mathbf{X}_1-\mathbf{X})} \rangle \tag{1.35}$$

with the convention (1.25), where the spatial average is an average over $\mathbf{X}_1$. Decoupling now the spatial and configurational averages as prescribed in eq. (1.26), one obtains

$$\begin{aligned} \langle \mathcal{I}^{\mathrm{coh}}(\mathbf{Q}) \rangle &= \sum_{\mathbf{X}} e^{i\mathbf{Q}\cdot\mathbf{X}} \sum_{\kappa_1,\kappa_2} e^{i(\mathbf{Q}-\mathbf{G})\cdot(\mathbf{x}_{\kappa_1}-\mathbf{x}_{\kappa_2})} \langle \overline{\mathcal{P}_{\kappa_1}} \rangle \langle \overline{\mathcal{P}^*_{\kappa_2}} \rangle \\ &= \delta_{\mathbf{Q},\mathbf{G}} \left| \langle \overline{\mathcal{P}} \rangle \right|^2 \end{aligned} \tag{1.36}$$

where $\overline{\mathcal{P}}$ is the spatial average of $\mathcal{P}(\mathbf{X})$, and the same relation holds between $\overline{\mathcal{P}_\kappa}$ and $\mathcal{P}_\kappa(\mathbf{X})$.

Moreover, one can write the order parameter as its spatial and configurational average plus its fluctuations,

$$\mathcal{P}_\kappa(\mathbf{X}) = \langle \overline{\mathcal{P}_\kappa} \rangle + \delta\mathcal{P}_\kappa(\mathbf{X}) \tag{1.37}$$

which can also be seen as a definition of $\delta\mathcal{P}_\kappa(\mathbf{X})$. Substituting relation (1.37) into (1.35) and taking into account that, by definition, $\langle \overline{\delta\mathcal{P}_\kappa} \rangle = 0$, one gets

$$\begin{aligned} \langle \mathcal{I}^{\mathrm{incoh}}(\mathbf{Q}) \rangle &= \langle \mathcal{I}(\mathbf{Q}) \rangle - \langle \mathcal{I}^{\mathrm{coh}}(\mathbf{Q}) \rangle = \\ &= \sum_{\mathbf{X}} e^{i\mathbf{Q}\cdot\mathbf{X}} \sum_{\kappa_1,\kappa_2} e^{i(\mathbf{Q}-\mathbf{G})\cdot(\mathbf{x}_{\kappa_1}-\mathbf{x}_{\kappa_2})} \left\langle \overline{\delta\mathcal{P}_{\kappa_1}(\mathbf{X}_1)\,\delta\mathcal{P}^*_{\kappa_2}(\mathbf{X}_1-\mathbf{X})} \right\rangle . \end{aligned} \tag{1.38}$$

But under the hypothesis of a translationally invariant system, the quantity under brackets will result to be dependent only on $\mathbf{X}$, thus eq. (1.38) becomes

$$\langle \mathcal{I}^{\text{incoh}}(\mathbf{Q}) \rangle \sim \mathcal{N} \sum_{\mathbf{X}} e^{i\mathbf{Q}\cdot\mathbf{X}} \sum_{\kappa_1,\kappa_2} e^{i(\mathbf{Q}-\mathbf{G})\cdot(\mathbf{x}_{\kappa_1}-\mathbf{x}_{\kappa_2})} \langle \delta\mathcal{P}_{\kappa_1}(\mathbf{X})\, \delta\mathcal{P}^*_{\kappa_2}(0) \rangle \qquad (1.39)$$

since the spatial average is now trivial, and gives a factor of the order of $\mathcal{N}$, the number of system sites. In the limit $|\mathbf{Q}-\mathbf{G}| \to 0$, one deduces

$$\langle \mathcal{I}^{\text{incoh}}(\mathbf{Q}) \rangle \sim \mathcal{N} \sum_{\mathbf{X}} e^{i(\mathbf{Q}-\mathbf{G})\cdot\mathbf{X}} \langle \delta\mathcal{P}(\mathbf{X})\, \delta\mathcal{P}^*(0) \rangle \ . \qquad (1.40)$$

The right hand side of eq. (1.40) is the Fourier transform of the correlation function of the fluctuations of the local order parameter $\mathcal{P}(\mathbf{X})$, connected to the susceptibility χ through the well-known fluctuation-dissipation theorem, namely

$$\langle \mathcal{I}^{\text{incoh}}(\mathbf{Q}) \rangle \sim \mathcal{N}\, k_B T\, \chi(\mathbf{Q}-\mathbf{G}) . \qquad (1.41)$$

This, together with (1.36), explains how the two contributions into which the scattering intensity can be factorized, are related to relevant thermodynamical quantities like the order parameter and its susceptibility. In the Appendix these general relations are written in two particular cases, in connection with a particular choice of the order parameters.

1.4.5 Scattering and critical exponents

In the preceeding Section it is shown as the coherent peak intensity is proportional to the square of an order parameter suitably defined according to the surface symmetry, while the incoherent part is proportional to its susceptibility. This relation can be approximately rewritten by making the temperature dependence of the various quantities explicit, that is

$$\langle \mathcal{I}(\mathbf{Q},T) \rangle \sim C' \langle \mathcal{P}(T) \rangle^2 \delta(\mathbf{Q}-\mathbf{G}) + C'' \chi(\mathbf{Q}-\mathbf{G},T) \qquad (1.42)$$

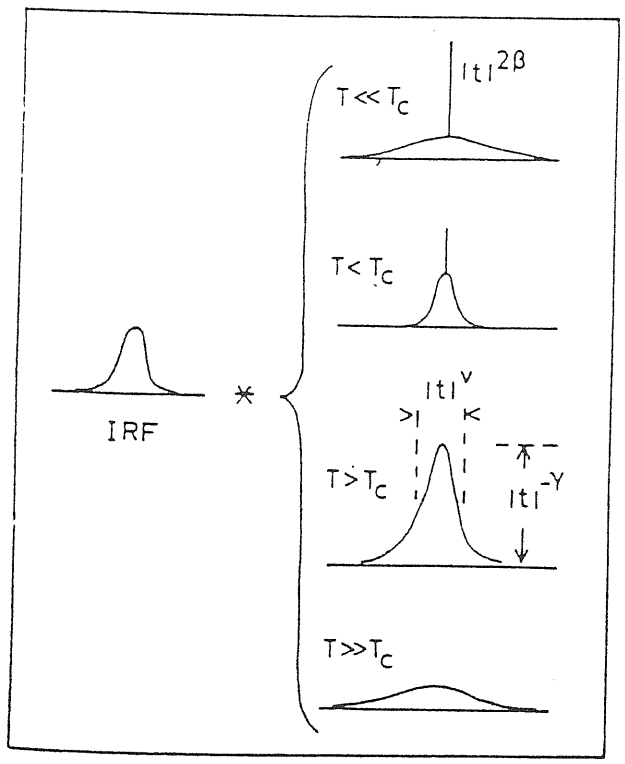

Figure 1.6. Diffraction spot profile showing long range order below T_C and short range order diffuse scattering above T_C in terms of the Fourier transform of the sample pair correlation critical exponents, convoluted with a Gaussian instrument response function IRF. From ref. [34].

with C' and C'' constants, eventually dependent on T. The first term gives a delta function which signals the reciprocal lattice vectors of a given surface symmetry, with intensity dependent on the square of $\langle \mathcal{P} \rangle$, the long range order parameter. The upper bound imposed on long range order by the finite extension of the ordered terraces actually broadens this delta function in a surface scattering peak which can be accurately fitted by a Gaussian function [34], whose height is now the quantity proportional to $\langle \mathcal{P} \rangle^2$. This term is dominant for $T < T_C$, T_C being the phase transition critical temperature, e.g. the deconstruction temperature , so that the critical exponent β can be determined after correcting for the Debye-Waller factor temperature-dependence, since $\mathcal{I}^{\text{coh}}$ is expected to vanish at T_C approaching zero as $t^{2\beta}$, with $t = \frac{T - T_C}{T_C}$.

As T_C is approached, fluctuations starts to appear and the peak profile can

no longer be fitted by a gaussian alone. The second term, already present but usually weak at $T \ll T_C$, is the only one present at $T > T_C$, and describes the fluctuations at and near the critical temperature. For relatively small values of t and momentum transfer $k = |\mathbf{Q} - \mathbf{G}|$, so that k is of the same order of magnitude of $1/\xi$ (ξ being the correlation length), this term may be approximated by a Lorentzian of the form [35]

$$\tilde{\chi}(q,T) = \frac{\chi(T)}{1 + \xi^2 k^2} \tag{1.43}$$

with half width $1/\xi$ and height $\chi(T)$, where $\chi(T)$ is the susceptibility associated with the order parameter $\mathcal{P}$ (see fig. 1.6). In this way, a careful fitting of the peak profile near T_C with a superimposition of a Gaussian and a Lorentzian leads in principle to the determination of the other two critical exponents γ and ν. In practice, however, surface imperfections and experimental resolution must be taken into account, in order to obtain reliable data.

From the incoherent scattering one can extract other useful information on the structure of the surface, for example the maximum of the incoherent part of the reconstruction peak in Au and Pt(110) can be shifted from the Bragg point. The shift reflects a global change of density of the top rows as that occurring for example between (2×1) domains at the opposite sides of step. From the analysis of sign and behaviour of the shift with temperature one can obtain information on the type and concentration of defects, thus gaining insight into the disordering process.

In order to conclude and clarify this section, it is worth noting that for a finite system it is not strictly necessary to distinguish between the coherent and incoherent parts for each value of $\mathbf{Q}$, since, as the delta functions of the preceeding section clearly indicate, the coherent contribution vanishes for all of the $\mathbf{Q}$-values compatible with quantization in a finite box, with the exclusion of the Bragg wavevectors. Above T_C, there will be no coherent peak intensity; at T_C, the coherent maximum merges into incoherent scattering.

1.4.6 Scattering from a rough surface

The scattering peaks show a peculiar behaviour around the roughening transitions temperature T_R. While the coherent part, as just noticed at the end of the previous Section, merges into the incoherent part, this starts diverging when $T \to T_R$ for $\mathbf{Q} \to \mathbf{G}$ (the Bragg wavevectors), the divergence assuming a power-law form in the neighbourhood of $\mathbf{G}$. A detailed theoretical treatment of the scattering peaks in this temperature region is provided, for example, by Villain *et al.* [36], who indeed describe a roughening process which refers to disordering of pre-existing step lines on a vicinal surface, and by Trayanov *et al.* [23], who instead study the creation of new steps on a (110) surface. They both agree in showing that for small $|K| = |\mathbf{Q} - \mathbf{G}|$, only the long-distance correlations on the surface are important, and that the logarithmic divergence of the height-height correlation function for $T > T_R$ leads to the incoherent intensity

$$\mathcal{I}^{\text{incoh}}(\mathbf{K}, q_z; T) \sim \left(\Lambda a_x^2 K_x^2 + \frac{a_y^2 K_y^2}{\Lambda} \right)^{-1+\frac{\tau(T,q_z)}{2}} \tag{1.44}$$

where Λ is an anisotropy parameter. According to Trayanov *et al.*, eq. (1.44) holds only in the case of atom scattering for the principal peaks, since at the superlattice (and, presumably, at the reconstruction) Bragg points the power-law divergence is suppressed by interference between the shadowing factors of eq. (1.18). Nonetheless, this important divergence can be extended to X-rays scattering intensities, since obviously the physics of the surface is the same, independently form the particular choice of the scattering probe. The exponent τ is a function of temperature and of perpendicular momentum transfer, its exact expression being

$$\tau(T, \hat{p}) = K(T)\, \hat{p}^2 \tag{1.45}$$

where $K(T)$ is the coefficient in front of the height-height correlation function in eq. (1.6) and $\hat{p} = q_z a_z - 2\pi k$, k integer and $|\hat{p}| \leq \pi$. For a Kosterlitz-Thouless roughening transition, from (1.8), τ turns out to be an increasing function of temperature and assumes the value 1 exactly at the roughening temperature and for $\hat{p} = \pi$, that is

$$\tau(T_R, \pi) = 1\,. \tag{1.46}$$

This result is commonly used by experimentalists to locate T_R from scattering data, through a fitting of the power-law tails of the peak lineshape (see, e.g., ref. [37], [38]); at the same time, the success of the fitting confirms the Kosterlitz-Thouless nature of the roughening transition.

1.4.7 Other considerations about scattering

This subsection is not strictly related to the general considerations about scattering done in the previous ones but more to some technical details about the calculation of scattering quantities relevant in the successive chapters; its position is justified here only for reasons of completeness.

The model which will be adopted for a description of the fcc (110) surfaces phenomenology is a SOS one, thus it is useful to specialize expression like eq. (1.17) to this case. Assigning the subscripts B and W to the sites of the two equivalent sublattices "black" and "white" which map out the surface, the positions of their atoms may be given as follows (see fig. 1.5)

$$\begin{aligned} \mathbf{R}_W &= \hat{n}_x a_x \hat{\mathbf{x}} + \hat{n}_y a_y \hat{\mathbf{y}} \\ \mathbf{R}_B &= \left(\hat{n}_x + \frac{1}{2}\right) a_x \hat{\mathbf{x}} + \left(\hat{n}_y + \frac{1}{2}\right) a_y \hat{\mathbf{y}} \end{aligned} \tag{1.47}$$

with $\hat{n}_x$, $\hat{n}_y$ integers. The sum over $\mathbf{R}$ can be split into two sums over $\hat{n}_x$ and $\hat{n}_y$, with $\hat{n}_x = 0, 1, \cdots N_x - 1$ and $\hat{n}_y = 0, 1, \cdots N_y - 1$, since for calculation purposes it is necessary to stick to a finite surface composed of $\mathcal{N} = 2N_x N_y$ atoms. Quantization in a finite box also imposes some constraint on the range spanned by the possible wavevectors $\mathbf{Q}$, which can assume only the following discrete values

$$\begin{aligned} \mathbf{Q}_x &= \frac{2\pi}{N_x a_x} n_x \\ \mathbf{Q}_y &= \frac{2\pi}{N_x a_y} n_y, \end{aligned} \tag{1.48}$$

n_x, n_y integers. No condition of the above kind is instead present on the values of the perpendicular momentum transfer q_z, since periodicity is broken in the z direction due to the presence of the surface itself. With this in mind, and rewriting $q_z h(\mathbf{R})$ as $p\,m(\mathbf{R})$, with $m(\mathbf{R})$ integer ($p = q_z a_z$, $h(\mathbf{R}) = a_z\, m(\mathbf{R})$), eq. (1.17) becomes

$$\mathcal{I}_A = \left| \sum_{n_x,n_y} \mathrm{e}^{i\frac{2\pi}{N_x} n_x \hat{n}_x} \mathrm{e}^{i\frac{2\pi}{N_y} n_y \hat{n}_y} \left[\mathrm{e}^{ipm(n_x,n_y)} \alpha(\hat{n}_x,\hat{n}_y) + \right.\right.$$
$$\left.\left. + \mathrm{e}^{i\pi\left(\frac{n_x}{N_x}+\frac{n_y}{N_y}\right)} \mathrm{e}^{ipm(n_x+\frac{1}{2},n_y+\frac{1}{2})} \alpha\left(\hat{n}_x+\frac{1}{2},\hat{n}_y+\frac{1}{2}\right) \right] \right|^2 \qquad (1.49)$$

where $m(\hat{n}_x,\hat{n}_y)$ stands for $m(\mathbf{R}_W)$, $m(\hat{n}_x+\frac{1}{2},\hat{n}_y+\frac{1}{2})$ for $m(\mathbf{R}_B)$, and the same holds for α. From (1.49) certain symmetries of the scattering intensity formula now becomes apparent. First of all, it is periodic in $\hat{n}_x$ and $\hat{n}_y$, with periodicity respectively $2N_x$ and $2N_y$ (or, equivalently, in $\mathbf{Q}_x$ and $\mathbf{Q}_y$ with periodicity $\frac{2\pi}{a_x}$, $\frac{2\pi}{a_x}$). This periodicity is somehow an artifact of the SOS model, i.e. of the fact that the atoms are supposed to remain in their bulk positions. In this approximation, the diffraction peaks (in bulk notation) $(0\,0\,l)$ with half integer l should have identical intensities, whereas the $l = 1$ peak should have zero intensity in a (2×1) reconstructed phase. In fact, as for example reported by Keane *et al.* [39], all of the $(0.06\;0.06\;l)$ peaks are observed in a X-ray scattering experiment, and the variation in intensity between the $l = \frac{1}{2}, \frac{3}{2}$ and $\frac{5}{2}$ peaks are of the order of 30. Allowing the top three layers of atoms to deviate from their bulk positions in the right directions and by suitable displacements, the resultant structure predicts a set of intensities which are in good agreement with the measured values of all reconstruction and surface peaks.

Coming back to SOS scattering, in the z direction, due to the integer values assumed by the height variables $m(\hat{n}_x+\frac{1}{2},\hat{n}_y+\frac{1}{2})$, a 2π periodicity in p results too. In this way a complete scattering pattern should require a calculation of the intensity in the parallelepiped

$$0 \leq n_x < 2N_x$$
$$0 \leq n_y < 2N_y$$
$$0 \leq p < 2\pi.$$

But not all the symmetries have been exploited as yet: in fact nothing changes in (1.49) if the following transformations are performed:

$$(n_x, n_y, p) \rightarrow (-n_x, -n_y, -p) \tag{1.50}$$
$$(n_x, n_y, p) \rightarrow (n_x, n_y + N_y, p + \pi)\,. \tag{1.51}$$

By applying transformation (1.51) one gets

$$(n_x, n_y, p) \rightarrow (n_x + N_x, n_y + N_y, p) \tag{1.52}$$

and if now the surface sample is square, that is $N_x = N_y$,

$$(n_x, n_y, p) \rightarrow (n_y, n_x, p) \tag{1.53}$$

These symmetries permit to restrict the calculation to a more limited range of the momentum transfer: for example, in the case $n_y = 0$, instead of the interval $0 \leq n_x < 2N_x$, $0 \leq p < 2\pi$, one can keep to the two intervals $0 \leq n_x < N_x$, $0 \leq p < \frac{\pi}{2}$ and $0 \leq n_x < N_x$, $\pi \leq p < \frac{3\pi}{2}$. Making use of (1.53) too, the square $0 \leq n_x < 2N_x$, $0 \leq n_y < 2N_y$ (for whatever value of p), can shrink to the wedge $0 \leq n_x < N_x$, $0 \leq n_y < n_x$.

Chapter 2

Phenomenology of (110) surfaces

Low temperature structures, thermal disordering, deconstruction and roughening transitions are presented in the following pages which review the main experimental aspects of the fcc (110) surfaces.

2.1 Reconstructed surfaces

2.1.1 Au(110)

In spite of the fact that probably Au(110) is so far one of the most studied surfaces from the point of view of its critical behaviour (it is in fact the "softest" among the fcc(110) reconstructing surfaces, thus easily experimentally accessible for its relatively low transition temperatures), the missing row nature of its (2×1) low temperature reconstruction has been controversial for several years. In addition, only very recently a roughening transition has been revealed in the high temperature deconstructed phase.

The (2×1) scattering patterns measured in the diffraction experiments of the '70s - early '80s[40,41] called in fact for a doubling of the unit cell in the [001] direction, which could be accounted for by several structural models such as, for example, the saw-tooth model proposed by Bonzel and Ferrer[42,43]. This proved unsuccessful, and the missing-row model was confirmed, among other experiments, by LEED analysis[44], x ray diffraction[45,46], low[47] and medium en-

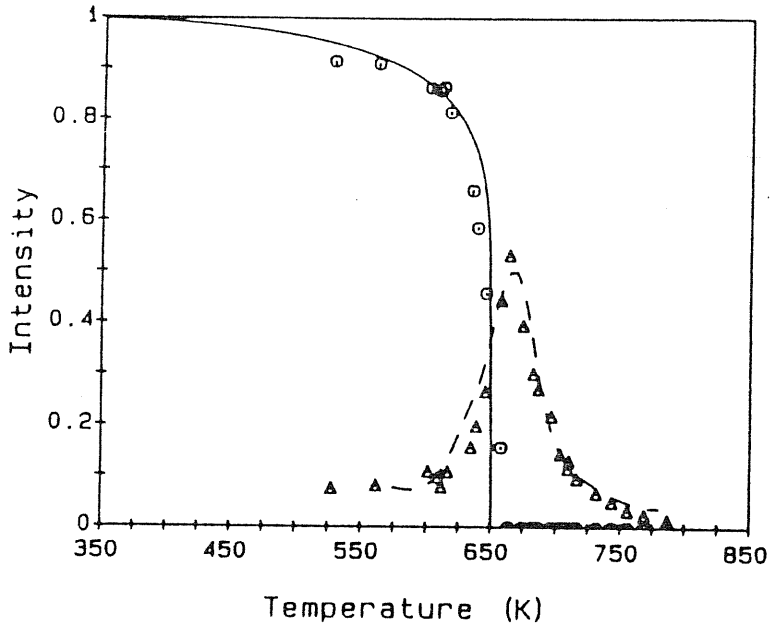

Figure 2.1. Au(110). Plot of the long range order (circles), Onsager's β=1/8 theoretical results (solid curve), fluctuations (triangles) obtained by the Lorentzian fitting. From ref. [52].

ergy ion backscattering[48], and its faceted (111) nature unambiguously detected by high resolution electron microscopy[49] and scanning tunneling microscopy[50]. The majority of these experiments also show relaxation effects within the missing-row structure (already addressed to in Chapter 1) such as a top layer spacing contraction, a second layer inward pairing and a third layer atomic buckling, confirmed by a recent careful X-ray diffraction experiment[51].

Wolf *et al.* [40] were the first experimental group to report (via LEED measurements) a phase transition from the (2×1) structure to some disordered phase around $700K$, even before the missing-row structure had been accepted as the low temperature phase of Au(110). However, both the transition temperature and, moreover, the critical exponent β were overestimated. The first LEED experiment intended to investigate in detail the critical behaviour of the (2×1) deconstruction transition was performed by Campuzano *et al.* [52,53]. By fitting the temperature variations of the half integer order diffraction profile with an expression of the form (1.42), they were able to derive for the critical exponents the

values $\beta = 0.13 \pm 0.02$, $\gamma = 1.75 \pm 0.10$ and $\nu = 0.93 \pm 0.09$, which are in fairly good agreement with those of the two dimensional Ising model, i.e. $\beta = 1/8$, $\gamma = 7/4$ and $\nu = 1$ (see fig. 2.1). Therefore this experiment would indicate that at a temperature of about $650K$, the (110) surface of Au undergoes a phase transition from an ordered (2×1) phase to a disordered phase, falling into the same universality class of the two dimensional Ising model as predicted from symmetry considerations by Bak[54]. The situation is actually more complex than envisaged by Bak, and his simple symmetry arguments based on the two-fold degeneracy of the ground state should be reexamined by considering that Au(110) has indeed four equivalent ground state configurations instead of two. This is due to the fact that besides the reconstruction order parameter, there is also a separate sublattice order parameter. Considerations of this kind will be done in Chapter 3, dedicated to a review of the theoretical work on the system, as well as in Chapter 6, where the results of the model adopted in the thesis will be presented. The Ising nature of the deconstruction transition, if confirmed, should not be considered a straightforward consequence of existing symmetry considerations.

This original LEED data did not identify the type of defects involved in disordering, nor provided evidence about roughening. From 1985 on, a wealth of other experiments confirmed and complemented Campuzano's first findings. Among these, the synchrotron X-ray scattering study of Keane *et al.* [39] reports of a deconstruction transition at a temperature significantly higher than that of Campuzano *et al.*, i.e. at $T_D = 735K$, characterized by proliferation of compact antiphase defects (in the language of Villain and Vilfan, a compact antiphase defect, or domain wall, is a pair of two bound surface steps of finite width, see Chapter 3). This transition is described by critical exponents which are roughly consistent with those predicted for the two dimensional Ising model, although there are some quantitative discrepancies perhaps due to finite-size rounding of the scattering data near T_D, or to sample impurity. In addition, around $T = 784K$, a significant increase in the density of both antiphase defects and also of single surface steps is found, signalled by a significant broadening of the integer order surface peak widths and by an upward shift in the position of the $(\frac{3}{2}\ 0.06\ 0.06)$ peak intensity (which has dramatically decreased as it should do far above T_D). This may be consistent with a surface roughening transition with onset between 752 and $784K$, though no power law lineshape fitting (see Section 1.4.6) is performed,

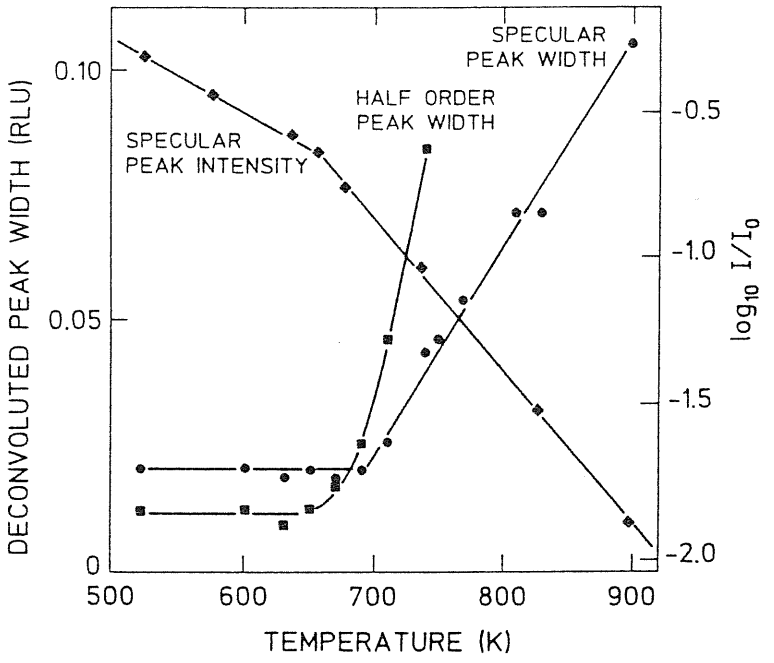

Figure 2.2. Au(110). Intensity of the in-phase specular peak (diamonds); width of antiphase specular peak (circles); width of half order peak under incidence conditions yielding minimum width (squares). The width is given in reciprocal lattice units $2\pi/a$=1.540Å^{-1}, intensity is in arbitrary units. From ref. [56].

which would settle down the question of the existence of surface roughening.

Such fitting is attempted on a Au(110) surface analyzed by means of He beam scattering by Cvetko *et al.* [55]. They observe an exponent τ which decreases from a value close to 2 at room temperature to 1.55 ± 0.1 at $723K$, so they cannot conclude positively in favour of a roughening transition but conclude that if roughening occurs, this can only be at a higher temperature. Nonetheless, broadening in the integer order peak width is a clear indication in favour of steps proliferation on the surface at that temperature. At a definitely lower temperature around $700K$ the half integer order peaks disappear and show a sudden broadening: here they place the deconstruction transition, caused by formation of domain walls (and not by steps, responsible for roughening) as also found by Keane *et al.* [39].

An experiment which has apparently been able to locate both the transitions is the recent He scattering experiment by Sprösser *et al.* [56]. By monitoring

both half order and integer peaks, they find a simple Debye-Waller exponential decrease of peak intensity between $100K$ and $650K$. Above $650K$ the half integer order peak width increases rapidly but the integer one still remains constant up to about $690K$. It increases dramatically above (fig. 2.2). They claim the former to be the the deconstruction transition temperature, the latter the roughening one, supporting this claim by the power law integer order lineshape fitting which clearly indicates the appearance of a state with logarithmic height-height correlations, compatible with Kosterlitz-Thouless roughening.

A word must now be spent on the different values of the transition temperature reported in the abovementioned experiments. In general, they agree on the difference $T_R - T_D$ to be a value around $40K$, but there is no agreement for the absolute values of T_D and T_R. This may be due to sample purity, as suggested by several facts. It is well known that the Au(110) surface is sensitive to submonolayer impurity coverage, even at levels barely detectable by Augier electron spectroscopy at low energy ion scattering. In some cases, trace impurities are responsible for higher order reconstruction of the surface, e.g. (3×1), as reported by Held *et al.* [57] (they further claim this symmetry to be lost at $T = 758 \pm 15K$ in a simultaneous deconstruction/roughening transition). Cesium deposited on the surface also induces Au (3×1) reconstruction via formation of extended (111) facets, probably due to charge-transfer effects [58]. As shown by McRae *et al.* [59], a 0.002 monolayer of Sn diffusing from the bulk and segregating at the surface results in a downward shift of 10-15K in the deconstruction temperature. The rate of segregation is appreciable around $675K$ and becomes relatively fast above $775K$, too. Some of these effects are reported by Keane *et al.* [39], while it is worth noting that they can also cause a rounding in the peak intensity decay affecting as a consequence the value of the critical exponents. In addition, sample contamination by Ca impurities is the reason why Cvetko *et al.* [55] could not push their investigation to higher temperatures.

Finally, there is a number of other experiments which corroborate what has just been presented. Van de Riet *et al.* [60], employing Ne ion scattering, report an onset of step proliferation on the surface around $650K$, the Campuzano *et al.* [52] deconstruction temperature, but also vacancy-adatom pair proliferation with a threshold temperature $120K$ below. From the analysis of LEED integer order spot profiles, Romahn *et al.* [61] find indications for roughening on Au(110):

a maximum broadening of the peak is observed at a temperature $T = 733K$, although no clear-cut temperature value for T_R is provided. They also find a smoothening of the surface, i.e. a decrease in the high step density some $50K$ above roughening, possibly due to surface melting effects. Precursor effects to the roughening transition are probably the cause of a minimum around $650K$ in the otherwise monotonic decrease of the blocking dip width in a ion channeling and blocking experiment [62]. This unexpected feature could in fact be explained by an enhancement of vibrational amplitudes due to the fact that the edge atoms participating in a step of a rough surface are assumed to have a larger and more anisotropic vibrational amplitude compared to the atoms of a smooth surface.

Lastly, Gimzewski *et al.* [63] presented a detailed STM room temperature investigation of the nature of atomic disorder on the Au(110) surface. The main usefulness of STM lies in elucidating the local shape and nature of steps and antiphase boundary structures and their temporal evolution, since for investigating the (2×1) domains diffraction methods are better suited, as they represent an average over mm-sized areas of the surface. The surface anisotropic behaviour is confirmed by the fact that, e.g., steps separating two perfect (2×1) terraces show long range ordering in $[1\bar{1}0]$ direction (corresponding to (111) microfacets), whereas kinks in [001] direction exposing (100) facets are rarely observed to be longer than several atomic distances. Steps, which are to be expected at the surface due to local crystal misorientations, tend to coalesce in bands. However in each band they remain distinctly monoatomic, and separated by small (2×1) elongated cells. No evidence is found for condensation of steps into facets of greater than monoatomic height, suggesting repulsion between steps which nevertheless exhibits bunching. This observation may indicate a longer range attractive interaction, while on the other hand another possible mechanism for the apparent condensation may be the pinning of steps which migrate over the surface during annealing cycles. Steps forming (111) microfacets may locally create (1×1) or (3×1) phases. The former is generally considered energetically unfavoured, and they are indeed rarely observed, while the latter appear to play a dominant role in surface structure at room temperature: the loss of evidence of significant atomic motion is an indication of their greater stability. Nonetheless, but to a much lesser extent, (331) microfacets (of low surface free energy) are observed too. Contamination, e.g. by CO adsorption, affects the reconstruction by just increasing the number

of (3×1) steps already interspersed in a more ordered sequence of (2×1) rows. This was seen in the first STM pictures of Au(110)[50] and, more indirectly, in the combined X-ray – ion backscattering experiment of Robinson *et al.* [46]. Individual adatoms are not detected on the surface, and surface mobility results in mass transport along the $[1\bar{1}0]$ direction, whereas atomic movements across the rows are not observed.

2.1.2 Pt(110)

Platinum lies in the same row of the periodic table as Au and could share some of the properties of gold. However, it is much "harder" and this fact should should shift all its eventual surface phenomena to higher temperatures, as well as increase the difficulties of experimental investigation.

Pt(110) is missing-row reconstructed as well. Evidence is provided, e.g., by low energy atom scattering spectroscopy[65], field-ion microscope images[66] and detailed LEED studies of (2×1) atomic relaxations[67,68]. A first attempt[69] to observe a deconstruction transition similar to that observed on gold with LEED was not successful, due to the difficulties intrinsic in LEED structure determination at high temperature because of the large vibrational amplitudes of the atoms. On the other hand, the core-level binding energy separation between surface and bulk atoms, as well as the intensity ratio of surface-to-bulk contributions in a photoemission spectrum strongly depend on the structure of a surface[70] So the surface core-level shift have been used as a probe of structural changes of a surface, also at high temperatures, by Dückers and Bonzel[71]. On the basis of a simple tight-binding model, the difference in $4f_{7/2}$ binding energies between surface and bulk atoms can be correlated with surface and bulk coordination numbers, leading to a prediction of lower values for the disordered (1×1) structure compared to the ordered (2×1) one, as the average coordination number of a disordered surface is lower. A clear decrease of the shift in the region $500K < T < 750K$ for Au(110) indicates a change in the surface structure, which further analysis identifies with a deconstruction transition at a $T_D = 620 \pm 50K$. The same kind of measures provides evidence for an analogous transition on Pt(110). Although potassium contamination could not be totally avoided, the experimental data are explained

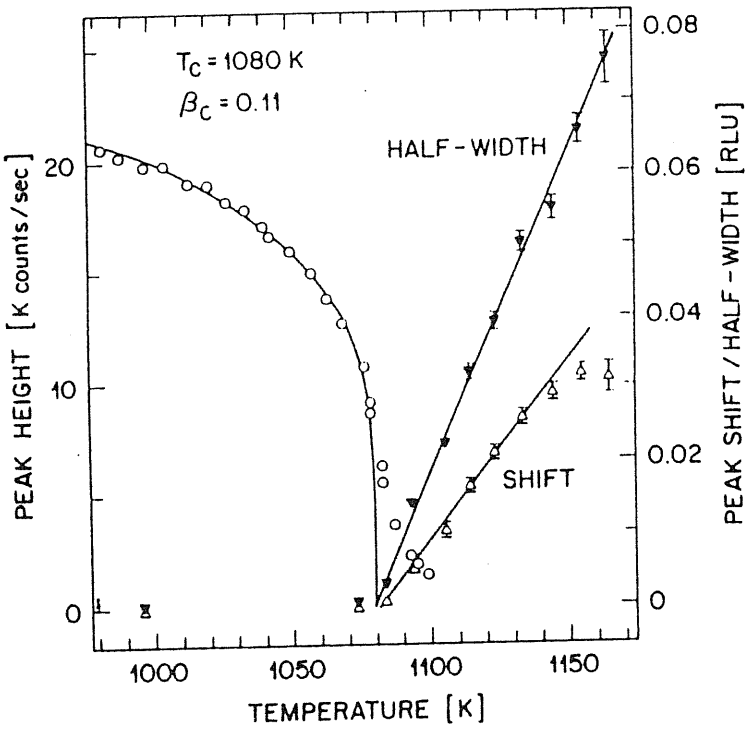

Figure 2.3. Pt(110). Left: peak height at (1.502 0.06 0.06) vs. temperature and its fit by $(T-T_D)^{2\beta}$. Right: variation of the fit values of half width and shift (from 1.5 reciprocal lattice units) of the Lorentzian that was convolved with the $T<T_D$ profile. From ref. [64].

in terms of an order-disorder transition located approximately at $940 \pm 50K$. In this way the authors find for the first time evidence of such a transition, and it is noteworthy that the transition temperature of Au(110) and Pt(110) ($620K$: $940K$) scale with the melting points of these metals ($1336K$: $2042K$).

The deconstruction transition was accurately studied in the X-ray diffraction experiments of Robinson, Vlieg and Kern[64,72], of somewhat controversial interpretation (fig. 2.3). Looking at the intensity decrease of the $\frac{3}{2}$ peak, they are able to locate the deconstruction transition temperature for Pt(110) at $T_D = 1080 \pm 50K$, finding a similar behaviour to Au(110) but with the important difference that above T_D steps are created spontaneously, and their density diverges with temperature. Because step proliferation is a central component of the disorder above T_D, the transition is classified as roughening (coinciding with

deconstruction), and not as simply a two-state two dimensional Ising transition, although the critical exponents are found to be consistent with those of the two dimensional Ising model ($\beta = 0.11 \pm 0.01$, $\nu = 0.95 \pm 0.09$), in good agreement with the case of Au(110).

The main indication of the presence of steps on Pt(110) is due to the shift of the half integer order peak. In accordance with Fenter and Lu's theory [73], randomly distributed single height steps on the surface should lead to an oscillation in the peak shift (shift in the maximum of the peak lineshape with respect to the central $h_s = \frac{3}{2}$ or $\frac{5}{2}$ position), as a function of the perpendicular momentum transfer q_z, which is indeed measured by Robinson *et al.* (but not by Campuzano *et al.* [52], for instance, as their measures were taken under diffraction conditions that corresponded to a position of zero shift). This shift is, moreover, temperature dependent and its increase above T_D, together with the dramatic broadening of the peak width, are clear indications of steps spontaneously appearing above T_D and hence that the phase transition is also a roughening one.

The main result of the experiment, the superposition of the deconstruction and roughening transitions, is considered by Villain and Vilfan [74] who are able to reconcile the apparent Ising nature of the transition with the presence of steps on the surface, in a model predicting a shift due to domain walls, i.e. antiphase step pairs of finite width, which are directly responsible for deconstruction. This could be a first step in a better understanding of the critical behaviour of Pt(110). A second step may be "just a question of terminology" [75]. Robinson *et al.* [64] did not fit any peak lineshape in search for a thermal behaviour of the exponent τ, but merely reported a sudden increase in step density. This could be explained as enhanced *roughness* of the surface [76], which is nevertheless a very distinct concept from a statistical mechanics definition of *roughening*, based on a logarithmically divergent height-height correlation function. Recent results from new He scattering experiments [77] suggest instead for Pt(110) two transitions, a deconstruction around $T_D = 1030K$ and roughening some $60K$ above, around $T_R = 1090K$, a very similar scenario to that of Au(110).

Robinson, Vlieg and Kern's experiment nonetheless remains as a landmark for the possibility of the merging of the transitions into one: this possibility and its consequences will be extensively addressed in the following chapters.

2.1.3 Ir(110)

Iridium is still harder a metal than platinum, as witnessed by the value of its bulk melting temperature, $T_M = 2682K$, and investigations on its structure as well as eventual phase transitions are still more complex. Nonetheless, Ir(110) was commonly believed to stand in row with Pt(110) and Au(110) and to exhibit a (2×1) missing-row structure at low temperatures[78–80]. Recent low energy ion scattering results[81,82] and ion scattering spectrometry[83,84], however, yield evidence for (3×1) and (1×1) phases to coexist on the surface. Preliminary evidence for an order-disorder transition around $1100K$ is found[82] but with a strong dependence of T_D upon the surface preparation and annealing procedures.

Results of combined STM and LEED investigations[85] on clean Ir(110) point to an unexpected new type of surface reconstruction: STM detects a rippled surface structure consisting of grooves which run parallel to the close-packed rows. The walls of the grooves are striped, stripes representing rows lying in successively deeper (110) layers: hence, they are formed by extended (331) facets with a slope of $\pm 13.3°$ along $[1\bar{1}0]$ with respect to the (110) plane, and not by the usual (111) facets found in Au and Pt (with the much steeper slope of 35.3°. On top of the grooves, local (1×1) regions are detected, and all the observations can be reconciled with the complex LEED patterns observed also by other authors[81,82] which, due to geometrical considerations, may appear to be a created by a (3×1) symmetry.

This seems to be a novel path for a fcc (110) metal surface to lower its free energy. Of course, new theoretical studies are now needed for Ir(110) to account for its structure and eventual phase transitions: this remains a completely open field and will not form one of the objects of the present thesis.

2.2 Unreconstructed surfaces

2.2.1 Ag(110)

An X-ray scattering experiment by Held *et al.* [37] provides a very direct information about the thermal dependence of the surface height-height correlation function $G(R)$, the behaviour of which is closely connected to the existence of a roughening transition. They look at the surface along the $(1\,\bar{1}\,l)$ crystal truncation rod, and choose a value of $l \approx 0$, corresponding to the position of a bulk-forbidden peak. This gives exact cancellation of intensity for a smooth surface but not for a disordered one and, as a consequence, provides a measurement sensitive to surface steps and to the behaviour of $G(R)$. They show how the peak evolves from a delta function to a power-law lineshape with an exponent τ (after a careful fitting which takes into account broadening due to finite-size effects on the surface as well as experimental resolution), and give evidence for a roughening transition on Ag(110) at a temperature $T_R = 723 \pm 25K$.

Preliminary He scattering data [86] seem to confirm the occurrence of a roughening transition on Ag(110), but at least $110K$ above the previously quoted value.

On the other hand, a completely new viewpoint is presented by Robinson *et al.* [87], who reject a model that involves equilibrium populations of steps within otherwise flat facets. They favour a phase separation of Ag(110) into a flat and a rough phase coexisting on the surface and forming different facets at a temperature-dependent angle α. This is the only possible way to explain the two-component lineshape of X-ray scattering peak which shows up for q_z values different from zero (noticeably enough, at the $(h\,k\,l)$ values adopted by Held *et al.* [37] no asymmetric lineshape was visible). A decreasing value of α as a function of temperature is an indication of the gradual replacement of flat regions by rough ones till α stops decreasing at a value coinciding with the miscut angle of the crystal. No flat faces are present anymore and the rough phase has spread all over the surface. This happens at a temperature which is given as the roughening temperature of that particular sample, $T_R = 790 \pm 20K$, but it is also possible, though with not much certainty, to indicate in $T_R^0 \approx 992K$ the temperature at which an improbable miscut-free surface would roughen.

2.2.2 Pb(110)

Problems of the kind just discussed for Ag(110) seemed to be absent for Pb(110), where a LEED experiment [38,88] locates at around $415K$ the roughening transition temperature. A clear LEED (1×1) pattern is shown at low temperatures. The authors then first look at the behaviour of the full width at half maximum of the peaks present along the beam as a function of q_z. The (0 0) beam width, for example, shows no q_z dependence for $T \sim 303K$, while a clear oscillatory behaviour of period $\frac{2\pi}{a_z}$ is found for $T \approx 475K$. This is a distinct signal of the presence of thermally generated steps, and the period indicates that only single atomic steps with a step height of a_z (the perpendicular inter-layer spacing) are contained on the surface. To make sure that a roughening transition has taken place on Pb(110), and to definitely locate T_R, a power-law lineshape fitting is also performed, leading to a value of $T_R = 415K$, at least $100K$ below the first surface melting effects, which are revealed by a sudden decrease of the integer order in phase peak intensity.

The picture seemed to be clear. However, the same authors in a subsequent paper [89] propose a novel scenario for the Pb(110) surface and its thermal evolution. They measure oscillations of the width of the (0 0) beam, as in the previous papers, but at $T = 361K$ an oscillation in q_z with period $\frac{\pi}{a_z}$ and not $\frac{2\pi}{a_z}$ is found. They report this observation as an evidence of an unpredicted appearance of double-height steps on the surface; a subsequent lineshape analysis rules out the possibility of a double-step roughening transition thus indicating that Pb(110) below the true roughening temperature, which is confirmed at $415 \pm 10K$, contains this kind of defects but still remains flat. Based on the sharp decrease of antiphase /scat near $380K$, the authors suggest this to be the first evidence of a formation of an up-down structure on the surface, i.e. of a Disordered Flat Phase (DOF) in the words of den Nijs *et al.* [90] due to the predicted (though never with double steps), but up-to-now never observed, pre-roughening transition. These findings, however, remain questionable, due to an obscure anisotropic behaviour in the decay of the DOF order parameter, which is a scalar, and should vanish when measured either along the [001] as well as along the $[1\bar{1}0]$ directions, if a true phase transition occurs on the surface, in contrast to what is experimentally observed.

2.2.3 Cu(110)

The first experiment aimed at revealing a phase transition on Cu(110) was carried out by Mochrie[91]. Considering the step-sensitive bulk-forbidden (001) X-ray peak, he just finds a decrease in intensity between $200°C$ and $650°C$ with no appreciable broadening of the width. Yet, he claims to have enough evidence to locate at $600°C$ a roughening transition, from an unusual increase in the root mean square atomic displacement $\langle u^2 \rangle^{\frac{1}{2}}$ (which is somehow related to the $\langle \delta h^2 \rangle^{\frac{1}{2}}$ of Section 1.3) fitted from the temperature dependence of the peak intensity, which he ascribes to the presence of thermally generated steps. No power-law lineshape fitting is performed.

In a subsequent careful helium scattering experiment[92] no thermal roughening is seen to take place on Cu(110) at least up to $900K$. They confirm a strongly enhanced mean square displacement of surface atoms for temperatures above $550K$, but demonstrate that there is no increase in step density up to $900K$, pointing out that an anomalous thermal behaviour of the coherent intensity is not a sufficient proof for the occurrence of a roughening transition. Ruling out the hypothesis of step proliferation, since no out of phase (i.e. near the bulk-forbidden condition) peak broadening is observed, no indication for roughening is found after the usual power-law lineshape fitting provides values for the exponent τ which are far above the crucial value 1. The sudden decrease of intensity above $550K$ has thus to be explained either by resorting to vacancy-adatom proliferation, or to an enhanced surface anharmonicity, giving rise to an anomalous Debye-Waller effect. The latter possibility is preferred by the authors. They monitor the diffuse elastic peak which is a standard measure for the estimation of the density of short-range scatterers, due to their large cross-section, and find again a decrease instead of an increase, as it would be the case if single or multi atomic defects were present on the surface.

Mochrie himself reconsidered his measurement[93] and found a miscut in his Cu(110) sample of 0.8°. This probably leads to a faceting of the misaligned surface into a sequence of sloped and flat regions, as shown by the asymmetry in low temperature X-ray Fresnel reflectivity peaks. As he points out, the observation of small copper crystals immediately below their melting point ($T_M = 1356K$) demonstrate that the (110) facet is absent from the equilibrium crystal shape at

this temperature[94]. This requires that either the (110) facet has a roughening transition at a temperature T_R below T_M or that the (110) is not a stable facet at any temperature. The latter improbable possibility would occur if the surface free energy of, say, the (111) facet were so much lower than that of the (110) that it would be energetically favourable for the surface to increase its area to form (111) facets rather than a flat (110) surface. A surface melting transition is likely to explain Stock and Menzel's data. in Cu(110) has been reported The crystal miscut can be the cause of the observed high temperature instability which may be of a kind similar to that found by Robinson *et al.* [87] on Ag(110).

In the debate surface defects vs. enhanced anharmonicity, an old paper by Lapujoulade *et al.* [95] seemed to choose the former as an explanation of the sudden drop in intensity in the elastic helium scattering peak (with a threshold temperature of $423K$). The heuristic explanation was given that thermal excitation of vacancies, adatoms and kinks is easier on less compact faces with respect to the close-packed (100) or (111) surfaces, where no such effects are measured.

Other He beam diffraction experiments tend to support the point-like defects hypothesis[96] and the anharmonic hypothesis[97] respectively, each of them not excluding formation of a small amount of disorder of the other kind. The question remains open and probably the two effects are intertwined, as a molecular dynamics study[98] seem to show. Indeed, in the presence of point defects the force constants are locally modified and may lead to large mean square displacements which may in turn facilitate the creation of additional point defects. Nonetheless, the results of another recent molecular dynamics simulation[99] point to anharmonicity as the leading effect on Cu(110) and not to thermal disorder (or roughening) between 600 and $850K$, since adatoms and vacancies are created but not below $900K$.

Though no definitive evidence for the occurrence of a roughening transition on Cu(110) has yet been provided, a combined Monte Carlo and molecular dynamics computation scheme seems to demonstrate that both a roughening and a surface melting transition occur on Cu(110)[100]. The identification of a roughening phase transition through molecular dynamics is difficult since computer runs cannot be long enough to produce good statistics for the height-height correlation function[101]. Irregular fluctuations in the occupation number of the first layer just signal that clusters of defects are forming on the surface, while the logarithmic divergence of the height-height correlation function is reproduced only in

a lattice-gas Monte Carlo version of the simulation (adopting the same realistic effective medium theory potential), which of course neglects important dynamical effects such as relaxation, atomic vibration and lattice distortion. With this method, a roughening transition is found around $1000K$, while molecular dynamics simulations point towards a surface melting phase transition around $1200K$. These results are not in contradiction with an ion scattering spectroscopy experiment [102] which detects structural changes of the Cu(110) surface above $1000K$, though it is not able to discriminate between a roughening transition or the formation of a quasi-liquid layer. No preroughening transition is reported for this surface.

2.2.4 Ni(110)

A high resolution LEED experiment shows the occurrence of successive different phenomena for the (110) surface of nickel [103]. First, a large increase in the mean square atomic displacement suggests anharmonicity (as in Cu(110) [97]) developing in the surface layers around $700K$. This is monitored via the decrease of both the in-phase (220) and the out of phase (110) peak intensities, and thus rules out step or point-like defect formation since this would leave the in-phase peaks unchanged, and no increase in the diffuse background is observed until $1150K$. At this temperature, the background-to-peak ratio sharply increases without a corresponding change in lineshape, suggesting vacancy formation. Finally, above $1350K$, a considerable (isotropic) broadening of the out of phase peaks (both the specular (110) with $|\mathbf{Q}| = 0$ and the off-specular ones, with $|\mathbf{Q}| \neq 0$) is observed, together with no appreciable change in the in-phase lineshapes. This is a clear signal that at these temperatures the step formation probability increases drastically. Although no determination of the logarithmic divergence in the height-height correlation function has been performed, a natural conclusion would lead towards a roughening phase transition above $1300K$.

2.2.5 Other (110) surfaces

A joint experimental (via medium energy ion scattering) and computational (via effective medium theory potentials) effort was carried out on **Al(110)** [104] to measure and simulate scattering yields from this crystal surface. Both experiment and theory agree well in showing how the onset of disordering is strongly correlated with the production of adatom-vacancy pairs, though the main contribution to scattering yields must be ascribed to disordering of other atoms in the top layers of the crystal which can be enhanced by defects formation. This mechanism can also explain why disordering of close-packed surfaces (e..g.Al(111)) below the melting point is much weaker than on open surfaces, since the energy involved in taking an atom out of the surface layer and placing it above it is much higher for the former surface than for the latter. No phase transition , however, apart from surface melting, has been investigated in this work.

The temperature dependence of the diffraction peak profiles for **Pd(110)** has been reported [105]. Slightly below room temperature, the authors observe that the diffraction beam shows a sharp decrease in intensity accompanied by a significant broadening. These results are interpreted as indicative of an order-disorder transition in which random displacements parallel to the surface lead to a breakdown in periodicity with increasing temperature. They are however not reproduced by other experimental groups [106] since nothing is observed but a normal Debye-Waller type of decrease of diffraction intensity with temperature. Furthermore the beam half widths are insensitive to surface temperature, at least up to $800K$. No explanation for this discrepancy is found, but the later results are probably more reliable.

2.3 An overview on fcc(110) surfaces

It is now time to summarize the main experimental evidence on fcc(110) surfaces and to signal the most relevant points of their phenomenology, as well as to present a general explanation of their behaviour.

Au(110) is the most studied between the reconstructed fcc metal surfaces, showing a missing-row reconstruction at low temperatures and two distinct phase

transitions when the temperature is raised, first a deconstruction and, at higher temperatures a roughening transition (apart from surface melting[62,107] which takes place slightly below bulk melting). The deconstruction transition appear to belong to the Ising universality class, and has to be ascribed to the thermally generated proliferation of defects of the domain wall type (bound step pairs). Above T_D the surface is deconstructed, disordered but still flat on average, though steps begin to appear. Steps between terraces are prevalently monoatomic and of the (3×1) kind (i.e. one of the sloping walls of a (3×1) groove), because energetically more favoured with respect to (1×1) ones, reflecting also in this aspect the faceting tendency of the surface. In the phase between T_D and T_R short range attractive forces between steps tend to prevail over entropic disordering, and roughening occurs approximately $40K$ above deconstruction. It is characterized not only by a roughness of the surface on the atomic scale but also by a logarithmic divergency of the height-height correlation function.

A very similar scenario is most probably present on Pt(110) too, where again deconstruction is of Ising kind and step proliferation occurs just above T_D, though the roughening transition temperature has not been clearly localized yet. The possibility of two distinct transitions or, on the other hand, of superimposed deconstruction/roughening are both theoretically intriguing and will be presented in detail in the following chapters.

Data on the Ir(110) phase transitions are scanty, since even its low temperature structure is still subject to experimental investigation. Novel routes to the minimization of surface free energy for fcc(110) metal surfaces may open for this element, which calls for a detailed theoretical treatment.

The (110) surface can be classified among the open surfaces, particularly exposed to disordering processes. Theoretical models would predict a roughening transition for all the metals like Ag, Cu, Ni, Pd, Pb and Al[23], whereas only in Pb and probably in Ni a clear transition has been detected. On Pb(110) surface roughening followed by melting of the topmost atomic layers at higher temperatures[108,109] has been found. Pb thus seems the best characterized between the unreconstructed (110) surfaces, were it not for a very recent and controversial experiment[89] claiming for a preroughening phase transition with a singular feature, i.e. the occurrence of double steps to separate the up and down terraces. For Cu and Al a strong increase in surface disorder which has to be ascribed either

to local defect creation or to enhanced surface anharmonicity has been detected, but this could not be immediately ascribed to roughening. A new scenario opens up for Ag(110), were there is clear evidence for a roughening transition[37] connected to a much more complex faceting mechanism[87]. This perhaps can be found on Cu(110) too[93] and resolves the controversy of whether or not there is a roughening transition on it. Unreconstructed surfaces, in addition, may easily (2×1) reconstruct under adsorption of, e.g., alkali atoms[110–115] and Au and Pt show (3×1) or higher order reconstructions[4,5] if covered by a suitable amount of Co or H (CO on Pt(110) stabilizes the (1×1) phase, while O leads to (3×1), (5×1) or even (7×1) reconstructions[69]). This is a clear signal of how subtle is the balance in surface free energy between (1×1), (2×1), (3×1) and higher order reconstructions, and how this may be influenced by the presence of impurities on the surface. The electronic charge transfer processes which certainly take place in this reordering have been the subject of many investigations, in particular, for the clean surfaces, towards the understanding of reconstruction processes[116,2,112].

The physical reason underlying all these phenomena (and which also make these surfaces good candidates for roughening, though step creation is very expensive energetically on low-Miller-index metal surfaces) can be traced back to the non-directional nature of cohesive forces in these metals. For a filled or nearly filled d-shell a large contribution to the cohesive energy can be obtained simply by a high coordination, irrespective of bond angles. This state of affairs seems well accounted for by some variant of the spherical many-body force methods ("embedded atom methods"[117] or "glue" models[3–5] recently proposed). In these formulations, the cohesive energy is given by the sum of a conventional two-body contribution $\phi(r)$, plus a many-body "glue" term $U(n)$:

$$V = \frac{1}{2} \sum_{ij} \phi\left(\mathbf{r}_i - \mathbf{r}_j\right) + \sum_i U\left(n_i\right),$$

$$n_i = \sum_{i \neq j} \rho\left(\mathbf{r}_i - \mathbf{r}_j\right), \tag{2.1}$$

where $\rho(r)$ is some decreasing function of distance. The two-body potential ϕ has a hard core preventing particle pairs form overlapping. The glue term $U(n)$ can be

chosen so as to be minimal at some optimal coordination number n_0 (for example $n_0 = 12$), so that it will increase for both insufficient and excessive coordination. For a surface atom, the value of n is always less than the bulk value n_0, and the glue forces become effective.

For a surface, the zero temperature effect of the glue is (a) to cause inward relaxation; (b) to reduce all surface energies, but more drastically so the energy of well-packed faces. The latter effect implies an increase in "anisotropy". By this, it is meant in particular that the ratio $\sigma_{(111)}/\sigma_{(110)}$ of $T = 0$ surface energies per unit area, already less than 1 for a two-body force system, becomes even smaller for a glue system. The crucial quantity is [23]

$$\Delta = \sqrt{\frac{3}{2}}\,\sigma_{(111)} - \sigma_{(110)}, \tag{2.2}$$

the factor in front of $\sigma_{(111)}$ arising form geometrical considerations, since the (111) face is tilted by an angle $\theta = \arccos\sqrt{3/2} \simeq 35°$ with respect to the (110) surface plane. If Δ is negative, as is the case for Au and Pt, the (110) surface reconstructs to the missing-row (2×1) structure at low temperature, but roughens at higher temperature due to the low energetic cost of formation of (111) facets, combined with the related increase in entropy.

In the lighter noble and near noble metals, instead, Δ is mildly positive, the unreconstructed (110) surface exists and it is smooth at $T = 0$ but again may roughen at higher temperature gaining entropy by becoming disordered. The increase of anisotropy is not sufficient to cause reconstruction on clean surfaces, but the fact that they can be readily reconstructed if not clean is a clear signal that they come quite close to it.

For "simple" metals such as Pb or Al the situation is not very clear. If Δ were positive, roughening would not be favoured for them, and maybe more complex mechanisms should be advocated for an understanding of their phenomenology.

Chapter 3

Theoretical models

In this Chapter a review is presented of the most recent and relevant theoretical models of the phase transitions which can occur on the fcc(110) surfaces: preroughening on the unreconstructed surface, deconstruction for the reconstructed ones, and roughening of both. The presence on the "hot" surface of many kinds of defects, from vacancies and adatoms to bound or free arrays of steps, may lead to an intriguing interplay between the various transitions which gives rise to the formulation of different disordering scenarios.

This rich variety has been reviewed in a comprehensive paper by Bernasconi[118], which will form the backbone of this Chapter†.

3.1 The preroughening transition

The idea of a DisOrdered Flat (DOF) phase and of a preroughening transition was introduced for the first time by den Nijs and Rommelse[90], who also studied the conditions for the stability of such a phase on a simple cubic (100) surface.

DOF is a novel type of phase appearing between the flat and the rough phases in the presence of short-range interactions between steps. In a few words, starting form the flat phase and as the temperature is increased, one first meets the transition from this to the DOF phase, called *preroughening*, next the surface undergoes

† For placing his work to my disposal prior to publication and for his constant critical advice I would like to warmly thank Marco Bernasconi.

a conventional Kosterlitz-Thouless transition from the DOF phase into a rough disordered phase.

The main ingredients are very simple. From now on, step rows on the surface will be sketched as wandering lines with an arrow which points upward if the surface is higher on its right. Two parallel (antiparallel) step rows are therefore labeled by a couple of up-up or down-down (up-down) lines. Rommelse and den Nijs consider a restricted solid on solid (RSOS) model (the nearest neighbour height difference can be just ± 1 or 0), and the following Hamiltonian

$$\mathcal{H}/k_BT = K \sum_{\langle \mathbf{RR}' \rangle} \delta\left(|h(\mathbf{R}) - h(\mathbf{R}')| - 1\right) + L_2 \sum_{(\mathbf{RR}')} \delta\left(|h(\mathbf{R}) - h(\mathbf{R}')| - 2\right) \quad (3.1)$$

where $\langle \mathbf{RR}' \rangle$ denotes nearest neighbours, $(\mathbf{RR}')$ next nearest neighbours on the square lattice and $h(\mathbf{R})$ are integer-valued column height variables. The nearest neighbor interaction K contributes to the step energy. Next nearest neighbour interactions (L_2) may cross more than one step. In particular, $L_2 > 0$ produces a short-range repulsion between parallel steps. Considering first the extreme limit where the repulsion is infinitely strong, $L_2 \to \infty$, steps with parallel arrows are forbidden to approach each other closer than the interaction range, while steps with antiparallel arrows are not affected by L_2, and may approach each other at will. Consequently the steps have larger meander entropy in configurations where they alternate in an up-down array, than in configurations where neighbouring steps have the same sign. This argument shows that the long range up-down-up order of steps, producing the DOF phase, is favoured by a combination of meander entropy and short range interaction between steps. This argument is indeed very general and not restricted to the particular choice of the model Hamiltonian (3.1) but it does not tell whether the effect is strong enough to stabilize the disordered flat phase.

A stronger statistical mechanics argument is obtained by considering a coarse-grained six vertex model written on the irregular lattice formed by the steps. By assigning an Ising spin $\sigma(\mathbf{R}) = \mathrm{e}^{i\pi h(\mathbf{R})}$ to each column height (thus representing its parity), Den Nijs shows that Hamiltonian (3.1) can be rewritten as an Ising model coupled with the six vertex model. In this formulation the partition function reads:

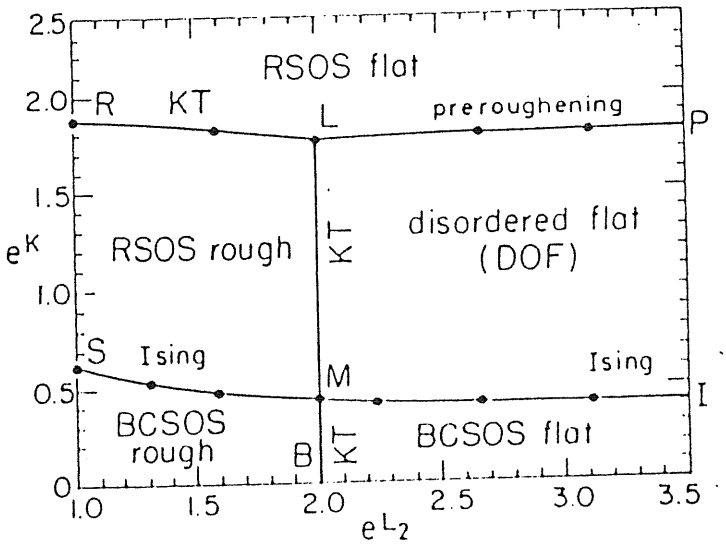

Figure 3.1. Phase diagram of the RSOS model with nearest neighbour interaction K and step repulsion L_2. From ref. [90].

$$Z = \sum_{\{\sigma(\mathbf{R})\}} e^{\left[-\frac{1}{2}K\sum_{(\mathbf{R},\mathbf{R}')}\left(\sigma(\mathbf{R})\sigma(\mathbf{R}')+1\right)\right]} \cdot Z_{6V}(\{\sigma(\mathbf{R})\}, L_2) \qquad (3.2)$$

where K governs the Ising-type order, i.e. the structure of the annealed fluctuating lattice of steps, while L_2 governs the antiferromagnetic order of arrows on the lattice of steps. The Boltzmann weight is e^{-L_2} for vertices 1-4, and 1 for vertices 5-6.

The phase diagram, obtained numerically by den Nijs who studied the properties of suitably-defined interfacial free energies, is shown in figure 3.1. For $K \to -\infty$ the Ising spin are antiferromagnetically ordered and the model reduces to the exact solvable BCSOS model on the square lattice. The BCSOS flat sector in fig. 3.1, obtained for large L_2 and negative K, represents the reconstructed phase of the model, since the Ising spins remain antiferromagnetically ordered for $K \ll 0$. The BCSOS geometry is achieved by rotating the resulting checkerboard structure by 45°, and it is addressed to in more details in subsequent works by den Nijs[119,120]. Starting from this state, the system undergoes a Kosterlitz-Thouless

roughening to a reconstructed rough phase along the line M-B.

By increasing K gradually, the Ising spins disorder along the Ising critical line S-M-I, corresponding to the deconstruction transition (it is worth noticing that the point (1,1) on this diagram corresponds to $T \to \infty$). For $K \approx 0$ the Ising spins are disordered, even at low temperature, and Ising-Bloch walls (steps) form a disordered array. This state contains disconnected finite terraces, but always includes an infinitely large connected backbone cluster, necessary to destroy the long range ferromagnetic order of spins. The backbone is not rigid, but has annealed fluctuations in its shape and number of bonds. The six vertex model defined on the backbone is controlled by L_2, and its stiffness for large e^{L_2} is alone responsible for the long range up-down-up order of steps (antiferromagnetic order of arrows). This flat phase at large values of L_2 represents the DOF phase.

On the other hand, the rough phase of the six vertex model at small values of L_2 represents the conventional rough phase of the RSOS. Since in general the universality class of a phase transition does not depend critically on the shape of the underlying lattice, one may expect the six vertex model on the backbone to undergo a conventional KT roughening (line L-M). The density of steps in the backbone is expected to decrease approaching the line R-L-P from above till the backbone disintegrates on line R-L-P. Above this line, only finite terraces survive, restoring the long range ferromagnetic Ising order of the RSOS flat phase. Along the line R-L-P the single step free energy vanishes, as required for the appearance of the backbone (for finite step free energy only finite terraces can be present). Along the preroughening line L-P, where the ratio L_2/K is sufficiently large, the surface is still smooth on average, because the height fluctuations are limited by the AF order of arrows in the backbone. Conversely if L_2/K is small, i.e. the energy for the generation of a step is large compared to the vertex energies, the six vertex model is already in its rough phase when the backbone appears. So along the line R-L the system undergoes a conventional KT transition from the RSOS flat to the RSOS rough phase.

The different phases are characterized by different order parameters, and the critical lines drawn on the global phase diagram correspond to the vanishing of these order parameters, and are numerically located by a transfer matrix finite-size scaling calculation of free energies of suitably set up interfaces between the various phases. The general criterion is that if a phase is void of a certain type of defects

(e.g. the RSOS phase, which has no infinitely long steps, though it can present terraces of finite dimensions), the free energy of that defect is finite, whereas its vanishing causes proliferation of energetically costless domain boundaries.

In particular, the thermal behaviour of the single step free energy, called $\eta^+(1)$ by den Nijs, is noteworthy, since above the S-M-I line it may be decomposed into two terms, η_I^F and $\eta_S^+(1)$. The former is the free energy of one Ising-Bloch wall (i.e. a step on the sc(100) surface), finite in the RSOS flat phase and zero everywhere else. The latter represents the additional free energy due to the presence of "wrong" (i.e neither 5 nor 6) vertices on the backbone, induced through the additional step imposed by the boundary conditions. It is nonzero only when the backbone exists in its smooth phase (i.e. in the BCSOS flat and DOF phases), vanishes at the roughening of the six vertex model, but also on the preroughening line where the backbone disappears. Thus, if one starts at low temperature in the RSOS flat phase where $\eta^+(1)$ is finite because η_I^F is finite, by raising the temperature entropic contributions cause η_I^F (and consequently $\eta^+(1)$) to vanish. The preroughening line is being crossed. At this point $\eta_S^+(1)$ is switched on due to the creation of the backbone of the DOF phase and $\eta^+(1)$ assumes again finite values, until it definitely vanishes at the roughening temperature, where $\eta_S^+(1) = 0$.

The non monotonic behaviour of $\eta_S^+(1)$ implies a maximum in this term as a function of temperature between T_{PR} and T_R, which can be explained with the presence of two competing effects. By increasing the temperature above T_{PR}, the average lattice constant of the backbone decreases (the backbone net thickens), implying an increase in the density of "wrong" vertices induced by an additional step. On the other hand, by increasing T the free energy $\eta_S^+(1)$ decreases on a lattice with fixed average density, due to the usual contribution of the meander entropy. The preroughening line has thus been identified numerically as the threshold where η_I^F vanishes and $\eta_S^+(1)$ becomes finite.

In a subsequent work, den Nijs[119] also showed that the inclusion of a hard-core attraction between antiparallel steps of the form $L_1 \sum_{\langle \mathbf{R}\mathbf{R}' \rangle} \delta\left(|h(\mathbf{R}) - h(\mathbf{R}')| - 1\right)$ modifies the phase diagram of fig 3.1. By taking for example $L = L_1 = \frac{L_2}{4}$, for large L the lines L-P and M-I merge in a line corresponding to a first order transition from the RSOS flat phase to reconstructed flat phase. The resulting phase diagram is shown in fig. 3.2.

Together with Rommelse, den Nijs showed numerically that the critical ex-

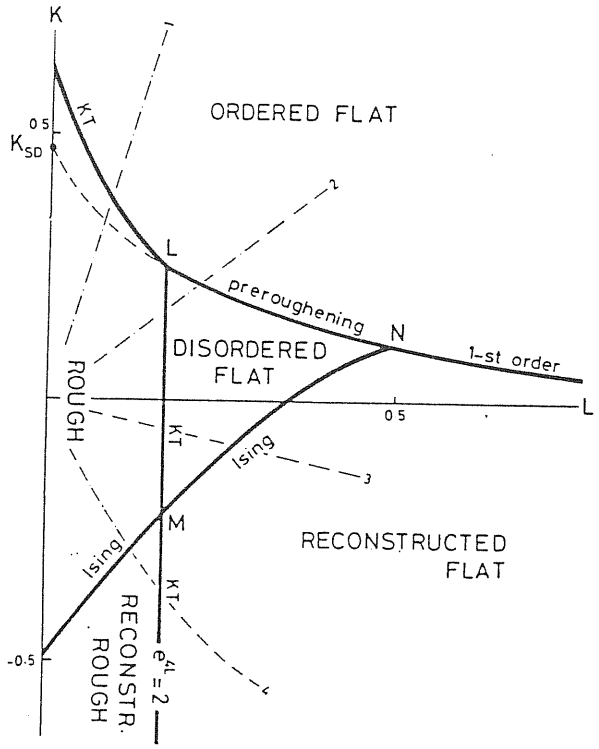

Figure 3.2. Phase diagram of Hamiltonian (3.1) with attraction between antiparallel steps. The dash-dotted lines represent characteristic experimental paths. From ref. [119].

ponents at point P along the PR line in fig. 3.2 (in the limit $L_2 \to \infty$) do not belong to the Kosterlitz-Thouless universality class. This result suggests that the preroughening line has *continuously varying critical exponents*, i.e. changing with the model's couplings. This prediction is confirmed by a renormalization group analysis of a continuous model presented in a successive paper [119].

Finally it is noteworthy to mention that den Nijs and Rommelse propose that the preroughening transition can be detected by means of scattering experiments. They showed that the coherent part of the specular peak in antiphase (i.e. the peak $(0\ 0\ \pi/a_z)$ in the notation of Chapter 1) is expected to vanish in the DOF phase, while the incoherent part has a Lorentian lineshape and diverges as a power-law at the roughening transition. As shown in Chapter 2, however, up to now no conclusive evidence of a preroughening transition has been found.

3.2 Scenarios for the reconstructed surfaces: the Bernasconi analysis

In Chapter 2 most experimental results have shown that for Au (and probably for Pt too) two distinct phase transitions occur on the (110) surface. Yet, not much attention has been payed till now to the structure of the deconstructed but flat phase in between. Bernasconi[118] provides a deep insight into this phase by proposing the study of two different order parameters, already introduced[121] but not fully understood in all the implications which follow from their different behaviour. The first is a deconstruction (or reconstruction) order parameter, $\mathcal{P}_{2\times1}$, which vanishes at the deconstruction temperature, while the second might be called $\mathcal{P}_{B/W}$ and determines which of the two sublattices of fcc(110), the black (even height variables) or white (odd height variables) corresponds to the atoms in the top layer. The exact definitions in terms of lattice size heights will be given at the end of Chapter 4 (these do not coincide exactly with those provided in ref. [118], but do embody the same physics and critical behaviour).

The (2×1) reconstructed phase shows four equivalent ground states (see also Section 4.6), which can be labeled by four different values of an angular variable θ, corresponding to the "colour" of the atoms on the top layer and to the parity of the missing row positions: in short, $\theta = 0\,(\pi)$ means black atoms on top with even (odd) parity of the missing rows, $\theta = \pm\pi/2$ white atoms on top instead.

A step on the surface is a boundary between two (2×1) terraces at different height levels, with different sublattice on top rows and opposite sign of $\mathcal{P}_{B/W}$. Across a (1×1) step the phase θ changes by $\pi/2$, while across a (3×1) step it changes by $-\pi/2$. A domain wall is instead a defect dividing two regions of the surface with the same height (same value of $\mathcal{P}_{B/W}$, i.e. same sublattice on top rows) but with $\mathcal{P}_{2\times1}$ of opposite sign (different parity of the missing rows): the change in θ is 0 or π. A domain wall is then represented by a bound pair of steps of opposite sign (up and down) with zero or finite width.

Step and domain wall free energies can be calculated, in general, by imposing the required change of θ as a boundary condition.

A joint study of $\mathcal{P}_{2\times1}$ and $\mathcal{P}_{B/W}$ can discriminate between two different possible structures of the flat phase. Since there are two order parameters, one can imagine that the vanishing of $\mathcal{P}_{2\times1}$ and $\mathcal{P}_{B/W}$ independently locates two phase

transitions at temperature T_D and $T_{B/W}$ respectively. These two transitions can differ or they can coincide, and this possibility opens up the following scenarios:

(i)-(iii) The deconstruction transition is driven by proliferation of domain walls with zero or finite width (i.e. a (1×1) (i) or (3×1) (ii) compact domain wall, or an extended (1×1) or (3×1) domain wall (iii) with a fixed average width l_w) due to the vanishing of the corresponding free energy. In particular, in scenario (iii) the mean extension of the wall l_w has non critical behaviour near T_D (while it can broaden above T_D). This mechanism destroys the reconstruction order parameter $\mathcal{P}_{2\times1}$ at T_D, but $\mathcal{P}_{B/W}$ is still finite above T_D. $T_D < T_{B/W}$, because inside the reconstructed domains only the two ground states with the same sublattice, say the black (even) one, on the top rows positions are involved. Bernasconi proposes for this the name of Deconstructed Even Flat (DEF) phase.

(iv) The free energy of a step vanishes at T_D but the surface is stabilized in a DOF phase, similar to the one proposed by Rommelse and den Nijs but realized in this case within a (2×1) reconstructed environment. Steps are no longer bound together but have long range up-down-up-down order, and the surface is still flat on average. All the four missing row ground states are involved locally in the reconstructed domains and with the same probability, implying the vanishing of the $\mathcal{P}_{B/W}$ order parameter, as well as of $\mathcal{P}_{2\times1}$: consequently $T_D = T_{B/W}$. The roughening transition at $T_R > T_D$ coincides with the vanishing of the long range up-down-up-down order.

(v) There is only one phase transition where the surface simultaneously roughens and deconstructs, $T_D = T_{B/W} = T_R$.

It is worth remarking that, whatever the deconstruction mechanism is, since roughening implies a proliferation of steps and since across two adjacent steps (either parallel or antiparallel) the reconstruction order parameter changes sign, the rough surface is in some sense deconstructed, i.e. it has $\mathcal{P}_{2\times1} = 0$. The roughening transition always implies a deconstruction transition, if the latter does not occur before, i.e. $T_D \leq T_R$. The same holds for $\mathcal{P}_{B/W}$ too, since in the rough phase atoms at each level have the same probability to be on top of the surface (the interfacial width diverges), so that there is no predominance of one sublattice and consequently $T_{B/W} \leq T_R$.

Scenarios (i)-(iii) and (iv) for the deconstruction transition differ substantially. In the first case a couple of steps is bound to form a domain wall with finite size l_w, while the size of the domain between two walls scales as the reconstruction correlation length $\xi_{2\times1}$ (diverging at T_D). In the DOF phase, on the other hand, between disconnected reconstruction domains an infinite fluctuating backbone of steps must exist in order to destroy the long range reconstruction order. This backbone forms a lattice which is not rigid but fluctuates in its shape and number of bonds. Below T_D the backbone disintegrates and only disconnected terraces survive, restoring the long range reconstruction order.

The difference between the two possible deconstructed phases may lead to different critical behaviour for the transitions at T_D and $T_{B/W}$. In the DEF phase of scenarios (i)-(iii) mainly one sublattice occupies top rows positions, thus reconstructed domains involve just two of the four degenerate missing row ground states while the other two are only assumed locally inside the domain walls. Symmetry considerations by Bak[54] apply to this case, which considers disordering of only the outermost layer, since the order parameter $\mathcal{P}_{2\times1}$ averages to zero for $T > T_D$ by assuming mainly two values at T_D, (i.e. $\theta = 0$, π, or $\theta = \pm\frac{\pi}{2}$). It can therefore be considered an Ising variable, and the deconstruction transition is expected to lie in the the 2D Ising universality class.

On the contrary, the DOF phase of scenario (iv) is formed by reconstructed domains of all the four missing row ground states, and no a priori argument is seen to predict the universality class of the deconstruction transition in this case.

3.2.1 The parity restoring transition

An open problem is represented by the behaviour of the $\mathcal{P}_{B/W}$ order parameter between T_D and T_R in scenarios (i)-(iv). If $l_w \ll \xi_{2\times1}$ above T_D and up to T_R, the domain wall width does not widen significantly and surface roughening is produced by a proliferation of "individual" steps thought of as independent entities with respect to the bound steps which form the domain walls. Depending on the nature of step-step interaction, one can contemplate two further possibilities. One is the case where the step free energy vanishes only at the roughening transition and $T_{B/W} = T_R$. The second, new possibility, is given by the vanishing of the

single step free energy vanishing at $T_{B/W} < T_R$. Above $T_{B/W}$ steps form a percolating network on the surface, superimposed to another network of domain walls with finite width l_w which has already caused the vanishing of the (2×1) order parameter. However, long range up-down-up-down order of steps still guarantees the flatness of the surface on average. Therefore in this case $T_{B/W}$ locates a new "parity restoring" transition from a DEF to a DOF phase. Once in the DOF phase, the roughening transition will occur at higher temperatures, following the same mechanism discussed in scenario (iv). In summary, three phase transitions are predicted at temperatures $T_D < T_{B/W} < T_R$, corresponding to the sequence of phases RECONSTRUCTED $(2 \times 1) \rightarrow$ DEF $\rightarrow$ DOF $\rightarrow$ ROUGH. This can happen, of course, only if scenarios (i)-(iv) are verified.

3.2.2 Experiments and scenarios for Au(110)

All that was proposed in the preceeding Sections is not just mere speculation, since every type of transition leaves a trace in the behaviour of some scattering peak. In Chapters 1 and 2 it has already been shown how the reconstruction peaks vanish at T_D and how the shape of the integer peaks, decomposed into a coherent and an incoherent part, changes at the roughening transition. Bernasconi in addition proposes that the behaviour of the specular peak in antiphase, $(0\,0\,\pi/a_z)$ in surface notation, can be used to discriminate the two different structures of the deconstructed surface previously discussed. It is been well-known [90] that the antiphase peak intensity vanishes at preroughening and inside the DOF phase, when $\mathcal{P}_{B/W}$ is zero. This particular peak, often measured in the scattering experiments, cannot unfortunately be reproduced by the atom scattering formula eq. (1.17), because with the choice (1.18) of the shadowing factors, it is exactly zero in the (2×1) reconstructed phase. However, with a different choice of the α's, for example including only contributions of the top atoms in the scattering intensity ($\alpha = 1$ if the atom has four nearest neighbours at a lower height, 0 otherwise), Bernasconi shows that the coherent part of the specular peak in antiphase is proportional to $\mathcal{P}^2_{B/W}$ (see Appendix for an exact derivation of this relation). Thus his analysis can be used to locate $T_{B/W}$, while a discontinuous increase of its width (related to $\xi_{B/W}$ which is approximately the mean extension of the grid of the fluctuating

step backbone) is expected at $T_{B/W}$.

In addition, as previously mentioned, from the analysis of the sign and the temperature behaviour of the shift of the half integer order peak, one can obtain information on the type and concentration of defects, which provides insight into the nature of the disordering process. By assuming a Markovian distribution of steps on a 2x1 surface, Fenter and Lu[73] obtain an oscillation of the shift as a function of q_z, with its maximum at $q_z = 0$, where it goes approximately as the inverse of the (2×1) domain width. If this condition might be replaced, as Bernasconi assumes, by the requisite that the two sublattices have the same probability of occupying top row positions (as is the case for scenarios (iv) and (v)), it is possible to predict, as Robinson *et al.* [64] do, a linear increase of the shift with temperature above T_D. In scenarios (i)-(iii) instead, the shift behaves quadratically with $T - T_D$, as shown by Villain and Vilfan[74,122]. Finally, it is worth noticing that the shift if zero if (3×1) and (1×1) steps are present on the surface with equal abundance (zero chirality).

From the simultaneous analysis of the integer and half integer order peaks it is therefore possible to discriminate between the different scenarios proposed.

In scenarios (i)-(iii) the half integer Bragg peaks vanishes at T_D and the shift goes quadratically with $T - T_D$. Above T_D the specular peak in antiphase still has a delta function term since $P_{B/W}$ is finite. If $T_{B/W} \neq T_R$ one expects that above $T_{B/W}$ this delta function term disappears, while the incoherent part is still finite, and a large increase of the peak width is expected (due to the presence of steps). At T_R the incoherent scattering intensity diverges as a power law near the Bragg peaks. Conversely, if $T_{B/W} = T_R$ the delta function term in the antiphase specular peak remains finite until $T = T_R$ where the incoherent peak shape becomes a power law.

In scenario (iv) the coherent part of both the reconstruction peak and the antiphase specular peak vanish at $T_D = T_{B/W}$. A noticeable broadening of the specular peak is expected at T_D, but only at T_R the incoherent part of the peak diverges as a power law. The half integer order peak shift behaves linearly with temperature above T_D.

Finally, scenario (v) can be distinguished from the preceeding one by the analysis of the power law of the integer peaks, though none of the theoretical models studied up to now has predicted the height-height correlation function to

diverge logarithmically as in a Kosterlitz-Thouless transition even for this unusual case. Should this not be the case, one could still discriminate between scenario (iv) and (v) by noticing that at $T_{B/W}$ only the coherent peak at $q_z = \pi/a_z$ vanishes, while at the roughening transition the coherent part of the peaks vanishes for every value of q_z.

With this in mind, it is now possible to analyze the different experiments to assign to Au and Pt(110) a position in one of the proposed scenarios.

The first experiments by Robinson *et al.* [64] seem to clearly open for Pt(110) a simultaneous deconstruction and roughening transition (scenario (v)). Nonetheless, if the discovery of two different transition temperatures is confirmed[77], or even if ref. [64] is not seen to provide enough evidence for the statement "$T_D = T_R$", a scenario of type (iv) may open too, due to the linear increase of the shift with temperature, the sign of which is however a clear indication of a proliferation of (3×1) steps. Unfortunately, experimental analysis on integer peaks, necessary to discriminate between scenario (iv) and (v), is not available.

On the other hand, the different values of the deconstruction and roughening temperatures measured on Au(110) definitely rule out scenario (v). Scenario (iv) is at first not excluded by the absence of a relevant shift in the half integer order peaks (it could be explained also within the DOF phase invoking small chirality, i.e. a small difference in the energetic cost for (1×1) and (3×1) steps). But it is independently ruled out by the absence of broadening of the antiphase specular peak at T_D as seen by Sprösser *et al.* [56]. Though the possibility of a third phase transition between deconstruction and roughening could still materialize on Au(110) and available experimental data are not stringent enough to exclude or to take it into account, most probably scenarios (i)-(iii) are good candidates for Au(110). A predominance of (3×1) steps on the (1×1) ones is expected, as observed for example by the sign of the shift of the reconstruction peak above T_D detected by Keane *et al.* [39].

3.3 The model of Levi and Touzani

Levi and Touzani[123] propose a model starting form a simple but interesting idea, that of an interacting six-vertex model but, due to the difficulty of monitoring the

deconstruction transition by a transfer matrix finite-size scaling approach, they just look at the roughening transition. Hence the model may be included with difficulty in one of the scenarios proposed by Bernasconi.

The starting point of Levi and Touzani is the six vertex model in its anisotropic version, as already proposed by Jayaprakash and Saam[20,21,22] for the study of the (110) face of fcc crystals. The antiferroelectric phase (i.e. the unreconstructed surface) corresponds to the inequality $\varepsilon_5 < \varepsilon_1 < \varepsilon_3$ for the vertex energies, whereas the missing-row structure is made of an ordered array of rows of vertices 1, 5, 2 and 6. Vertices 1 form the ascending slopes, 5 the ridges, 2 the descending slopes and 6 the valleys, so that no two adjacent vertices belong to the same type. Thus, it would look natural at first to increase the density of vertices 1 and 2 by changing the order of the inequality to $\varepsilon_1 < \varepsilon_5 < \varepsilon_3$. Unfortunately, this change brings the six vertex model to the ferroelectric phase, the structure of which is disappointingly simple: up to the transition all vertices are type 2 (or 1, which is the same). This situation does not correspond to reconstruction but to a constant descent in the surface with a slope $\alpha = \arccos\sqrt{2/3} = 35°16'$, i.e. to an effective replacement of the (110) surface by a (111) surface. In order to really obtain a missing row ground state, the six vertex model has to be modified, and it can be done mainly in three ways: 1) by introducing, along with the energy inequality $\varepsilon_1 < \varepsilon_5 < \varepsilon_3$, a repulsive interaction ε_{11} between adjacent vertices of the same type to discourage the creation of a (111) facet; 2) by still considering $\varepsilon_5 < \varepsilon_1 < \varepsilon_3$, which favours the unreconstructed (110) surface, but encouraging reconstruction by introducing a repulsive energy ε_{56} between adjacent vertices of type 5 and 6; 3) by introducing both ε_{11} and ε_{56} (e.g. of the same strength).

However, in order to perform a transfer matrix finite-size scaling, a drastic simplification must be employed, that is to consider the interactions between vertices in a direction only, and to put them to zero in the other. All the three models give qualitatively the same results, in terms of the parameter $\gamma = (\varepsilon_1 - \varepsilon_5)/\varepsilon_{\text{int}}$ (where $\varepsilon_{\text{int}} = \varepsilon_{11}$ in model 1, $\varepsilon_{\text{int}} = \varepsilon_{56}$ in models 2 and 3). They find that for very low values of γ the ground state forms a faceted (111)-like phase (a "macroscopic sawtooth"), then for increasing γ a (2×1) reconstructed phase, and finally a (1×1) unreconstructed phase. They are able to locate the roughening transition temperature of their models by looking at the vanishing of a quantity strictly connected to the step free energy, drawing in the end a phase diagram where a

smooth phase (of one of the three forms listed above, according to the value of γ) occurs at low temperature and a rough one at higher temperature.

The results obtained contrast the existence of other phase transitions like an order-disorder transition occurring at intermediate temperatures from the (2×1) phase to a modulated one in the presence of higher order reconstructions or directly to a rough phase. This is probably just due to the fact that such transition has simply not been looked for, due to the difficulties of defining suitable quantities to monitor in a transfer matrix formalism. In the model of Levi and Touzani, however, the roughening transition remains in the Kosterlitz-Thouless universality class.

3.4 The models of Jug, Tosatti and Kohanoff

Jug and Tosatti propose a model[124] successively studied with Kohanoff[125,126], based on a SOS description of the surface. The black and white sublattices, however, are not treated on the same ground: a slight (unphysical) asymmetry is introduced by considering on them two different sets of integer height variables, $\{h_i\}$ and $\{l_i\}$, in an Hamiltonian of the form

$$\begin{aligned} H/J = \alpha \sum_i & [(h_i - l_i)(l_i - h_{i+\mathrm{x}}) + (l_i - h_{i+\mathrm{x}})(h_{i+\mathrm{x}} - l_{i+\mathrm{x}})] + \\ & + \sum_i [(h_i - l_i)(l_i - h_{i+\mathrm{y}}) + (l_i - h_{i+\mathrm{y}})(h_{i+\mathrm{y}} - l_{i+\mathrm{y}})] + \\ & - \beta \sum_i (h_i - h_{i+\mathrm{x}})^2 + \Delta H(\alpha)/J \end{aligned} \tag{3.3}$$

where

$$\Delta H(\alpha)/J = (1+\alpha) \sum_i [(h_i - l_i)^2 + (l_i - h_{i+\mathrm{x}})^2]$$

is an ordinary nearest neighbours SOS contribution needed in order to fix J as the effective step energy cost in the y direction and impose the ± 1 n. n. height jumps. Here, as usual, x and y are respectively the soft and hard (missing-row) directions and $\hat{\mathrm{x}}$ and $\hat{\mathrm{y}}$ their unit vectors. The first two terms in eq. (3.3) induce

at sufficiently low temperatures (so that the height jumps between two nearest neighbour sites $s_i \equiv h_i - l_i$ are constrained to be ± 1), a ferromagnetic ordering in the "spins" s_i, corresponding to the ordered (1×1) structure. The parameter α $(0 < \alpha < 1)$ measures the local anisotropy in the x vs y directions. The next term corresponds to next-nearest-neighbour interactions, inducing a more stable missing row profile in the x direction for $\beta > 0$.

Ground state energy considerations show that in this model $E^{\circ}_{(1\times1)} \leq E^{\circ}_{(2\times1)}$ for $\beta \leq \frac{1}{2}\alpha$. Hence, at zero temperature it behaves like an Anisotropic Next Nearest Neighbour Ising (ANNNI) model[127,128] in terms of the spins s_i, in that there is a switch from the ferromagnetic (1×1) phase to the $\langle + + - - \rangle$ (2×1) phase as a function of the parameter $\kappa = 4\beta - 2\alpha$. On the other hand, the true symmetry of the model is that of an SOS model, so it is likely to exhibit a roughening transition. The model thus has all the needed properties to describe the noble metal (110) surfaces, together with the presence of higher energy, higher order reconstructions.

Two possible solutions can be attempted. The first is an analytic low-temperature investigation[124] of the properties of the model near the multiphase point at $\kappa = T = 0$, where both (2×1) and (1×1) phases coexist with all the reconstructed $(n \times 1)$ phases, with $n = 3, 4, \ldots$, which are all degenerate ground states provided only the first-layer $n - 1$ rows are missing (these structures are called "shallow reconstructions"). The different (actually ∞) domain walls between all these structures are then considered within a free-fermion approximation, as done by Villain and Bak[127] for the 2D ANNNI model.

The second possibility is a transfer-matrix finite-size scaling[125,126] performed on Hamiltonian (3.3) with the additional (six vertex) constraint of ± 1 height jumps between nearest neighbours heights (restricted Jug-Tosatti model).

Both approaches agree in predicting $T_C < T_R$, T_C being the deconstruction temperature, T_R the roughening one. However, T_C now strictly denotes a pseudo-transition, characterised by a non-divergent peak in the heat capacity, while T_R denotes a transition of the Kosterlitz-Thouless type. Between the two transitions a sequence of disordered incommensurate phases, arising from the presence of the shallow reconstruction states degenerate at $T = 0$, is present as a precursor to roughening. Physically, the lower transition at T_C should correspond to a proliferation of defects in the missing-row structure, while it is only at T_R that

these defects become unbound to form steps.

The deconstructed flat phase and the overall deconstruction mechanism may be attributed to a scenario of type (ii), that is of compact domain walls, since no terraces with long range up-down order are present on the surface. Nevertheless, the results of the calculation lead to enlarge the type of dephasing defects from (3×1) to higher reconstruction order ones, which appear as grooves on the flat surface, running along the $[1\bar{1}0]$ direction (apart form kinks and other local defects).

Noticeably enough, this model is able to predict two transitions, one of order-disorder character and a roughening transition at a higher temperature, also for fcc (110) surfaces which do not reconstruct. No detailed analysis has been performed for this disordering transition, but it presumably may lie in some preroughening class. Then, precisely at the point where reconstruction sets in ($\kappa = 0$), the disordering temperature appears to vanish, unlike the roughening one, so that not only the physics of, say, Au(110) , but also that of Cu(110) may be accounted for by the Jug-Tosatti model, by employing for the latter a small negative value of κ, which ensures a (1×1) phase at low temperature. For $\kappa < 0$ (unreconstructed surfaces) T_C presents variable critical exponents.

3.5 The models of Villain and Vilfan

Scenarios (i) and (ii) have been studied by Villain and Vilfan [129,122]. They calculate the free energy of steps and walls, not by solving a bulk problem defined by suitably chosen boundary conditions, but just by considering the configuration entropy of the (one dimensional) interface. This procedure was discussed previously by E.Muller-Hartmann and Zittartz[130], who showed that for the 2D Ising model the interface free energy obtained from the solution of the bulk problem is equal to the free energy obtained by summing over all the configurations of the interface, supposed to traverse the lattice without bending backwards (i.e. overhangs are forbidden). This may happen due to a fortuitous cancellation of errors. Nonetheless the method provides a valuable approximation which is assumed by Villain and Vilfan to produce a correct evaluation of the critical temperature also for systems different from the 2D Ising model. In this procedure step-step interaction is neglected. The transition temperature can be obtained as the temperature

above which the free energy of the interface vanishes. The infinitely long defects in figure 3.3 are ground state configurations of the interface, and at finite temperature are interrupted by kinks. The interface jumps to neighbouring atomic rows through intermediate excited states. Figure 3.4 describes a possible configuration with intermediate excited states for the meandering of a 4×1 step.

Villain and Vilfan assign energies per unit length for each of the infinitely extended configurations of fig. 3.3 with respect to the ground state, and another value to the breaking of a bond along $[1\bar{1}0]$. Since direct transition between ground state in neighboring rows requires the simultaneous breaking of several bonds along $[1\bar{1}0]$, their contribution to the partition function of the interface is neglected by Villain and Vilfan. Using a saddle point approximation for the interface partition function, they obtain expressions for the critical temperatures, as a function of the defects' energy of figure 3.3. The vanishing of step free energies provides values for the roughening temperature, while that of a domain wall yields the deconstruction temperature. This transition is therefore likely to occur in scenarios (i)-(iii).

It is of great importance to note that T_D can be lower than T_R even if the energy of a compact domain wall is equal or higher than twice the energy of a step. This occurs, provided that the intermediate excited states for the meandering of a step have energy sufficiently higher than the intermediate excited states of the domain wall.

After assigning a hierarchy between the energies of the defects (γ, ε, η, δ, etc.), the lowest temperature amongst those obtained by locating the vanishing of defect free energies is really meaningful. If it corresponds to the vanishing of a domain wall, either of (1×1) or (3×1) type, one argues that a deconstruction transition occurs before roughening, while a roughening inducing deconstruction occurs if a step free energy vanishes first.

Vilfan and Villain [122] also analysed scenario (iii) for (3×1) extended domain walls. They calculate the partition function of a system composed by two (3×1) steps with opposite sign. Each step is assumed to traverse the surface in the x direction without bending backwards. The pair is described for each value of x by the state $|m, n\rangle$, where m and n are the steps coordinates; the "motion" of the pair in the x direction is described within the transfer matrix formalism. The transfer matrix is then an operator on the states $|m, n\rangle$, and its elements are expressed as a function of the energies of defects of figure 3.3. By increasing the temperature

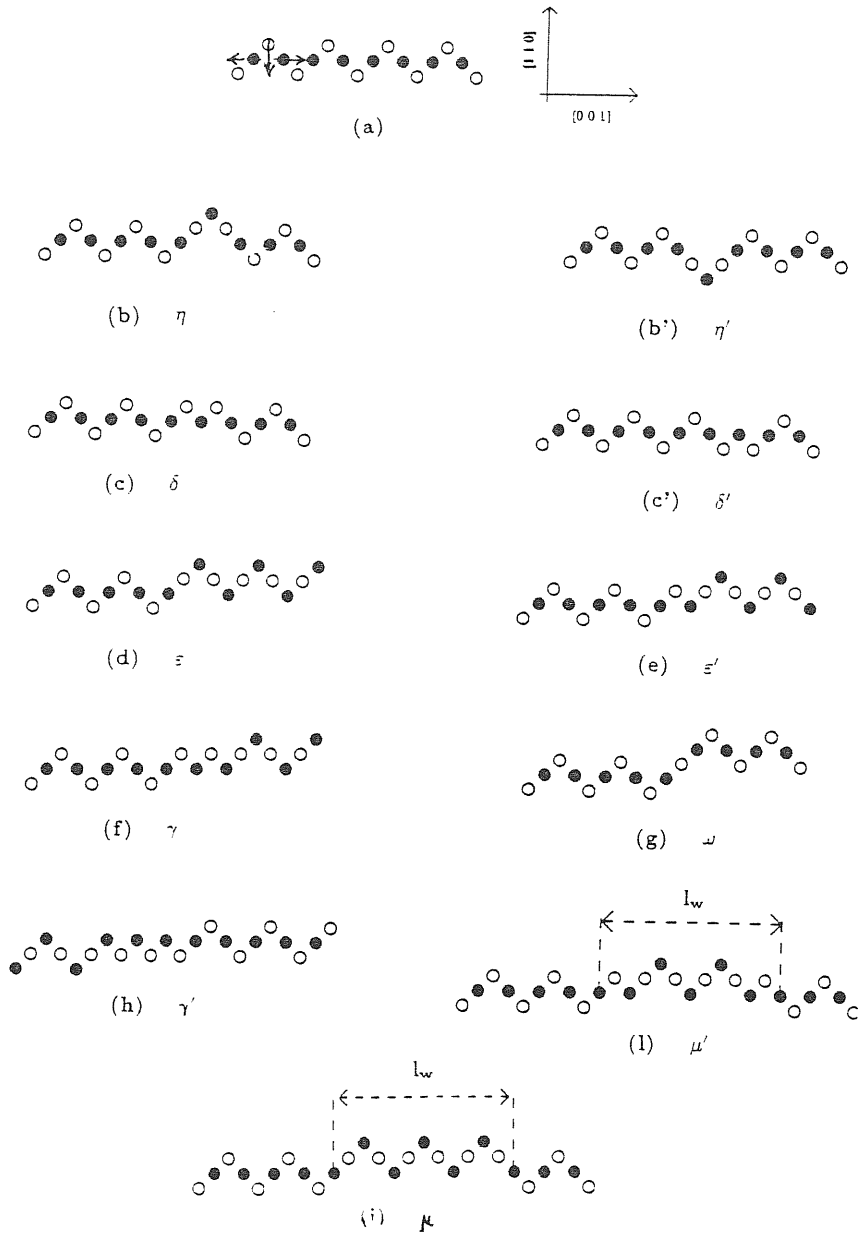

Figure 3.3. Side view of 2×1 phase and possible elementary excitations. Ideal structure (a). The arrows show the direction of surface-atoms relaxation. Defects configurations (b)-(p). Greek letters denote creation energy per atom along $[1\bar{1}0]$. From ref. [118].

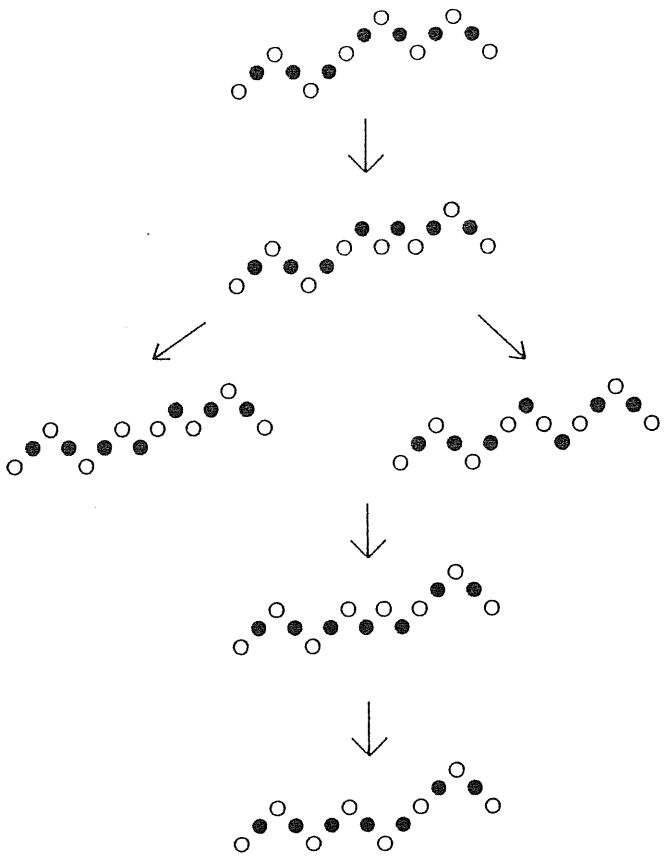

Figure 3.4. Intermediate excited states for the meandering of a 4×1. Greek letters denote the energy of the defects. From ref. [118].

there are two effects. On the one hand, a bound pair of steps becomes unstable at a certain temperature where the largest eigenvalue corresponds to a couple of unbound steps. On the other hand the wall free energy decreases by increasing temperature and could vanish before the unbinding of the pair occurs. In the latter case an Ising deconstruction transition is expected before the roughening transition identified with the unbinding of the steps. As in the former analysis of compact domain walls, the free energy of an interface strongly depends on the energies of the intermediate excited states necessary for the meandering. The condition for

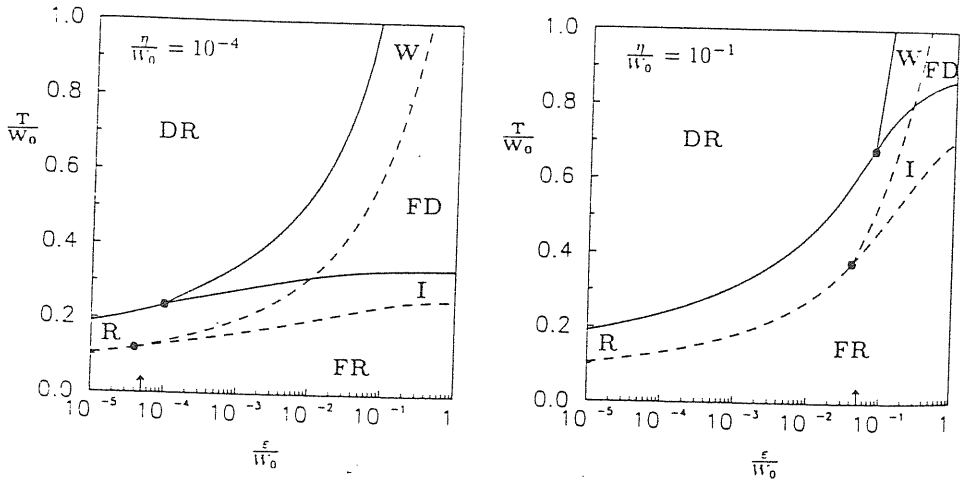

Figure 3.5. Phase diagrams of the model by Villain and Vilfan for two different η/W_0 ratios. Solid and dashed lines refer to different choices of the defects energies. Solid: for $\varepsilon'=\delta=\infty$; dashed lines are for $\varepsilon'=2\varepsilon$, $\delta=3\varepsilon'/2$. R, I and W are the roughening, Ising, and wetting (roughening) critical lines, respectively. FR, FD and DR are the Flat Reconstructed, Flat Disordered and Disordered Rough phases respectively. The arrow indicates the case $\varepsilon=\eta/2$. The figure is taken from ref. [122].

the occurrence of an Ising deconstruction transition before roughening is thus a complicate algebraic expression involving most of the defects' energy parameters. The binding of the steps is not due to long range interactions, since there are only short range interactions ($\eta \leq 2\varepsilon$ in figure 3.3). However the larger meander entropy of the compact (3×1) domain wall with respect to the (3×1) step, which favours the crossing of the two steps, gives rise to an effective long-range entropic attraction.

The phase diagram proposed by Villain and Vilfan [122] is depicted in fig. 3.5 for two possible choices of the energies of intermediate excited states. The separation between T_D and T_R widens by decreasing the energy of a (3×1) compact domain wall with respect to the (3×1) step, but still T_D can be lower than T_R even if $\eta = 2\varepsilon$, due to different energies of the intermediate excited states for the meandering of a wall and a step. In other words antiparallel steps can be bound even if there is no energetic attraction between them (pure entropic attraction). In the analysis by Villain and Vilfan the condition $T_D \leq T_{B/W} = T_R$ is assumed. The model is not able to tell what happens when l_w, increasing monotonically above

T_D, starts to compete with the reconstruction correlation length. Furthermore the analysis of the critical behaviour at roughening is beyond the scope of the model itself. An important message which comes out from the investigation of Villain and Vilfan is that, by tuning the energy of intermediate excited states, it should be possible to move from a scenario where two phase transitions are predicted to a scenario where only the roughening transition survives.

3.6 The four-state clock step model of den Nijs

An alternative model for the deconstruction and roughening described in scenarios (i)-(iii) has been recently proposed by den Nijs [120]. It contemplates also a possible description of scenario (v), i.e. of a simultaneous deconstruction and roughening, but still with critical behaviour of the reconstruction order parameter in the 2D Ising universality class. Instead of considering Hamiltonians, such as an SOS model, den Nijs prefers a "coarse grained" description of the system. He defines a rectangular lattice oriented along the grooves of the missing rows. Its lattice constant is large compared to the missing row unit cell, but small compared to the reconstruction correlation length. He associates to each unit cell on the lattice a height and a four-state variable $\theta = 0, \pm\pi/2, \pi$ which describes the phase of the (2×1) order parameter in the four degenerate ground states. The boundary between the unit cells can be a wall or a step, depending on the value of $d\theta$. He introduces a Hamiltonian with interactions between cells, assigning an energy to the boundary along [001] which represents steps and wall energies, and energies to the boundaries along $[1\bar{1}0]$ which represent kink energies. Notice that in this model the wall has zero size on the coarse grained scale, being the boundary between adjacent cells. He considers the following partition function:

$$Z = \sum_{\{\theta_{n,m}\}} e^{\sum_{n,m}[K_m \cos(\theta_{n,m}-\theta_{n,m+1}-\Delta)+Q_m \cos(2\theta_{n,m}-2\theta_{n,m+1})]} \cdot e^{\sum_{n,m}[K_n \cos(\theta_{n,m}-\theta_{n+1,m})+Q_n \cos(2\theta_{n,m}-2\theta_{n+1,m})]} \cdot Z_{6V}\left(\left\{d\theta = \pm\frac{\pi}{2}\right\}, L\right) . \tag{3.4}$$

This is a four-state clock model, where K_m, Q_m and Δ assign steps and wall energies. Δ represents the chirality, i.e. the energy difference between (1×1) and (3×1) steps. K_n and Q_n represent the energies of the kinks. Every configuration of the θ variables is weighted by a six vertex (6V) model which includes the height degrees of freedom. The six vertex arrows represent the change in height at the steps. The vertices are defined on the annealed fluctuating lattice, formed by the $d\theta = \pm\frac{\pi}{2}$ boundaries of the clock model (similar to the DOF). A couple of parallel and antiparallel steps divide two surface regions with the same configuration of the θ variables, thus having the same energy in the clock model (Hamiltonian (3.4) depends only on θ, not on h). Only the step-step hard-core interaction, assigned by the six vertex model, is sensitive to the additional height degrees of freedom. L in (3.4) represents the parameter of the six vertex model, favoring up-down-up step order.

The model is quite complex, and up to now only the simplest case has been examined via the analysis of interface free energies, in finite-size transfer matrix framework. If $\eta(d\theta, dh)$ represents the free energy of the interface introduced through the boundary condition $d\theta$ and dh along [001], the vanishing of $\eta(\pi, 0)$ (free energy of a compact domain wall) indicates the disappearance of long range reconstruction order, while the the vanishing of $\eta(0, 2)$ (free energy of a couple of parallel steps) indicates surface roughening. One can then simplify the model, assuming zero chirality, isotropic interactions between cells along $[1\bar{1}0]$ and [001], and neglect step-step interactions ($L = 0$). Only two parameters survive: the wall energy E_w and the step energy E_s. The phase diagram as determined by den Nijs is shown in fig. 3.6.

For $E_w < 2E_s$ there is an Ising deconstruction transition followed by a Kosterlitz-Thouless roughening transition, while for $E_w > 2E_s$ the deconstruction and roughening lines merge together. In the first case one finds $T_D < T_{B/W} = T_R$. The wall width cannot widen above T_D, since it has zero dimension. When $E_w > 2E_s$, the $\eta(\pi, 0)$ interface is reasonably composed by a couple of independent steps in the simplified model analysed numerically. Neglecting step-step interaction (as the model does) the free energies of a couple of parallel or antiparallel steps is expected to vanish simultaneously. This should explain naively why the critical lines $\eta(\pi, 0) = 0$ and $\eta(0, 2) = 0$ merge for $E_w > 2E_s$. Moreover, den Nijs provides some evidences that a small, but finite chirality does not change the

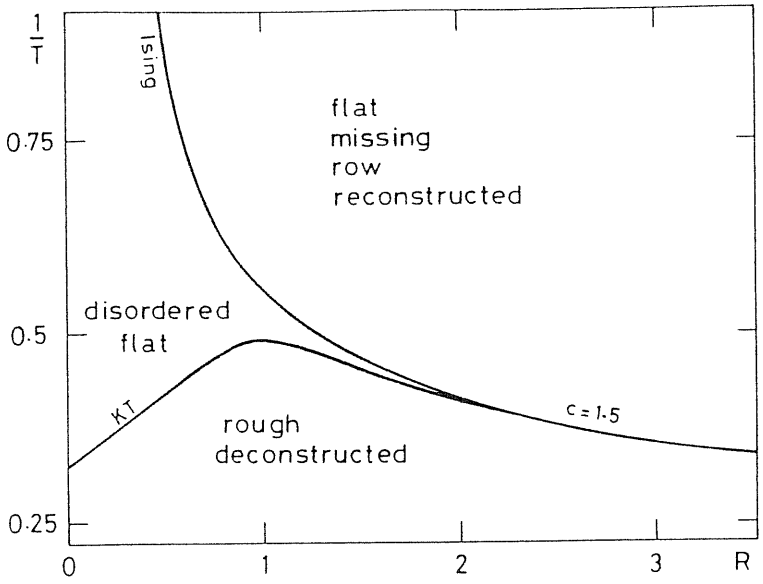

Figure 3.6. Phase diagram of the four-state chiral clock-step model with $R{=}E_W/E_S$, and temperature T in units of E_S. The figure is taken from ref. [120].

critical properties. Hence, the experimental data of Robinson *et al.* [64] on Pt(110) can be consistent with a simultaneous deconstruction and roughening. Information on height-height correlation function are not available from the numerical results presented. This information is necessary to predict the behaviour of integer peaks at roughening.

The phase diagram of den Nijs (fig. 3.6) and of Villain and Vilfan (fig. 3.5) are indeed very similar. The position of the multicritical point N, occurring at $E_W = 2E_S$ in fig. 3.6, is actually dependent on the energies of intermediate excited states for the meandering of walls and steps, as shown in the preceeding Section. This effect should be recovered in the general model (3.4) of den Nijs, by introducing the anisotropy of the surface, i.e. $Q_n \neq Q_m$ and $K_n \neq K_m$ in (3.4).

The deconstructed phase in fig 3.6 is actually a DEF phase; den Nijs does not discuss the role of the $P_{B/W}$ order parameter in model (3.4), neither analyses the role of vertex energies in the phase diagram of the four-state clock-step model. Following up on the arguments by Rommelse and den Nijs [90], Bernasconi [118] predicts that for a sufficiently large value of L in (3.4) the KT line could split into a preroughening line, where $P_{B/W}$ vanishes, plus a true roughening line correspond-

ing to the roughening of the six vertex model, suggesting in this way that the model (3.4) with $L \neq 0$ could be used to analyze the properties of a third novel phase transition between deconstruction and roughening (the parity-restoring transition, with $T_D < T_{B/W} < T_R$).

3.7 The strong chirality limit and the global phase diagram

In the previous section results for the zero chirality limit of the model Hamiltonian (3.4) have been presented. On the opposite limit of infinite chirality the problem can be mapped onto a system of quantum fermions in one dimension, as first pointed out by Villain and Vilfan[131]. In this section results obtained from this mapping by Villain and Vilfan and recently by Balents and Kardar[132] are presented. Finally the global phase diagram for all values of chirality, as recently proposed by den Njis[133], is sketched.

In the limit of strong chirality only one type of step is considered. Neglecting terraces of finite dimensions on the surface, the configurations are composed of lines oscillating along the $[1\bar{1}0]$ direction without overhangs and crossing the whole surface from the top to bottom. There are two types of lines, corresponding to up and down steps. Villain and Vilfan assumed that lines of the same sign cannot cross, while lines of opposite sign can cross with some crossing energy c, which can be positive, negative or zero. For $c < 0$ a pair of steps forms a bound state at $T = 0$. The situation is analogous to the models for commensurate-incommensurate transitions (CIT), the only essential difference being the number of species allowed for each line. The statistical mechanics of directed lines in two dimension can be mapped into the quantum mechanics of fermions in one dimension, and since in this case there are two types of steps the fermion are spin-1/2 particles. The Hamiltonian which describes this situation corresponds to the one dimensional Hubbard model, which has been exactly solved by Lieb and Wu[134]. For $c = 0$, and $c = \infty$ the solution is straightforward. It has been discussed by Villain and Vilfan[131]. A Pokrovsky-Talapov (PT) roughening transition is expected at a temperature T_R assigned by the vanishing of the free energy of a single step. For $T < T_R$ the density of steps is zero, but it is finite above, and the surface is rough but it is a "floating" or "incommensurate" solid with respect to reconstruction

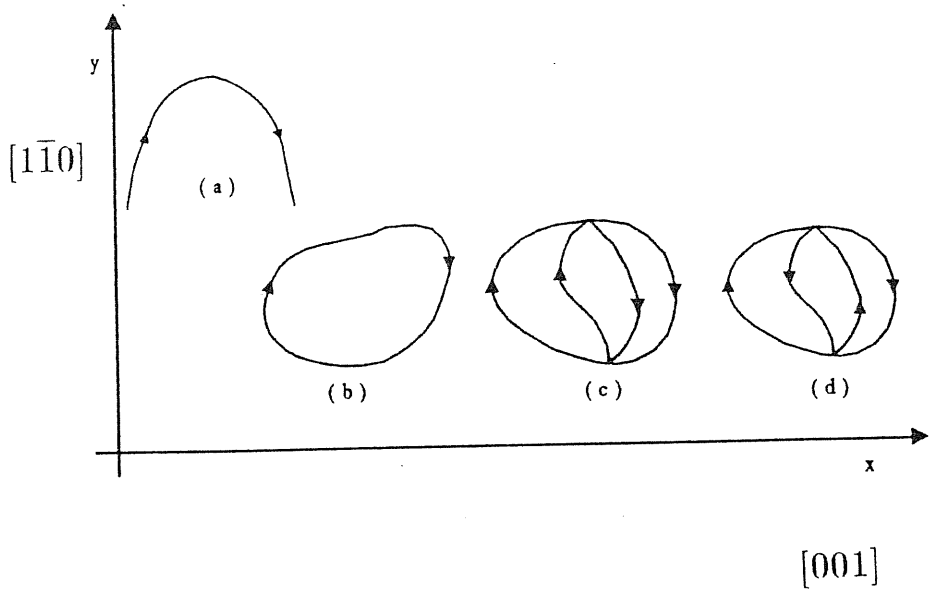

Figure 3.7. Topology of two allowed (c,d), and two forbidden (a,b) configurations of steps in the 2×1 phase. Arrows denote the sign of the steps. From ref. [118].

order. This means that $\mathcal{P}_{2\times1} = 0$, but the reconstruction correlation function decays as a power law, since the transition is maximally anisotropic, being driven by a proliferation of infinitely long steps in one direction only.

Very recently Balents and Kardar[132] applied the full power of the fermionic mapping of the problem. They deduced the full phase diagram for all values of the interaction energy c and they studied the stability of the system with respect to the proliferation of the closed islands of fig. 3.7(c,d), by including in the model the possibility of a simultaneous annihilation and creation of four fermions with total spin zero.

In fact, as previously observed by Villain and Vilfan[131], when walking on the reconstructed surface along the [001] direction, the order parameter $\mathcal{P}_{2\times1}$ changes sign after crossing two steps. Therefore simple closed terraces (fig. 3.7(b)) are forbidden and the simplest allowed closed terrace (fig. 3.7(c)) or closed reconstruction domain (fig. 3.7(d)) are made up by two pairs of simple steps which merge to a point (where four fermionic lines annihilate).

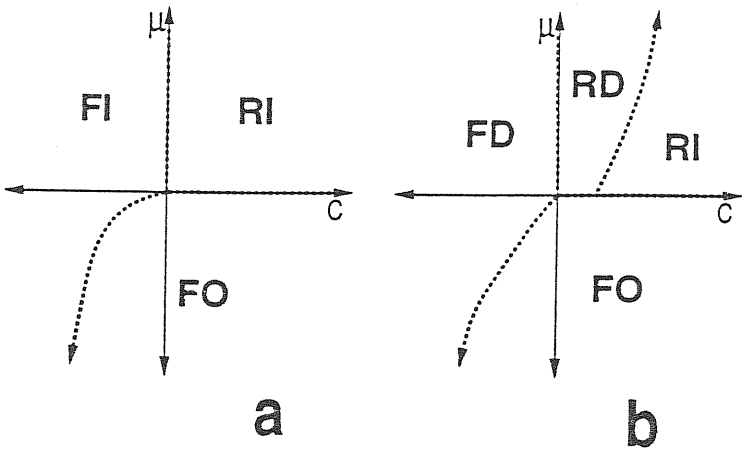

Figure 3.8. Phase diagram of the model by Balents and Kardar without finite islands (a) and in the presence of finite islands (b). From ref. [132].

Balents and Kardar, starting form the continuum version of the Hubbard Hamiltonian, find out a solution in the limit of weak coupling ($n/c \gg 1$, n the mean step density). In the strong coupling limit instead they applied a renormalization group analysis, and draw a phase diagram with a flat ordered (FO) phase in which no steps are present, a flat incommensurate (FI) phase in which up and down steps are bound to form walls and a rough incommensurate phase (RI). In the FI and RI phases the surface is deconstructed, but the correlation function decays as a power law. In the rough phase the height-height correlation function diverges logarithmically, as in the conventional SOS models. The FI-FO and RI-FO transitions are both in the PT universality class, while the RI-FI boundary is an infinite order phase transition, different from the KT universality class. Balents and Kardar showed that choices for the step-step interaction distinct from the contact interaction typical of the Hubbard model can assign a KT universality class to the RI-FI boundary. The PT universality class of the deconstruction and roughening transitions is due to the extreme anisotropy of the system of travelling lines.

The introduction of finite islands partly regains the spatial isotropy and can modify the critical behaviour. In fact, Balents and Kardar showed that for $c < 0$

the system is unstable with respect to islands formation, while it is stable for large positive c. The instability for $c < 0$ is easy to understand: in the regime the fermion lines are paired up into bound states of up and down steps. As those bound states act effectively as single lines, the requirement for four fermion lines meeting at a vertex in fig. 3.7(c) reduces to only two bound pairs intersecting. This is a much probable event. The stability for large positive c is also easily understood, as in this case the lines are completely mutually avoiding. The phase diagram proposed by Balents and Kardar, modified by the presence of islands is reported in fig. 3.8(b). For the (2×1) case, the FO-FI transition is now replaced in fig. 3.8(b) by a conventional deconstruction transition into a flat disordered phase (FD) where finite islands proliferate and where the reconstruction correlations decays exponentially. The FD is a DEF phase in the language of the preceeding Sections. The proliferation of finite islands modify the critical behaviour of the deconstruction transition, which is now Ising-like as expected on a symmetry ground for a systems of walls. Analogously the FI-RI transition is replaced by a conventional KT roughening into a rough disordered (RD) phase with reconstruction correlation decaying still exponentially. For $c \gg 1$ the surface first undergoes a PT transition into a rough phase with power law reconstruction correlations, and at higher temperature the proliferation of finite terraces induces a transition into the RD phase. Fig. 3.8(b) shows a boundary between the RD and the simple FO phase. The existence of this boundary should imply the instability of the FO phase with respect to island formation also for small positive c. Unfortunately, this range of values of c is outside the range of applicability of the renormalization group approach with the inclusion of finite terraces. So the existence of the FO-RD transition at infinite chirality is still an open problem. Moreover Balents and Kardar show that if simple loops (fig. 3.7(b)) were permitted the system would be unstable with respect to loop formation for all c. Actually, it is the condition of infinite chirality that has frozen out the possibility for steps to turn backwards. If one decreases the chirality, a step could turn backwards by changing from a (3×1) step to a (1×1) step. Hence for zero chirality the simple closed terraces are fully allowed and the results by Balents and Kardar imply that the PT roughening is replaced by a roughening into the RD phase. This is in agreement with the results of the 4-state clock-step model at zero chirality by den Njis.

Very recently den Nijs [133] deduced a phase diagram for the 4-state clock step model at infinite chirality which is essentially equal to fig. 3.8(b). In the limit of infinite chirality the 4-state clock-step model can be mapped into the fermionic problem previously discussed, including dislocations (i.e. finite islands). den Nijs decouples the fermionic Hamiltonian into the sum of two terms. The phase diagram of each single term can be deduced and the phase diagram of the full Hamiltonian is described as the superposition of the phase diagrams of the single terms. The result is equivalent to fig. 3.8(b), except for the boundary FO-RD which is absent in the phase diagram proposed by den Nijs. The superposition of the two phase diagram is an heuristic procedure and it does not exclude the existence of the boundary FO-RD at infinite chirality proposed by Balents and Kardar. From the topology of the phase diagram at infinite chirality, and from the phase diagram at zero chirality in fig. 3.6, den Nijs sketched a global phase diagram for the 4-state chiral clock-step model eq. (3.4), which is reported in fig. 3.9: Δ is the chirality, $R = E_w/E_s$ and T is in unit of E_s.

Three paths are distinguished by den Nijs on the phase diagram. Path 3 in fig. 3.9 describes the Ising-like deconstruction transition of scenarios (i)-(iii) and the subsequent KT roughening; the critical properties are not affected by the chirality. Across the line marked as L the sequence and the nature of the phase transitions change. Two paths may be distinguished, type 4a path and type 4b; both describe a simultaneous deconstruction and roughening and correspond to the FO-RI and FO-RD transitions discussed by Balents. The existence at low chirality and the precise location of the critical line L are the major uncertainties in the structure of the phase diagram in fig. 3.9. Path 4a corresponds to the simultaneous deconstruction and roughening predicted by the 4-state clock-step model at zero chirality: the correlations of the reconstruction order parameter decay exponentially above $T_D = T_R$ and the shift of the reconstruction peaks is expected to increase above T_R as approximately as $|T - T_R|$. Along path 4b, at strong chirality, the surface roughens via a Pokroski-Talapov transition leading to an incommensurate solid with respect to the reconstruction order; the reconstruction peaks start to shift at the transition as $|T - T_R|^{\frac{1}{2}}$. At higher temperature the reconstruction degrees of freedom melt via a Kosterlitz-Thouless transition; the correlation change from power law to exponential and the line shape of reconstruction peaks consequently changes from power-law to Lorentzian. Scenario (v)

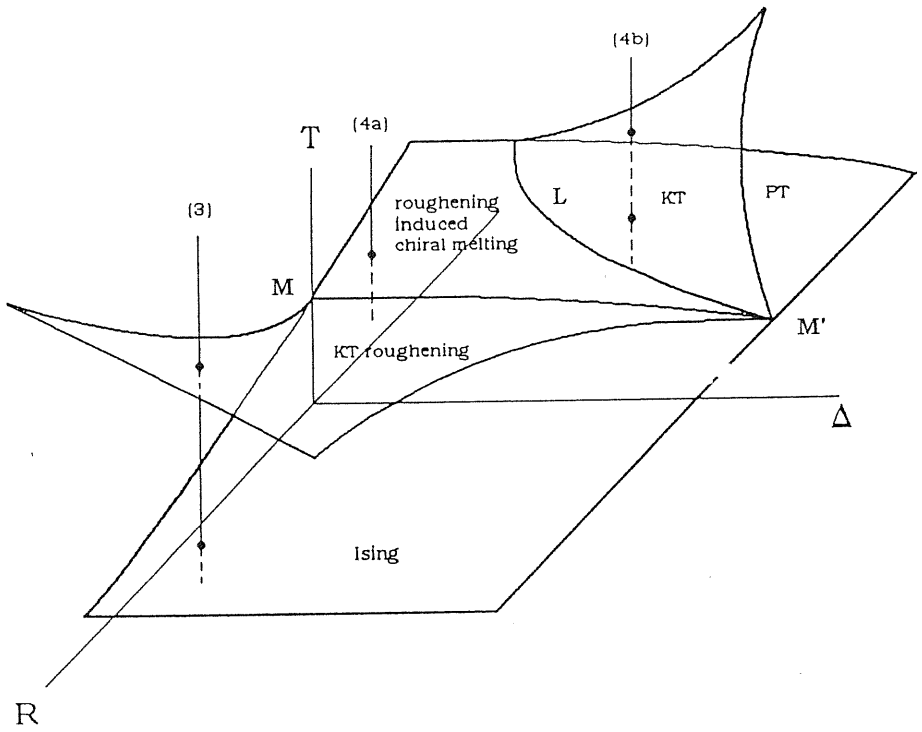

Figure 3.9. Schematic structure of the full diagram of the 4-state chiral clock-step model of den Nijs, with $R{=}E_W/E_S$, $\Delta{=}$ *chirality*, and the temperature T measured in unit of the step energy E_S. The figure is taken from ref. [133].

can be thus split in two scenarios, say (v) and (v'), corresponding to paths 4a and 4b in fig. 3.9.

In the global phase diagram there is still room for the critical line $\langle \mathcal{P}_{B/W} \rangle = 0$. This is expected to coincide with the roughening line, if step-step interaction is neglected in Hamiltonian (3.4), but in real system (and in the 4-state clock-step model by assuming $L \neq 0$ in (3.4)), the mechanisms discussed in the previous Sections could split the $\langle \mathcal{P}_{B/W} \rangle = 0$ line from the roughening one, and stabilize the DOF phase of scenario (iv). The experimental results on Pt(110) by Robinson *et al.* [64], indicating a shift of the reconstruction peaks increasing linearly with temperature, is compatible with the condition of strong chirality if the deconstruction transition of scenario (iv) is assumed. Conversely, the previous analysis of fig.

3.6. indicates that, by excluding scenario (iv), the results by Robinson *et al.* on the shift should imply a small chirality limit, since they are compatible only with path 4a.

Finite terraces have been supposed to play an important role in the stabilization of the DOF of scenario (iv), as will be discussed in Section 6.3; moreover they are the key ingredient for the location of the critical line L in fig.3.9. The role of finite terraces has been included only in an approximate way in the works discussed in this Chapter. Its full characterization could come from Monte Carlo simulations of Hamiltonians which are sufficiently rich to include all the mechanism discussed. A first step in this direction has been realized by the model proposed in this thesis which will be discussed in detail in the following Chapters.

Chapter 4

The model and the method

For a study of the phase transitions on fcc(110) metal surfaces, a SOS model has been employed and a Monte Carlo simulation procedure adopted.

4.1 A description of the model

The model is defined through a BCSOS Hamiltonian written for the fcc(110) lattice made up of two interpenetrating sublattices (fig. 1.3). These are called "BLACK" (B) and "WHITE" (W) sublattices but they are completely equivalent from the physical point of view. The geometry of the unreconstructed fcc(110) surface arises by choosing one of them as the topmost layer in the ground state and keeping the other at a distance $a_z = a/2\sqrt{2}$ (a = fcc lattice parameter) below in the vertical direction. The lattice is rectangular in shape, i.e. anisotropic, hence it is necessary to distinguish between the "soft" [001] direction (x) and the "hard" [1$\bar{1}$0] direction (y), along which the close-packed rows of atoms run (soft and hard respectively referring to the coupling between atoms).

The ordered surface alternates in height by exactly one unit from B to W sites, and the disordered surface contains only steps of unit height. The additional constraint is imposed on the m_i that height differences between nearest neighbouring sites (i.e. a white and each of the four surrounding black ones) are bound to be ± 1. Such restriction is quite physical, since ± 3 jumps are energetically very costly and thus highly improbable. This corresponds to an interaction energy J_0 between nearest neighbouring sites which is let to go to infinity, this description

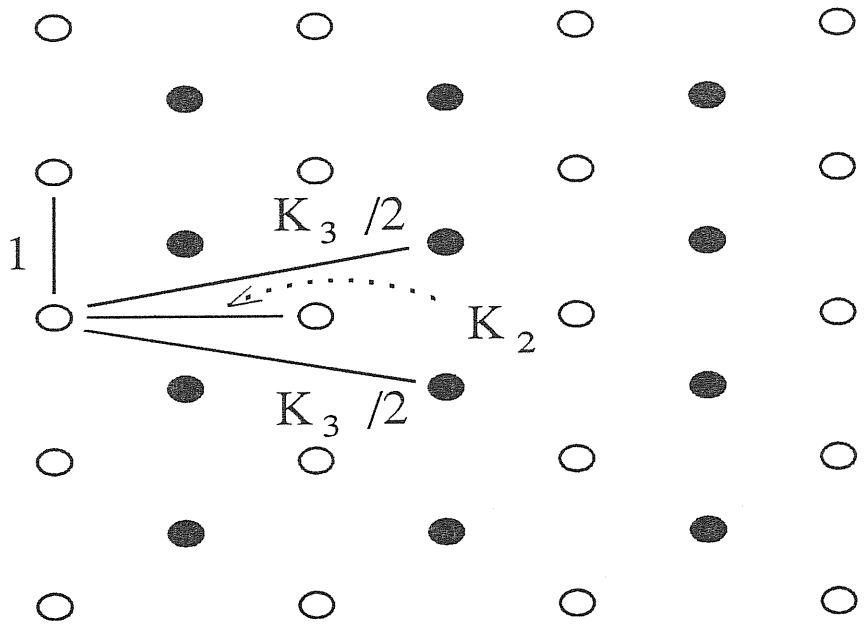

Figure 4.1. The structure of the couplings between sites. The parameters are expressed in units of J.

being meaningful only because of inward relaxation of the top layer, a common feature for both reconstructed and unreconstructed fcc(110) surfaces. Without that relaxation, the assumption $J_0 = \infty$ would be inappropriate, as in its absence and for a pairwise potential, J_0 equals some in-plane coupling (or is even smaller than that, if outward relaxation takes place). On the other hand, form the statistical mechanics point of view this is exactly the "six vertex" constraint imposed by van Beijeren on the BCSOS model, and enables a mapping of surface configurations into vertex configurations, which will prove useful in the following chapters.

Given a column height distribution m_i, the Hamiltonian taken is

$$\mathcal{H}/J = \sum_i (m_i - m_{i+\mathrm{y}})^2 - K_2 \sum_i (m_i - m_{i+\mathrm{x}})^2 + \\ + \frac{1}{2} K_3 \left[\sum_i (m_i - m_{i+\frac{3}{2}\mathrm{x}+\frac{1}{2}\mathrm{y}})^2 + \sum_i (m_i - m_{i+\frac{3}{2}\mathrm{x}-\frac{1}{2}\mathrm{y}})^2 \right]. \qquad (4.1)$$

Here, J is a measure of the atomic cohesion energy and is set as the scale of energies (and temperatures) in the model; $\hat{\mathrm{x}}$ and $\hat{\mathrm{y}}$ are the sublattice unit vectors in the [001] and $[1\bar{1}0]$ directions respectively. The structure of the couplings in (4.1) is drawn in fig. 4.1. Due to the abovementioned anisotropy of the surface, the relation $JK_2 \equiv J_2 < J$ holds for the nearest neighbour interaction energy in the x direction. An additional next nearest neighbours interaction $JK_3 \equiv J_3$, the relevance of which will be discussed below, is included in the model.

4.2 Ground state considerations

It is easy to capture the main features which have led to Hamiltonian (4.1) by examining it at $T = 0$ and determining which different ground state configurations show up by varying the value of the energy parameters. At $T = 0$, the first term $\sum_i (m_i - m_{i+\mathrm{y}})^2$ assigns an energy cost to neighbouring sites willing to be at different heights on each sublattice in the hard y direction, encouraging in this way the formation of uninterrupted rows in this direction. The second term $-K_2 \sum_i (m_i - m_{i+\mathrm{x}})^2$ has either a similar or opposite effect on the surface configurations in the x direction, according to whether $K_2 < 0$ or $K_2 > 0$. A negative value for K_2 induces the formation of rows also in this direction, thus of an overall flat (1×1) surface. A positive value would encourage the surface to perform a constant descent (or rise) in the x direction instead, so that the (110) starting surface is effectively replaced by a (111) system, which can also be described in terms of a $(\infty \times 1)$ reconstruction.

The model has been devised to fit (110) noble metal surfaces, both reconstructed and unreconstructed. But in the former case, a (2×1) stabilizing term is necessarily needed: this is represented by $\frac{1}{2}K_3 \left[\sum_i (m_i - m_{i+\frac{3}{2}\mathrm{x}+\frac{1}{2}\mathrm{y}})^2 + \sum_i (m_i - m_{i+\frac{3}{2}\mathrm{x}-\frac{1}{2}\mathrm{y}})^2\right]$, which, with $K_3 > 0$, acts to interrupt the descent of the surface induced by a negative K_2 by raising third neighbour sites in the x direction to height values as near as possible (hereafter, unless otherwise stated, it will always be considered $K_3 \geq 0$).

A ground state phase diagram is easy to draw, provided the energies of all the possible $(n \times 1)$ reconstructions are calculated and compared. The $(n \times 1)$ reconstruction is intended to be a structure showing a periodicity of n sublattice

sites in the x direction, but no broken bonds in the y direction, so that the y rows are preserved in their lengths. Its side view along the y direction is of a sawtooth configuration.

If $\mathcal{N} = 2N_xN_y$ is the total number of sites (where N_x, N_y are, respectively, the number of lattice sites in the two in-plane directions, and the factor two arises due to the presence of the two sublattices), the result is

$$\begin{aligned} E_{1\times1}/J\mathcal{N} &= K_3 \\ E_{2\times1}/J\mathcal{N} &= -2K_2 + K_3 \\ &\vdots \\ E_{n\times1}/J\mathcal{N} &= -4\frac{n-1}{n}K_2 + \frac{9n+16}{n}K_3 \\ E_{\infty\times1}/J\mathcal{N} &= -4K_2 + 9K_3 \end{aligned} \tag{4.2}$$

with E_0 constant contribution which can be neglected by suitably fixing the zero of energies.

It is easy to show that three distinct cases are possible for the ground state, depending on the value of the parameter $K = K_2/K_3$ (for $K_3 > 0$):

1) $K < 0$: the ground state is (1×1)

2) $0 < K < 4$: the ground state is (2×1)

3) $K > 4$: the ground state is $(\infty \times 1)$

and the points $K = 0$ and $K = 4$ are points of coexistence of two different phases. As noted before, the sign of K_2 has a primary influence in deciding if the surface will remain flat (1×1) or will be replaced by a sloping $(\infty \times 1)$. A value of K_3 greater than $\frac{1}{4}K_2$ is sufficient to stabilize the (2×1) missing row reconstructed phase at the expenses of the $(\infty \times 1)$ phase. From now on, the interval $0 < K < 4$ (neglecting the faceting region $K > 4$) will be addressed to as "the right side" of the phase diagram, the $K < 0$ as its "left" part.

It is worth noting that, at fixed K, the model assigns higher energies to all possible "shallow reconstructions", that is reconstruction with formation of $(n \times 1)$ grooves, $n = 3, 4, \cdots$, hence ruling out these phases.

It is also possible to enrich Hamiltonian (3.2) by enlarging the number of interactions, in order to include the fourth, fifth,..., neighbours too. For example, by adding a term of the form

$$\mathcal{H}_4/J = K_4 \sum_i (m_i - m_{i+2x})^2 \tag{4.3}$$

which represents a fourth neighbours interaction, one gets for the ground state a two-dimensional phase diagram in terms of the variables K_2/K_3 and K_4/K_3 which, in addition to (1×1) , (2×1) and $(\infty \times 1)$ phases, also contains a (3×1) region. It is probable, moreover, that by adding a fifth neighbours interaction, a (4×1) region in a three dimensional phase diagram would appear, and so on (sixth neighbours interaction $\rightarrow$ (5×1) phase, etc ...). The additional terms have not been considered in what follows, but may turn out to be relevant if the object of study goes beyond the (2×1) deconstruction transition. A more detailed description of the reconstructed phase would result, as some (3×1) facets have been experimentally observed[50], and the energy of the (3×1) phase obtained in the "glue" model appears to be only slightly higher than that of the (2×1) phase. In addition, a further neighbour term like (4.3) leads to a larger parameter space, hence it could open wider possibilities also for the reproduction of some of the scenarios presented in Chapter 3, thus enriching the model and its predictive power.

4.3 Energy parameters

If one wishes to describe a real physical situation, it is necessary to assign specific values to the energy parameters of the model. They are chosen so as to match the $T = 0$ energies of some fcc facets, as obtained from eq. (4.1), to their "experimental" values. Real metal data available in the literature, however, refer to the high temperature surface tension of a generic metal surface[135] (i.e. not specifically the (110)) and, moreover, are surface free energies including entropic contributions not present in expressions like (4.2). The only solution at one's disposal is provided by the choice to match expressions for the ground state surface energies to the

values obtained by many body theories through molecular dynamics calculations at $T = 0$.

The scope of this work is to investigate in detail some of the possible scenarios opening for the fcc(110) surfaces, thus two prototype surfaces are chosen, one form the reconstructed part of the phase diagram and the second from the unreconstructed part, namely **gold** and **silver** (110). These names, assigned to these two cases, refer to different values of the parameters given to Hamiltonian 4.1 which are extracted form molecular dynamics simulations of gold and silver respectively. They are nonetheless suited to describe a general situation more than the exact phenomenology of the corresponding real metal surfaces, especially for the case of silver. The statistical mechanics nature of the model in fact requires it to contain the main physical aspects, yet to be simple enough to permit its study via the Monte Carlo technique. Hence more complex features like, for example, faceting are necessarily ruled out from the possible resulting surface configurations, and should be looked at with the aid of more realistic models. These on the other hand fail in giving a complete picture of the fcc(110) phase transitions, especially from the point of view of their critical behaviour. This is the main target of the present work, which loses out in the care for particulars (such as, e.g., the high-precision determination of transition temperature values) but gains in the general insight into the rich phase diagram shown by the fcc(110) surfaces.

Au - For the "right" $K > 0$ part of the phase diagram, the $T = 0$ energies needed are obtained from the calculations of Ercolessi *et al.* [4] for Au, based on the "glue" model briefly described in Section 2.3. The values which represent energies per surface area and are calculated for the (100), (111) and both the reconstructed and unreconstructed (110) surfaces, are as follows:

$$\begin{aligned} \mathcal{E}_{100} &= 128.5 \text{ meV/Å}^2 \\ \mathcal{E}_{110} &= 122.5 \text{ meV/Å}^2 \\ \mathcal{E}_{111} &= 96.6 \text{ meV/Å}^2 \\ \mathcal{E}_{2\times1} &= 107.4 \text{ meV/Å}^2 \end{aligned} \tag{4.4}$$

All these energies refer to relaxed $T = 0$ configurations, i.e. starting from a perfect bulk-truncated arrangement of the atoms and letting them relax into their

equilibrium surface positions. This is the only possible way (though obviously not satisfactory) in which relaxations effects are included into an otherwise two dimensional rigid lattice model.

The corresponding expressions obtained from Hamiltonian (4.1), under the form of energies per site, are

$$\begin{aligned} E_{100}/\mathcal{N} &= E_0 + 4J + J_3 \\ E_{110}/\mathcal{N} &= E_0 + J_3 \\ E_{111}/\mathcal{N} &= E_0 - 4J_2 + 9J_3 \\ E_{2\times1}/\mathcal{N} &= E_0 - 2J_2 + J_3 \end{aligned} \tag{4.5}$$

where the additional energy constant E_0 is added, becoming another unknown variable to be fitted together with the others. A geometric conversion factor $\mathcal{A}/\cos\theta$ has to be inserted to multiply each value of (4.4) for a comparison with (4.5). Here $\mathcal{A} = \frac{1}{2}\frac{\sqrt{2}}{2}a{\cdot}a$ is the area per atom of the (110) surface (for Au, the lattice parameter $a = 4.07$ Å $\rightarrow$ $\mathcal{A} = 5.85$ Å^2) and $\cos\theta$ arises from the projection of the (111) and (100) surfaces onto the (110) face. The tilting angles are $\theta_{111} = \arccos\sqrt{2/3} \simeq 35°$ and $\theta_{100} = 45°$. The comparison, finally, yields

$$\begin{aligned} E_0 &= 698.4 \text{ meV} \\ J &= 86.7 \text{ meV} \\ K_2 &= 0.51 \\ K_3 &= 0.22 \\ K &= K_2/K_3 = 2.3 \quad . \end{aligned} \tag{4.6}$$

Two important features are worth noticing. First, the anisotropy expected from preliminary considerations is actually confirmed by the numerical values (4.6), since the coupling in the hard direction is twice that in the soft one. In addition, the next nearest neighbour interaction strength K_3 is approximately half the nearest neighbour one K_2, hence $K = K_2/K_3 = 2.3$, which places the ground state of the system in the (2×1) phase, as it should be for Au(110). A good self-consistency test for the parameters (4.6) is the calculation of the energy of the $T = 0$ (3×1) reconstructed phase, and its comparison with the "glue" values. The first

procedure gives 111.0 meV/Å^2, the second 109.8 meV/Å^2. The values are very similar and, what is more, show that the model reproduces the correct behaviour of the energies of the reconstructed phase, yielding a value for $E_{3\times1}$ which is slightly greater than $E_{2\times1}$, as previously observed with the "glue" data.

Among the values (4.6), J due to the form of the Hamiltonian (4.1), fixes the temperature scale. From now on, temperatures will be expressed in reduced dimensionless units, each unit corresponding to $J \simeq 1000K$.

Ag - The procedure of fitting the interaction values for the case of an unreconstructed surface is similar but has to resort to some other effective medium theory calculations, since no "glue" values are available, for instance, for silver. At least four surface energies are needed to extract four parameters (J, K_2, K_3 and E_0), thus Chen and Voter's "embedded atom method" data[136] are chosen, which provide values for the (110), (210) and (310) surfaces, each of the last ones unreconstructed and (2×1) reconstructed. The tilting angle with respect to the (110) surface are $\theta_{(210)} = \arctan 1/3 \simeq 20.5°$, and $\theta_{(310)} = \arctan 1/2 \simeq 29.5°$.

The energies of the different faces of Ag calculated by Chen and Voter † are

$$\begin{aligned} \mathcal{E}_{100} &= 879.6 \text{ mJ/m}^2 & \mathcal{E}_{210} &= 1014 \text{ mJ/m}^2 \\ \mathcal{E}_{111} &= 802.7 \text{ mJ/m}^2 & \mathcal{E}_{210,R} &= 1006 \text{ mJ/m}^2 \\ \mathcal{E}_{110} &= 967 \text{ mJ/m}^2 & \mathcal{E}_{310} &= 992 \text{ mJ/m}^2 \\ \mathcal{E}_{110,R} &= 972 \text{ mJ/m}^2 & \mathcal{E}_{310,R} &= 999 \text{ mJ/m}^2 \end{aligned} \tag{4.7}$$

(where R means (2×1) reconstructed), whereas the corresponding expressions obtained from (4.1) are

† The values for the (100) and (111) surfaces have been calculated by Furio Ercolessi adopting the potentials kindly provided by Art Voter himself. I would like to thank them both.

$$
\begin{aligned}
E_{100}/\mathcal{N} &= E_0 + 4J + J_3 & E_{210}/\mathcal{N} &= E_0 + \frac{4}{3}J + J_3 \\
E_{111}/\mathcal{N} &= E_0 - 4J_2 + 9J_3 & E_{210,R}/\mathcal{N} &= E_0 + \frac{4}{3}J + J_3 \\
E_{110}/\mathcal{N} &= E_0 + J_3 & E_{310}/\mathcal{N} &= E_0 + 2J + J_3 \\
E_{110,R}/\mathcal{N} &= E_0 - 2J_2 + J_3 & E_{310,R}/\mathcal{N} &= E_0 + 2J + J_3 - J_2
\end{aligned}
\tag{4.8}
$$

Taking into account the usual geometric factors (also, the Ag lattice constant is very close to the Au value, that is $a = 4.08\text{Å}$), it is straightforward to match the expressions (4.8) with the energies (4.7). However, the problem of fitting the needed four parameters of Hamiltonian (4.1) employing the eight energy values provided above is obviously overdetermined. A meaningful solution is not easy to find as, for example, the two different structures of the (210) phase are separated 8 mJ/m^2 in energy but share the same expression of the form (4.8). The most sensible way to extract J, K_2, K_3 and E_0 is the following. By grouping together the available energies into sets of four and taking care not to include in the same set both the values of $\mathcal{E}_{210}$ and $\mathcal{E}_{210,R}$ which would give rise to an undetermined linear system, one ends up with 24 different sets, each one providing a unique solution for the values of the parameters. These solutions are spread in a certain range of the parameter space. The choice criterion is first to eliminate the solutions giving rise to positive values of K_2 or to negative values of K_3, then to perform a rough averaging procedure by picking up the central value of each restricted parameter interval. Positive values of KJ_2 are rejected as leading to a (2×1) ground state, whereas Ag has an unreconstructed ground state. Also positive values of K_3 are out, since if K_3 is negative the phase diagram of the model changes into a new one with only two phases, the $(\infty \times 1)$ extending for $K' > -\frac{1}{2}$ and the (1×1) for $K' < -\frac{1}{2}$, $K' = K_2/(-K_3)$, so that it is not sufficient anymore that K_2 be negative for the stability of the unreconstructed symmetry.

The result of this procedure is

$$\begin{aligned} E_0 &\simeq 356.4 \text{ meV} \\ J &\simeq 25.875 \text{ meV} \simeq 300K \\ K_2 &\simeq -0.1 \\ K_3 &\simeq 0.025 \\ K &= K_2/K_3 \simeq -4.0 \quad . \end{aligned} \tag{4.9}$$

The element which (110) unreconstructed surface has been taken for investigation in this way has no more right to be called "silver" than "copper" or "lead" or any other metal. This undoubtedly uneasy procedure however leads to a point in parameter space which lies on the left side of the phase diagram and can be considered as a starting value for the study of the critical behaviour of the model on that side of the diagram, nonetheless keeping some connection with real surfaces.

4.4 The Monte Carlo algorithm

In order to investigate the thermodynamic properties of the model, a standard Monte Carlo technique[137] is applied to a lattice of $\mathcal{N} = 2 \times N_x \times N_y$ sites, with $N_x = N_y = 12, 16, 20, 24, 28$ and 32, and with periodic boundary conditions. As is well known, this technique allows for the evaluation of statistical averages of thermodynamic observables through the sampling of significant configurations $\{m_i\}$, after equilibration has been achieved. Employing the standard Metropolis sampling algorithm[138], the energy change $\Delta E = \mathcal{H}(\{m_i'\}) - \mathcal{H}(\{m_i\})$ is evaluated after the interfacial configuration has been changed by randomly removing or depositing one atom at a random site – if allowed by the BCSOS constraints – on a randomly chosen sublattice. This means that each SOS column height is changed by either $+2$ or -2, preserving the parity of the sublattice, and, moreover, that the six vertex constraint is imposed on every new configuration. Hence the mean surface height is not conserved. This procedure yields a grandcanonical ensemble where the chemical potential is the same in both the solid and the vapour phases. The usual Metropolis acceptance criterion (accept the new configuration if $\Delta E \leq 0$, otherwise accept it if $\exp(-\Delta E/k_B T) > R$, R being a random number in the interval $0 \leq R < 1$; reject it in the other cases) is adopted. Each attempted

move per site (either accepted or rejected) is referred to as 1 Monte Carlo step, and $\mathcal{N}$ steps are referred to as 1 Monte Carlo configuration. The initial $2 \cdot 10^4$ configurations are discarded for equilibration, and at least $5 \cdot 10^5$ configurations used to compute averages. To avoid excessive correlation between quantities evaluated in two different steps, averages of relevant thermodynamic quantities are collected every 5 to 10 Monte Carlo configurations. Nonetheless, some correlation remains in this procedure, especially for large systems and near the critical points where the well-known phenomenon of critical slowing down takes place, due to the large correlation length. No particular technique is employed to circumvent this problem: longer runs are simply adopted (up to 10^6 configurations or more). Error bars are estimated by dividing the simulation into 10 to 20 independent runs and, for some temperature values, the errors have been checked by calculating the statistical correlation length of the related quantity (a more accurate, but lengthy, procedure[139]). Finally, no significant differences in the simulation scheme for gold or silver are utilized. Mainly, different quantities are evaluated to match the needs of different physical requests: in this respect more details will be given in the following section.

4.5 The relevant quantities

In order to closely follow the thermodynamics of the system, about 20 values of temperature are examined, and for each of them a set of thermodynamic quantities, which proves to be relevant for the present investigation, are evaluated. All of them are normalized per site, in order to allow for an easier finite-size scaling analysis; $\mathcal{N}$ is the number of system sites, and in the following formulæ the symbol $\langle \cdots \rangle$ will mean "Monte Carlo average", that is

$$Q = \langle \mathcal{Q} \rangle = \frac{1}{N_C} \sum_{n=1}^{N_C} \mathcal{Q}_n \tag{4.10}$$

where N_C is the number of Monte Carlo configurations, $\mathcal{Q}_n$ (written in calligraphic letters) is the generic quantity evaluated in the n-th configuration, whereas Q (in roman font) is the Monte Carlo average of $\mathcal{Q}$.

Apart for the order parameters, to which a separate section is devoted, the relevant quantities are the first three cumulants of the energy, the height fluctuations and the scattering intensities. In detail:

- the total configurational energy per site

$$E = \frac{1}{\mathcal{N}} \langle \mathcal{E} \rangle \tag{4.11}$$

- the specific heat C_V, defined as

$$C_V = \frac{1}{\mathcal{N}} \frac{1}{k_B T^2} \left[\langle \mathcal{E}^2 \rangle - \langle \mathcal{E} \rangle^2 \right], \tag{4.12}$$

where $k_B = 1$ and T is measured in units of J;

- the first temperature derivative of the specific heat, always per site

$$\frac{dC_V}{dT} = \frac{1}{\mathcal{N}} \frac{1}{k_B T^3} \left[-2 \left(\langle \mathcal{E}^2 \rangle - \langle \mathcal{E} \rangle^2 \right) + \frac{1}{T} \left(\langle \mathcal{E}^3 \rangle - 3 \langle \mathcal{E} \rangle \langle \mathcal{E}^2 \rangle + 2 \langle \mathcal{E} \rangle^3 \right) \right] \tag{4.13}$$

where the second term is the third cumulant of the energy (the first term is the second cumulant, proportional to C_V). This quantity will prove essential only for silver.

- The height fluctuations (square of the interfacial width), relevant for the roughening transition

$$\langle \delta h^2 \rangle = \frac{1}{\mathcal{N}} \sum_i \left\langle (m_i - \bar{m})^2 \right\rangle \tag{4.14}$$

where $\bar{m} = \sum_i m_i / \mathcal{N}$ (not necessarily an integer number) is the nominal surface height for a given configuration, and the sum is carried out over the lattice sites. Eq. (4.14) makes sure that the only statistical height fluctuations taken into account arise from thermal fluctuations, while $k = 0$ – capillary wave (Goldstone mode) wandering, which comes out from the invariance of

Hamiltonian (4.1) for global vertical translation of the interface, $m_i \to m_i + m$, is neglected.

- The total atom scattering intensity (obtained by simple rewriting eq. (1.17))

$$I_A(\mathbf{Q}, q_z) = \frac{1}{\mathcal{N}^2}\langle \mathcal{I}_A(\mathbf{Q}, q_z)\rangle = \frac{1}{\mathcal{N}^2}\left\langle \left| \sum_i \mathrm{e}^{i\mathbf{Q}\cdot\mathbf{R}_i}\mathrm{e}^{iq_z h_i}\alpha_i \right|^2 \right\rangle \tag{4.15}$$

where $\mathbf{R}_i$ is the position of the i-th site on the surface plane, $h_i = a_z m_i$ and $\alpha_i = \alpha(\mathbf{R}_i)$;

- The total X-ray scattering intensity (eq. (1.20))

$$I_X(\mathbf{Q}, q_z) = \frac{1}{\mathcal{N}^2}\langle \mathcal{I}_X(\mathbf{Q}, q_z)\rangle = \frac{1}{\mathcal{N}^2}\frac{1}{\left|1 - \mathrm{e}^{-2(ip+\mu)}\right|^2}\left\langle \left| \sum_i \mathrm{e}^{i\mathbf{Q}\cdot\mathbf{R}_i}\mathrm{e}^{iq_z h_i} \right|^2 \right\rangle . \tag{4.16}$$

For particulars on these formulæ, see Chapter 1, the scattering Section.

4.6 Order parameters

In order to monitor a phase transition it is necessary to study the behaviour of some suitably defined order parameter as a function of temperature. Since, however, this thesis presents an investigation of both the reconstructed and the unreconstructed part of the phase diagram of model (4.1), different parameters have to be defined for different symmetries of the ground state. The first of these quantities, envisaged to monitor the (2×1) deconstruction transition on the right side of the phase diagram, is defined by making use of the mapping of the surface height variables into an Ising spin configuration. The restriction, in fact, that nearest neighbours height differences be ± 1 enables one to associate to each bond connecting the two sublattices a spin variable s_j by writing $s_j = (m_W - m_B)_j$, j

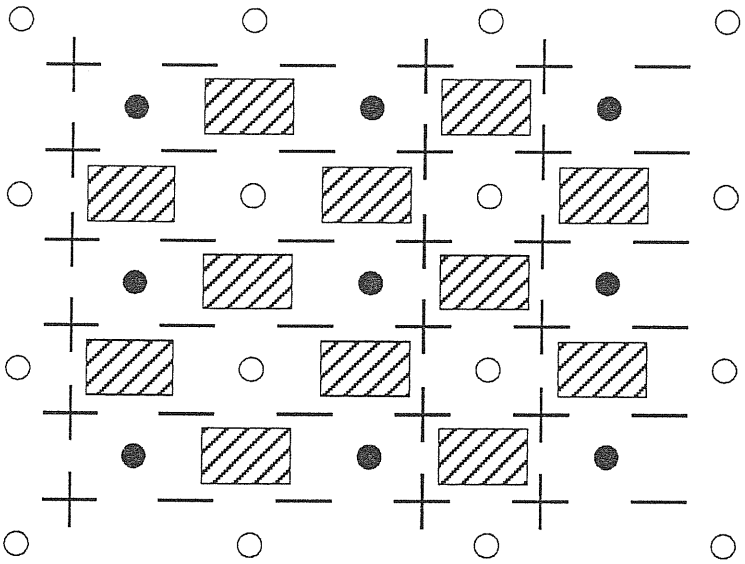

Figure 4.2. The spin configuration corresponding to the height configuration of figure 1.3. The shaded regions indicate on which spin plaquettes the height conservation constraint is imposed.

running on the lattice of bonds of W ∪ B, m_W and m_B being the heights of the sites connected by each bond.

In this way, a $\mathcal{N}$ - site height configuration is mapped onto a $2\mathcal{N}$ - spin one, and this procedure leads to an Hamiltonian of the ANNNI (Anisotropic Next Nearest Neighbours Ising) model type[127,128]. However, the important constraint is imposed that height conservation be respected on every other square of the resulting Ising checkerboard lattice (those which do not include the atoms). The requirement $s_1 - s_2 + s_3 - s_4 = 0$, where s_1 is the upper left corner spin of a 4-spin plaquette and the others follow clockwise (this can alternatively be seen as the ice-rule for the equivalent six-vertex representation of the model), leads to important new physics with respect to the 2D ANNNI model. For instance, "spin" excitations in the present model must occur through the flipping of four neighbouring spins, rather than of a single spin as normal (see fig 4.2).

It is now easy to verify that while the spin configuration corresponding to the (1×1) phase is a simple ferromagnetic arrangement, four degenerate spin ground states are allowed to correspond to the ordered (2×1) phase, namely

those described by the repeated sequences $\langle++--\rangle$, $\langle+--+\rangle$, $\langle--++\rangle$ and $\langle-++-\rangle$ (here the symbol $\langle\cdots\rangle$ denotes repeated spin units).

By grouping together the vertical columns of spins so as to put in each group all the columns having the same integer coordinate in the x direction (modulo 4), it is possible to form four "column magnetizations" defined by summing over the spins in each group of columns: $M_\alpha = 4\sum_i s_i^{(\alpha)}/\mathcal{N}$, $\alpha = 1,2,3,4$. Four (2×1) order parameters can be defined in terms of the M_α:

$$\begin{aligned} M_{\langle++--\rangle} &= (+M_1 + M_2 - M_3 - M_4)/4 \\ M_{\langle+--+\rangle} &= (+M_1 - M_2 - M_3 + M_4)/4 \\ M_{\langle--++\rangle} &= (-M_1 - M_2 + M_3 + M_4)/4 = -M_{\langle++--\rangle} \\ M_{\langle-++-\rangle} &= (-M_1 + M_2 + M_3 - M_4)/4 = -M_{\langle+--+\rangle} \end{aligned} \tag{4.17}$$

and an overall reconstruction order parameter will be obtained in terms of the root-mean-square magnetization [140]

$$\mathcal{P}_{2\times1} = \sqrt{\frac{1}{2}\left[M^2_{\langle++--\rangle} + M^2_{\langle+--+\rangle} + M^2_{\langle--++\rangle} + M^2_{\langle-++-\rangle}\right]}\,, \tag{4.18}$$

averaged over all Monte Carlo configurations, $P_{2\times1} = \langle\mathcal{P}_{2\times1}\rangle$. This parameter, as the one below, is well defined in the sense that its value is 1 in the (2×1) low temperature phase and 0 in the high temperature disordered or (1×1) ordered phase. For a scattering interpretation of $\mathcal{P}_{2\times1}$ see Appendix A.

Another way to define an order parameter on a fcc(110) surface is to make use of the fact that the surface lattice is made up of two equivalent sublattices and by specifying which of them prevails in the topmost layer. This parameter, designed as $\mathcal{P}_{B/W}$ (or "sublattice" order parameter) where B/W stands for BLACK and WHITE from the two sublattice colouring, has already been addressed to in Chapter 3 when presenting different deconstruction and roughening scenarios. Since by definition one of the requirements for $\mathcal{P}_{B/W}$ is the demand that it assumes a value 1 in an ordered phase and 0 in a disordered one, its expression will necessarily be dependent on the symmetry of the ground state (i.e. on different sides of the phase diagram), making sure that different formulæ do embody the same physics. Hence, the expressions are

– (2×1) symmetry

$$\mathcal{P}_{B/W} = \frac{1}{2\mathcal{N}} \left| \sum_{i,W} |S_{i,W}| - \sum_{i,B} |S_{i,B}| \right|, \tag{4.19}$$

with $S_{i,W}(S_{i,B})$ the sum of the four Ising spins defined on the four nearest neighbour bonds relative to a white (black) site, and
– (1×1) symmetry

$$\mathcal{P}_{B/W} = \frac{2}{\mathcal{N}} \left| \sum_{B} m_B - \sum_{W} m_W \right|, \tag{4.20}$$

the absolute value ensuring a meaningful averaging procedure. Monte Carlo averages are taken as usual by bracketing the quantity under consideration, i.e. $P = \langle \mathcal{P} \rangle$.

For each of these order parameters $\mathcal{P}$, the related susceptibility

$$\chi = \frac{\mathcal{N}}{k_B T} \left[\langle \mathcal{P}^2 \rangle - \langle \mathcal{P} \rangle^2 \right] \tag{4.21}$$

is evaluated and its critical behaviour studied too.

In the Appendix it is shown how $\mathcal{P}_{B/W}$, as well as $\mathcal{P}_{2\times1}$, is related to the scattering intensities under particular conditions (see also Sections 1.4.4).

Chapter 5

The BCSOS model

This chapter is dedicated to the study of the roughening transition on the BCSOS model. Its aim is threefold. First, it can be seen as a check for the techniques and, in general, for the global simulation procedure against an exactly solvable model. Secondly, an important concept like that of a sublattice order parameter is introduced and studied in connection with known exact results. Lastly, a deeper insight into a quantity which has remained hitherto unexplored, the staggered susceptibility, is provided [141].

Surface roughening phenomena are often studied within Solid on Solid (SOS) models. The simplest of such models, such as the Discrete Gaussian or the Absolute SOS models, have no sublattice structure and therefore roughening takes place without any accompanying change of symmetry. Real surfaces, however, commonly exhibit two, and sometimes three or more, sublattices. For example: fcc (100) and (110), as well as bcc (100) and (111), have two sublattices, fcc (111) and bcc (110) have three, and so on. Their ground states are accordingly at least n-fold degenerate, corresponding to the equivalent possibilities of the topmost layer to belong to one of the n sublattices. At finite temperatures, one can therefore associate any thermodynamic state of the surface with a well defined *sublattice order parameter* $\mathcal{P}$. Moreover, this order parameter is expected to vanish identically in the rough state (where all sublattices must enter with equal weight). It follows that a sublattice disordering phase transition is expected to take place, either below the roughening temperature T_R, or at T_R itself. It should be stressed that, apart from this constraint, the two phenomena, sublattice disordering and roughening, are distinct. They will in general occur at different temperatures, and belong to

different universality classes. den Nijs [90] as well as the Trieste group [124,125] have introduced models which address this type of situation. Sublattice disordering is indeed analogous to the "pre-roughening" of den Nijs, who calls "disordered flat" the ensuing phase. Hence, it is highly desirable to understand sublattice disordering, if present, in simpler models, where a good deal of experience has accumulated over the years.

The simplest surface model which is of the SOS type, but does embody the presence of two sublattices, is van Beijeren's well-known BCSOS model [14]. As shown in Section 1.3.1, it is mapped onto the F version of the six-vertex model, for which many properties are known exactly. It is therefore of interest to enquire about sublattice disordering within the BCSOS model.

The Hamiltonian (4.1) is equivalent to the BCSOS one provided its parameters assume particular values. It is easy to see that the requirements are

$$\begin{aligned} K_2 &= -1 \\ K_3 &= 0 \,. \end{aligned} \tag{5.1}$$

Moreover, one can express the parameter J in terms of the energy ε of vertices 1, 2, 3 and 4 of the F model in the following way. The energy per site corresponding to a (111) surface is, from (4.5) and (5.1) neglecting the background constant E_0

$$E_{111}/\mathcal{N} = E_{\infty\times 1}/\mathcal{N} = 4J$$

but a (111) surface is represented by an ordered array of vertices of type 1, so that the total energy of the surface per vertex is ε. One obtains the relation

$$\varepsilon = 4J \,.$$

As seen in section 1.3.1, the roughening transition of the BCSOS model occurs at $k_B T_R = \varepsilon/\ln 2$, so that in terms of J it will result

$$k_B T_R = \frac{4J}{\ln 2} = 5.771 J \tag{5.2}$$

while the peak of the specific heat will be located at

$$k_B T_{Peak} \simeq 0.81 k_B T_R = 4.67 J\,.$$

5.1 The sublattice order parameter

A natural definition, within the BCSOS model, for the sublattice order parameter of (unreconstructed) bcc (100) and fcc (110) surfaces is as follows. Denoting, as usual, the two interpenetrating sublattices which make up the surface as B (black) and W (white), the ground state appears doubly-degenerate and consists of the B sites at height +1 with respect to the W sites at height 0 (or viceversa). For a thermally excited configuration define probabilities of stepping up and stepping down from a given B site to one of its W nearest neighbours, $P_B^+ = 1 - P_B^-$ and P_B^-, where

$$P_B^- = \sum_{\text{odd } m=-\infty}^{+\infty} p_m b_m \tag{5.3}$$

and the sum extends over all the odd B site heights m. The analogous definition holds for P_W^-, where the sum runs over all even heights. Here p_m is the probability to find a surface atom at height m (fixing the flat surface reference height at $m = \frac{1}{2}$), while b_m is the probability of stepping down from an atom at level m. For the F model it is necessary to recall, in Lieb's notation [16], the definition (1.11) of the parameter Δ,

$$\Delta = -\cosh\lambda = \frac{a^2 + b^2 - c^2}{2ab}$$

with $a = b = \exp(-\epsilon/k_B T)$ and $c = 1$ the Boltzmann weights associated with the vertices of the F model. Then, the above probabilities read [142]

$$p_m = const \times \exp\left[-\lambda(m - \frac{1}{2})^2\right] \tag{5.4}$$

and [30]

$$b_m = \begin{cases} \sum_{n=0}^{\infty}(-1)^n \exp[-\lambda n(n+2m-1)] & \text{for } m > 0, \\ 1 - b_{-m+1} & \text{for } m \leq 0. \end{cases} \tag{5.5}$$

The order parameter is then defined through

$$\mathcal{P}_1 = \frac{P_B^- - P_W^-}{P_B^- + P_W^-} \tag{5.6}$$

and takes values +1 (or -1) in the ground state and 0 in the disordered rough phase. At intermediate temperatures this quantity singles out which of the two sublattices' atoms are predominantly present in the surface top layer. The special feature of this quantity is that it vanishes with all its temperature derivatives at the roughening temperature T_R. This behaviour characterizes the sublattice order parameter of the infinite-order roughening transition.

Another definition of order parameter was given by Baxter for the F model[143,144]. In the notation of Baxter, after partitioning the (dual) vertex lattice in two sublattices A and B, an energy $-s$ $(+s)$ is associated to every horizontal (vertical) arrow pointing from an A vertex to a B vertex and $+s$ $(-s)$ if it points from B to A. In this way s has the character of a staggered external field and is the equivalent of the magnetic field of the Ising model as is able to lift the degeneracy of the ground state. Thus the order parameter which corresponds to this field is simply:

$$\mathcal{P}_2 = -\left(\frac{\partial f}{\partial s}\right)_T \tag{5.7}$$

where f is the free energy per vertex. With the introduction of the field, the F model becomes insolvable, except for $T = 2T_R$[143]. However, the order parameter $\mathcal{P}_2$ in zero field is known exactly at all temperatures and is given by[144]

$$\begin{aligned} \mathcal{P}_2(s \to 0^+) &= \left[\prod_{n=1}^{\infty} \tanh(n\lambda)\right]^2 \\ &= \left[1 + 2\sum_{n=1}^{\infty}(-1)^n \exp(-2n^2\lambda)\right]^2 \end{aligned} \tag{5.8}$$

It can be shown at this point that the series expansions for $\mathcal{P}_1$ and $\mathcal{P}_2$ are identical, so that the two order parameters are taken to be one and the same $\mathcal{P}$ which, for uniformity with previous definitions will be called $\mathcal{P}_{B/W}$. No information is available, however, on the behaviour of the staggered field susceptibility, $\chi = -(\partial^2 f/\partial s^2)_T$, except again at $T = 2T_R$ and $s \to 0^+$ where it diverges as $\ln s$. Nevertheless, Baxter[144] has proposed that for $s = 0$ and in the neighbourhood of T_R this susceptibility should obey the scaling ansatz:

$$\chi \sim \mathcal{P}_{B/W}^2 / f_{sing} \tag{5.9}$$

where f_{sing} is the singular part of the free energy. If one considers that $f_{sing} \sim \exp(-\pi^2/\lambda)$ and that

$$\mathcal{P}_{B/W} \sim \lambda^{-1} \exp(-\pi^2/4\lambda) \tag{5.10}$$

one arrives at

$$\chi \sim \lambda^{-2} \exp(\pi^2/2\lambda) \tag{5.11}$$

which implies an extremely strong divergence at T_R, since, near T_R, $\lambda \sim (T_R - T)^{\frac{1}{2}}$. In a finite size lattice, the operative definition of the order parameter has to be modified as follows. Since for the BCSOS model lattice topology implies $P_B^- + P_W^- = \frac{1}{2}$, one gets form 5.6:

$$\mathcal{P}_{B/W} = 4P_B^- - 1\,.$$

The stepping down probability P_B^- can be evaluated from the thermal and site average of the local $p_B^-(\mathbf{R}_i)$ which, for a given configuration and B site i, is given by:

$$p_B^-(\mathbf{R}_i) = \frac{1}{4}\left[1 + m_B(\mathbf{R}_i) - \frac{1}{4}\sum_{\mathbf{D}} m_W(\mathbf{R}_i + \mathbf{D})\right] \tag{5.12}$$

where $\mathbf{D}$ runs over the four neighbouring W sites. Taking the site average, $\mathcal{P}_{B/W}$ reads (the absolute value ensuring a meaningful averaging procedure):

$$P_{B/W} = \langle \mathcal{P}_{B/W} \rangle = \left\langle \frac{2}{\mathcal{N}} \left| \sum_B m_B - \sum_W m_W \right| \right\rangle$$

where $\mathcal{N}/2$ is the number of B (or W) sites and the angular brackets denote thermal (Monte Carlo) averaging. This is exactly the expression of eq. (4.20); the related susceptibility is given by an expression like (4.21).

5.2 Exact results verified

Six different lattice sizes, $N_x = N_y = N = 10$, 16, 20, 24, 28 and 32 are employed in the Monte Carlo simulation to permit a meaningful finite-size scaling analysis.

In figure 5.1 the peculiar behaviour of the specific heat is reported: no singularity of any kind is present at the transition temperature $T_R = 5.771$ (in units of J), while a rounded peak appears around $T_{Peak} \simeq 4.67$, as theoretically predicted. Thus, the main feature of the specific heat is the absence of any divergence as seen in the practically null dependence on the system size. This same characteristic may be encountered again in figure 5.2 which represents the behaviour of a quantity which actually has no great interest in itself here but that will prove of wide utility especially in Chapter 7, the first derivative of the specific heat (from eq. (4.13)). The roughening transition in the BCSOS model is of infinite order, that is the free energy shows a non singular behaviour at T_R and no singularity in any of its derivatives will appear which, in a Monte Carlo calculation on finite system sizes will result in no appreciable difference from one size to another (for large enough sizes). From fig. 5.1 and 5.2 one thus can also make sure of the fact that the infinite system critical behaviour is already reached for $N \approx 20$, and no other differences apart from statistical fluctuations are to be found for larger size values.

A more quantitative confirmation that meaningful information can be drawn from not exceptionally large systems is the procedure to extract the roughening transition temperature T_R from the analysis of the height fluctuations. This

should cast aside all the legitimate doubts that can arise, for example, after ref. [145] where it is shown that spurious finite size effects connected with the ± 1 height difference restriction could mask the asymptotic behaviour in a numerical simulation. The height fluctuations, defined in eq. (1.9), are shown in figure 5.3 as a function of temperature for different sizes, and in fig. 5.4 as a function of the logarithm of the size for various temperatures. The first graph shows a marked size effect in the intermediate and high temperature regions, which is reflected in the second graph where it is clear that for low temperatures the quantity is independent of the size, while the slope of $\langle \delta h^2 \rangle$ vs. $\ln N$ increases for higher temperatures. This behaviour is not only consistent with what expected for the BCSOS model, but provides a method of establishing whether a roughening transition takes place in the system, allowing for the estimate of T_R. In fact, from equations (1.7) to (1.10) it is known that the height fluctuations of an infinite system remain finite for $T < T_R$, diverging instead logarithmically with the size for $T \geq T_R$. In a finite system, the divergence of the correlation length ξ (which causes this behaviour) saturates to the value of the linear size of the system. Nonetheless relevant information may be extracted from the universal properties of the quantity $K(T)$ of formula (2.6), which for $T \to T_R^+$ behaves like (see formula (1.8))

$$K(T) = \frac{1}{\pi^2} + C\sqrt{T - T_R} \tag{5.13}$$

The quantity $K(T)$ is nothing but the slope of $\langle \delta h^2 \rangle$ vs. $\ln N$, and is shown in fig. 5.5 At first sight, $K(T)$ behaves as expected, since it increases with temperature and assumes the critical value $1/\pi^2$ at the transition temperature $T_R = 5.771$. A more quantitative analysis is performed by plotting the quantity $\left[K(T) - \frac{1}{\pi^2}\right]^2$ vs. T, since, from eq. (5.13)

$$\left[K(T) - \frac{1}{\pi^2}\right]^2 \simeq C'\,(T - T_R) \tag{5.14}$$

The linear behaviour of the data in fig. 5.6 for $T > T_R$ is well reproduced, and extrapolation of this form yields

$$T_R = 5.66 \pm 0.11 \tag{5.15}$$

which is only above 2% below the exact value. Longer Monte Carlo runs would certainly provide better accuracy. Possible finite size effects of ± 1 height restriction thus should not affect in a relevant way the determination of T_R. A somewhat larger error is found for the coefficient C of eq. (5.13) which is found to be $(4.3 \pm 0.7) \times 10^{-2}$, against an exact value of 3.2×10^{-2}: this may in fact be related to these size effects.

Notice that although $K(T)$ can be derived from the above mentioned finite-size analysis only for $T > T_R$, it is convenient to extend the fitting also to lower temperatures. In order to produce plots like fig. 5.5 – 5.6, this has indeed been extended to all temperature values where a more careful analysis should instead be adopted starting from expressions like (1.6). Nonetheless, since ξ diverges at T_R, right below T_R there is a range of temperatures where $\xi \gg L$, L being the system size adopted. Within this range $\langle \delta h^2 \rangle$ is already logarithmic in L and the applied fitting is legitimate.

In figure 5.7 the Monte Carlo results for the temperature dependence of the order parameter $P_{B/W}$ is reported. For this quantity, the infinite system critical behaviour (also reported for convenience) is approached slowly, like $L^{-\frac{1}{2}}$ at T_R as finite-size scaling would suggest, when the size $L = Na$ (a being the lattice spacing) is increased. Below T_R, however, one may attempt to fit the largest size data with the infinite-system asymptotic form, eq. (5.10). We select a temperature window $0.70 < T/T_R < 0.88$ in order to avoid finite-size effects in the immediate neighbourhood of T_R, yet capturing the critical region temperature dependence. Our fitting is consistent with the form (5.10), yielding an exponential $\exp(-A/(T_R - T)^{\frac{1}{2}})$ having $A = 2.50 \pm 0.15$, which compares well with the exact value $A = \frac{\pi^2}{2\sqrt{2}\ln 2} = 2.517\cdots$. Moreover, the same fitting yields a value of $T_R = 5.73 \pm 0.08$, to be compared with 5.771 of eq. (5.2).

All these results for the BCSOS model show that the adopted procedure, both for the simulation program and the successive data analysis seems to work well, and can thus be pushed towards unexplored regions.

5.3 The staggered field susceptibility

Having checked the method against exact results, it is now possible to report novel data for the staggered field susceptibility χ, as shown in figure 5.8. In the infinite system, χ diverges at T_R remaining infinite above. For a finite lattice, we find a divergence with the size of the lattice typical of infinite-order transitions of the form

$$\chi(L,T) \sim L^{\omega(T)} \tag{5.16}$$

with a temperature-dependent unknown exponent ω. Exactly at T_R, Baxter's ansatz, eq. (5.11), would imply (barring logarithmic corrections)

$$\omega(T_R) = 1 \tag{5.17}$$

This follows from the asymptotic form $\xi \sim \exp(\pi^2/2\lambda)$ for the correlation length which becomes of the order of L in a finite system at T_R. The data are compatible with $\omega(T_R) = 1$ (see figure 5.9). Furthermore we observe that the peak in $\chi(L,T)$ (which might be taken as a measure of T_R) shifts very slowly towards T_R, like $(\ln L)^{-2}$ to be precise, as L is increased. In turn, this whole procedure might represent a way of determining the sublattice disordering temperature in models of the BCSOS type where the transition point is unknown. Indeed, χ is the only sensible diverging quantity in an otherwise smooth phase transition.

The exact and finite-size behaviour of the sublattice order parameter and related staggered susceptibility of the BCSOS model have thus been examined, together with the verification of the validity of Baxter's conjecture for the asymptotic diverging behaviour of χ at T_R. Sublattice disordering and roughening occur together at $T = T_R$, and with the same Kosterlitz-Thouless behaviour, in this model. The sublattice disordering in the BCSOS model is driven by the thermal excitation of steps which are responsible for roughening. However, the definition of sublattice order parameter and susceptibility, as well as the Monte Carlo finite size scaling method which allows for a separate study of sublattice disordering and of roughening, can now be taken over to more realistic surface models. For many

of these models the two phenomena should become totally distinct. This is the scenario addressed in the following chapters.

5.4 The exponent ω

The temperature dependent exponent ω is known at T_R if the Baxter's conjecture is, as it seems, verified. However, a more careful analysis leads to a simple prediction for the exact behaviour of this exponent in the whole interval $T > T_R$.

Considering the planar six vertex lattice, that is a square two dimensional lattice with arrows on the bond which satisfy the ice-rule, if the lattice sites are labeled by the index $\mathbf{R} = (n, m)$, the arrow-arrow correlation function $G_{AA}(R)$ is defined as the thermal average of the product of two arrows separated by a distance $R = |\mathbf{R}|$. Its evaluation in full generality is extremely difficult, however when the parameter Δ (eq. (1.11)) vanishes (condition known as the "free fermion" case), which is equivalent in the F model to the condition $T = 2T_R$, its exact evaluation is possible[146]. In this case its asymptotic behaviour for large R reads

$$G_{AA}(R) \sim \frac{2}{\pi^2 R^2}\left[\cos\pi(n-m) + \frac{m^2-n^2}{r^2}\right]. \tag{5.18}$$

In particular, for two arrows belonging to the same row (i.e. $m = 0$: notice, moreover, that the square arrow lattice is 45° degree rotated with respect to the BCSOS site lattice), eq. (5.18) simplifies to

$$G_{AA}(n) \sim \begin{cases} 0, & \text{if } m \text{ even} \\ -\frac{4}{\pi^2 n^2} & \text{if } m \text{ odd} \end{cases} \tag{5.19}$$

where it is evident that this arrow-arrow correlation function oscillates from odd to even sites, and it decays like R^{-2} at $T = 2T_R$. As Youngblood, Axe and McCoy[147] noticed, the rapidly oscillating contributions decay more slowly than R^{-2} for $T < 2T_R$ till, as T tends towards T_R from above, they will become increasingly important. Ultimately at $T = T_R$, where the transition to a state of antiferroelectric long range order takes place, the discreteness of the lattice will be essential. Unfortunately, for $T \neq 2T_R$ no exact expression is available for $G_{AA}(n)$.

Nonetheless its asymptotic behaviour is known from a calculation employing the quantum inverse scattering method [148] by Bogoliubov, Izergin and Korepin, which leads to the following generalization of eq. (5.19)

$$G_{AA}(n) \sim \frac{K(T)}{n^2} + (-1)^n \frac{K'(T)}{n^{\theta(T)}} \tag{5.20}$$

valid in absence of ferroelectric long range order (when the vertical polarization is zero, that is for any temperature in the F model in the absence of a vertical electric field coupled to the arrows).

It is important to note that the coefficient in front of the non-oscillating term in eq. (5.20), $K(T)$, is exactly the same coefficient multiplying the logarithmic divergence of the height-height correlation function, eq. (1.6) (this correlation function is readily obtained by a suitable integration of (5.20)), and Bogoliubov *et al.* [148] main result is the relation between the exponent θ and K, that is

$$\theta(T) = \pi^2 K(T)\,. \tag{5.21}$$

The predictions of Youngblood *et al.* are thus confirmed by the behaviour of eq. (5.20) in the range $T_R < T < 2T_R$ with the use of eq. (5.21).

The staggered susceptibility χ is related in a simple way to the arrow-arrow correlation function through the usual fluctuation dissipation formula which reads

$$\chi = \int_a^L dR^2 G_{Stagg.}(R)\,. \tag{5.22}$$

Here a is the lattice spacing acting as a small distance cutoff, L is the linear system size and a factor $(-1)^n$, due to the need of a staggered expression, has to be inserted as follows: $G_{Stagg.}(n) = (-1)^n G_{AA}(n)$. The resulting formula written in the discrete limit, is (apart from irrelevant numerical constants)

$$\chi \sim \lim_{n\to\infty} -K(T) \sum_{j=1}^{n} \frac{(-1)^j}{j} + K'(T) \sum_{j=1}^{n} \frac{1}{j^{\theta(T)-1}}$$

where in the asymptotic limit the first series is convergent to a constant, and the second becomes $K'/n^{\theta(T)-2}$. The susceptibility becomes, again in the continuum limit,

$$\chi(L,T) \sim A(T) + \frac{B(T)}{L^{2-\theta(T)}} \tag{5.23}$$

with $A(T)$ and $B(T)$ functions of temperature not relevant for the present study. A comparison with eq. (5.16) yields immediately the relation

$$\omega(T) = 2 - \theta(T) = 2 - \pi^2 K(T), \qquad T > T_R \tag{5.24}$$

which gives the behaviour of the exponent ω as a function of temperature in the whole interval $T > T_R$ (for $T < T_R$, ω is not defined since the susceptibility is not a divergent quantity).

The Monte Carlo simulation data are in very good agreement with such formula and the resulting exponent $\omega(T)$ is shown as a function of temperature in fig. 5.9. This is compared with the Monte Carlo data for $2 - \pi^2 K(T)$ and the exact behaviour of this quantity, which from the exact solution of the BCSOS model reads

$$K(T) = \frac{1}{\pi \arccos \Delta(T)} \tag{5.25}$$

with Δ given by eq. (1.11). The simulation data compare well with the exact results, though maybe the errorbars are a little underestimated. Finite-size effects in fact may show up, as already noticed, in the constants, but not in the square root behaviour of a quantity like $K(T)$ just above T_R.

Instead of resorting to the quantum inverse scattering method, eq. (5.24) could probably be obtained through some more phenomenological approach including scattering quantities[149] and work is currently in progress in this direction. It is nonetheless interesting to further investigate the implications contained in eq. (5.24). Since the function $K(T)$ increases with temperature, one gets for the exponent $\omega(T)$

$$\begin{aligned} K(T=T_R) &= \frac{1}{\pi^2} & \omega(T=T_R) &= 1 \\ K(T=2T_R) &= \frac{2}{\pi^2} \quad \rightarrow & \omega(T=2T_R) &= 0 \\ K(T=\infty) &= \frac{3}{\pi^2} & \omega(T=\infty) &= -1 \end{aligned} \tag{5.26}$$

which confirms Baxter's ansatz for $T = T_R$ and shows that no divergence, at least of the power-law type, is to be found for $T = 2T_R$ (in fact for $T = 2T_R$ formulæ (5.19) and (5.22) give $\chi(L, 2T_R) \sim \log L$, and the Monte Carlo data are compatible with this kind of behaviour). What is more, (5.26) shows that no further divergence with size is to be expected in the staggered susceptibility for $T > 2T_R$. Hence, this quantity shows a singular behaviour only in the range $T_R \leq T < 2T_R$, and no other singularities below T_R or above $2T_R$. At first sight, this result may appear strange, but it may be reconciled with known concepts of the theory of liquids, like that of a "disorder point" in a $P - T$ phase diagram above the critical point. Though it is possible to continuously vary the thermodynamical variables and succeed in passing from the liquid to the gas phase with no phase transition, yet this path still crosses a line of disorder points (on the prolongation of that connecting the triple point to the critical point), below which correlations are oscillating, that is more liquid-like, and above which they show instead a monotonic, gas-like behaviour. This is exactly what is happening in this case, since the point $2T_R$ is known as a disorder point of the F model. A quick inspection of eq. (5.20) together with (5.24) shows that below $2T_R$ the dominant correlations are the oscillating ones ($\theta < 2$), while above $2T_R$ the monotonic ones prevail ($\theta > 2$).

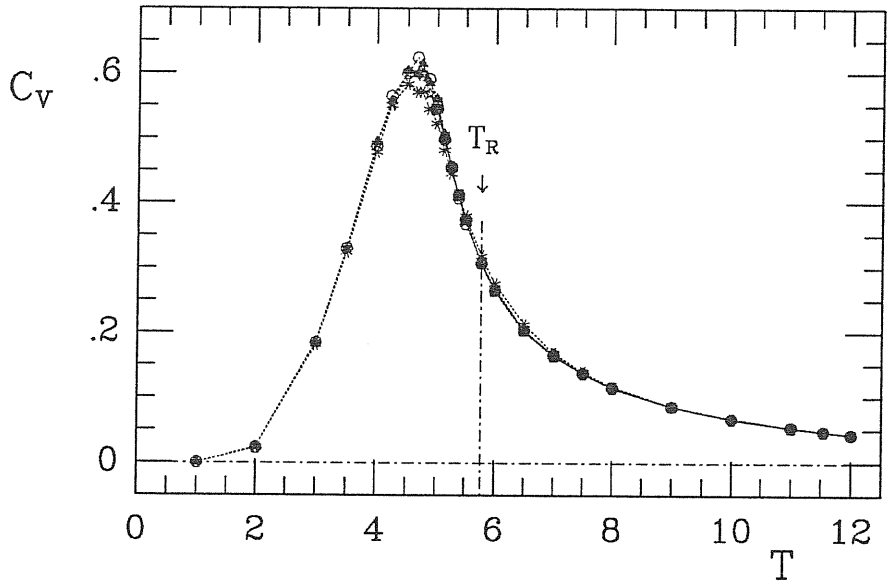

Figure 5.1. Specific heat vs. temperature in the BCSOS model for six system sizes. The arrow indicates the position of the roughening temperature. In this and all subsequent figures, temperatures are expressed in units of J.

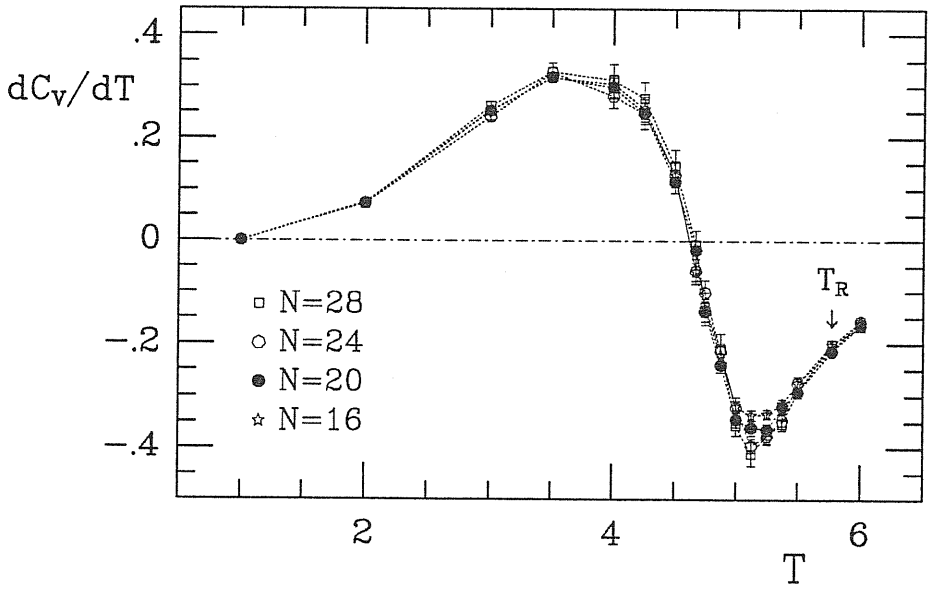

Figure 5.2. The first derivative of the specific heat vs. temperature in the BCSOS model.

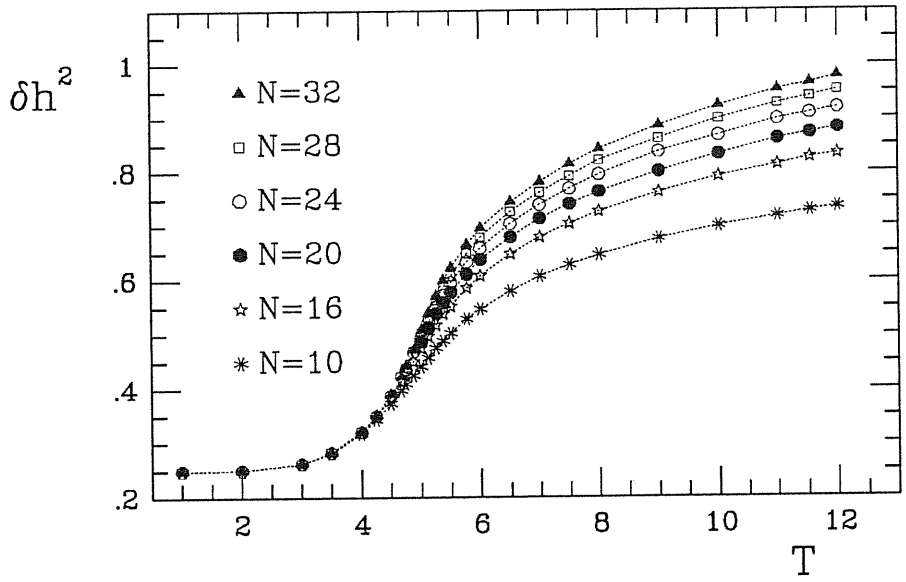

Figure 5.3. Finite size behaviour of the height fluctuations vs. temperature in the BCSOS model. In this and all subsequent figures, no errorbar is plotted if smaller than the point size.

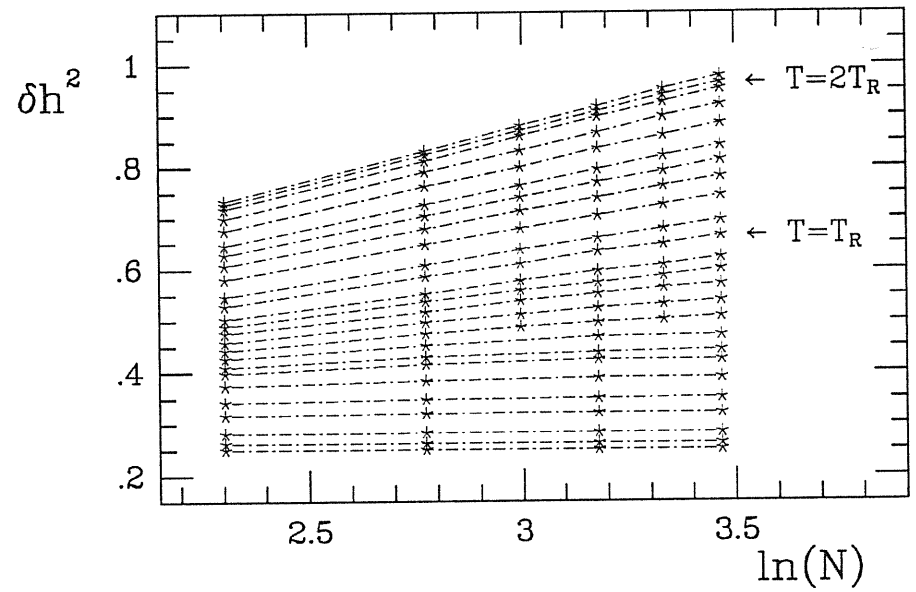

Figure 5.4. Height fluctuations vs. logarithm of the size in the BCSOS model for the temperatures investigated. The lines plotted should be straight only for $T \geq T_R$.

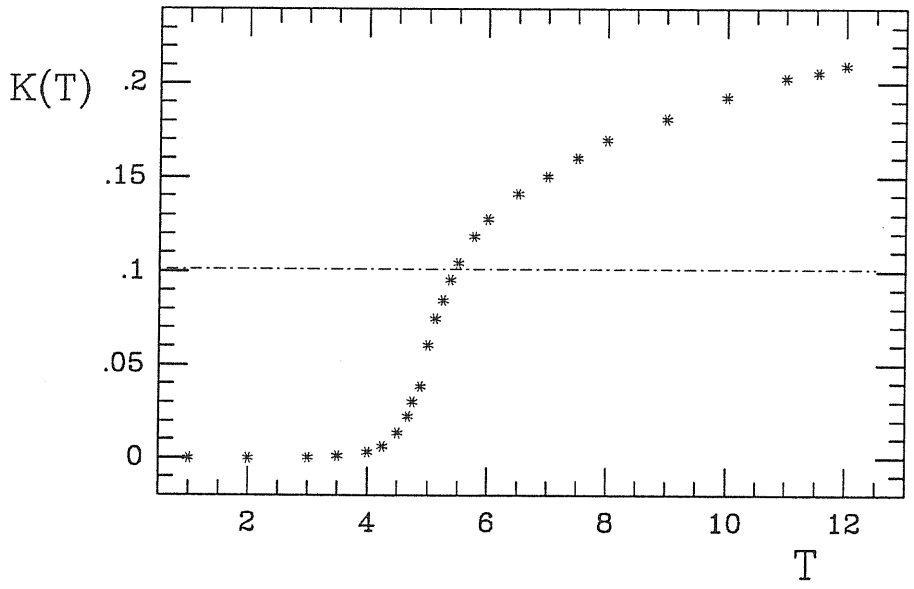

Figure 5.5. $K(T)$ vs. temperature in the BCSOS model. The line indicates the position of the universal value $1/\pi^2$.

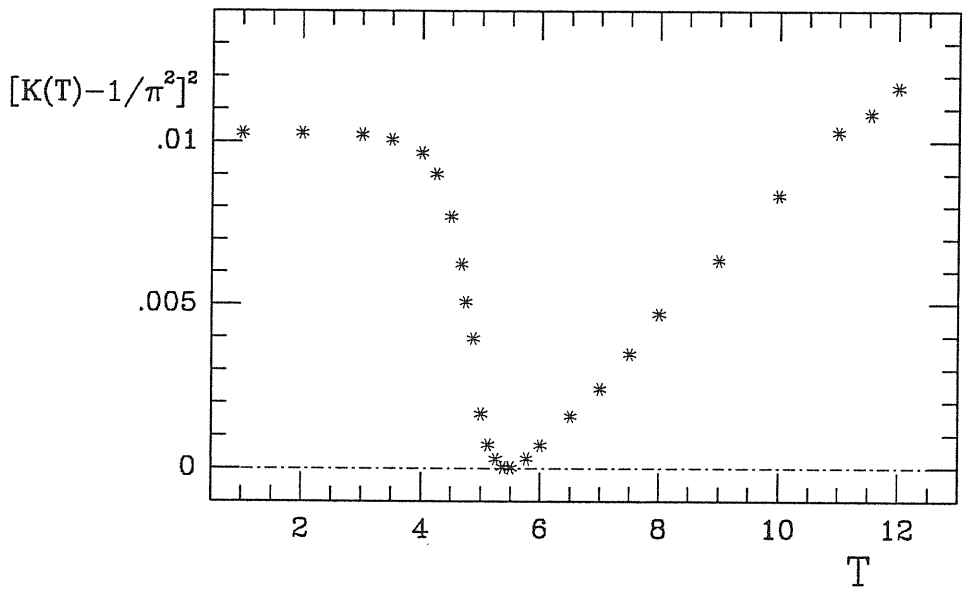

Figure 5.6. $\left[K(T)-1/\pi^2\right]^2$ vs. temperature in the BCSOS model.

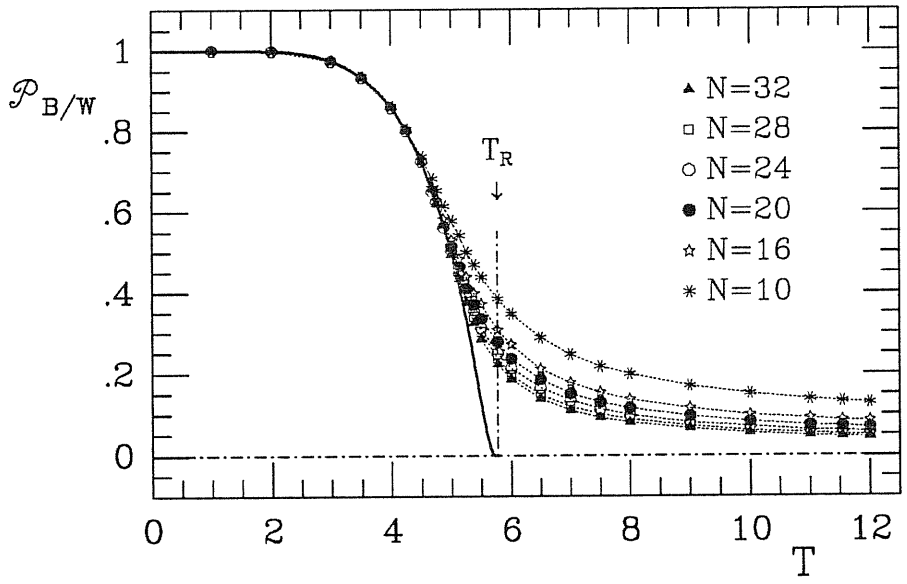

Figure 5.7. Sublattice order parameter in the BCSOS model. The solid line represents the infinite system exact behaviour.

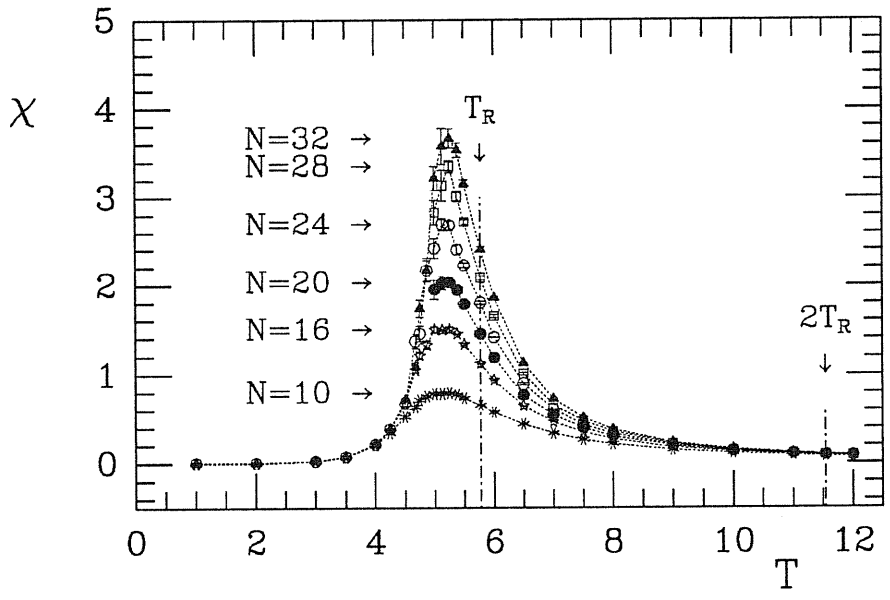

Figure 5.8. Staggered field susceptibility in the BCSOS model.

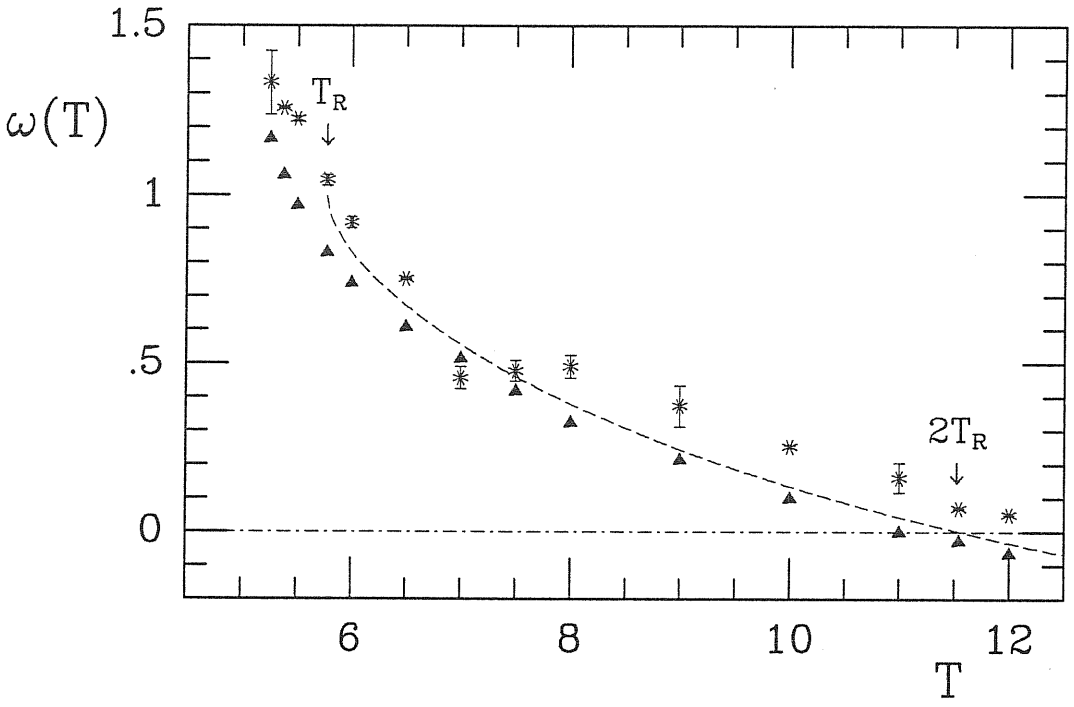

Figure 5.9. The exponent ω as a function of temperature. The asterisks are extracted from a fitting of the staggered susceptibility, the triangles are expression of the formula $\omega(T)=2-\pi^2 K(T)$ (with $K(T)$ of figure 5.5), the dashed line is obtained from the exact behaviour of $K(T)$.

Chapter 6

Gold(110)

In this Chapter the Monte Carlo simulation results for our BCSOS model simulating gold(110) are presented, and two separate phase transitions are detected to take place on the surface[121].

6.1 Deconstruction and roughening

A strong indication for a second order phase transitions taking place on the surface is provided by the temperature behaviour of the specific heat data, as well as of the order parameter and the related susceptibility, eq. (4.12), (4.18) and (4.21).

The specific heat data are very different from those obtained for the BCSOS model, especially for the presence of a sharp peak around $T \sim 3.0$, in the rapid rise of the peak height as the system size increases (suggesting a divergent behaviour for $N \to \infty$), and in the concomitant narrowing of the peak width (fig. 6.1). The presence of a critical transition is corroborated by the behaviour of the (2×1) order parameter and related susceptibility. The former (fig 6.2), starting from the value 1 of the ordered missing-row phase, shows a sudden decrease in the same critical temperature region, and vanishes for higher temperatures. Finite-size effects, as usual, tend to smooth down an otherwise sharp behaviour, as it is apparent from the fact that the larger the size the steeper is the drop and the lower is the value approached by the parameter at high temperatures. The susceptibility $\chi_{2\times1}$ (fig. 6.3) shows a similar feature as the specific heat around the same temperature, that is a peak rapidly increasing with size. The evidence presented here is therefore

suggestive of a second order phase transition. A naive plot of the maximum of C_V and of $\ln \chi_{2\times 1}$ versus $\ln L$ reveals the characteristic exponents of the 2D Ising universality class (figure 6-4 (a,b)). Indeed, from the finite-size scaling theory of critical phenomena[150], the following behaviour is expected

$$\begin{cases} C_V(L,T_D) &= A_1 L^{\alpha/\nu}, & \text{non} - \text{Ising} \\ C_V(L,T_D) &= A_2 + A_3 \ln L, & \text{Ising},\ \alpha = 0 \end{cases} \tag{6.1}$$

and

$$\chi_{2\times 1}(L,T_D) = A_4 L^{\frac{\gamma}{\nu}} \tag{6.2}$$

at the infinite system critical point temperature T_D (where D stands for "deconstruction"), with A_1, A_2, A_3, A_4 constants. The position of the χ-peak seems to be practically independent of the size, and thus it is possible to extract the behaviour of eq. (6.1) and (6.2) from the Monte Carlo data with an exponent ratio $\frac{\gamma}{\nu}$ consistent with $\frac{7}{4}$, and with the logarithmic trend in C_V. This unmistakably characterizes a 2D Ising transition. In order to further check the finite-size scaling analysis, the phenomenological renormalization method introduced by Barber and Selke[151] is used. For a critical quantity $Q(L,T)$ characterized by an exponent ω, in its size divergence, this method predicts a "crossing of the curves", each defined for a pair of sizes L_1, L_2:

$$f^Q_{L_1 L_2}(T) = \frac{\ln\big(Q(L_1,T)/Q(L_2,T)\big)}{\ln(L_1/L_2)} \tag{6.3}$$

at the point $(T_D, \frac{\omega}{\nu})$ for $L_1, L_2 \to \infty$, with T_D the infinite system critical temperature. As seen in figure 6-5 (a,b), this method leads to the critical temperature

$$T_D/J = 2.903 \pm 0.015 \tag{6.4}$$

from both C_V and $\chi_{2\times 1}$, the latter with an exponent

$$\frac{\gamma}{\nu} = 1.8 \pm 0.2, \tag{6.5}$$

which is compatible with $\frac{7}{4}$ and is associated with the 2D Ising deconstruction transition in the model proposed for Au(110).

A similar analysis is performed for $P_{B/W}$ and its related susceptibility. At first sight, these two quantities seem to behave exactly in the same as $P_{2\times1}$ and $\chi_{2\times1}$, and this prediction is confirmed by the usual finite-size scaling analysis which again provides Ising values for the exponent of the diverging susceptibility and an estimation of the transition temperature coinciding, within error bars, with eq. (6.4). This is an important indication of the nature of the transition, where sublattice disordering, monitored by $P_{B/W}$ occurs together and with the same critical behaviour of deconstruction, ruling out therefore some of the scenarios proposed in Chapter 3 and pointing in the direction of a loss of long-range order by proliferation of steps between (2×1) terraces, that is in the direction of scenario (iv).

The indication for a second phase transition of infinite order at a slightly higher temperature comes from the analysis of the height fluctuations. The procedure is the same adopted to determine the occurrence of a roughening transition and to localize T_R in the BCSOS model, given in Section 5.2 This begins by considering the plot of $\langle \delta h^2 \rangle$ vs. T for different sizes (fig. 6.8) and vs. $\ln L$ for different temperatures (fig 6.9). The data for $\langle \delta h^2 \rangle$ vs. T show a clear size effect, not only for T sufficiently high ($T \geq 3$), but also for lower temperatures, where the size effect appears to be reversed. This implies a peculiar behaviour of the slope $K(T)$ of the straight lines $\langle \delta h^2 \rangle$ vs. $\ln L$, as shown in fig. 6.10. Starting from zero slope (no size effect), negative values are first seen ("reversed" size effect), followed by positive ones, which slowly increase for higher temperatures. Finally, from figures 6.10 and 6.11 it can be seen that the universal Kosterlitz-Thouless features for a roughening transition, both the value of $K(T)$ at the transition temperature and the asymptotic behaviour characterizing the rough phase are attained in the case of Au(110) too, for $T > T_R$ where

$$T_R = 3.09 \pm 0.04\,. \tag{6.6}$$

Therefore, the roughening transition takes place at a slightly, but definitely higher temperature than reconstruction (about 6 % above, in reasonable, although perhaps fortuitous, agreement with data reported by recent experiments[56]). This

temperature difference is well beyond the statistical errors, thus confirming two separate transitions for our model of Au(110).

6.2 Scattering intensities results

The correlation properties of the system can best be evidenced through the behaviour of the scattering intensities. In particular, these can shed light on the nature of the intermediate phase which exists between T_D and T_R.

Important effects of shift and broadening are expected in the deconstructed scattering pattern above T_D. Both shift and width depend on q_z and T, the shift being particularly interesting as it is related to the incommensurability. This can appear due to the mismatch arising from surface areas separated by 1×1, 3×1, 4×1 or higher reconstruction defects, seen as pairs of bound steps (as envisaged in previous works by Jug and Tosatti[124]), as well as from individual unbound steps.

The nomenclature of the peaks is the same introduced in Section 1.4.1. In particular, the half integer order peaks monitor the deconstruction transition, the integer order peaks are instead related to roughening. The scattering intensities are obtained by means of Monte Carlo simulations on the largest system available, $N = 32$, with a choice of $p = q_z a_z = 0$ for atom scattering and $p = \pi/8$ for X-rays scattering, and a value of the intensity attenuation factor $\mu_I = 2.7 \cdot 10^{-5}$ taken as typical for a 10 keV beam on Au[31]. This selection of values for the perpendicular momentum transfer is due to the fact that for $q_z = 0$ there exist an exact relation between the atom scattering reconstruction peaks and the (2×1) order parameter (see Appendix), whereas the $q_z = 0$ case lies outside the range of validity of the X-rays kinematic treatment, therefore the nearest to zero value available for q_z, i.e. $q_z a_z = \pi/8$ has been chosen. In the following analysis, the y component of the parallel momentum transfer has always been kept equal to zero, that is $Q_y = 0$. With this choice, and following the notation expressed in eq. (1.48), in the range $0 \leq \frac{n_x}{N_x} \leq 2$, reconstruction peaks are those labeled by $(\frac{1}{2}\,0)$, $(\frac{3}{2}\,0)$, principal peaks are $(0\,0)$, $(2\,0)$ and the only superlattice one is located at $(1\,0)$.

Figure 6.12-(a) present the X-rays scattering at a temperature just below T_D, when principal and reconstruction peaks are present (incoherent scattering being

one order of magnitude weaker, as is the case for the intensity of the superlattice peak at this value of q_z). Figure 6.12-(b) reports the pattern at a temperature intermediate between T_D and T_R. As can be observed, the $(\frac{1}{2},0)$ peak intensity is strongly reduced with respect to the value just below T_D and has merged with the incoherent background, which is at its maximum at T_D. The separation between coherent and incoherent contributions is carried out in figure 6.12-(b); the coherent intensity is non-zero owing to finite-size effects in this range of temperature. The scattering pattern is fitted to the sum of five specular Lorentzians, of adjustable height, width and, for reconstruction, centre. The position of this scattering peak centre gives the shift with respect to the commensurate $(\frac{1}{2},0)$ spot, hence a measure of the surface modulation. Figure 6.12-(c) gives the situation above T_R (when the coherent reconstruction peak has merged into the background).

The patterns are very similar in the case of atom scattering. Figures 6.13-(a,b,c) present the data for the $(\frac{1}{2},0)$ peak height, incoherent width and its shift, in the case of atom scattering. The coherent (Bragg) peak height is seen to cut off more sharply near T_D than the total, including incoherent scattering from critical fluctuations. The practical difficulty in subtracting off the latter may have led in the past to an overestimate of T_D, as figure 6.13-(a) clearly demonstrates. As for the width of figure 6.13-(b), the general order of magnitude and linear temperature dependence is in agreement with experimental data from atom scattering for $T > T_D$ as reported by Sprösser et al. for Au(110) at $q_z \simeq 0$ [56]. The linear dependence upon $T - T_D$ implies for the correlation length of in-plane fluctuations an exponent $\nu = 1$, which again agrees with the Ising-like nature of the deconstruction transition. Notice that in the simulation the value of the incoherent width is bounded from below owing to finite-size effects; for $L \to \infty$ it should vanish at T_D. The basically negligible shift in the position of the peak centre shown in figure 6.13-(c), on the other hand, indicates virtually no modulation as seen by atoms towards lower **Q**-values, in the temperature range $T_D < T < T_R$.

Figure 6.14-(a) reports Monte Carlo predictions for the X-ray scattering intensities. The half-order peak width (figure 6.14-(b)) again shows a linear dependence on temperature, as for atom scattering, while the shift (figure 6.14-(c)) is a monotonically decreasing function of T and, while still small, is substantially larger than for atom scattering. This shift clearly denotes proliferation of defects of higher-order reconstruction types, however its smallness may explain why it has so far

not observed in Au(110)[39].

6.3 Discussion

The model proposed in Hamiltonian (4.1) has proved capable of describing the structure of a reconstruction fcc(110) surface and to reproduce both (2×1) missing-row deconstruction and the roughening phase transitions. With an appropriate choice of parameters this model appears to be a possible realization of the physics of Au(110) (and perhaps of Pt(110)).

If the value of $J = 1005.2$ K is taken at face value, these results would imply a deconstruction transition occurring at $T_D \simeq 2900$ K, followed by a roughening transition at $T_R \simeq 3100$ K, for Au(110). Both values are obvious overestimates of the reality, a fact that calls for a few words of caution in the use of the $T = 0$ model parameters, as suggested by the glue model. Conclusions of a study by Bernasconi[118] indicate that the glue model energy parameter J may be simply too large. In turn, this may be related to the general overestimate of relaxations already noted for the (2×1) missing-row surfaces. Apart from this, one should note that a renormalization of the defect energy at temperatures $T > 0$ takes place owing to two separate mechanisms which cannot be easily included in the derivation of the preceeding Sections, which relies on a rigid lattice model. i) Relaxation effects near defects may cause a lowering of the effective surface energy, and hence of the value of J. ii) Diffusion of atoms along the missing-row direction, possibly enhanced by vacancy formation[60], also implies a dynamical renormalization of the effective model parameters at temperatures close to disordering. Both mechanisms hint to a lowering of J. Were one to fix J at, say, $J = 250$ K, this would provide a value of T_D and T_R in reasonable agreement with the experiments[56].

This discrepancy on energy scales however does not invalidate the information obtained from these Monte Carlo results on the interplay between roughening and deconstruction, and the existence of two distinct phase transitions: an Ising-like deconstruction transition and a Kosterlitz-Thouless roughening.

Amongst the different scenarios proposed by Bernasconi[118] and reviewed in Chapter 3 for the above mentioned interplay, scenario (v) is obviously ruled out, as it also happens from the experimental point of view for Au(110) and maybe for

Pt(110). It is interesting now to investigate which of the other previously discussed cases (i)-(iv) applies to the results reported before, and to try to understand why.

$T = 0$ calculations of the energetics of the most common defects on the surface provide for the (3×1) wall energy a value around 24% below that of a (1×1) wall, with the choice of parameters of eq. (4.6). This is in accordance with a careful inspection of some surface configurations as obtained by Monte Carlo snapshots in the intermediate temperature region between T_D and T_R (see figures 6.15 – 6.17), as well as with the shift in the half integer order peaks, which clearly indicates a proliferation of (3×1) steps against (1×1) steps. This feature signals a small, but definitely non zero, chirality, in the sense of den Nijs, towards high order facets formation. This is also in reasonable agreement with experiments, where such a shift is not observed between T_D and T_R, due maybe to its smallness, but is actually observed above T_R (like in Keane *et al.* [39] case), and it shows to be in the right "3×1" direction. Not to mention, of course, the STM experiments of Binnig *et al.* [50] where (3×1) facets are predominant defects on the (2×1) reconstructed surface. Scenario (i), suggesting a proliferation of compact (1×1) domain walls, could thus be safely excluded.

The main point is now to elucidate the following problem: the structure of Hamiltonian (4.1) assigns the same $T = 0$ energies for a pair of (3×1) infinitely long steps, either parallel or antiparallel, and for a 4×1 step. Stabilization of a flat, but disordered phase, requires instead some effective interaction between steps, either a repulsion of antiparallel steps or an attraction for parallel steps, therefore this can be provided in the model proposed only by entropic reasons, due to the meandering of the steps and to the intermediate excited states encountered when one of them is displaced to a neighbouring row. A similar mechanism is present, for example, in the case of Villain and Vilfan [122], where also at the point of the phase diagram corresponding to the situation $E_{Wall} = 2E_{Step}$, two separate transitions can still occur (see Section 3.4 for discussions). This mechanism is absent in the phase diagram proposed by den Nijs [120], fig. 3.6, only because he neglects anisotropy and assumes zero chirality, which takes an essential role in the delicate energetic balance for the intermediate excited states.

However, the physics showed by the model of the present thesis can be better attributed to scenario (iv), than to scenarios (i)-(iii), mainly for two reasons. First, if one applies (as Bernasconi does) the analysis of Villain and Vilfan with the choice

of defect energies assigned by Hamiltonian (4.1) with the parameters (4.6), it turns out that the step free energy vanishes before that of a compact or extended 3x1 wall. So the model by Villain and Vilfan predicts that steps are unbound at the point of the parameter space explored. Moreover, the order parameter $\mathcal{P}_{B/W}$ behaves as $\mathcal{P}_{2\times1}$, i.e. it vanishes at T_D. Its susceptibility also has a maximum at T_D, the intensity scaling with size in an Ising fashion.

The first point is maybe not conclusive, since an analysis *á la* Villain and Vilfan is obviously oversimplified. It gives useful indications on the structure of the phase diagram but it probably cannot accurately locate the positions of the critical lines. The second point is instead more convincing, and strongly suggests the presence of the DOF phase, since the deconstructed phase of scenario (iv) is the only flat phase able to destroy $\mathcal{P}_{B/W}$ as well as $\mathcal{P}_{2\times1}$. The problem of stability of such a DOF phase is however not been solved yet. The discussion which will follow is an attempt towards its elucidation[118].

When the backbone typical of the DOF phase appears, because of the vanishing of the step free energy, the six vertex model defined on the backbone must be in its antiferroelectric phase. This occurs provided the Boltzmann weight $a_5 = \mathrm{e}^{-\beta\varepsilon_5}$ of vertex 5 is sufficiently larger than those of vertex 1 and 3, a_1 and a_3.

The four "arms" of the vertices are made up of (3×1) steps. Since, however, a step running perpendicular to the the "hard" $[1\bar{1}0]$ direction is much more costly than one running parallel to it for the number of energetically expensive broken bonds (thus very rarely present on a real surface), the vertex arms will never lie parallel to each one of the two directions but will form an angle with them. In the DOF phase vertex 1 represent the intersection between two parallel steps, i.e. a 4×1 step; vertex 5 represents the intersection between two antiparallel steps, i.e a (3×1) compact wall; vertex 3 corresponds to exchange of sign of two antiparallel steps at their crossing, and requires the breaking of three bonds along $[1\bar{1}0]$ (fig. 6.18). Because of the large bond-breaking energy, vertex 3 is energetically much more costly than vertex 5. Hence, it seems possible to have $a_1 < a_5$ and stabilize the DOF phase, just by requiring a larger energy of the 4×1 step with respect to the (3×1) wall (the symmetric version of the six vertex model $a_1 = a_2$, $a_3 = a_4$, $a_5 = a_6$ is assumed).

In reality a vertex is presumably a rather complex object, instead of a point as assumed so far. Schematically, we may think of a region of radius R, large

compared with the lattice parameter a, but small compared with the correlation length $\xi_{B/W}$. The steps have no intersections outside R, but they can cross each other many times and have indirect interactions mediated by finite terraces inside R. Therefore one can assign a vertex free energy as $f = F_{vertex} - F_{periodic} - 2F_{step}$, where F_{vertex}, $F_{periodic}$, and F_{step} are respectively the free energy of a sample of dimension $\xi_{B/W} \times \xi_{B/W}$ with the boundary conditions imposed by the vertex, the free energy of a sample with periodic boundary condition and the free energy of a single step.

Different mechanisms can be envisaged which favour the configuration with two adjacent antiparallel steps of vertex 5, with respect to the configuration of vertex 1 with two adjacent parallel steps. For example, in real surfaces there is an elastic repulsion between parallel steps, which turns out to be an attraction between antiparallel steps but of course it cannot happen in a rigid SOS model. Perhaps the most probable mechanism is provided by a larger meander entropy of a (3×1) compact wall, with respect to the a 4×1 step, since no energetic contributions are given by Hamiltonian (4.1). This should occur via a very subtle interplay between the energy of the intermediate excited states.

No exact proof of the relation $f_5 < f_1$ is available, but the arguments presented above should be convincing enough, and are sufficient to stabilize the DOF phase. In fact, though $a_3 < a_5$ is no more automatically true if the vertices are not points but extended objects, f_3 could be larger than f_5 because of an indirect interaction between the steps of the backbone, mediated by finite terraces. In figure 6.19 are displayed the configurations of vertices 5 (a), 4 (b) and 1 (c) in the presence of a finite terrace. One recognizes the presence of subvertices at the intersections between the steps of the backbone and the finite terrace. It is easy to recognise that vertex 5 is the only one which does not contain any subvertex of type 1. If one assumes that indeed $f_5 < f_1$, then the absence of subvertices 1 in vertex 5 justifies a lower free energy of vertex 5 with respect to vertex 4. In other words, if we assume a stronger repulsion, either energetic or entropic, between parallel steps, one concludes that the presence of finite terraces hinders the crossing (exchange of sign) between two antiparallel steps.

A DOF phase, with a predominance of 5 and 6 vertices, the cheapest in free energy, is thus stabilized.

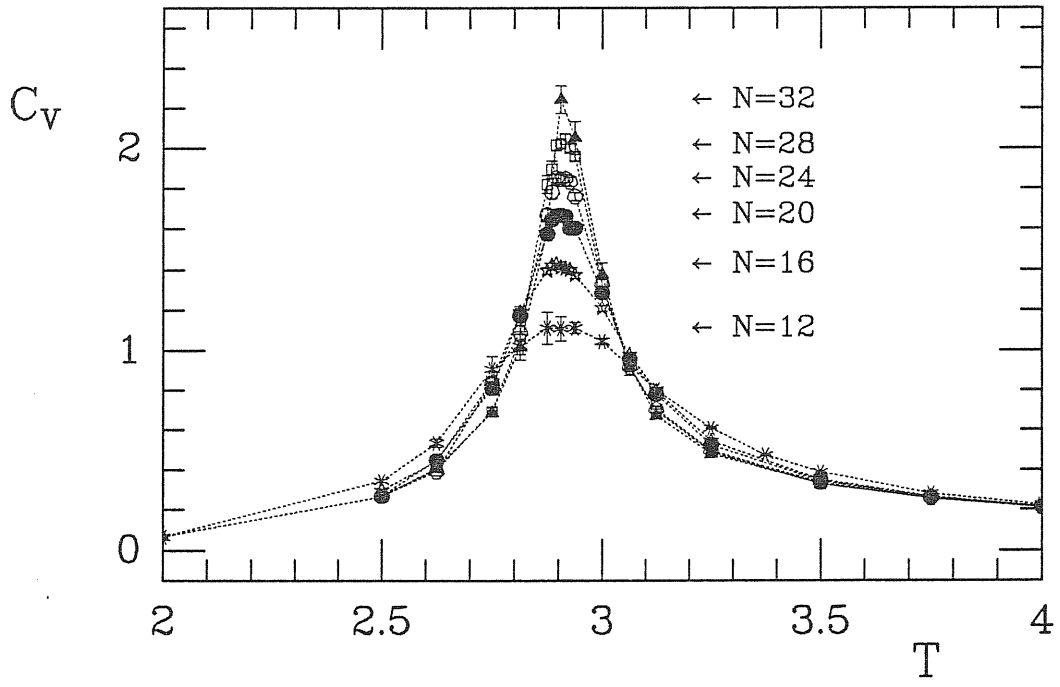

Figure 6.1. Specific heat vs. temperature.

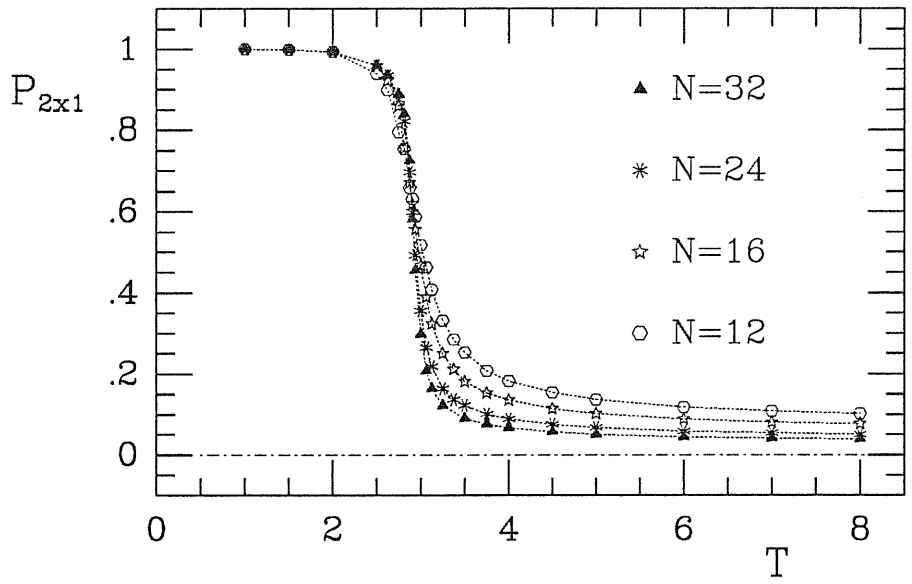

Figure 6.2. Deconstruction order parameter vs. temperature.

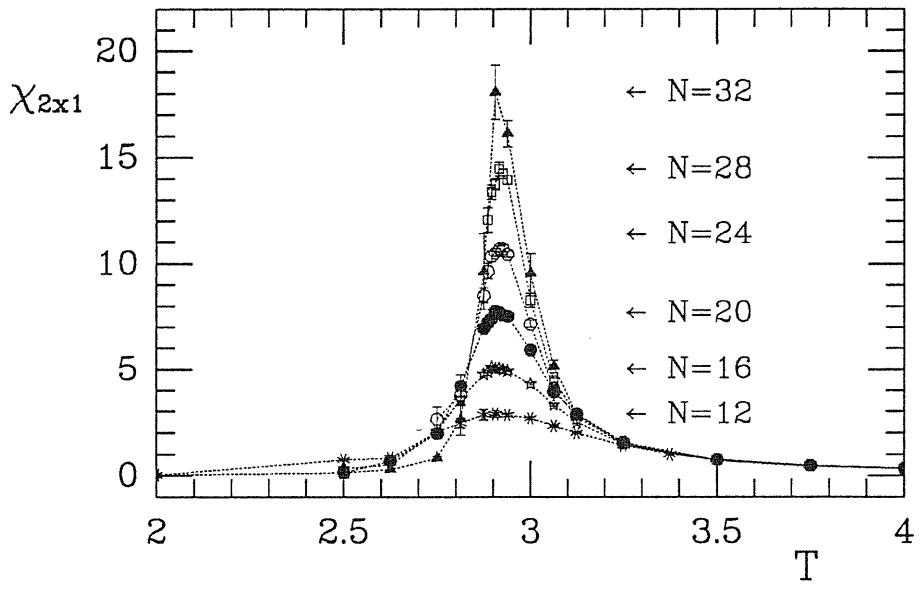

Figure 6.3. Susceptibility $\chi_{2\times1}$ vs. temperature in the critical region: the scale is enlarged with respect to fig. 6.2

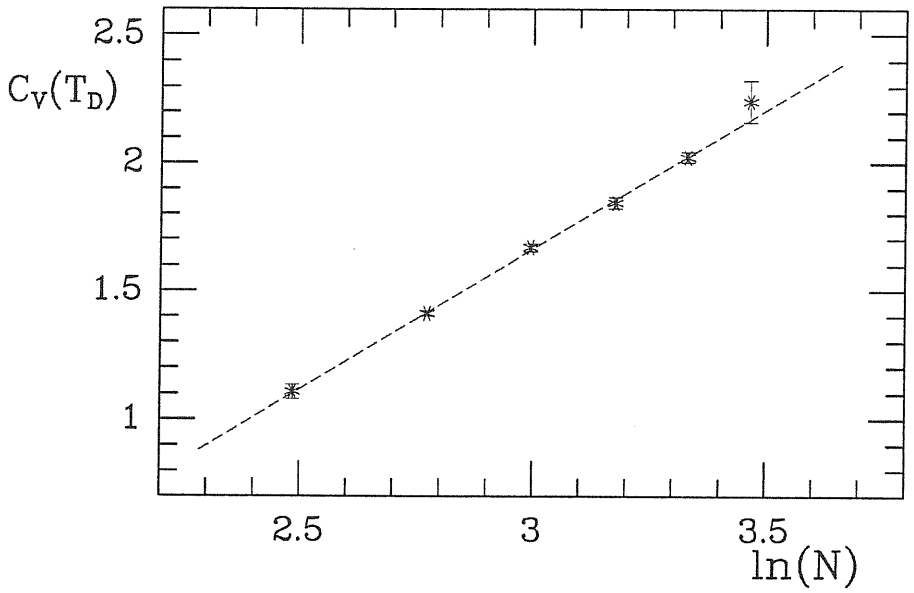

Figure 6.4. Scaling of the heat capacity peak height $C_V(N,T_{max})$ with system size N.

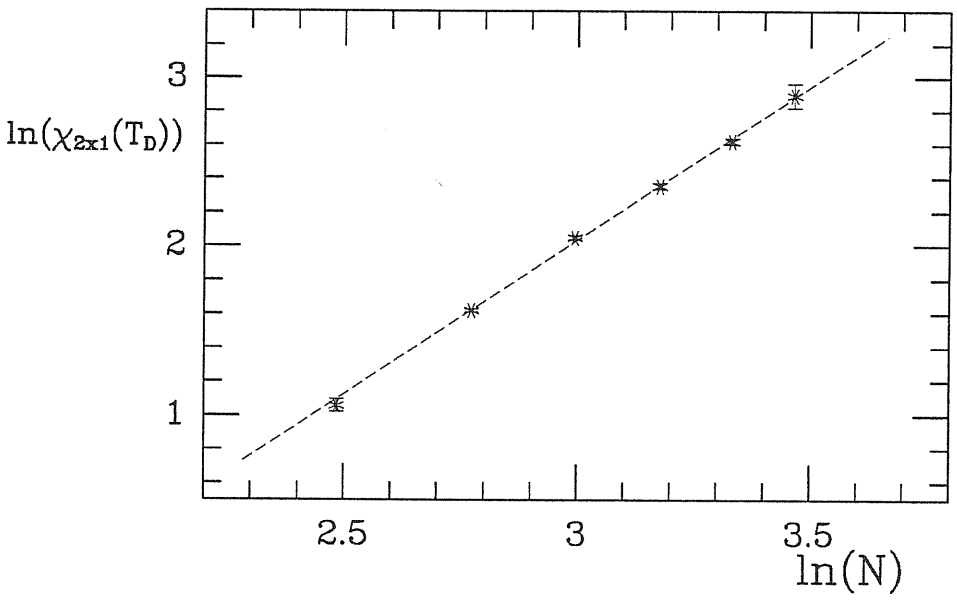

Figure 6.5. Scaling of the susceptibility peak height $\chi_{2\times1}(N,T_{max})$ with system size N.

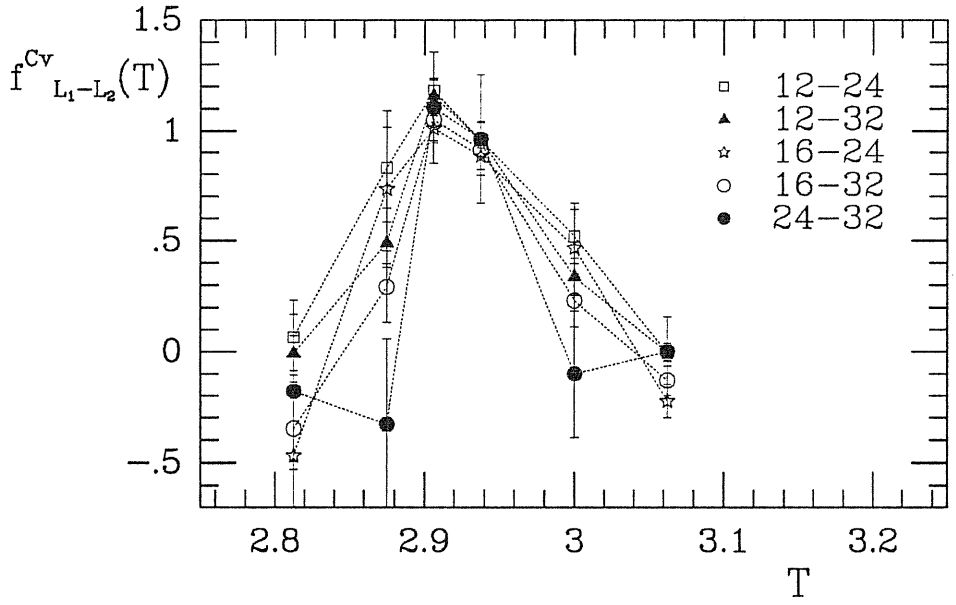

Figure 6.6. Determination of T_D from the phenomenological renormalization method.

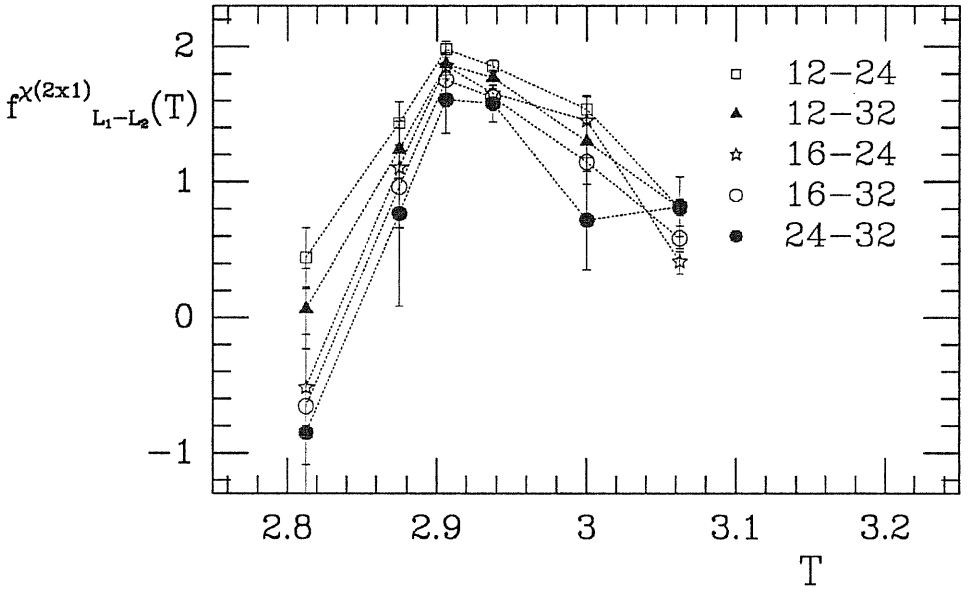

Figure 6.7. Determination of T_D and γ/ν from the phenomenological renormalization method. Notice that, as it often occurs, curves approach each other near the would-be crossing point.

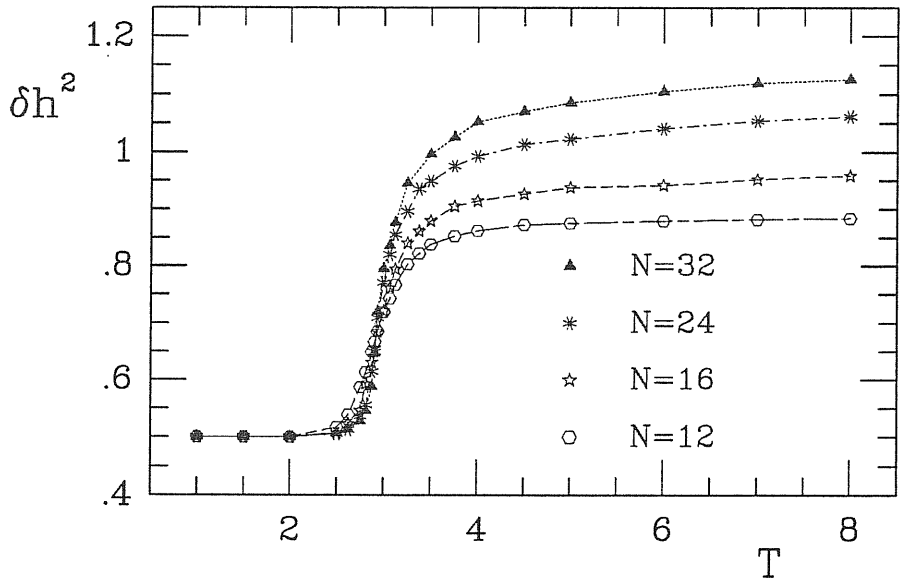

Figure 6.8. Finite size behaviour of the height fluctuations vs. temperature.

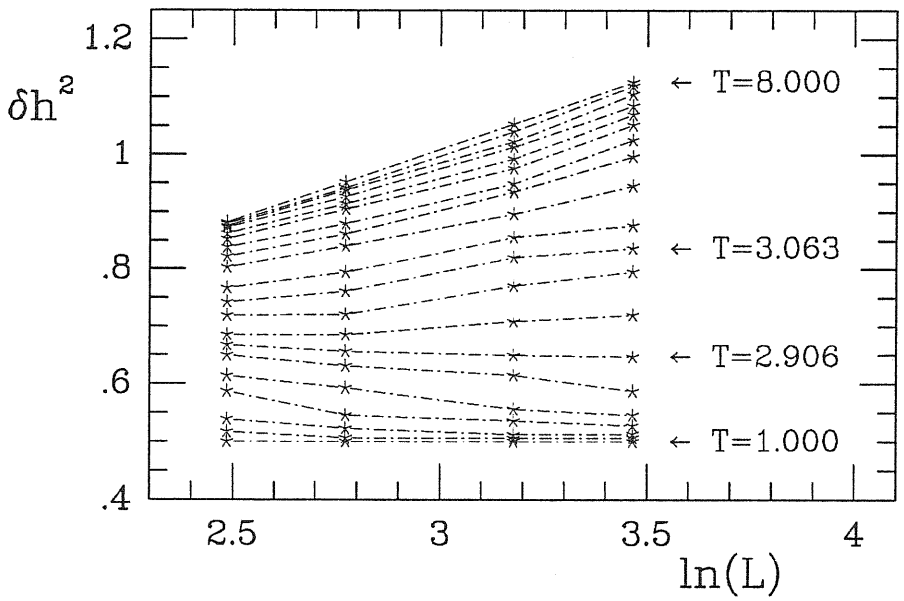

Figure 6.9. Size dependence of the height fluctuations for different temperatures. The lines should be straight only for $T \geq T_R \simeq 3.063$.

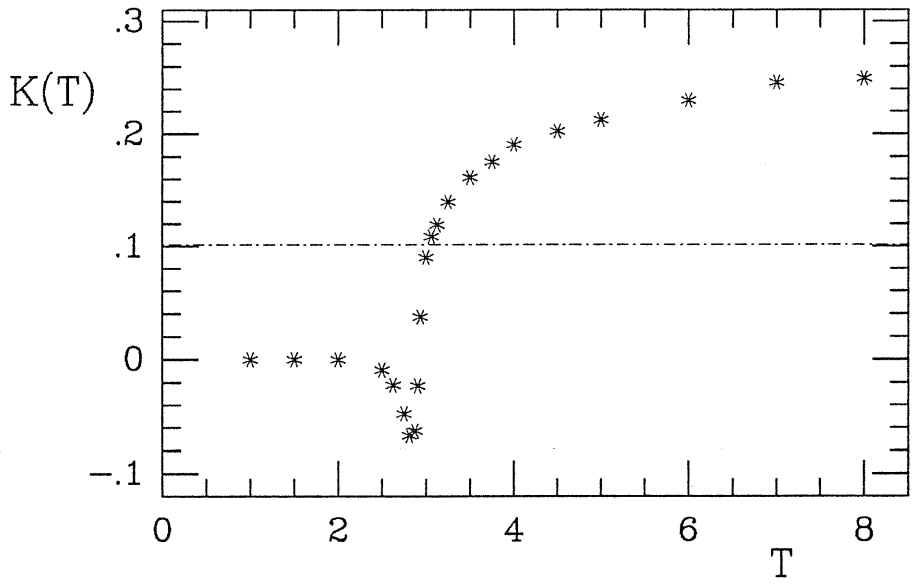

Figure 6.10. K(T) plotted as a function of temperature. The line indicates the position of the universal value $1/\pi^2$.

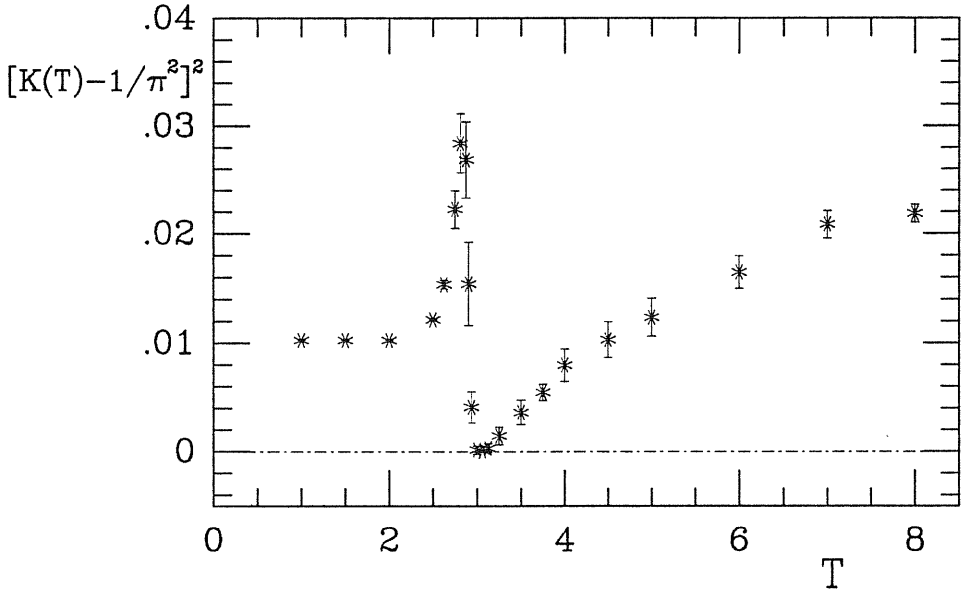

Figure 6.11. Search for the linear temperature dependence of $\left[K(T)-1/\pi^2\right]^2$ in order to identify T_R.

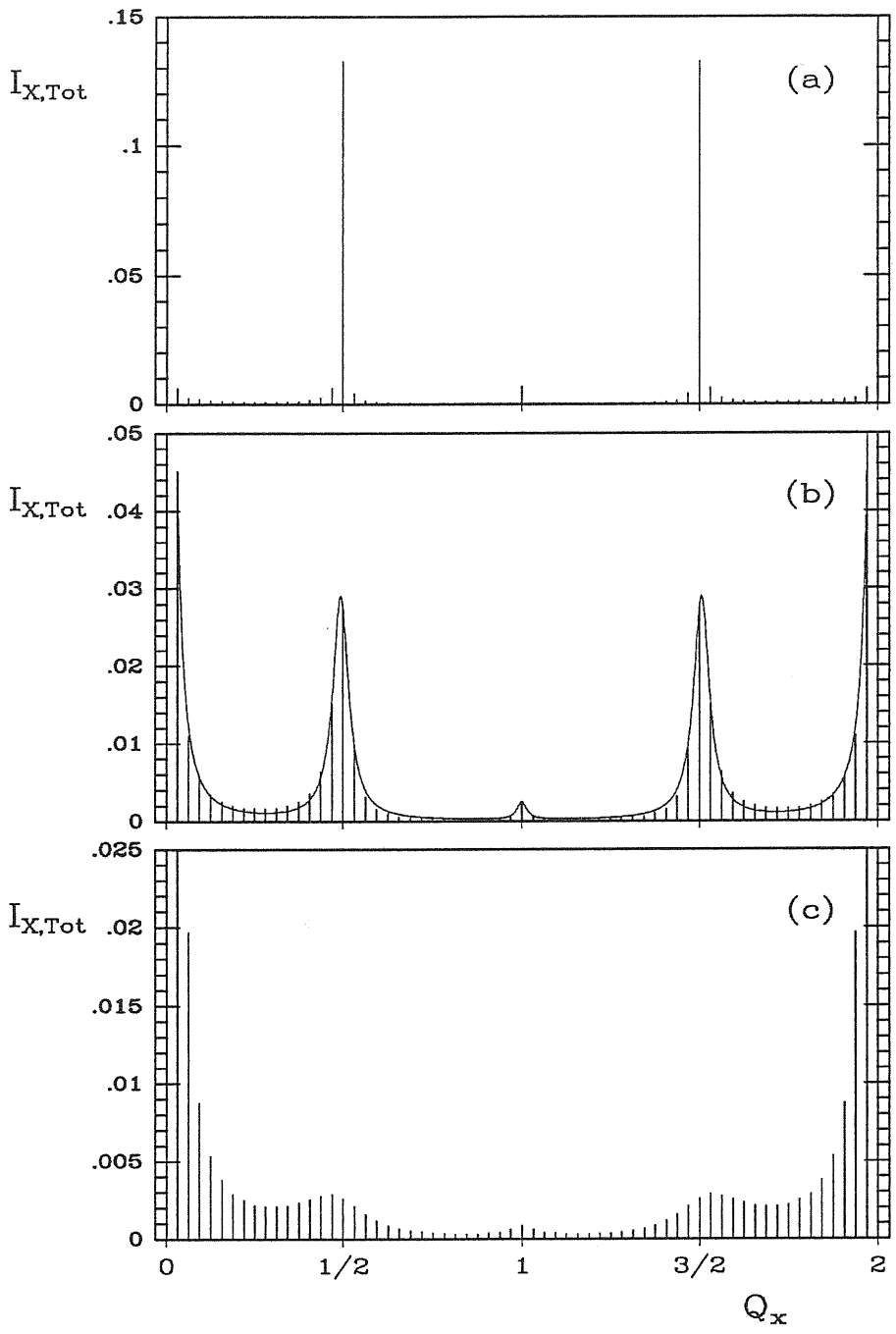

Figure 6.12. (a) Scattering pattern for X-rays scattering at $q_z=\pi/8$, $\mathbf{Q}=(Q_x,0)$ at $T/J=2.875$. (b) As in (a), but for $T/J=3.0$ and including a fitting to a Lorentzian lineshape. Notice that the incoherent background is asymmetric with respect to the (1/2 0) peak position, leading to a shift in the centering of the corresponding Lorentzians. (c) As in (a), but for $T/J=3.5$. The inverse length unit is $2\pi/a$, a=4.08Å being the Au lattice spacing.

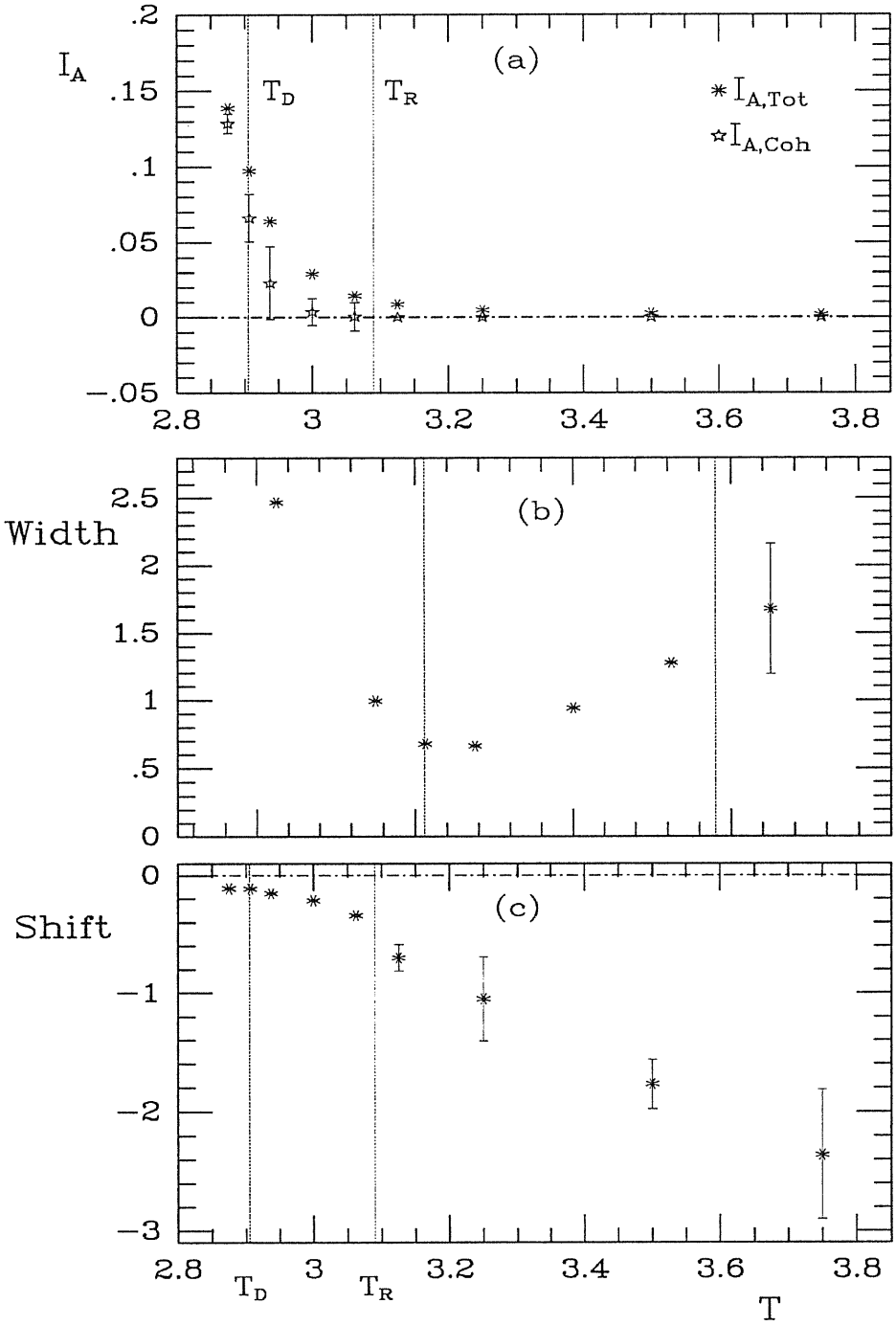

Figure 6.13. Temperature dependence of: (a) the fitted reconstruction (total and coherent) peak heights, (b) the incoherent peak width and (c) the peak shift. All the figures refer to atom scattering with q_z=0. The vertical axis inverse lengths in (b) and (c) are given in units of $2\pi/Na$=0.048$\mathring{A}^{-1}$.

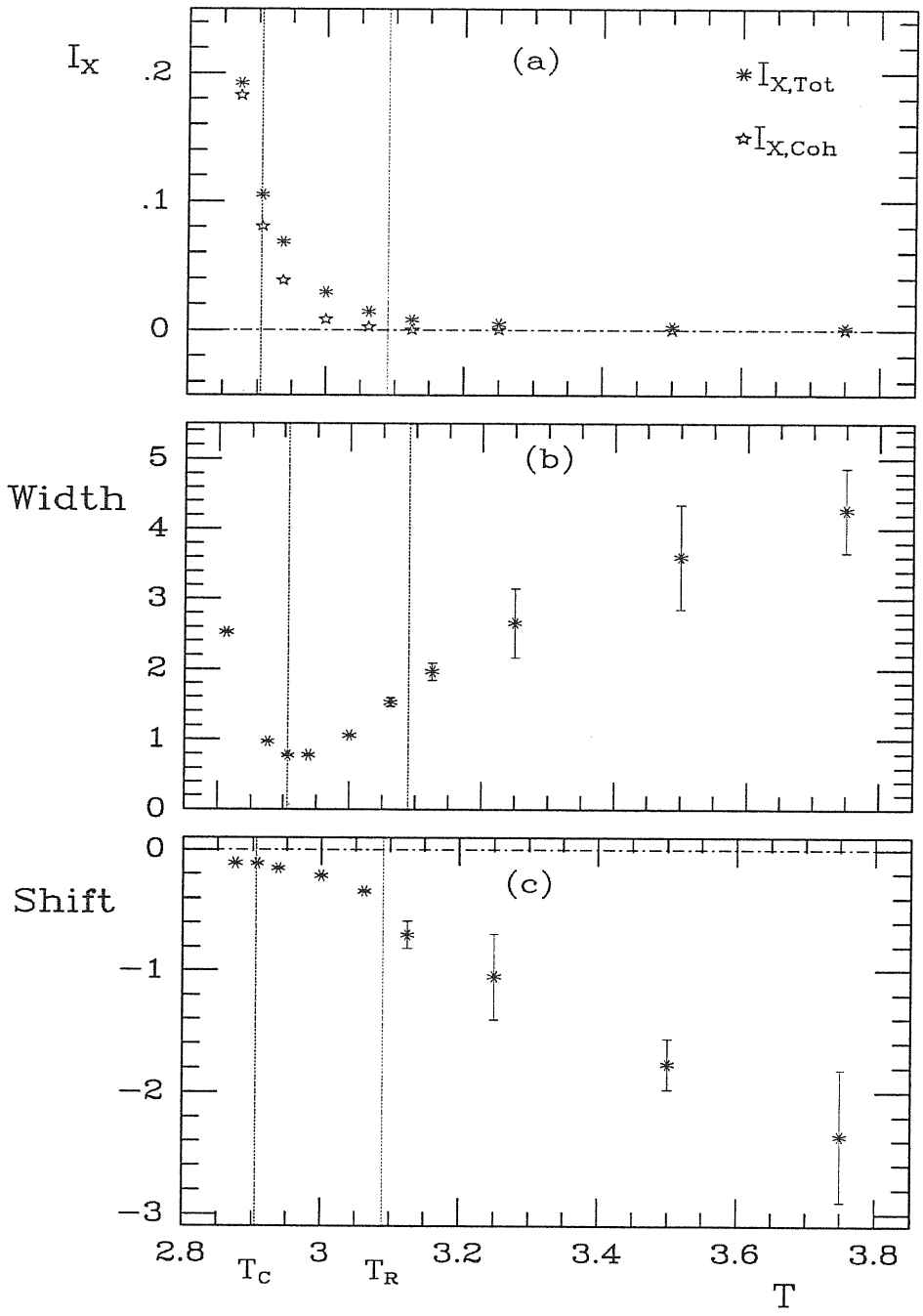

Figure 6.14. As in figure 6.13, but for X-rays scattering, and for $q_z=\pi/8$.

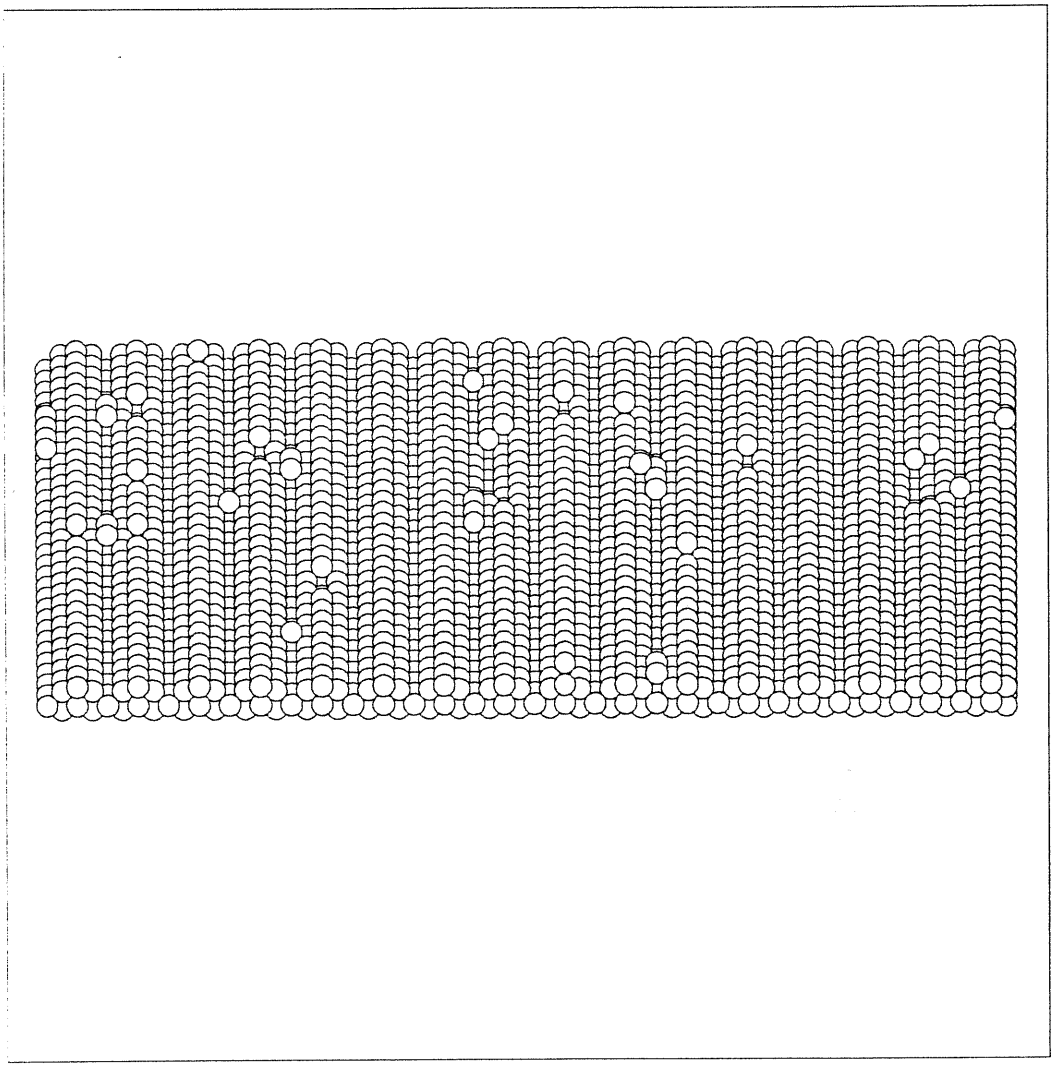

Figure 6.15. Snapshot of the Au(110) surface configuration at a temperature T/J=2.812 below T_D. Here and the successive pallographies refer to the largest size system (N=32). Atoms are added below the surface to help visualization of the configuration, though the Monte Carlo program generates only the surface layer.

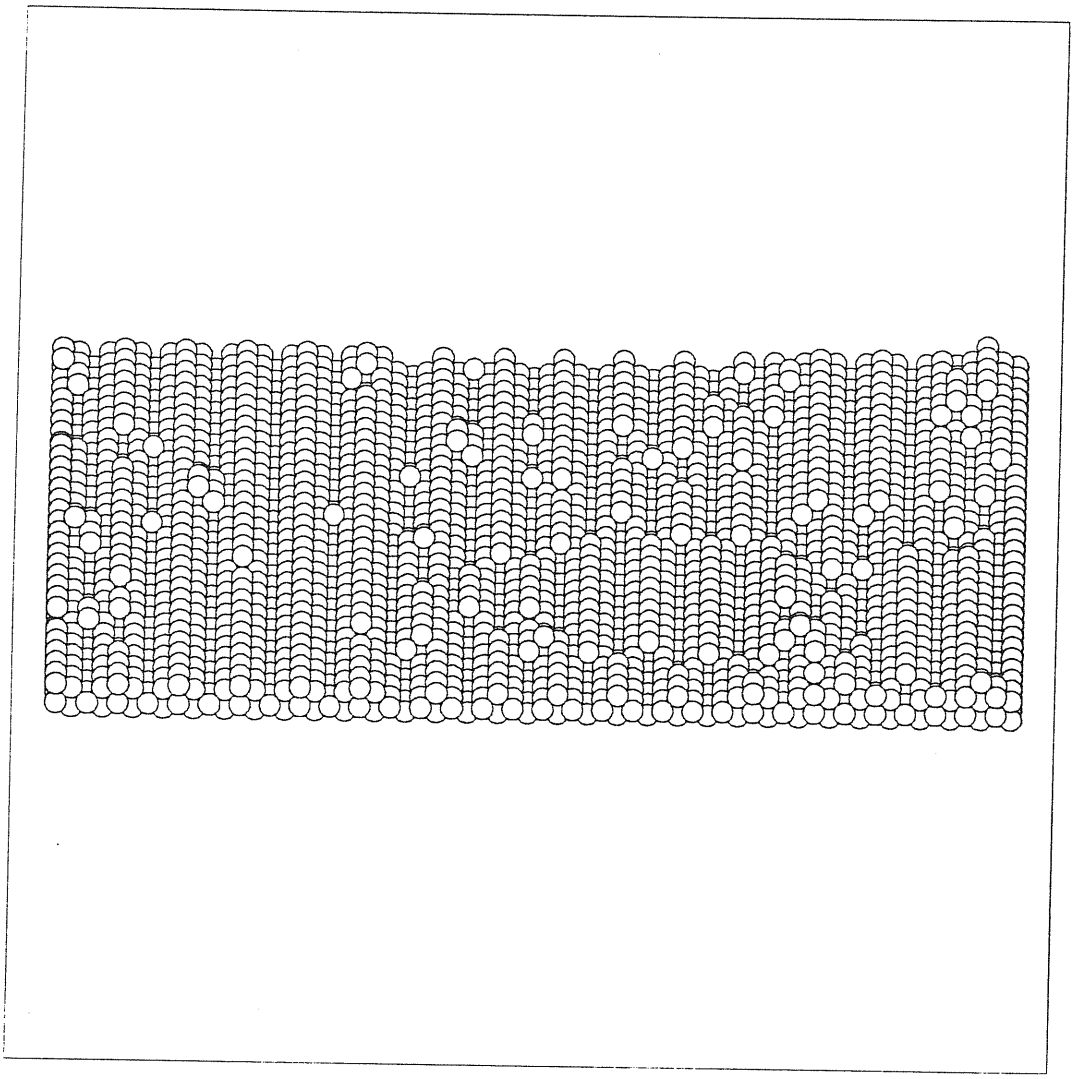

Figure 6.16. Snapshot of the Au(110) surface configuration at a temperature T/J=2.937, between T_D and T_R.

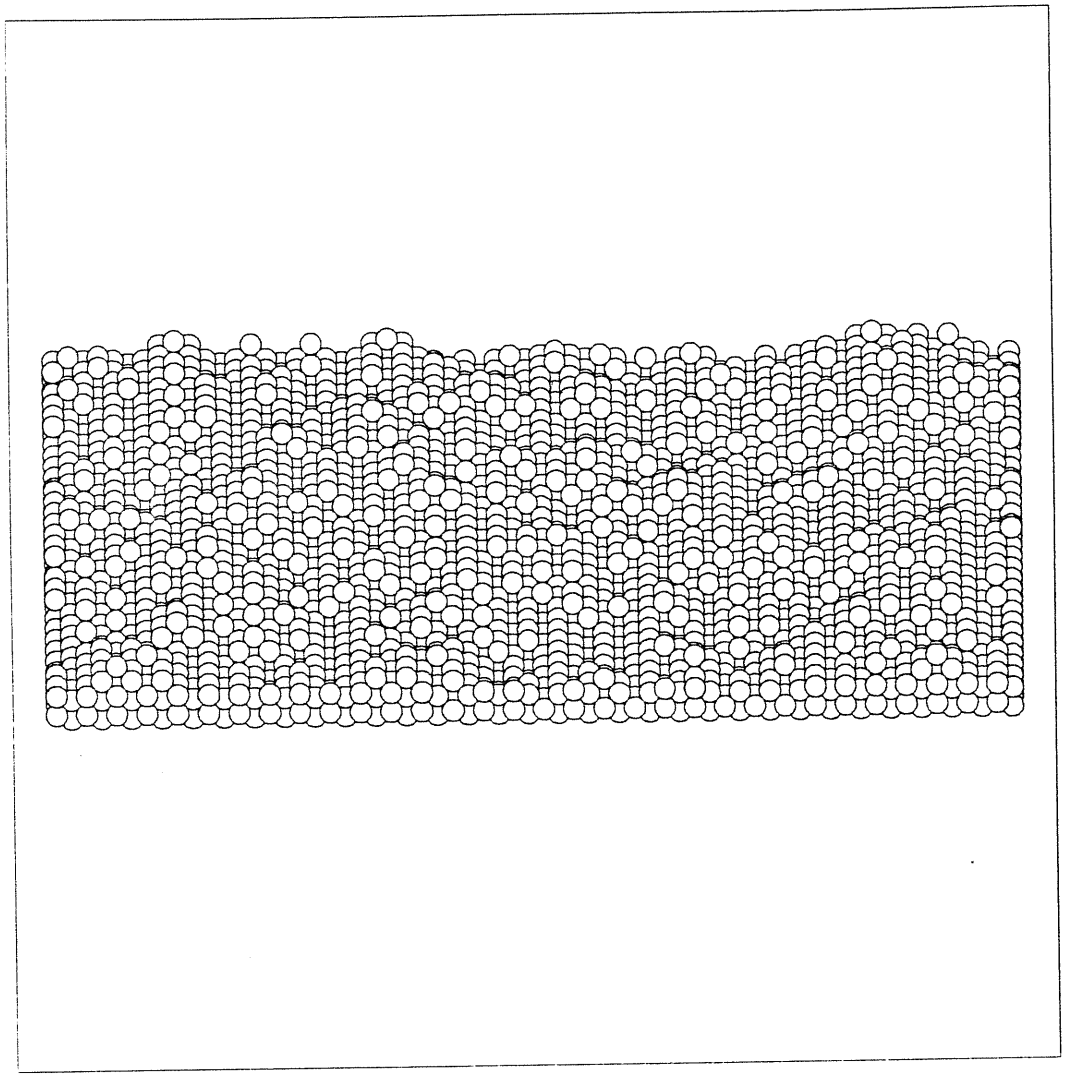

Figure 6.17. Snapshot of the Au(110) surface configuration at a temperature T/J=8.000, above T_R.

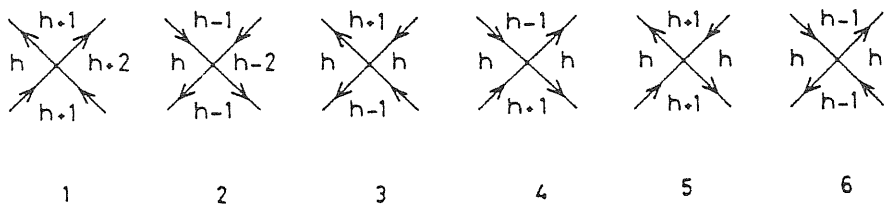

Figure 6.18. The six vertices with the relative corresponding surface heights. From ref. [90].

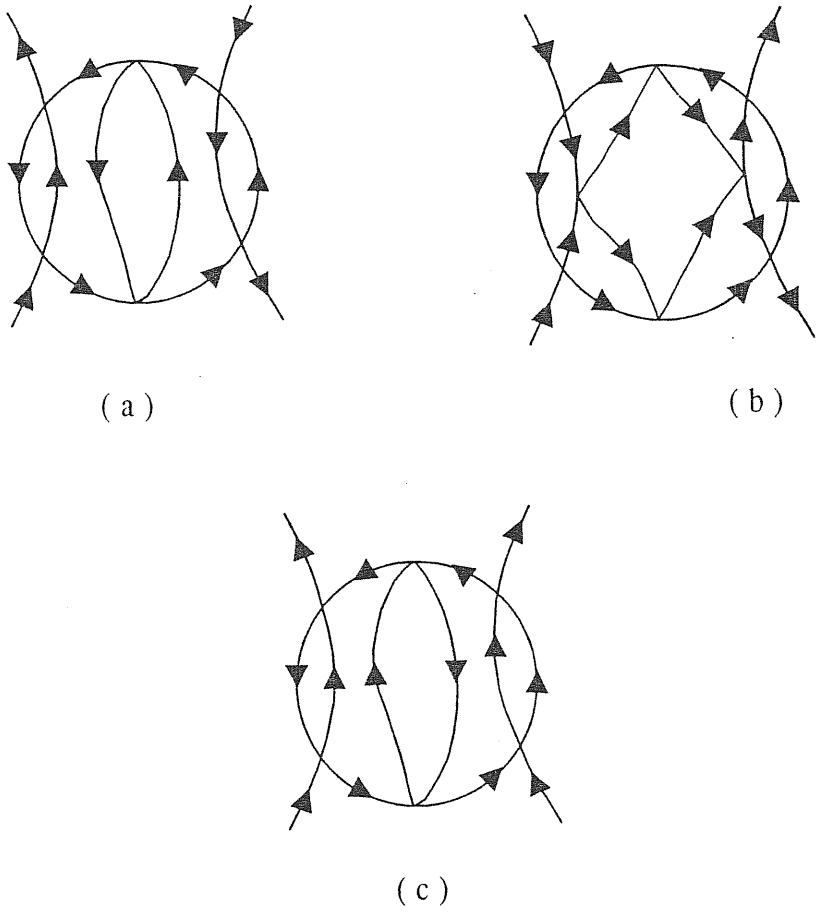

Figure 6.19. Configurations of vertex 5 (a), vertex 4 (b) and vertex 1 (c) in presence of a finite terrace. From ref. [118].

Chapter 7

Silver(110)

In Chapter 4 two choices of energy parameters for Hamiltonian (4.1) have been selected: the former was meant to describe a (2×1) reconstructed fcc(110) surface, the latter an unreconstructed one. Here results for the unreconstructed one, which has been called "Ag(110)", are presented. The most important feature is the occurrence of a non-Ising sublattice disordering phase transition on the flat (1×1) surface before the roughening one.

7.1 Sublattice disordering and roughening

Before addressing the evidence of a sublattice disordering phase transition, the occurrence of a roughening transition on this unreconstructed surface is briefly described. Its detection through the study of the interfacial width behaviour as a function of temperature and system size, clarified in figures 7.1 to 7.4, follows exactly the same reliable method adopted for the BCSOS model as well as for Hamiltonian (4.1) with the Au(110) energy parameters, and provides the value of

$$T_R = 2.25 \pm 0.07 \tag{7.1}$$

for the roughening transition temperature. The linearity of data for $T > T_R$ in fig. 7.4 is actually impressive, providing a strong indication for the Kosterlitz-Thouless behaviour of the transition and a self-consistency test of the validity of the method, since at least for this choice of the energy parameters the square root

region of eq. (1.8) extends far above T_R.

The plot of the specific heat as a function of temperature (fig. 7.5) opens up a new scenario for an in-plane surface disordering phase transition. Instead of showing a sharp divergence around a certain temperature as in the case of Au(110), it exhibits a rounded peak which presents no sign of increasing with increasing size, but rather saturates. A rapid inspection of the susceptibility $\chi_{B/W}$ for the sublattice order parameter $P_{B/W}$ (fig. 7.7) (the only parameter to be defined on the (1×1) unreconstructed surface) does not help to clarify the situation. Its pronounced size divergence is not by itself evidence for a critical phase transition, since very similar behaviour is observed for the $\chi_{B/W}$ in the BCSOS case (see fig. 5.8).

The size dependence of the order parameter (fig. 7.6) is different from that exhibited by $P_{B/W}$ in the BCSOS case (fig. 5.7). In that case, the finite size values detached from the exact (infinite size) curve at a temperature which is higher the larger the size (making thus possible a fitting for an independent extrapolation of T_R too). Here, on the contrary, all the lines seem to join in a narrow temperature region, remaining definitely below the infinite system (unknown) behaviour for lower temperatures, above for higher temperatures. This is much similar to what happens for $P_{2\times1}$ in the case of Au(110), but it is not sufficient, of course, for claiming the occurrence of a critical phase transition.

The clear proof that such a transition indeed takes place on the surface comes from the analysis of the first derivative of the specific heat dC_V/dT (from eq. (4.13)), figure 7.8. Though statistical fluctuations affect higher order energy cumulants more than lower order ones, so that wider spurious oscillations in the values are to be expected, (cured only by means of longer Monte Carlo runs), this quantity nonetheless shows a distinct behaviour as a function of temperature. It presents a node in correspondence of the maximum of C_V and two absolute extremes below and above, which heights tend to increase with increasing size. The details about what is happening in this region will be addressed immediately below. Here it is necessary to stress that, however, a critical phase transition undoubtedly is taking place on the surface, this being evidenced by the comparison with the behaviour of the same quantity shown in the BCSOS case (fig. 5.2). In that case, a practically-absent size dependence was the confirmation of the "singularity-free" nature of the free energy and of its derivatives. This evidence transforms here into the prediction of a free energy f singular in some of its derivatives. Most

probably, however, the critical exponent α is negative otherwise the divergence would be apparent already in the second derivative (the specific heat itself).

The derivation of a value for α (or, better, for α/ν) has to resort to a new procedure. An interesting quantity to analyze would be the second derivative of the specific heat since it should again show a peak at the transition temperature, critical with size. Statistical fluctuations would on the other hand most surely cover all relevant information contained in this quantity related to the fourth cumulant of the energy. A straightforward numerical differentiation method is employed to extract its value from the critical region of dC_V/dT (an enlarged graph of which is shown in fig. 7.9). For each system size, the slope of dC_V/dT is obtained and a logarithmic plot as a function of size is drawn from these values, which represent a quantity proportional to d^2C_V/dT^2, in order to extract the ratio between critical exponents of the form $(\alpha+2)/\nu$ (figure 7.10).

This procedure might seem to rest on a shaky ground due to the possible influence of statistical fluctuations in the extraction of meaningful values. It has therefore been tested in a simulation on a simple 2D Ising model, where all the critical exponents are known. Fig. 7.12 shows the results of this calculation performed on a square lattice of linear dimension $N = 16$, 24, 32 and 48 spins (smaller than the size adopted in the simulation of Hamiltonian (4.1) since a surface square lattice with $\mathcal{N}$ sites is equivalent to a lattice of $2\mathcal{N}$ spins). The specific heat is clearly size dependent and the same same appears for dC_V/dT though the peak in C_V shown by the $N = 48$ is slightly displaced to higher temperature with respect to the infinite system critical temperature, $T_{C,Ising} = 2.2692$. The exponents $(\alpha+2)/\nu$ (fig. 7.13) and γ/ν (the latter obtained by a finite size scaling analysis of the magnetic susceptibility χ, defined as in eq. (4.21) where the Ising magnetization replaces the order parameter), taken at $T_{C,Ising}$, provide an excellent estimate of the Ising critical exponents. One gets:

$$\begin{aligned} \frac{\alpha+2}{\nu} &= 1.92 \pm 0.11 \\ \frac{\gamma}{\nu} &= 1.71 \pm 0.03 \end{aligned} \tag{7.2}$$

that is

$$\begin{aligned} \alpha &= -0.04 \pm 0.06 \\ \nu &= 1.02 \pm 0.02 \\ \gamma &= 1.74 \pm 0.05 \end{aligned} \tag{7.3}$$

all in agreement (within error bars) with the exact values ($\alpha = 0$, $\nu = 1$, $\gamma = 1.75$).

Having checked the method against exact results, it is now possible to analyze in a similar way the quantity dC_V/dT calculated in the case of silver. The transition temperature may be located at the point where dC_V/dT is nearer to zero, which corresponds to the peak value of C_V, that is at

$$T_C = 1.81 \pm 0.03\,, \tag{7.4}$$

T_C being the critical temperature related to the vanishing of $\mathcal{P}_{B/W}$. Sublattice disordering thus occurs at 4/5 of the roughening temperature with present parameters. The ratio between critical exponents obtained from the abovementioned finite size scaling analysis is

$$\frac{\alpha + 2}{\nu} = 1.58 \pm 0.19 \tag{7.5}$$

A similar analysis is performed on the susceptibility, which peak value for the larger size available coincides with eq. (7.4). Again the plot of $\ln \chi_{B/W}$ as a function of $\ln L$ (fig. 7.11) yields a linear behaviour described by the value

$$\frac{\gamma}{\nu} = 1.56 \pm 0.02\,. \tag{7.6}$$

From these values it is possible to obtain all the critical exponents for sublattice disordering in our model of Ag(110), the most relevant to the present investigations being

$$\begin{aligned} \alpha &= -0.23 \pm 0.12 \\ \nu &= 1.12 \pm 0.06 \\ \gamma &= 1.74 \pm 0.10 \end{aligned} \tag{7.7}$$

The value assumed by α lies in the range $-1 \leq \alpha \leq 0$, which is consistent with the saturation of finite size effects observed in C_V, where a non critical large background dominates on a non divergent critical contribution, and with the size effects present in dC_V/dT. This undoubtedly rules out the possibility of a transition of the Ising type (this transition is actually "weaker" than Ising, i.e. α is negative), although the γ value practically coincides with the Ising value 7/4.

The values (7.7) point towards a critical phase transition at T_C with non-universal exponents for different surfaces (energy parameters), as envisaged by den Nijs [90,119] for the preroughening transition as well as by Kohanoff *et al.* [125,126] in the Jug-Tosatti model.

7.2 Scattering intensities results

As in the case of Au(110), also for this unreconstructed Ag(110) surface intensities for both atoms and X-ray scattering are calculated.

The exact value of the amplitude absorption coefficient μ for X-ray scattering is not essential since it appears just in a prefactor in front of formula (1.20). Nevertheless $\mu = 1.66 \cdot 10^{-5}$ is chosen, extracted from the tables [31] in correspondence with the value of 8.05 KeV employed by Held *et al.* [37] in their diffraction experiment.

Fig. 7.14 shows the atom scattering pattern (the X-ray one looks similar, thus it is not shown) calculated for the largest system available ($N = 32$), for $Q_y = 0$, $q_z = 0$ and Q_x in the whole range of investigation, $0 \leq Q_x \leq 4\pi/a_x$ ($0 \leq n_x/N_x \leq 4$), for a temperature $T = 1.875$ between T_C and T_R, together with the Lorentzian fitting adopted. The central peak is equivalent, via the symmetry relations of Section 1.4.7, to the specular peak in antiphase $(0\,0\,\pi/a_z)$ which directly monitors the behaviour of the order parameter $\mathcal{P}_{B/W}$ (see Appendix). The main feature of the plot is, together with the disappearance of the half integer order reconstruction peaks with respect to the case of Au(110) (fig. 6.12), the absence of a shift, however small, of the peak, which is maintained also for $T > T_R$.

A fitting of the incoherent part (excluding the central peak where both coherent and incoherent contributions are superimposed) with a Lorentzian function is performed on the data. It is particularly appropriate in that temperature range

where the lineshape should actually be Lorentzian, i.e. neither for too low temperatures nor for too high ones, where it changes to a power-law (for $T \geq T_R$). The coherent contribution is thus obtained by subtracting from the total intensity an extrapolated value of the incoherent intensity at the peak position, which has been chosen to be that taken at the maximum of the Lorentzian.

In fig. 7.15-(a) the intensity of the specular peak in antiphase is reported as a function of temperature, both for the total and the coherent part. The incoherent one is shown in fig. 7.15-(b). It has a peculiar bell-shaped form, with a maximum not exactly placed at T_C but slightly shifted upward in temperature, a feature which is sometimes observed experimentally [52,53], see for example fig. 2.1.

Finally, the width of the incoherent peak is shown as a function of temperature in fig. 7.15-(c). It has a feature similar to that of the half integer order peak width in the Au(110) case, that is a minimum at a certain temperature (more or less coinciding with that of the maximum in the incoherent intensity), but it increases above it due to a proliferation of defects on the surface. Its boundedness for lower temperatures is due only to finite size effects and to the fitting procedure, which becomes more inappropriate the lower the temperature.

The coherent part of the specular peak in antiphase should behave as the sublattice order parameter, thus should vanish at T_C. However, this is not clearly seen in fig. 15-(a) where it shows a sharp decrease, which nonetheless does not permit to locate the transition temperature with precision. This is mainly due to finite size effects, evidently more important here than in Au(110).

For X-ray scattering the situation looks exactly in the same way, thus no additional scattering diagram is reported.

A better understanding of the features arising from the scattering calculations can be provided by looking at snapshots of surface configurations taken at different temperatures (fig. 7.16 – 7.18). For $T < T_C$ only isolated local defects are found on an otherwise flat (110) surface. Their density increases as a function of temperature and compact domain walls start to appear. None of them causes sublattice disordering which is instead driven by steps with a long range up-down order, as shown in fig. 7.17. Their appearance is also an explanation of the absence of the shift of the specular peak found in the scattering patterns. Two of them in fact are sufficient to cause the vanishing of $\mathcal{P}_{B/W}$ on a finite system, but of course this is not enough to induce a shift which is instead driven by a global increase of the

lattice spacing in the x direction. This would arise due to proliferation of (2×1) compact domain walls, for example, but this is clearly not the case. By raising the temperature, the disordered but flat structure evolves into the usual rough structure with delocalized interface, and this is apparent too from fig. 7.18.

In conclusion, Ag(110) shows two distinct transitions, the second located through the divergence of the height-height correlation function, the first through the vanishing of the $\mathcal{P}_{B/W}$ order parameter. This can be classified into a class of preroughening transitions envisaged by den Nijs and by Kohanoff, Jug and Tosatti by introducing a long range interaction in a nearest neighbour Hamiltonian, which is represented in this case by the K_3 coupling in the Hamiltonian. The occurrence of a DOF phase stabilized by long range antiferromagnetic order of steps is a crucial structure in the preroughening mechanism. It can be deduced from theoretical arguments, as well as clearly seen in snapshots of the surface configurations like fig. 7.17.

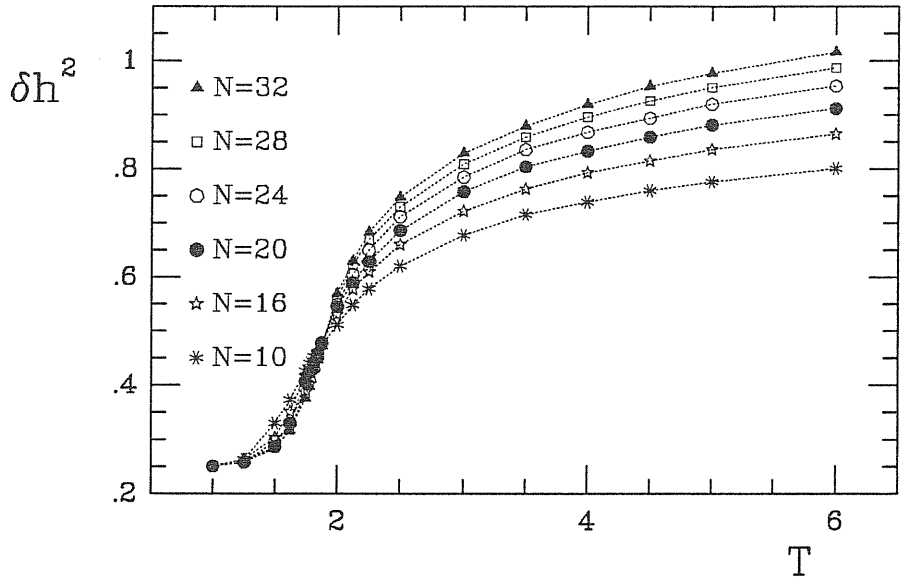

Figure 7.1. Finite size behaviour of the height fluctuations vs. temperature.

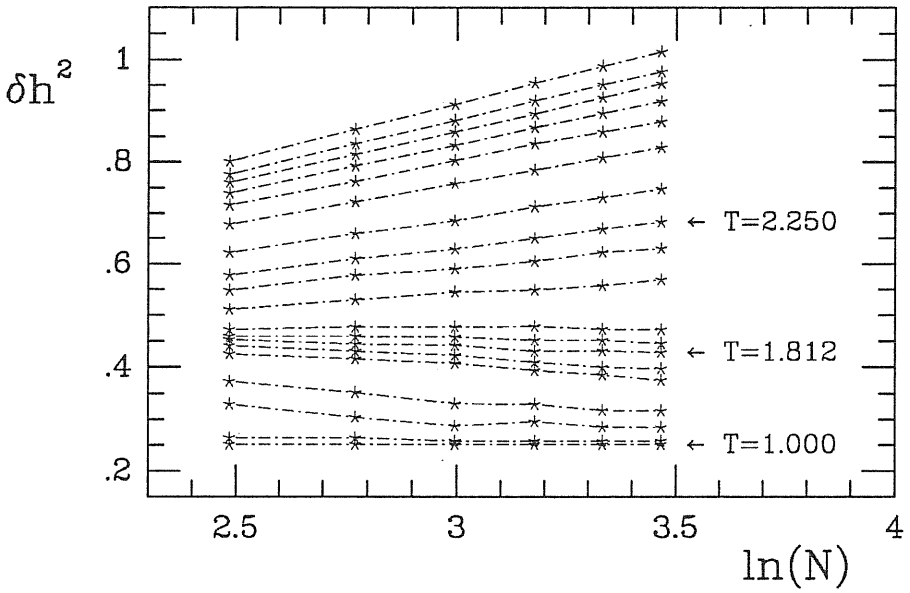

Figure 7.2. Size dependence of the height fluctuations for different temperatures. The lines should be straight only for $T \geq T_R \simeq 2.25$.

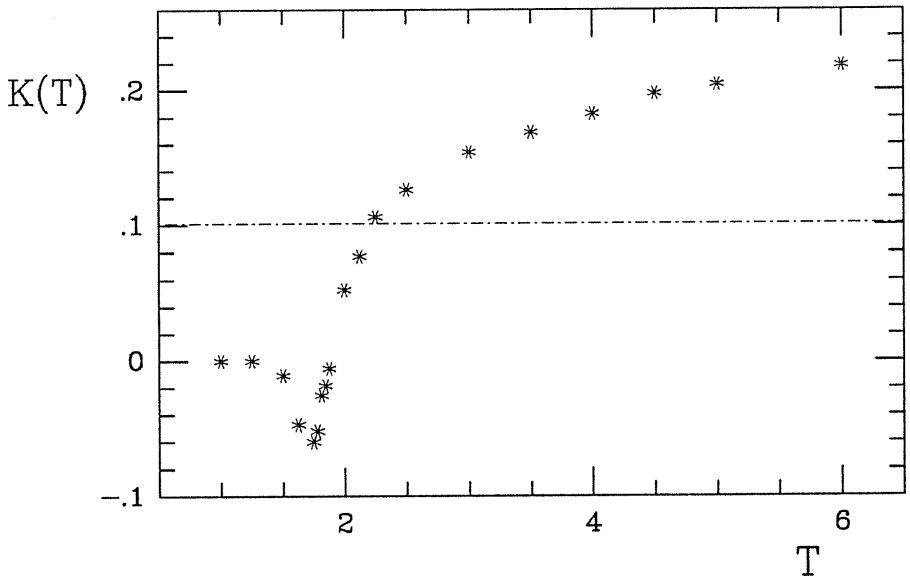

Figure 7.3. K(T) plotted as a function of temperature. The line indicates the position of the universal value $1/\pi^2$.

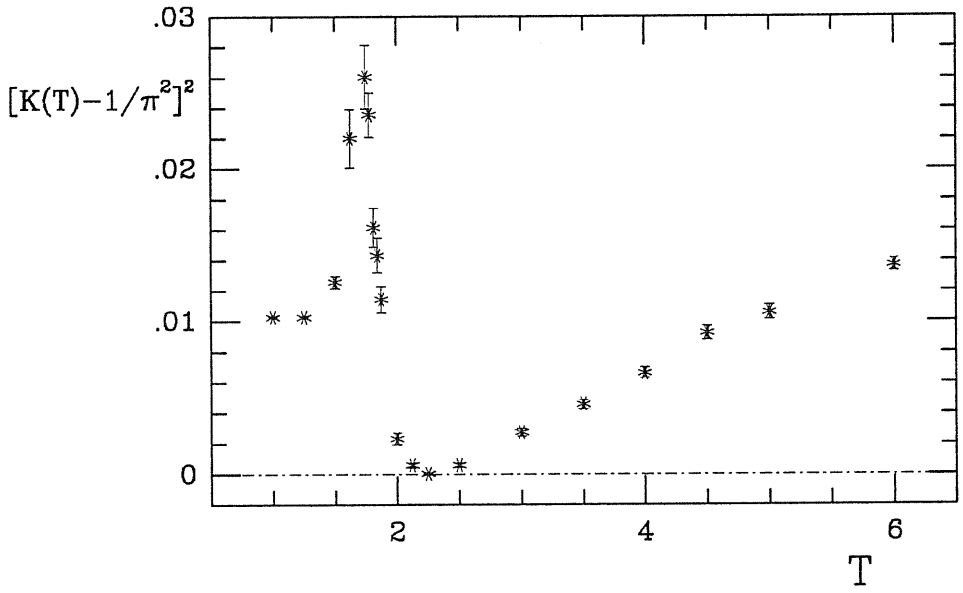

Figure 7.4. Plot of the linear temperature dependence of $\left[K(T)-1/\pi^2\right]^2$ in order to identify T_R.

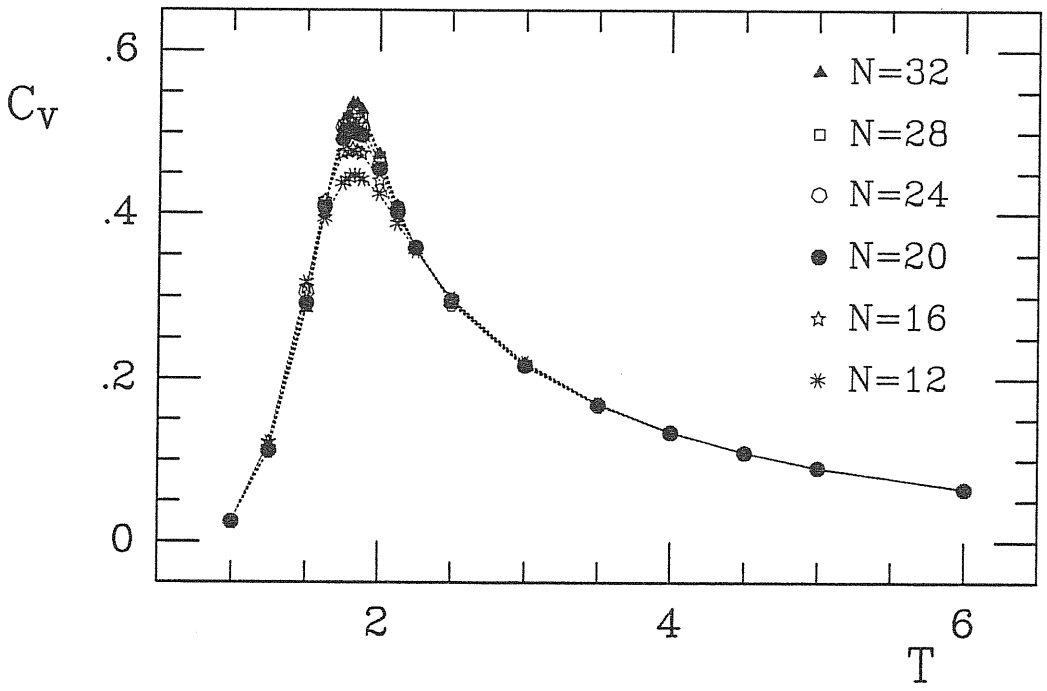

Figure 7.5. Specific heat vs. temperature.

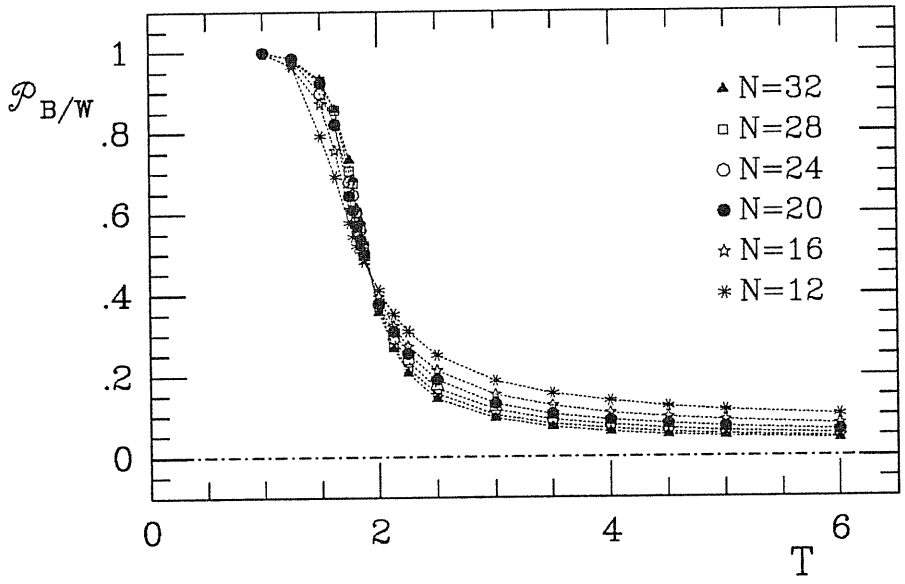

Figure 7.6. Sublattice order parameter vs. temperature.

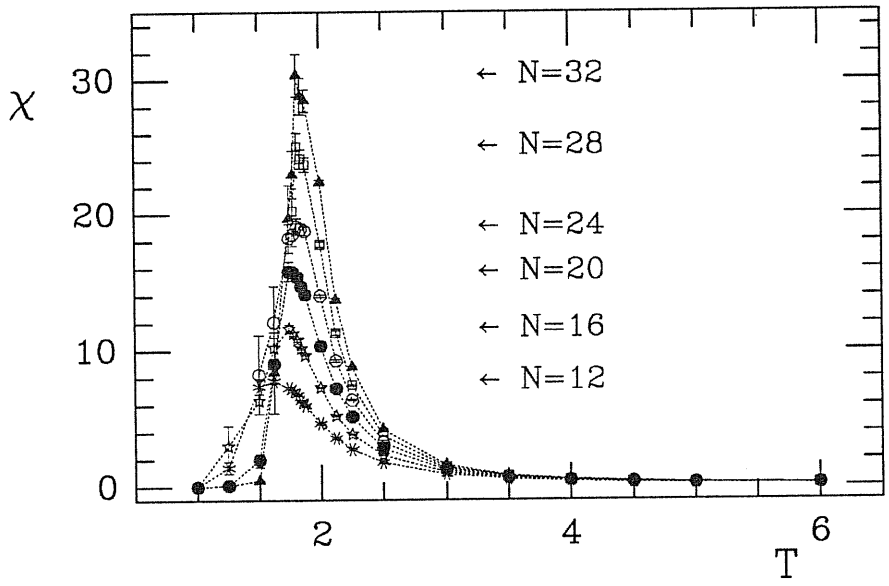

Figure 7.7. Susceptibility χ vs. temperature.

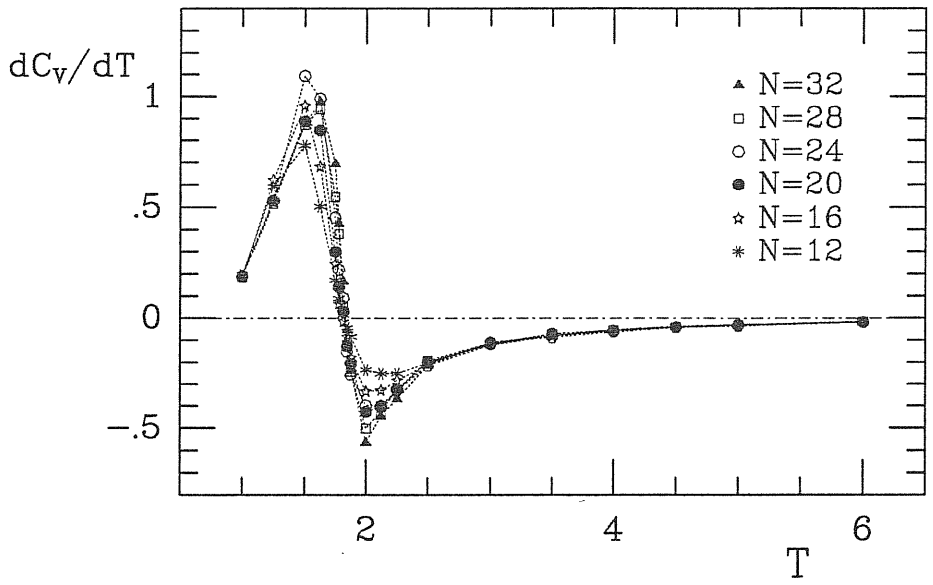

Figure 7.8. The first derivative of the specific heat vs. temperature.

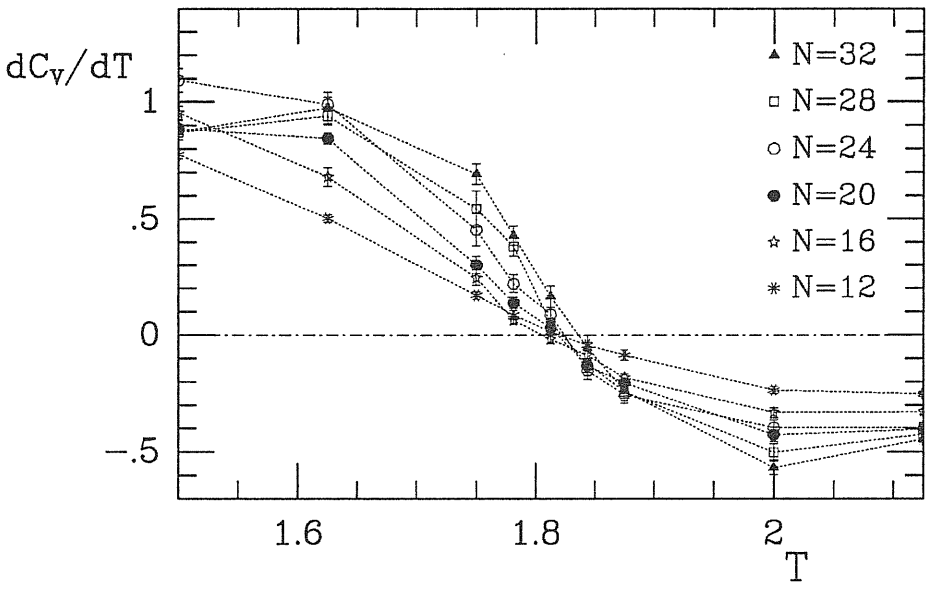

Figure 7.9. As in figure 7.8, with an enlarged scale in the critical region.

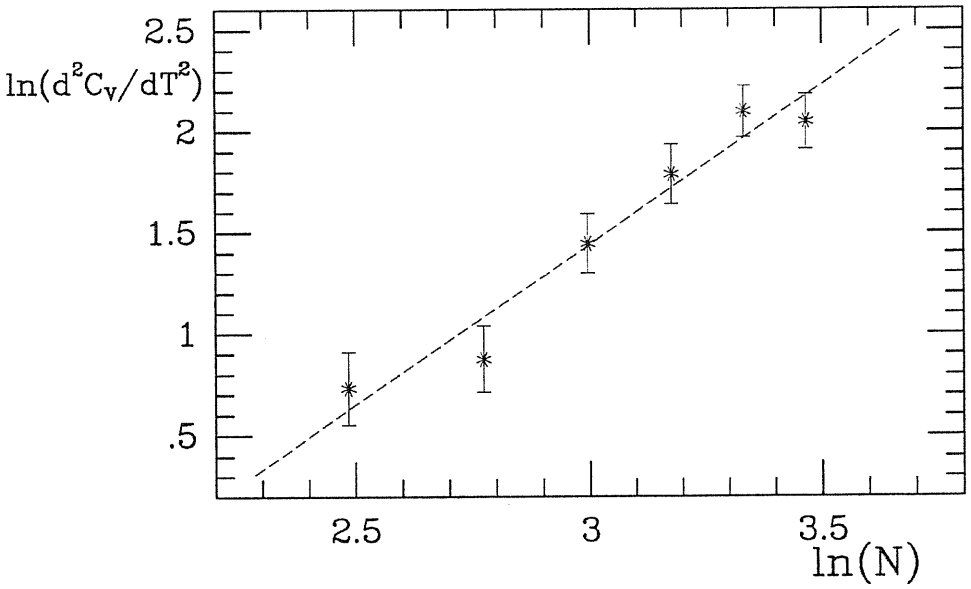

Figure 7.10. Scaling of the slope of dC_V/dT (proportional to the second derivative of the specific heat) in the critical region.

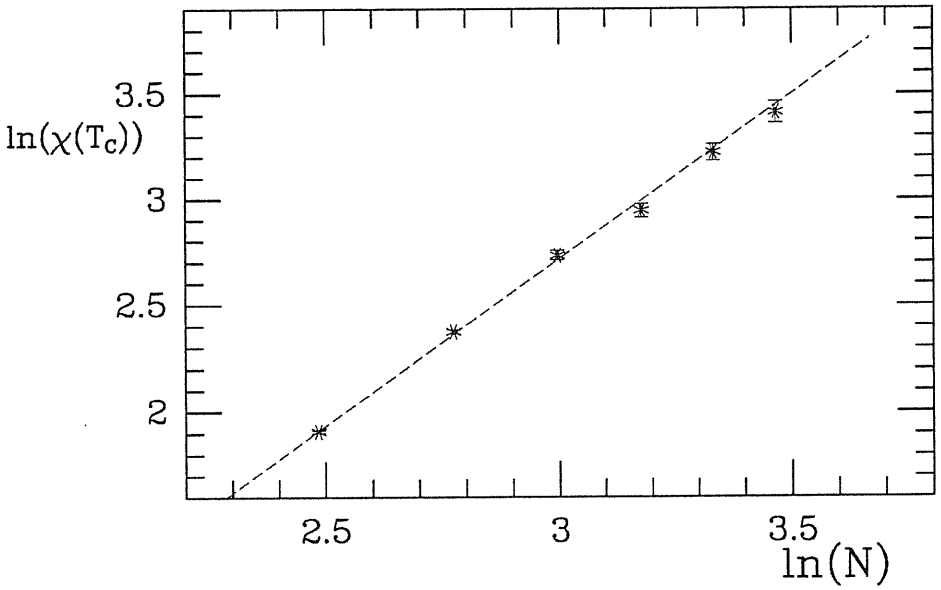

Figure 7.11. Scaling of the susceptibility peak height $\chi(N,T_{max})$ with system size N.

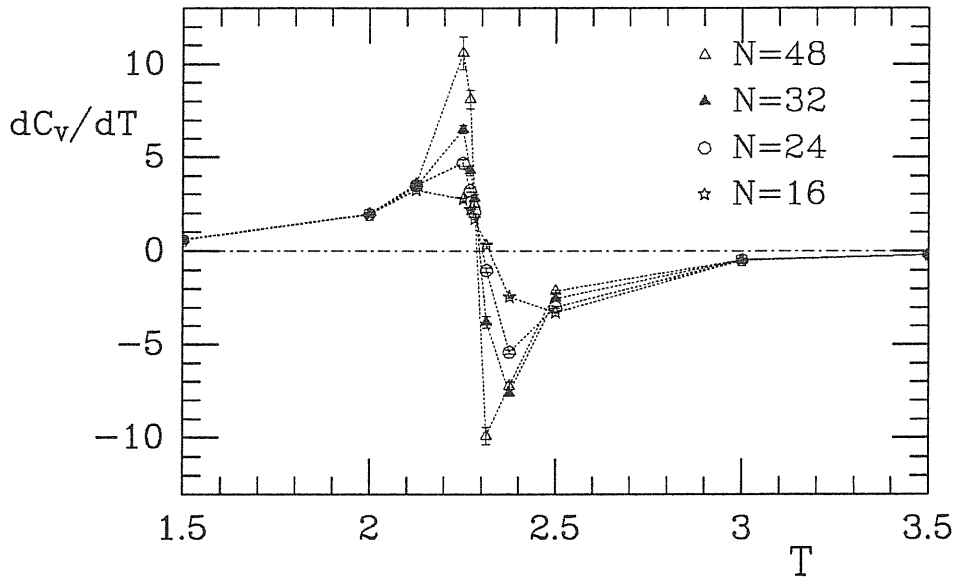

Figure 7.12. The first derivative of the specific heat vs. temperature in the Ising model.

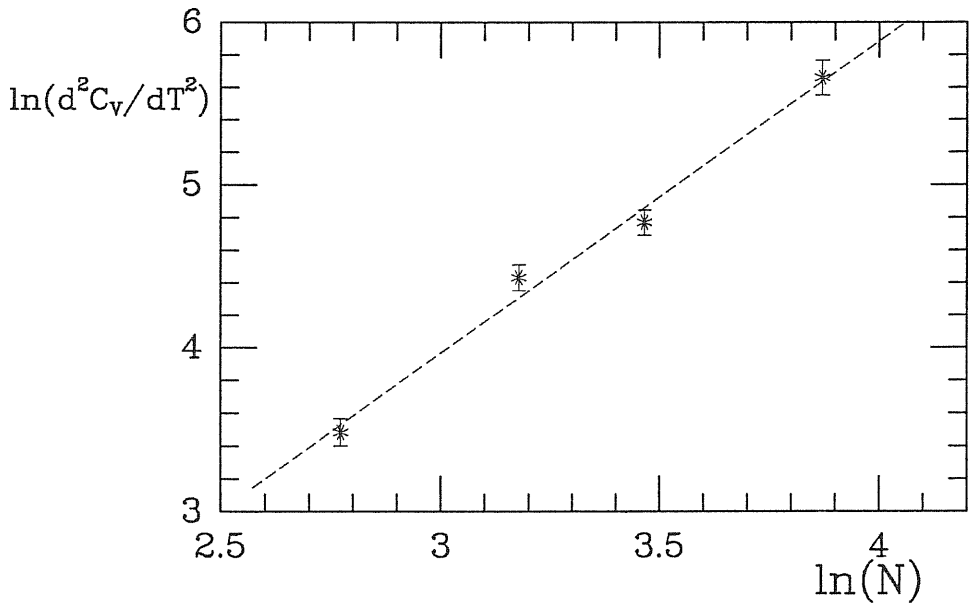

Figure 7.13. Scaling of the slope of dC_V/dT in the Ising model.

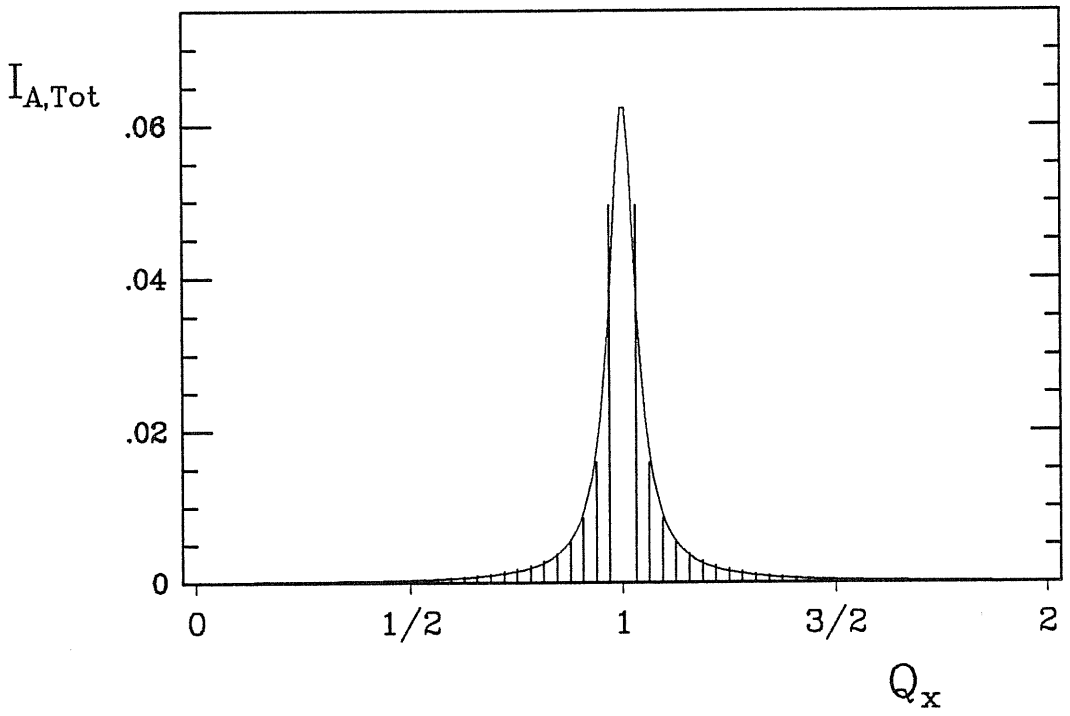

Figure 7.14. Incoherent atom scattering pattern for the specular peak in antiphase, fitted with a Lorentzian function. The coherent part (at $Q_x = 1$) is not reported since out of scale.

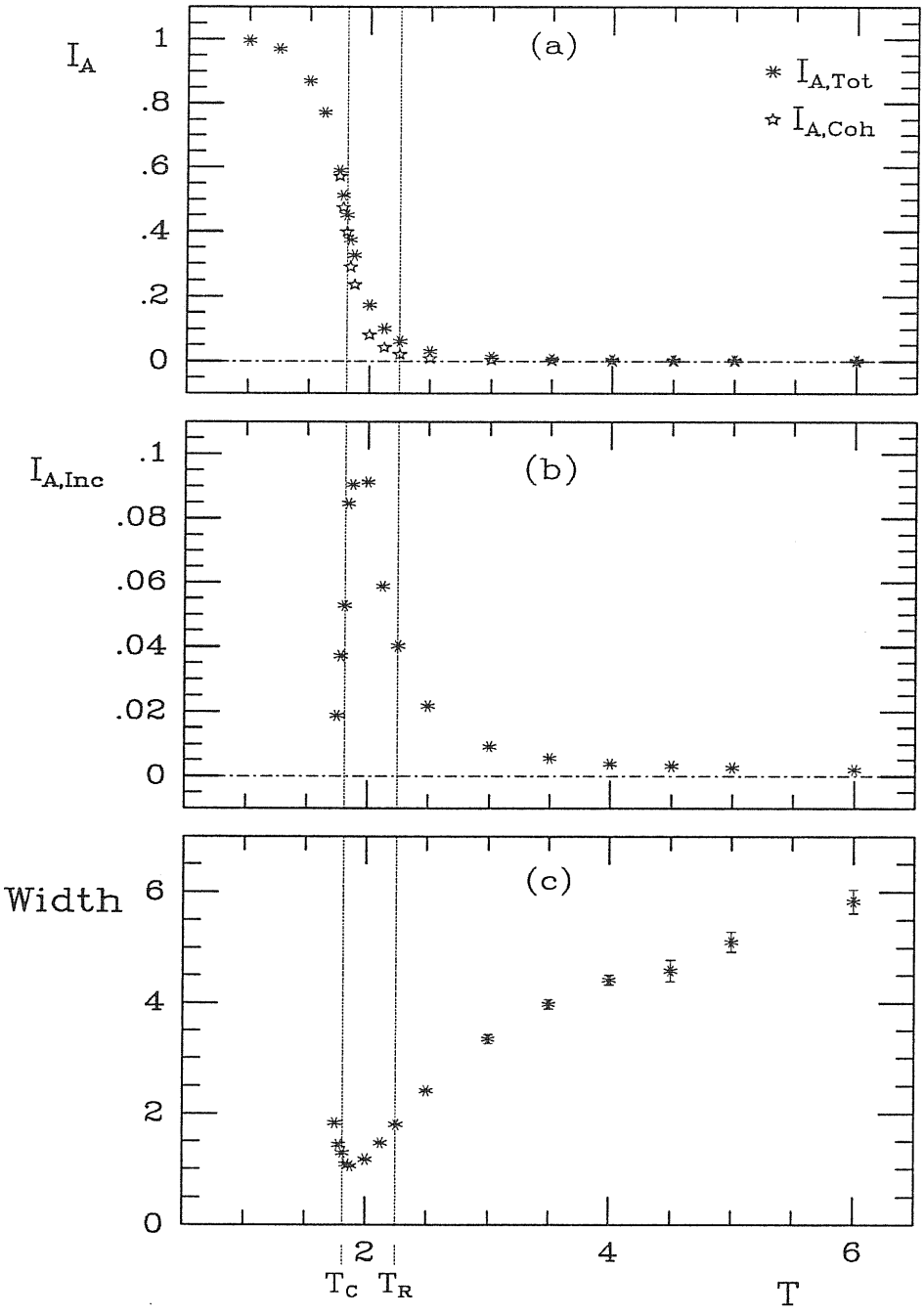

Figure 7.15. Temperature dependence of: (a) the total and the coherent part of the specular peak in antiphase $(0\,0\,\pi/a_z)$; (b) the incoherent contribution and (c) the incoherent peak width. All the figures refer to atom scattering. The vertical axis inverse lengths in (b) and (c) are given in units of $2\pi/Na$=0.048$\mathring{A}^{-1}$.

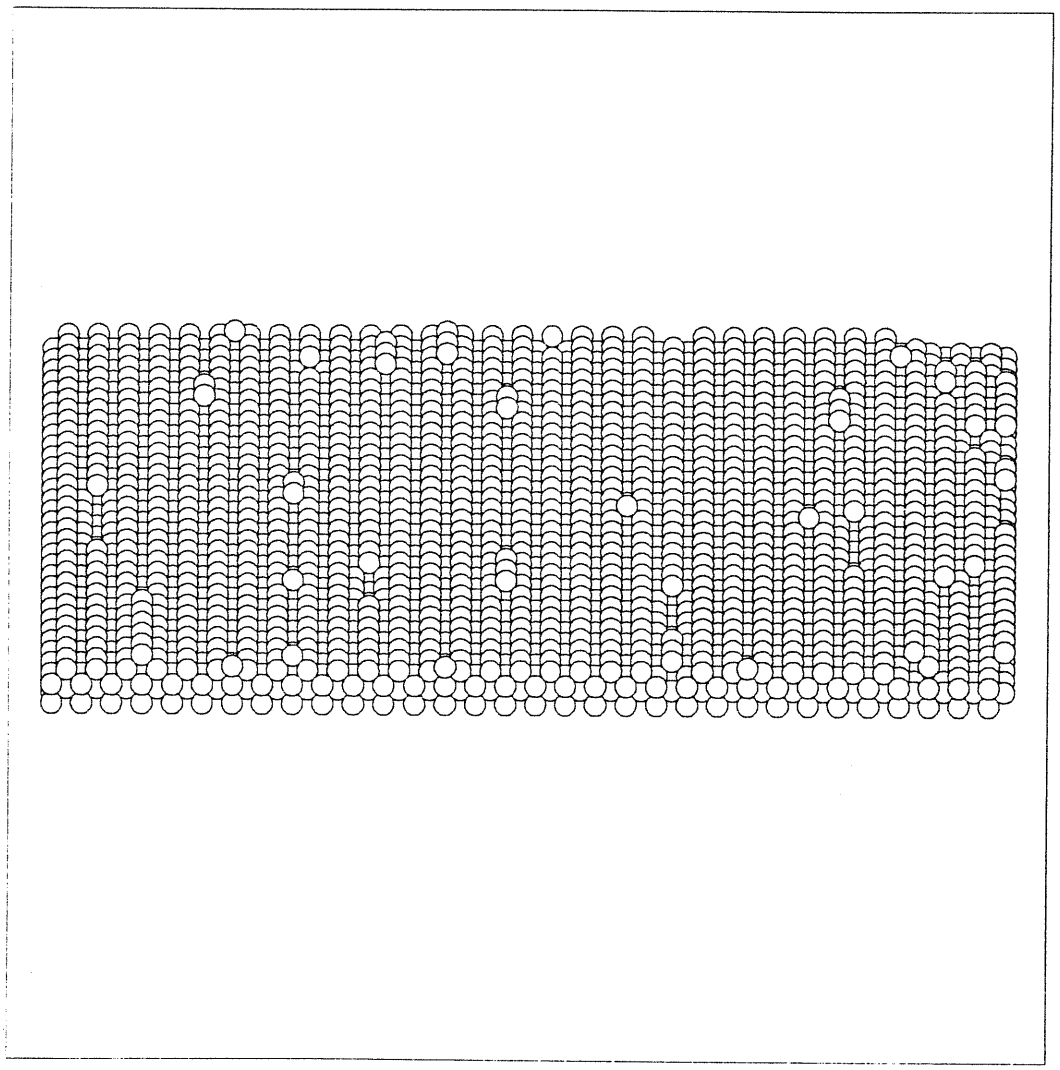

Figure 7.16. Snapshot of the Ag(110) surface configuration at a temperature T/J=1.750, below T_C.

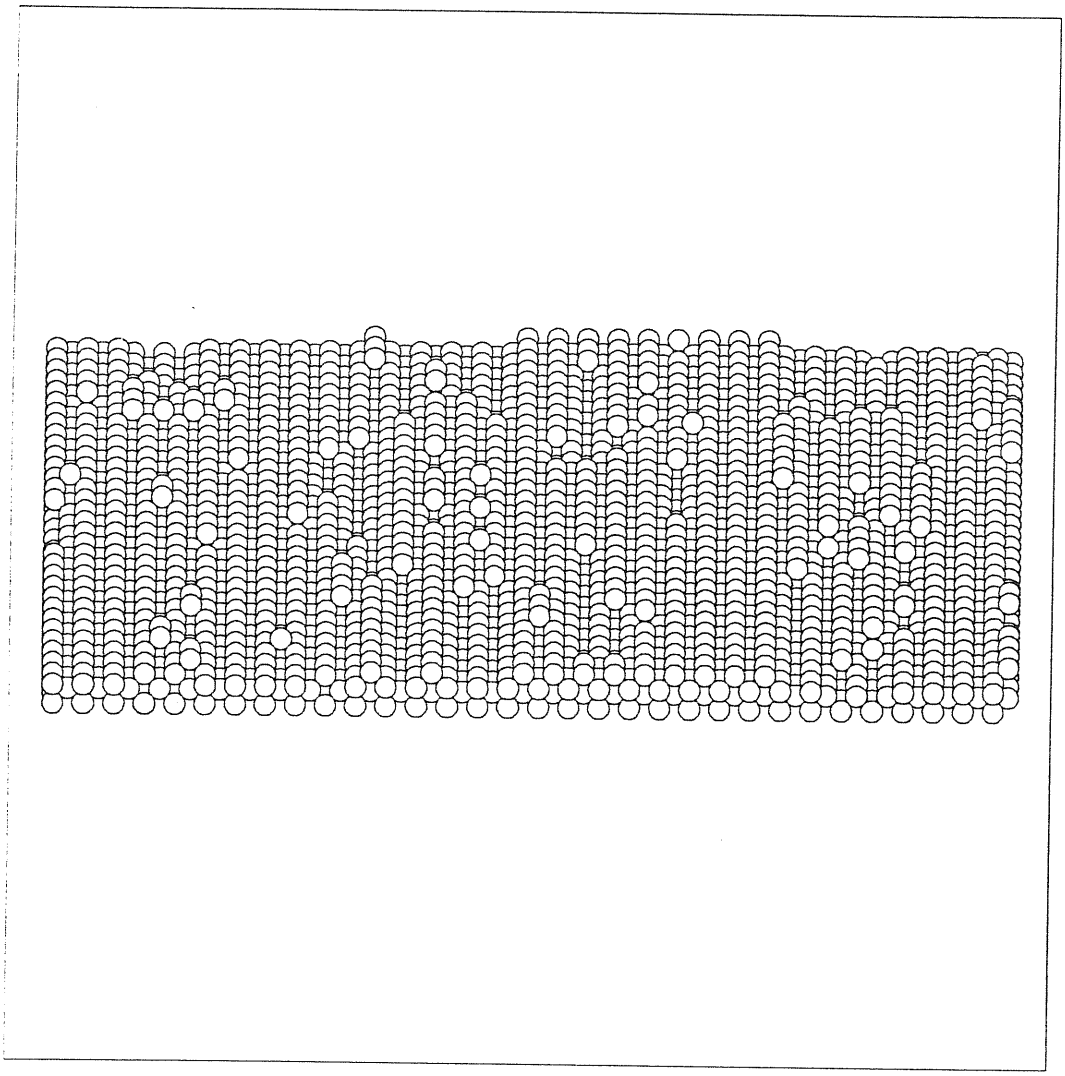

Figure 7.17. Snapshot of the Ag(110) surface configuration at a temperature T/J=2.000, between T_C and T_R.

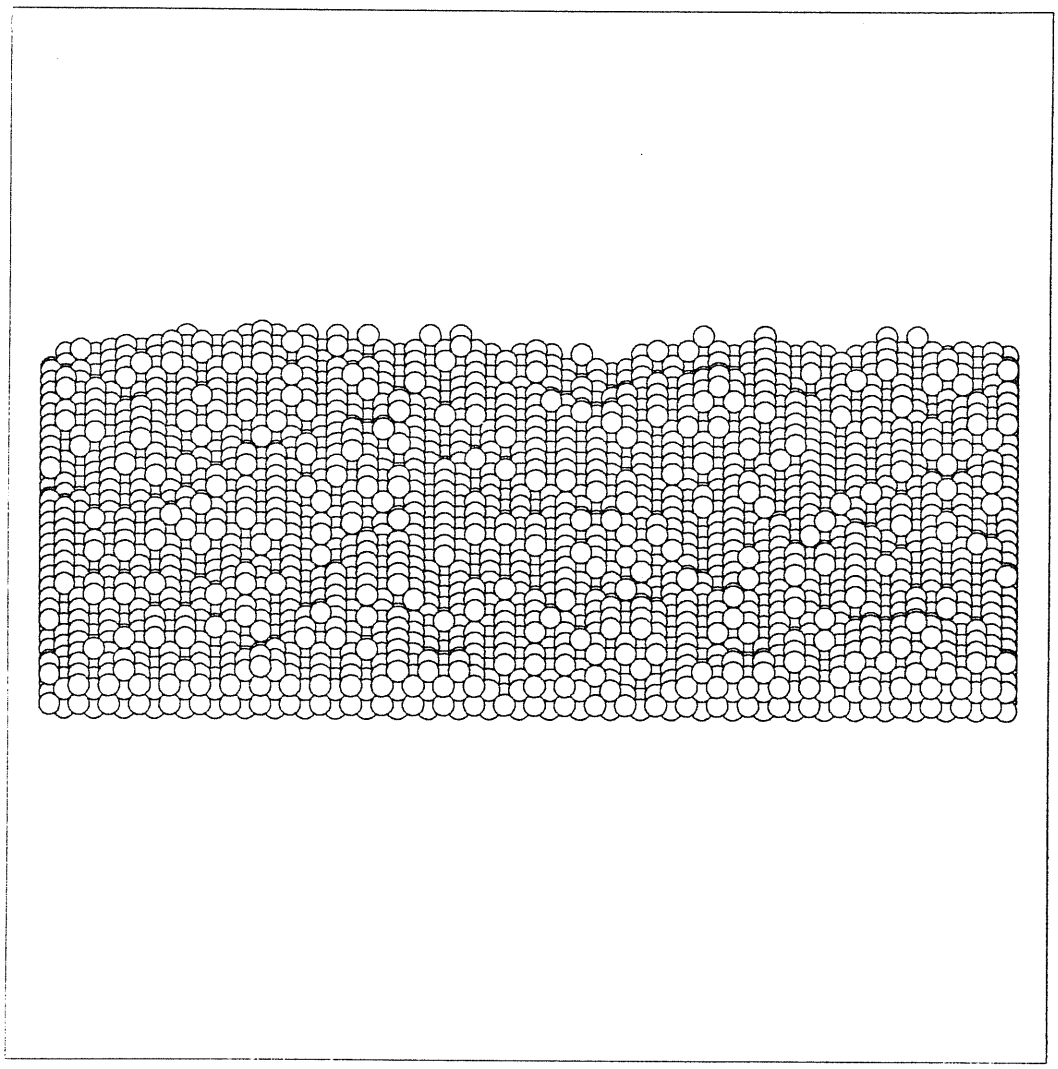

Figure 7.18. Snapshot of the Ag(110) surface configuration at a temperature T/J=6.000, above T_R.

Conclusions

The model proposed in Hamiltonian (4.1) has been shown to be capable of describing a variety of different phenomena occurring on the noble and near noble metal fcc(110) metal surfaces. With a suitable choice of parameters it can be used to characterize both (2×1) reconstructed surfaces like Au(110) and Pt(110) and the (2×1) unreconstructed surfaces like Ag(110), Pb(110), etc..., and to reproduce the phase transitions which occur on these systems as the temperature is raised. In the first case, evidence for a (2×1) deconstruction transition, followed 6% above in temperature by a roughening one, is extracted by the Monte Carlo data produced. In the second case, apart form the roughening transition again observed, at lower temperatures a new sublattice disordering critical phase transition is detected and characterized to lie in the class of non-universal "preroughening" transitions first envisaged by den Nijs and Rommelse[90] and by Kohanoff, Jug and Tosatti[124,125,126].

Coming to discuss the right side of the phase diagram relative to the reconstructed surface, it is apparent that a (2×1) deconstruction transition is found and characterized, which turns out to be, with convincing accuracy, Ising-like in nature. It is to be noticed that this is in agreement with the elementary discussions based on the symmetry of the order parameter for the reconstructed structure[54]. However, in these considerations the interference with the off-plane degrees of freedom was never taken into account. Hence any treatment which includes these must produce an Ising point in a rather non-trivial fashion. In fact, one should bear in mind that the degeneracy of the ground state is actually fourfold and naive symmetry consid-

erations would call for a transition of 4-state Potts universality class, for example. Yet, the existence of the six-vertex constraint enforced on half of the plaquettes of the spin checkerboard lattice leads to a spontaneous symmetry breaking inherent to the topology of the two-sublattice system (see figure 4.2). This corresponds to an ordered structure with an effectively lower symmetry "dynamically" imposed by the constraint on the excitations leading to disordering. Thus, the symmetry group is split into the product $Z_2 \bigotimes Z_2$ and leads to an effective Ising critical point. This is in agreement with the results obtained by other authors on the basis of different but related models[122,120,133]. In order to further elucidate this point, calculations of the sublattice order parameter $\mathcal{P}_{B/W}$ show it behaves as $\mathcal{P}_{2\times1}$, as far as critical properties are concerned.

The defect structures leading to deconstruction into a flat disordered phase appear to be of the higher-order 3×1, 4×1, ... as well as 1×1 types, with a predominance of 3×1, as seen by examining typical surface configurations. Indeed, the fact that the $(\frac{1}{2}, 0)$ peak position does show a small but non-zero shift towards lower Q_x values in the scattering calculation, confirms the presence of such dephasing higher-order defects (see below). In the language of den Nijs[90], this is a "chirality" effect.

It has also been shown that the surface becomes rough at a temperature $T_R \simeq 1.06 T_D$. Amongst the different scenarios proposed by Bernasconi[118], this rules out scenario (v), where $T_R = T_D$. This is connected to the question of whether steps consisting of (111) microfacets are not bound in pairs made of step up and step down or, if so, what is the origin of the step-step attraction. Indeed, the geometrical constraints are such that the meandering entropy of domain walls is higher when steps of opposite sign are bound than when steps of the same sign pair together (see Section 3.2). Geometry and entropy therefore play a most prominent role in the model, as it is not possible to distinguish between pairs of up-down and up-up (down-down) steps in terms of their energy. Under such conditions, pairing of steps of opposite sign is expected, leading to the appearance of a smooth phase right above deconstruction (T_D strictly lower than T_R).

Though it is not possible to definitely rule out scenarios (i)-(iii) (deconstruction driven by compact antiphase domains), the evidence of the $\mathcal{P}_{B/W}$ order parameter vanishing at the same temperature and with the same critical behaviour of the deconstruction order parameter $\mathcal{P}_{2\times1}$ is a clear indication of a scenario of

type (iv) occurring on the simulated surface, i.e. a DOF phase where a backbone of (3×1) steps proliferate in a up-down-up-down long range order, thus ensuring the average flatness of the disordered surface. This DOF phase is again stabilized by a subtle entropic mechanism between steps, owing also to the important role played by anisotropy in surface interactions.

Should a repulsion between steps be included by hand, one might expect it to cause $T_D = T_R$, as well as no one can exclude that for different values of the model parameters T_D and T_R may coincide. On the other hand, if an attraction is added, the gap between T_D and T_R ought to widen even further, as in the Villain and Vilfan [122] and in the den Nijs [120] models. In the model studied in this thesis, where no proper step-step interaction is present at $T = 0$, the gap between the two transitions is however a reality, despite its smallness. Indeed, at T_D and, more importantly, at $T_D + \Delta T_D$ (where ΔT_D is the statistical error), the coefficient $K(T)$ is well below the value $1/\pi^2$ taken up at T_R. Hence the surface is still flat. $K(T)$ is in fact negative in the region between T_D and T_R, i.e. large systems show a smaller interface width than small systems; no explanations for this feature has yet been found.

An important point in this theoretical study of the Au(110) surface is represented by the analysis of the scattering intensities for atom as well as for X-ray diffraction experiments. Results indicate that the position of the incoherent peak (and also its width and intensity) changes with temperature (and perpendicular momentum transfer q_z) above deconstruction, in broad agreement with experimental data obtained for Au(110) (and also Pt(110) [64]). This represents some important evidence that the surface generated by the statistical-mechanical model adopted is modulated (but flat and disordered) above T_D, as predicted by earlier theoretical treatments [124], before roughening at T_R. However, the half-order peak shift predicted for Au(110) with the present choice of the model parameters turns out to be quantitatively small, at least below T_R. This seems to be well borne out both by X-ray [39] and by He [55] scattering.

As on the right reconstructed side of the phase diagram, on the left, unreconstructed side a crucial role is played by the sublattice order parameter. On the extreme left ($K = -\infty$) one encounters the BCSOS model, where only a roughening transition is known to occur. This transition can be signalled by monitoring the behaviour of $\mathcal{P}_{B/W}$ of an infinite system and by looking at its vanishing, though

for finite systems this is carried out with a certain difficulty, due to finite size effect and also to the peculiar non-critical vanishing of $\mathcal{P}_{B/W}$ at T_R.

It is presumable, however, that as soon as one moves away from this particular point of the phase diagram, a new transition will appear on the surface, namely preroughening or sublattice disordering. This has been tested only for one value of the energy parameters, but it should be a general feature of Hamiltonian (4.1). In a way, roughening and sublattice disordering are two distinct transitions which are found to coincide only in the BCSOS case, but are ready to disentangle from one another as soon as a next nearest neighbour coupling K_3 is added to a BCSOS - like Hamiltonian. In this way, K_3 acts equivalently as the longer range term introduced by den Nijs in a SOS Hamiltonian , which gives rise to preroughening. The mechanism which causes this transition and, also, the stabilization of a DOF phase before roughening is much simpler than that envisaged in the Au(110) case, since it involves energetic considerations and not only entropic ones. In fact, the structure of (4.1) is such that with the choice of parameters 4.9, two parallel (2×1) steps are energetically more favoured than a (3×1) step, due to the presence of the positive K_3 term. This introduces a hard-core repulsion between parallel (2×1) steps of the same nature of that added by den Nijs in Hamiltonian (3.1), preventing them to merge into a single (3×1) step. Such mechanism leads to a stabilization of the DOF phase delimited by (2×1) steps. Incidentally, if (3×1) steps had been favoured, they would have connected terraces of the same type of atoms on top rows, and $\mathcal{P}_{B/W}$ would not have vanished. This stability temperature region survives till at T_R the step free energy definitely goes to zero and the interface delocalizes.

Pictures like 7.16 - 7.18 are an example of the realization of a DOF phase on a fcc(110) surface. Steps connecting flat terraces at different height levels are predominantly monoatomic, and the presence on the terraces of local thermal defects, like vacancies and adatoms, helps the disordering process but does not constitute the main source of relevant excitations which lead to the preroughening transition, these being composed only by the above mentioned steps.

Scattering experiments on the unreconstructed surfaces show particular features in the behaviour of the peaks with temperature which have been attributed either to local defect proliferation or to enhanced anharmonicity, but never to preroughening. The scattering calculations presented in Chapter 7 instead show

a sharp decrease in scattering peaks (a particularly sensitive peak is the specular peak in antiphase, as shown in the Appendix) which should vanish at the pre-roughening transition. The results of a statistical mechanics model, built up to mimic the physics of real systems and carefully reproducing the main features experimentally found on Au(110), should not, of course, necessarily be true also for unreconstructed (110) surfaces, especially if much more complex phenomena like faceting, which cannot be easily introduced in the model, occur. Nonetheless, this thesis should act as a suggestions to experimentalists to set up new measurements, sharply focused in the temperature region below the roughening transition.

Appendix

This Appendix is intended to explain the link between order parameters and scattering intensities (already discussion in Section 1.4.4), in two particular cases.

$\boxed{\otimes}$ The atom scattering intensities (1.17) for the reconstruction point $Q_x = \frac{1}{2}\frac{2\pi}{a_x}$, $Q_y = 0$, $q_z = 0$ is related to the reconstruction order parameter $\mathcal{P}_{2\times 1}$ (4.18). In fact, with this choice of momentum transfer values, $\mathcal{I}_A$ reads

$$\mathcal{I}_A\left(\frac{\pi}{a_x}, 0, 0\right) = \left|\sum_{\mathbf{R}} \mathrm{e}^{iQ_x R_x}\alpha(\mathbf{R})\right|^2 . \qquad (A.1)$$

The sum over all the lattice sites can be decomposed in the following manner. R_x, after (1.47) and similarly to Section 1.4.3 is written as $\mathbf{X}$, which runs over the position of the left corner atoms of each unit cell doubled due to reconstruction, plus $\mathbf{x}_\kappa$, which labels the four columns of black and white atoms within each unit cell, $\mathbf{x}_\kappa = 0, \frac{a_x}{2}, a_x, \frac{3}{2}a_x$. In this way

$$\sum_{\mathbf{R}} = \sum_{R_x, R_y} \longrightarrow \sum_{\mathbf{X}, \kappa, r_y} = \sum_{\kappa, \mathbf{R}_\kappa} \qquad \kappa = 1, 2, 3, 4$$

where $\mathbf{R}_\kappa$ labels each of the four sets obtained by grouping together every four columns, starting from the κ-th one. The phase factor $\mathrm{e}^{iQ_x R_x}$, after (1.47), is $\mathrm{e}^{i\pi n_x}$ for white sites, $\mathrm{e}^{i\pi(n_x+1/2)}$ for black ones, thus it depends only on κ (it can be written $\mathrm{e}^{i\frac{\pi}{2}(\kappa-1)}$, $\kappa = 1, 2, 3, 4$), and (A.1) transforms into

$$\mathcal{I}_A\left(\frac{\pi}{a_x},0,0\right) = \left|\sum_{\mathbf{R}_1}\alpha(\mathbf{R}_1) + i\sum_{\mathbf{R}_2}\alpha(\mathbf{R}_2) - \sum_{\mathbf{R}_3}\alpha(\mathbf{R}_3) - i\sum_{\mathbf{R}_4}\alpha(\mathbf{R}_4)\right|^2 =$$
$$= \left|\left(\sum_{\mathbf{R}_1}\alpha(\mathbf{R}_1) - \sum_{\mathbf{R}_3}\alpha(\mathbf{R}_3)\right) + i\left(\sum_{\mathbf{R}_2}\alpha(\mathbf{R}_2) - \sum_{\mathbf{R}_4}\alpha(\mathbf{R}_4)\right)\right|^2 . \tag{A.2}$$

On the other hand, the shadowing factor $\alpha(\mathbf{R})$ of eq. (1.18) can be rewritten as

$$\alpha(\mathbf{R}) = 1 + m(\mathbf{R}) - \frac{1}{4}\sum_{\mathbf{D}} m(\mathbf{R}+\mathbf{D}) \tag{A.3}$$

with $m(\mathbf{R})$ and $m(\mathbf{R}+\mathbf{D})$ respectively the heights of two nearest neighbour sites, located at $\mathbf{R}$ and $\mathbf{R}+\mathbf{D}$, and where the sum over $\mathbf{D}$ runs over the four nearest neighbour positions. With this expression, one gets

$$\sum_{\mathbf{R}_1}\alpha(\mathbf{R}_1) = \sum_{\mathbf{R}_1}\left[1 + m(\mathbf{R}_1) - \frac{1}{4}\sum_{\mathbf{D}} m(\mathbf{R}+\mathbf{D})\right] =$$
$$= \frac{\mathcal{N}}{4} + \sum_{\mathbf{R}_1} m(\mathbf{R}_1) - \frac{1}{4}\,2\left[\sum_{\mathbf{R}_2} m(\mathbf{R}_2) + \sum_{\mathbf{R}_4} m(\mathbf{R}_4)\right] =$$
$$= \frac{\mathcal{N}}{4} + \sum_{\mathbf{R}_1} m(\mathbf{R}_1) - \frac{1}{2}\sum_{\mathbf{R}_2} m(\mathbf{R}_2) - \frac{1}{2}\sum_{\mathbf{R}_4} m(\mathbf{R}_4)\,, \tag{A.4}$$

since every set of columns group together $\frac{\mathcal{N}}{4}$ sites, and of the four sites nearest neighbour to one of the set 1, two belong to set 4 and two to set 2. The two sets respectively preceeding and following the set κ are labeled by $(\kappa-1)\,(mod4)$ and $(\kappa+1)\,(mod4)$. Therefore

$$\mathcal{I}_A\left(\frac{\pi}{a_x},0,0\right) = \Bigg| \quad \Big(+\frac{\mathcal{N}}{4} + \sum_{\mathbf{R}_1} m(\mathbf{R}_1) - \frac{1}{2}\sum_{\mathbf{R}_2} m(\mathbf{R}_2) - \frac{1}{2}\sum_{\mathbf{R}_4} m(\mathbf{R}_4) +$$

$$- \frac{\mathcal{N}}{4} - \sum_{\mathbf{R}_3} m(\mathbf{R}_3) + \frac{1}{2}\sum_{\mathbf{R}_2} m(\mathbf{R}_2) + \frac{1}{2}\sum_{\mathbf{R}_4} m(\mathbf{R}_4)\Big) +$$

$$+ i\Big(+\frac{\mathcal{N}}{4} + \sum_{\mathbf{R}_2} m(\mathbf{R}_2) - \frac{1}{2}\sum_{\mathbf{R}_1} m(\mathbf{R}_1) - \frac{1}{2}\sum_{\mathbf{R}_3} m(\mathbf{R}_3) \; +$$

$$- \frac{\mathcal{N}}{4} - \sum_{\mathbf{R}_4} m(\mathbf{R}_4) + \frac{1}{2}\sum_{\mathbf{R}_1} m(\mathbf{R}_1) + \frac{1}{2}\sum_{\mathbf{R}_3} m(\mathbf{R}_3)\Big)\Bigg|^2 =$$

$$= \left|\left(\sum_{\mathbf{R}_1} m(\mathbf{R}_1) - \sum_{\mathbf{R}_3} m(\mathbf{R}_3)\right) + i\left(\sum_{\mathbf{R}_2} m(\mathbf{R}_2) - \sum_{\mathbf{R}_4} m(\mathbf{R}_4)\right)\right|^2 =$$

$$= \left[\left(\sum_{\mathbf{R}_1} m(\mathbf{R}_1) - \sum_{\mathbf{R}_3} m(\mathbf{R}_3)\right)^2 + \left(\sum_{\mathbf{R}_2} m(\mathbf{R}_2) - \sum_{\mathbf{R}_4} m(\mathbf{R}_4)\right)^2\right] . \quad (A.5)$$

But this is exactly the square of the order parameter $\mathcal{P}_{2\times1}$ defined in equation (4.18). In fact, using (4.17), (4.18) rewrites as

$$\mathcal{P}_{2\times1} = \left[M^2_{\langle++--\rangle} + M^2_{\langle+--+\rangle}\right]^{\frac{1}{2}}$$

and

$$M^2_{\langle++--\rangle} = \left[+M_1 + M_2 - M_3 - M_4\right]/4$$

$$M^2_{\langle+--+\rangle} = \left[+M_1 - M_2 - M_3 + M_4\right]/4\,;$$

but remembering the relation spins - height variables, it is straightforward to rewrite

$$M_1 = \sum_{\mathbf{R}_1} m(\mathbf{R}_1) - \sum_{\mathbf{R}_2} m(\mathbf{R}_2) \qquad M_3 = \sum_{\mathbf{R}_3} m(\mathbf{R}_3) - \sum_{\mathbf{R}_4} m(\mathbf{R}_4)$$

$$M_2 = \sum_{\mathbf{R}_3} m(\mathbf{R}_3) - \sum_{\mathbf{R}_2} m(\mathbf{R}_2) \qquad M_4 = \sum_{\mathbf{R}_1} m(\mathbf{R}_1) - \sum_{\mathbf{R}_4} m(\mathbf{R}_4)$$

so that

$$M_{\langle ++--\rangle} = \frac{1}{2}\left[\sum_{\mathbf{R}_1} m(\mathbf{R}_1) - \sum_{\mathbf{R}_3} m(\mathbf{R}_3)\right]$$

$$M_{\langle +--+\rangle} = \frac{1}{2}\left[\sum_{\mathbf{R}_4} m(\mathbf{R}_4) - \sum_{\mathbf{R}_2} m(\mathbf{R}_2)\right]$$

and finally

$$\mathcal{P}_{2\times 1} = \frac{1}{2}\left[\left(\sum_{\mathbf{R}_1} m(\mathbf{R}_1) - \sum_{\mathbf{R}_3} m(\mathbf{R}_3)\right)^2 + \left(\sum_{\mathbf{R}_2} m(\mathbf{R}_2) - \sum_{\mathbf{R}_4} m(\mathbf{R}_4)\right)^2\right]^{\frac{1}{2}} .$$

Normalizing the intensity such that it takes on the value 1 in the (2×1) ground state, it is apparent that

$$\mathcal{I}_A\left(\frac{\pi}{a_x}, 0, 0\right) = \mathcal{P}^2_{2\times 1} . \tag{A.6}$$

⊗ A relation of the same kind holds also in the unreconstructed case, where it is possible to show that the specular atom scattering intensity in antiphase (i.e. for $q_z a_z = \pi$) is proportional to the square of the $\mathcal{P}_{B/W}$ order parameter given in eq. (4.20). In fact, with the usual separation of the lattice into B and W sites,

$$\mathcal{I}_A\left(0,0,\frac{\pi}{a_z}\right) = \left|\sum_{\mathbf{R}} e^{i\pi m(\mathbf{R})}\alpha(\mathbf{R})\right|^2 =$$

$$= \left|\sum_{\mathbf{R}_W} e^{i\pi m(\mathbf{R}_W)}\alpha(\mathbf{R}_W) + \sum_{\mathbf{R}_B} e^{i\pi m(\mathbf{R}_B)}\alpha(\mathbf{R}_B)\right|^2 .$$

But, by definition, white (black) sites have odd (even) integer height variables, so that $e^{i\pi m(\mathbf{R}_W)} = -1$ and $e^{i\pi m(\mathbf{R}_B)} = +1$, and the scattering intensity writes

$$\mathcal{I}_A\left(0,0,\frac{\pi}{a_z}\right) = \left|\sum_{\mathbf{R}_W} \alpha(\mathbf{R}_W) - \sum_{\mathbf{R}_B} \alpha(\mathbf{R}_B)\right|^2 ;$$

utilizing again relation (A.3), this transforms into

$$\mathcal{I}_A\left(0,0,\frac{\pi}{a_z}\right) =$$

$$= \left|\sum_{\mathbf{R}_W} m(\mathbf{R}_W) - \frac{1}{4}\sum_{\mathbf{R}_W,\mathbf{D}} m(\mathbf{R}_W,\mathbf{D}) - \sum_{\mathbf{R}_B} m(\mathbf{R}_B) - \frac{1}{4}\sum_{\mathbf{R}_B,\mathbf{D}} m(\mathbf{R}_B,\mathbf{D})\right|^2$$

but

$$\sum_{\mathbf{R}_W,\mathbf{D}} m(\mathbf{R}_W,\mathbf{D}) = 4\sum_{\mathbf{R}_B} m(\mathbf{R}_B)$$

$$\sum_{\mathbf{R}_W,\mathbf{D}} m(\mathbf{R}_B,\mathbf{D}) = 4\sum_{\mathbf{R}_W} m(\mathbf{R}_W)$$

so that

$$\mathcal{I}_A\left(0,0,\frac{\pi}{a_z}\right) = 4\left|\sum_{\mathbf{R}_W} m(\mathbf{R}_W) - \sum_{\mathbf{R}_B} m(\mathbf{R}_B)\right|^2$$

$$\sim \mathcal{P}^2_{B/W} \qquad (A.7)$$

as obtained from relation (4.20).

A last word about scattering intensities and order parameters. All the relations proven have the form

$$\mathcal{I} = \mathcal{P}^2$$

where $\mathcal{I}$ is not the coherent intensity but the total one. Now, by taking the Monte Carlo average, one straightforwardly gets

$$\begin{aligned} \langle \mathcal{I} \rangle = \langle \mathcal{P}^2 \rangle = \langle \mathcal{P}^2 \rangle - \langle \mathcal{P} \rangle^2 + \langle \mathcal{P} \rangle^2 = \\ = \langle \mathcal{P}^2 \rangle \frac{k_B T}{\mathcal{N}} \chi \end{aligned} \tag{A.8}$$

(this last relation is obtained via eq. (4.21)), which is exactly a formula with the same structure of those written in Sections 1.4.4 – 1.4.5., thus enforcing the validity of the choice of decoupling spatial and Monte Carlo averages taken there.

Bibliography

[1] K. M. Ho and K. P. Bohnen, *Europhys. Lett.* **4**, 345 (1987).

[2] K. M. Ho and K. P. Bohnen, *Phys. Rev. Lett.* **59**, 1833 (1987).

[3] F. Ercolessi, E. Tosatti and M. Parrinello, *Phys. Rev. Lett.* **57**, 719 (1986).

[4] F. Ercolessi, A. Bartolini, M. Garofalo, M. Parrinello and E. Tosatti,*Physica Scripta* **T19**, 399 (1987).

[5] F. Ercolessi, M. Parrinello and E. Tosatti, *Philos. Mag.* **A58**, 213 (1988).

[6] W. K. Burton and N. Cabrera, *Disc. Faraday Soc.* **5**, 33 (1949).

[7] W. K. Burton, N. Cabrera and F. C. Frank, *Philos. Trans. R. Soc. Lond.* **243A**, 299 (1951).

[8] L. Onsager, *Phys. Rev.* **65**, 117 (1944).

[9] J. D. Weeks, in *Ordering in Stongly Fluctuating Condensed Matter Systems*, Ed. T. Riste (Plenum Press, New York, 1980), p. 292.

[10] H. van Beijeren and I. Nolden, in *Structure and Dynamics of Surfaces II*, Eds. W. Schommers and P. von Blanckenhagen (Springer, Heidelberg, 1987), p. 259.

[11] S. T. Chui and J. D. Weeks, *Phys. Rev.* **B14**, 4978 (1976).

[12] J. M. Kosterlitz and D. Thouless, *J. Phys.* **C6**, 1181 (1973).

[13] J. M. Kosterlitz, *J. Phys.* **C7**, 1046 (1974).

[14] H. van Beijeren, *Phys. Rev. Lett.* **38**, 993 (1977).

[15] H. E. Lieb, *Phys. Rev. Lett.* **18**, 1046 (1967).

[16] H. E. Lieb and F. Y. Wu, *Two dimensional ferroelectric models*, in *Phase Transition and Critical Phenomena*, Eds. C. Domb and M. S. Green (Academic Press, New York, 1972), p. 331.

[17] R. J. Baxter, *Exactly Solved Models in Statistical Mechanics* (Academic Press, London, 1982).

[18] L. Pauling, *J. Am. Chem. Soc.* **57**, 2680 (1935).

[19] J. C. Slater, *J. Chem. Phys.* **9**, 16 (1941).

[20] C. Jayaprakash, W. F. Saam and S. Teitel, *Phys. Rev. Lett.* **50**, 2017 (1983).

[21] W. F. Saam, C. Jayaprakash and S. Teitel, in *Quantum Fluids and Solids - 1983*, Eds. E. D. Adams and G. G. Ihas (A.I.P., New York, 1983), p. 371.

[22] C. Jayaprakash and W. F. Saam, *Phys. Rev.* **B30**, 3916 (1984).

[23] A. Trayanov, A. C. Levi and E. Tosatti, *Surf. Sci.* **233**, 184 (1990).

[24] G. Wulff, *Z. Krist. Mater.* **34**, 449 (1901).

[25] C. Herring, *Phys. Rev.* **82**, 87 (1951).

[26] J. C. Heyraud and J. J. Métois, *Surf. Sci.* **128**, 334 (1983).

[27] I. K. Robinson, *Phys. Rev.* **B33**, 3830 (1986).

[28] U. Garibaldi, A. C. Levi, R. Spadacini and G. E. Tommei, *Surf. Sci.* **48**, 649 (1975).

[29] G. E. Tommei, A. C. Levi and R. Spadacini, *Surf. Sci.* **125**, 312 (1982).

[30] A. C. Levi, R. Spadacini and G. E. Tommei, in *The Structure of Surfaces II*, Eds. J. F. van der Veen and M. A. Hove (Springer, vol 11, 1988).

[31] K. Debertin and R. G. Helmer, in *Gamma and X-rays Spectrometry with Semiconductor Detectors* (North-Holland, Amsterdam, 1988), p. 342.

[32] R. Colella, *Phys. Rev.* **B43**, 13827 (1991).

[33] E. Vlieg, J. F. van der Veen, S. J. Gurman, C. Norris and J. E. Macdonald, *Surf. Sci.* **210**, 301 (1989).

[34] R. F. Willis, in *Dynamical Phenomena at Surfaces*, Eds. F. Nizzoli, K. H. Rieder and R. F. Willis (Spinger, Berlin, 1985), p. 126.

[35] E. Bauer, in *Structure and Dynamics of Surfaces II*, Eds. W. Schommers and P. von Blanckenhagen (Springer, Heidelberg, 1987), p. 115.

[36] J. Villain, D. R. Grempel and J. Lapujoulade, *J. Phys.* **F15**, 809 (1985).

[37] G. A. Held, J. L. Jordan-Sweet, P. M. Horn, A. Mak and R. Birgeneau, *Phys. Rev. Lett.* **59**, 2075 (1987).

[38] H.-N. Yang, T.-M. Lu and G.-C. Wang, *Phys. Rev. Lett.* **63**, 1621, (1989).

[39] D. T. Keane, P. A. Bancel, J. L. Jordan-Sweet, G .A .Held, A. Mak and R. J. Birgeneau, *Surf. Sci.* **250**, 8 (1991).

[40] D. Wolf, H. Jagodzinski and W. Moritz, *Surf. Sci.* **77**, 265 (1978); **77**, 283 (1978).
[41] W. Moritz and D. Wolf, *Surf. Sci.* **88**, L29 (1979).
[42] H. P. Bonzel and S. Ferrer, *Surf. Sci.* **118**, L111 (1982).
[43] H. P. Bonzel and S. Ferrer, *Surf. Sci.* **119**, 234 (1982).
[44] W. Moritz and D. Wolf, *Surf. Sci.* **163**, L655 (1985).
[45] I. K. Robinson, *Phys. Rev. Lett.* **50**, 1145 (1983).
[46] I. K. Robinson, Y. Kuk and L. C. Feldman, *Phys. Rev.* **B29**, 4762 (1984).
[47] J. Möller, J. Niehus and W. Heiland, *Surf. Sci.* **166**, L111 (1986).
[48] M. Copel and T. Gustafsson, *Phys. Rev. Lett.* **57**, 723 (1986).
[49] L. D. Marks, *Phys. Rev. Lett.* **51**, 1000 (1983).
[50] G. Binnig, H. Rohrer, Ch. Gerber and E. Weibel, *Surf. Sci.* **131**, 1379 (1983).
[51] E. Vlieg, I. K. Robinson and K. Kern, *Surf. Sci.* **233**, 248 (1990).
[52] J. C. Campuzano, M. S. Foster, G. Jennings, R. F. Willis and W. Unertl, *Phys. Rev. Lett.* **54**, 2684 (1985).
[53] J. C. Campuzano, G. Jennings and R. F. Willis, *Surf. Sci.* **162**, 484 (1985).
[54] P. Bak, *Solid State Commun.* **32**, 581 (1979).
[55] D. Cvetko, A. Lausi, A. Morgante, F. Tommasini and K. C. Prince, *Surf. Sci.* **269/270**, 68 (1992).
[56] J. Sprösser, B. Salanon and J. Lapujoulade, *Europhys. Lett.* **16**, 283 (1991).
[57] G. A. Held, J. L. Jordan-Sweet, P. M. Horn, A. Mak and R. Birgeneau, *Solid State Commun.* **72**, 37 (1989).
[58] P. Häberle, P. Fenter and T. Gustafsson, *Phys. Rev.* **B39**, 5810 (1989).
[59] E. G. McRae, T. M. Buck, R. A. Malik and G. H. Wheatley, *Phys. Rev.* **B36**, 2341 (1987).
[60] E. van de Riet, H. Derks and W. Heiland, *Surf. Sci.* **234**, 53 (1990).
[61] U. Romahn, H. Zimmermann, M. Nold, A. Hoss, H. Göbel, P. von Blanckenhagen and W. Schommers, *Surf. Sci.* **251/252**, 656 (1991).
[62] A. Hoss, M. Nold, P. von Blanckenhagen and O. Meyer, *Phys. Rev.* **B45**, 8714 (1992).
[63] J. K. Gimzewski, R. Berndt and R. R. Schlitter, *Phys. Rev.* **B45**, 6844 (1992).
[64] I. K. Robinson, E. Vlieg and K. Kern, *Phys. Rev. Lett.* **63**, 2578 (1989).
[65] H. Niehus, *Surf. Sci.* **145**, 407 (1984).
[66] G. L. Kellog, *Phys. Rev. Lett.* **55**, 2168 (1985).

[67] C. Sowa, M. A. van Hove and D. L. Adams, *Surf. Sci.* **199**, 174 (1988).
[68] P. Fery, W. Moritz and D. Wolf, *Phys. Rev.* **38**, 7275 (1988).
[69] M. Salmeron and G. Somorjai, *Surf. Sci.* **91**, 373 (1980).
[70] J. F. van der Veen, F. H. Himpsel and D. E. Eastman, *Phys. Rev. Lett.* **44**, 189 (1980).
[71] K. Dückers and H. P. Bonzel, *Europhys. Lett.* **7**, 371 (1988).
[72] I. K. Robinson, E. Vlieg and K. Kern, *Phys. Rev. Lett.* **65**, 1831 (1990).
[73] P. Fenter and T. M. Lu, *Surf. Sci.* **154**, 15 (1985).
[74] J. Villain and I. Vilfan, *Phys. Rev. Lett.* **65**, 1830 (1990).
[75] M. Wortis, in *Phase Transitions in Surface Films 2*, Eds. H. Taub, G. Torzo, H. J. Lauter and S. C. Fain Jr., NATO ASI Series Vol. **B 267** (Plenum Press, New York, 1991), p. 479.
[76] Elias Vlieg, private communication.
[77] Klaus Kern, private communication.
[78] C.-M. Chan, M. A.van Hove, W. H. Weinberg and E. D. Williams, *Surf. Sci.* **91**, 440 (1980).
[79] C.-M. Chan and M. A.van Hove, *Surf. Sci.* **171**, 226 (1986).
[80] M. Copel, P. Fenter and T. Gustafsson, J. Vac. Sci. Technol. **A5**(4), 742 (1987).
[81] W. Hetterich and W. Heiland, *Surf. Sci.* **210**, 129 (1989).
[82] W. Hetterich, C. Höfner and W. Heiland, *Surf. Sci.* **251/252**, 731 (1991).
[83] H. Bu, M Shi, F. Masson and J. W. Rabalais, *Surf. Sci.* **230**, L140 (1990).
[84] M Shi, H. Bu and J. W. Rabalais, *Phys. Rev.* **B42**, 2852 (1990).
[85] R. Koch, M. Borbonus, O. Haase and K. H. Rieder, *Phys. Rev. Lett.* **67**, 3416 (1991).
[86] G. Bracco, C. Maló and R. Tatarek, Vuoto **12**, 195 (1991).
[87] I. K. Robinson, E. Vlieg, H. Hornis and E. H. Conrad, *Phys. Rev. Lett.* **67**, 1890 (1991).
[88] H.-N. Yang, T.-M. Lu and G.-C. Wang, *Phys. Rev.* **B43**, 4714 (1991).
[89] H.-N. Yang, K. Fang, G.-C. Wang and T.-M. Lu, *Europhys. Lett.* **19**, 215 (1992).
[90] K. Rommelse and M. den Nijs, *Phys. Rev. Lett.* **59**, 2578 (1987); M. den Nijs and K. Rommelse, *Phys. Rev.* **B40**, 4709 (1987).
[91] S. J. G. Mochrie, *Phys. Rev. Lett.* **59**, 304 (1987).

[92] P. Zeppenfeld, K. Kern, R. David and G. Comsa, *Phys. Rev. Lett.* **62**, 63 (1989).

[93] B. M. Ocko and S. G. J. Mochrie, *Phys. Rev.* **B38**, 7378 (1988).

[94] K. D. Stock and E. Menzel, *Surf. Sci.* **61**, 272 (1976).

[95] J. Lapujoulade, J. Perreau and A. Kara, *Surf. Sci.* **129**, 59 (1983).

[96] D. Gorse and J. Lapujoulade, *Surf. Sci.* **162**, 847 (1985).

[97] G. Armand and P. Zeppenfeld, *Phys. Rev.* **B40**, 5936 (1989).

[98] B. Loisel, J. Lapujoulade and V. Pontikis, *Surf. Sci.* **256**, 242 (1991).

[99] L. Yang and T. S. Rahman, *Phys. Rev. Lett.* **67**, 2327 (1991).

[100] H. Häkkinen, J. Merikoski, M. Manninen, J. Timonen and K. Kaski, University of Jyväskylä (Finland) preprint no. 10, 1992.

[101] Marco Bernasconi, private communication.

[102] H. Dürr, R. Schneider and Th. Fauster, *Phys. Rev.* **B43**, 12187 (1991).

[103] Y. Cao and E. H. Conrad, *Phys. Rev. Lett.* **64**, 447 (1990).

[104] A. W. Denier van der Gon, D. Frenkel, J. W. M. Frenken, R. J. Smith and P. Stoltze, *Surf. Sci.* **256**, 385 (1991).

[105] S. M. Francis and N. V. Richardson, *Phys. Rev.* **B33**, 662 (1986).

[106] A. M. Lahee, J. P. Toennies and Ch. Wöll, *Surf. Sci.* **191**, 529 (1987).

[107] F. Ercolessi, S. Iarlori, O. Tomagnini, E. Tosatti and X. J. Chen, *Surf. Sci.* **251/252**, 645 (1991).

[108] J. W. M. Frenken and J. F. van der Veen, *Phys. Rev. Lett.* **54**, 134 (1985).

[109] J. F. van der Veen, in *Phase Transitions in Surface Films 2*, Eds. H. Taub, G. Torzo, H. J. Lauter and S. C. Fain Jr., NATO ASI Series Vol. **B 267** (Plenum Press, New York, 1991), p. 289, and references therein.

[110] B. E. Hayden, K. C. Prince, P. J. Davie, G. Paolucci and G. M. Bradshaw, *Solid State Commun.* **48**, 325 (1983).

[111] S. M. Francis and N. V. Richardson, *Surf. Sci.* **152/152**, 63 (1985).

[112] J. W. M. Frenken, R. L. Krans, J. F. van der Veen, E. Holub-Krappe and K. Horn, *Phys. Rev. Lett.* **59**, 2307 (1987).

[113] C. J. Barnes, M. Lindroos and D. A. King, *Surf. Sci.* **201**, 108 (1988).

[114] R. Spitz, H. Niehus, B. Poelsema and G. Comsa, *Surf. Sci.* **239**, 243 (1990).

[115] K. Kern, H. Niehus, A. Schatz, P. Zeppenfelf, J. Goerge and G. Comsa, *Phys. Rev. Lett.* **67**, 855 (1991).

[116] V. Heine and L. D. Marks, *Surf. Sci.* **165**, 65 (1986).

[117] S. M. Foiles, M. I. Baskes and M. S. Daw, *Phys. Rev.* **B33**, 7983 (1986); *Phys. Rev.* **B37**, 10378(Err.) (1988).
[118] M. Bernasconi and E. Tosatti, S.I.S.S.A. preprint (1992).
[119] M. den Nijs, *Phys. Rev. Lett.* **64**, 435 (1990).
[120] M. den Nijs, in *Phase Transitions in Surface Films 2*, Eds. H. Taub, G. Torzo, H. J. Lauter and S. C. Fain Jr., NATO ASI Series Vol. **B 267** (Plenum Press, New York, 1991), p. 247; *Phys. Rev. Lett.* **66**, 907 (1991).
[121] G. Mazzeo, G. Jug, A. C. Levi and E. Tosatti, *Surf. Sci.* **273**, 237 (1992).
[122] J. Villain and I. Vilfan, *Surf. Sci.* **257**, 368 (1991).
[123] A. C. Levi and M. Touzani, *Surf. Sci.* **218**, 223 (1989).
[124] G. Jug and E. Tosatti, *Phys. Rev.* **B42**, 969 (1990); *Physica* **A175**, 59 (1990).
[125] J. Kohanoff, G. Jug and E. Tosatti, *J. Phys.* **A23**, L209, (1990).
[126] J. Kohanoff, G. Jug and E. Tosatti, *J. Phys.* **A**, 5625 (1990).
[127] J. Villain and P. Bak, *J. Phys. (Paris)* **42**, 657 (1981).
[128] W. Selke, *Phys. Rep.* **170**, 213 (1988).
[129] J. Villain and I. Vilfan, *Surf. Sci.* **199**, 165 (1988).
[130] E. Muller-Hartmann and J. Zittartz, *Z. Phys.* **B27**, 261 (1977).
[131] J. Villain, J. L. Rouviere and I. Vilfan, in *Phase Transitions in Surface Films 2*, Eds. H. Taub, G. Torzo, H. J. Lauter and S. C. Fain Jr., NATO ASI Series Vol. **B 267** (Plenum Press, New York, 1991), p. 201.
[132] L. Balents and M. Kardar, *Harvard University preprint.*
[133] M. den Nijs, preprint (1992).
[134] E. H. Lieb and F. Y. Wu, *Phys. Rev. Lett.* **20**, 1445 (1968).
[135] V. K. Kumikov and Kh. B. Khokonov, *J. Appl. Phys.* **54**, 1346 (1983).
[136] S. P. Chen and A. F. Voter, *Surf. Sci.* **244**, L107 (1991).
[137] K. Binder, in *Monte Carlo methods in statistical physics*, Ed. K. Binder (Springer, 1979), p. 1.
[138] N. Metropolis, A. W. Rosenbluth, M. N. Rosenbluth, A. H. Teller and E. Teller, *J. Chem. Phys.* **21**, 1087 (1953).
[139] G. Jacucci and A. Rahman, *Nuovo Cim.* **4D**, 341 (1984).
[140] D. P. Landau, *Phys. Rev.* **B27**, 5604 (1983).
[141] G. Mazzeo, G. Jug, A. C. Levi and E. Tosatti, *J. Phys.* **A**, in press.
[142] P. Forrester, *J. Phys* **A19**, L143 (1986).
[143] R. J. Baxter *Phys. Rev.* **B1**, 2199 (1970).

[144] R. J. Baxter *J. Phys* **C6**, L94 (1973).

[145] M. den Nijs *J. Phys.* **A18**, L549 (1985).

[146] B. Sutherland, *Phys. Lett.* **26A**, 532 (1968).

[147] R. W. Youngblood, J. D. Axe and B. M. McCoy, *Phys. Rev.* **B21**, 5212 (1980).

[148] N. M. Bogoliubov, A. G. Izergin and V. E. Korepin, *Nucl. Phys.* **B275**, 687 (1986).

[149] Lei-Han Tang, private communication.

[150] M. N. Barber, in *Phase Transition and Critical Phenomena*, Eds. C. Domb and J. M. Lebowitz, Vol. 8 (Academic Press, London, 1983).

[151] M. N. Barber and W. Selke, *J. Phys.* **A15**, L617 (1982).

Ringraziamenti

Ringrazio di cuore tutti coloro che sentono di meritarsi tale ringraziamento.